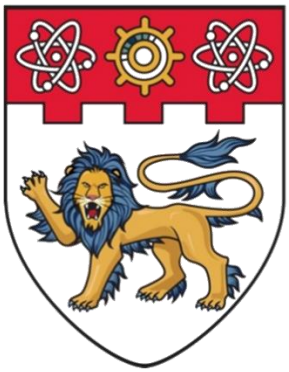

NANYANG TECHNOLOGICAL UNIVERSITY
SINGAPORE

School of Chemical and Biomedical Engineering

Thesis Report

Antimicrobial Polymers: From Theoretical Studies to Real-life Applications

Student Name: HOU ZHENG

Matric Number: G1400576C

Degree: Doctor of Philosophy

Supervisor: Prof Mary Chan-Park Bee Eng

2019

Antimicrobial Polymers: From Theoretical Studies to Real-life Applications

Hou Zheng

School of Chemical and Biomedical Engineering

Thesis submitted to The Nanyang Technological University In partial fulfilment of the requirements for the degree of Doctor of Philosophy

2020

Statement of Originality

I hereby certify that the work embodied in this thesis is the result of original research, is free of plagiarized and has not been submitted for a higher degree to any other University or Institution.

. . . . . 22-Aug-2019. . . . .  . .

Date Hou Zheng

Supervisor Declaration Statement

I have reviewed the content and presentation style of this thesis and declare it is free of plagiarism and of sufficient grammatical clarity to be examined. To the best of my knowledge, the research and writing are those of the candidate except as acknowledged in the Author Attribution Statement. I confirm that the investigations were conducted in accord with the ethics policies and integrity standards of Nanyang Technological University and that the research data are presented honestly and without prejudice.

22 Aug 2019

Date

Prof. Chan Bee Eng, Mary

Authorship Attribution Statement

This thesis contains material from **1** paper published in the following peer-reviewed journal in which I am listed as a co-first author.

Chapter 4 is published as Zheng Hou, Yogesh Vikhe Shankar, Yang Liu, Feiqing Ding, Jothy Lachumy Subramanion, Vikashini Ravikumar, Rubí Zamudio-Vázquez, Damien Keogh, Huiwen Lim, Moon Yue Feng Tay, Surajit Bhattacharjya, Scott A. Rice, Jian Shi, Hongwei Duan, Xue-Wei Liu, Yuguang Mu, Nguan Soon Tan, Kam C. Tam, Kevin Pethe, Mary B. Chan-Park* Nanoparticles of Short Cationic Peptidopolysaccharide Self-Assembled by Hydrogen Bonding with Antibacterial Effect against Multidrug-Resistant Bacteria. ACS Appl. Mater. Interfaces2017 9 44 38288-38303 https://doi.org/10.1021/acsami.7b12120

- Prof. M.B. Chan-Park provided the initial project direction and edited the manuscript drafts. Dr. Yogesh Vikhe Shanker and I prepared the manuscript drafts. Prof. M.B. Chan-Park, and I revised the manuscript.

- I conduced all biophysical tests, mechanism studies such as zeta potential, light scattering, isothermal titration calorimetry with help from Kam C. Tam and Surajit Bhattacharjva. As well as animal studies with help from Nguan Soon Tam in the facilities provided by NTU-SCBE, and NTU-SBS. I analysed the data.

- Dr Yogesh Vikhe Shankar synthesized the copolymer for testing with help from Feiqing Ding, Hongwei Duan and Xue-wei Liu and Dr Yang Liu did the computational simulation of antimicrobial mechanism with supervision from Yuguang Mu. Rubí Zamudio-Vázquez, Damien Keogh, Huiwen Lim, Moon Yue

Feng and Shi Jian Tay did the microbial biological tests with help from Kevin Pethe and Scott A. Rice.

. . . . . 22-Aug-2019. . . . .  . . . . .

Date Hou Zheng

Acknowledgement

I want to give my sincere appreciation to my supervisor Prof. Chan Bee Eng, Mary for her guidance and support throughout my entire Ph.D. study. Thank you for recruiting me into your lab and giving me the chance to widen my horizon in the field of antimicrobial polymer science.

I want to thank Prof. Li Peng, Dr. Pu Yuji, Dr Ding Feiqing, Dr Zhou Chao, and Dr Xu Chen

for their help in the development of my topic of thesis and their guidance in chemistry synthesis, and biological tests

I want to thank Dr. Liu Bo, Dr. Jo Thy Subramanian, Mr.Wu Yang, Mr. Li Jianghua, and Miss Sheethal Reghu for your valuable advices and help in my research. I want to thank A/Prof. Wang Mingfeng and A/Prof. Duan Hongwei to be my thesis advisory committee members.

I appreciate the research scholarship granted by NTU and financial aid from Prof. Chan Bee Eng, Mary.

Last but not least, I want to thank all my friends and my family members for your love and motivations throughout the PhD candidature

Table of Contents

List of Tables

Table 5.6 *In vivo* toxicity of DAC, effect on liver and kidney functions as well as balance of electrolytes in the blood.

List of Figures

(D) *S aureus* 29213. For DISC3(5) dye leakage assay, triton is used as control to break inner cell membrane completely; for NPN dye leakage assay, Polymyxin B is used as control with same concentration as polymer (100μg/mL) ATPase assay of (E) *E. coli* K12, and (F) MRSA BAA-40.

Figure 4.16 Fluorescence microscopy images of E. coli K12, MRSA BAA-40 and E. faecalis V583 incubated with Rho-CSM5-K5

Figure 4.17 Cryo-TEM images of MRSA treated with CSM5-K5 at 8×MIC. (A) MRSA Control without treatment by CSM5-K5; (B) Separation of Cell membrane from cell wall after treatment of CSM5-K5; (C) Shrinking of cell membrane after treatment of CSM5-K5; (D) Irregular cell wall after treatment of CSM5-K5; Scale bar=500nm.

Figure 4.18 Summary of enthalpy profile (kcal/mol) change with mole ratio of polymer added into liposomes determined by isothermal titration calorimetry study of CSM5-K5 interaction with (i) POPC: LPS liposome with LPS from *E coli;* (ii) POPC: LPS liposome with LPS from *P .aeruginosa* PAO1; (iii) POPC: POPG liposome; (iv) Pure POPC liposome

Figure 4.19 illustration of cationic copolymer binding on Liposome models: (A) the polymer has very strong interaction with liposome and cause the aggregation of liposome (POPC: LPS). (B) the polymer can bind with liposome (POPC: POPG), (C) the polymer has no interaction with liposome (Pure POPC).

Figure 5.1 NMR spectrum of 2,6-DAC synthesis(A) N-Phthaloyl Chitosan (B) 6-deoxy-6-bromo-N-phthaloyl-chitosans (C) 6-azido-6-deoxy-N-phthaloyl-chitosan (D) 2,6-Diamino Chitosan

Figure 5.2 FTIR characterization of synthesis of 2,6-diamino chitosan (3) 6-deoxy-6-bromo-N-phthaloyl-chitosans (4) 6-azido-6-deoxy-N-phthaloyl-chitosan (5) 2,6-Diamino Chitosan

Figure 5.3 NMR spectrum of other chitosan derivatives (5b) 6-EG Diamine Chitosan, (5c) 6-Spermine Chitosan, (5d) 6-DET Chitosan, (5e) 6-EDA Chitosan, (5f) 6-Triamine Chitosan, (5g) 6-Aminopropyl imidazole Chitosan, (5h) 6-Diamino Triazole Chitosan, (5i) 6-Amino Triazole Chitosan, (5j) 6-3 Amino 4-Carboxamide Imidazole Chitosan

Figure 5.4 Time-killing essay of 2,6-DAC against *A. baumanii* AB-1

Figure 6.7 Biocompatibility against mammalian cells, blood immune cells and antithrombogenic efficacy of the coatings. (A) Mammalian cell compatibility of extractants from soaking modified catheters in DMEM for 24hrs following ISO10993-5. (B). Antithrombogenic efficacy of the coatings measured by platelet activation and surface thrombus formation. (C) Activation of blood immune cells. (D) Blood protein fouling on catheters.

Figure 6.8 Scanning Electronic Microscopy images of thrombus formed on catheters, Left: before incubation with rabbit whole blood. Right: after 2hrs incubation with rabbit whole blood bar=10μm. Red circle: partially coverage of thrombus.

Figure 6.9 *In vivo* antibacterial efficacy (A) Murine subcutaneous model (i) illustration of subcutaneous implantation and infection. (ii) *In vivo* antibacterial efficacy for subcutaneous infection model. (iii) Images of infected subcutaneous pocket and recovered catheter after 24hrs implantation. (a) Serious sign of infection found in the subcutaneous pocket implanted with unmodified catheter (b) Minimal sign of infection found in the subcutaneous pocket implanted with #10 H(N)-b-S catheter. (c) Clotted blood found on unmodified catheter. (d) No blood clotting found on #10 H(N)-b-S catheter.

List of Schemes

List of Abbreviations

ACVA	4,4′-Azobis(4-cyanovaleric acid)
AFM	Atomic Force Microscopy
AMP	Antimicrobial Peptide
AMPTMA	(3-acrylamidopropyl)-trimethylammonium chloride
Ar	Argon
ATCC	American Type Culture Collection
ATR	Attenuated Total Reflectance
ATRP	Atom transfer radical polymerization
BHI	Brain heart infusion
BMA	butyl methacrylate
CAUTI	Catheter Associated Urinary tract infection
Cbz	Carboxybenzyl
CD	Circular dichroism
CFU	colony-forming unit
CLABSI	Central Line Associated Blood Stream Infections
CPCPA	4-Cyano-4-(phenylcarbonothioylthio) pentanoic acid
CS	Chitosan
DAC	Diamino chitosan
DET	Diethylenetriamine
DI water	De-ionized water
DISC35	3,3'-Dipropylthiadicarbocyanine Iodide
DLS	Dynamic Light Scattering
DMF	Dimethylformamide
DMSO	Dimethyl sulfoxide
DMEM	Dulbecco's Modified Eagle Medium
EDA	Ethylene diamine
EtOH	Ethanol
FACS	Fluorescence-activated cell sorting
FBS	Fetal bovine serum
FIC	Fractional inhibitory concentration
GPC	Gel permeation chromatography
HAI	Healthcare Associated Infection
HDF	Human Dermal Fibroblasts
HEMA	2-Hydroxyethyl methacrylate
HEK	Human embryonic kidney 293 cells
IP	Intraperitoneal
IPA	Isopropyl alcohol

LB	Lysogeny Broth
LPS	Lipopolysaccharides
MALDI	Matrix-assisted laser desorption/ionization
MBC	Minimum bactericidal concentration
MD	Molecular Dynamic
MeOH	Methanol
MDR	Multi-drug resistant
MHB	Muller-Hinton Broth
MIC	Minimum Inhibitory Concentration
MRSA	Methicillin-resistant Staphylococcus aureus
MTT	Thiazolyl Blue Tetrazolium Blue
M.W.	Molecular weight
NCA	N-carboxyanhydride
NMP	N-Methyl-2-pyrrolidone
NMR	Nuclear magnetic resonance
NO	nitric oxide
NPN	N-Phenyl-1-naphthylamine
ORSA	Oxacillin-resistant Staphylococcus aureus
POPC	1-palmitoyl-2-oleoyl-sn-glycero-3-phosphocholine
POPG	palmitoyl-oleoyl phosphatidylglycerol
PAA	poly acrylic acid
pDADMAC	Polydiallyldimethylammonium chloride
PEG	Polyethylene glycol
PEI	Polyethyleneimine
PSS	polystyrene sulfonate
PU	Polyurethane
PBS	phosphate buffered saline
RAFT	Reversible addition−fragmentation chain-transfer polymerization
RBC	Red blood cell
ROP	Ring Opening Polymerization
SBMA	[2-(Methacryloyloxy) ethyl] dimethyl-(3-sulfopropyl) ammonium hydroxide
SDS	Sodium dodecyl sulphate
SEM	Scanning Electronic Microscopy
SLS	Static Light Scattering
STED	Stimulated emission depletion
TFA	Trifluoroacetic acid
TSB	Tryptic Soy Broth
VRE	Vancomycin-resistant enterococci
YM	Yeast Mold broth

Abstract

Developing antibiotic agents against multidrug resistance bacteria is considered as an urgent and important healthcare challenge. Many cationic antimicrobial peptides (AMPs) or polymers have been developed to overcome resistance, but it is difficult to balance the mammalian cell compatibility and bactericidal efficacy because most cationic AMPs or polymers are based on cationic and hydrophobic components which also interrupt mammalian cell membrane. In this thesis, based on natural chitosan, the cationic peptidopolysaccharide (CSM5-K5) and polysaccharide (2,6-DAC) without hydrophobic components were synthesized with excellent antimicrobial efficacy and mammalian cell compatibility.

The short peptidopolysaccharide chitosan-graft-oligolysine (CSM5-K5) was synthesized with excellent antimicrobial activity measured by MIC values ranging from 16 to 64 μg/mL against broad spectrum of Gram-positive and Gram-negative bacteria including Methicillin-resistant *Staphylococcus aureus* (MRSA), *Escherichia coli*, *Pseudomonas aeruginosa* and *Salmonella*. CSM5-K5 also have excellent *in vitro* compatibility towards mammalian cells. The *in vivo* tests demonstrated that CSM5-K5 can reduce the load of Methicillin-resistant *Staphylococcus aureus* (MRSA) by 3.3$\log_{10}$ orders in a murine wound model. The antimicrobial mechanism of cationic peptidopolysaccharide was also studied and compared with linear cationic polylysine (K100).

Further, an antimicrobial cationic polysaccharide diamino chitosan (2,6-DAC) was synthesized mimic the cationic peptidopolysaccharide (CSM5-K5). The 2,6-DAC also shows excellent and broad intrinsic antimicrobial efficacy against *Staphylococcus aureus, Listeria, E. coli, Pseudomonas aeruginosa* and *A. baumannii* (MIC from 8-32 μg/mL) and excellent compatibility towards mammalian cells. Moreover, the 2,6-DAC shows synergism with various antibiotics including protein synthesis inhibitor (Tobramycin), DNA gyrase inhibitor (Novobiocin) and β-lactamase inhibitor (Tazobactam). The *in vivo* study shows 2,6-DAC combined with antibiotics can achieve $2\log_{10}$ orders inhibition of *A. baumannii* in murine intraperitoneal infection model and lung infection model.

Even though sterilization techniques are developing very fast, infections associated with medical implants/devices cannot be totally eradicated. To further reduce the possible bacterial infection caused by contamination on surface of medical device such as catheter, a novel coating strategy of catheter (H(N)-b-S) was developed with excellent and broad spectrum antibiofilm efficacy. The modified catheter can inhibit $>4\log_{10}$ orders of bacterial contamination in both *in vivo* and in *vitro* studies for 24 hrs against all pathogens tested (*Enterococcus, S. aureus, K. pneumonia, A. baumannii, P. aeruginosa, E. coli,* and *Candida*). The modified catheter also has good compatibility with blood immune cells and mammalian cells. The potential ability for large scale manufacture of such coated catheter was proved by coating of 30cm long commercially available polyurethane catheter successfully and achieving $3\log_{10}$ inhibition of *P.*

aeruginosa and *S. aureus* biofilm formation for 30 days under intraluminal flow test.

The findings reported in this thesis provide a package of solutions to prevent and treat bacteria/fungus infections.

Chapter 1. Introduction

Overcoming antibiotic resistance in bacteria is a critical challenge in healthcare. Antibiotics generally work by inhibition of cell wall synthesis and protein synthesis(Neu, 1973). The fundamental mechanisms of antimicrobial resistance are degradation of antibiotic, alteration of targeting protein of antibiotic, and changing membrane efflux pumps effusing the antibiotic(Dever LA, 1991). The root cause of antimicrobial resistance mechanisms arises from gene expression and mutation(Nikaido, 2009). Bacteria can still evolve antimicrobial resistance even if new antibiotics are consistently invented. Therefore, it is urgent to explore other bactericidal mechanisms, to which bacteria may evolve resistance less easily. Perturbation of bacteria cytoplasmic membrane is a newer bactericidal mechanism exerted by antimicrobial peptides (AMPs)(H.-G. S. Robert E W Hancock, 2006) and their analogues. Whilst more than about 2000 antimicrobial peptides have been reported, their low biocompatibility is a general problem(David Andreu, 1998). Most AMPs have cationic amino acids for electrostatically binding to anionic bacterial cell surfaces but also hydrophobic amino acids for insertion of the peptides into the bacterial lipids. However, charge and hydrophobicity are non-selective so there is great difficulty in finding peptide sequences with good bactericidal activity but without hemolysis.

To improve the selectivity of synthesized biopolymers against pathogen over mammalian cells, diverse designs of cationic peptide or peptide analogues

have been explored. Blocked, grafted or star-shaped polymers combining cationic charge and other components for targeting bacteria to improve the selectivity have been reported. In recent research, glucosamine is reported to have broad binding affinity with peptidoglycan hydrolase found in various bacteria cell wall(Audrey Beaussart, 2013). Various antimicrobial co-polymers functionalized with glucosamine oligomer are also reported to have good biocompatibility as well as antimicrobial activity(Peng Li, 2012). In our previous work(Peng Li, 2012), the peptidoglycan-mimic cationic chitosan(CS)-polylysine is reported to have excellent antimicrobial activity and hemocompatibility. Chitosan is a poly(glucosamine) and resembles the composition of bacterial cell wall. However, the mechanism by which CS-*graft*-polylysine interacts with and kills bacteria has not yet been reported.

In this thesis, I firstly studied the bactericidal killing mechanism of chitosan-graft-oligolysine (hereafter denoted as CSM5-K5) via various solution and biophysical techniques. CSM5-K5 is synthesized via the N-Carboxyanhydride (NCA) Ring-Opening Polymerization (ROP) of lysine initiated from a chitosan macroinitiator, followed by acidic hydrolysis. The excellent antimicrobial activities against various pathogenic bacteria such as MRSA, ORSA and *E. coli* 958 are shown in *in vitro* tests. In a murine MRSA-infected wound model, CSM5-K5 at a dose of about 2.5mg/kg reduces bacterial load by 3.3 log. We use light scattering, TEM, circular dichroism and computer simulation to show that CSM5-K5 aggregates into nano-sized particles of around 37 nm hydrodynamic radius (R_h). Further, these particles are shown by pH-

potentiometric titrations to be proton sponges. Membrane assays (ATP leakage, DISC35 and NPN) show the nanoparticles disrupt bacterial membrane better than the linear polycationic peptide polylysine K100. Cryo-TEM is also applied to study the effect on the cell wall and membrane. Aggregation of CSM5-K5 as well as binding of CSM5-K5 to cell membrane are simulated by molecular dynamics (MD) simulation. With all various techniques, we attempted to understand how the self-assembles of CSM5-K5 is critical for antibacterial activity.

Further, a 2,6 Diamino chitosan (2,6-DAC) is synthesized to mimic the cationic short peptidopolysaccharide (CSM5-K5), with simplified synthesis steps and antimicrobial efficacy comparable to CSM5-K5. The 2,6-DAC is then combined with commercially available antibiotics, and the synergy between cationic polysaccharide and antibiotics is studied. The cationic polysaccharide is found to synergize *in vitro* with various classes of antibiotics such as DNA gyrase inhibitor (Amikacin and Tobramycin), protein synthesis inhibitor (Novobiocin) and β-lactamase inhibitor (Tazobactam) against Gram-Negative bacteria AB-1, with combined minimum inhibitory concentration (MIC) less than 1μg/mL. Synergy is also present in *in vivo* models of intraperitoneal and lung infection with AB-1. The combination of 2,6-DAC with the antibiotic Novobiocin reduces AB-1 load by $>2\log_{10}$ in intraperitoneal fluid and different organs (kidney, lung, spleen, liver).

Antimicrobial therapies are essential for treatment of established bacterial infections, but it is always preferable to prevent infection. An important cause of

bacterial infections is the contamination of the surfaces of medical devices. Healthcare associated infections (HAIs) including central line-associated bloodstream infection (CLABSI) and catheter-associated urinary tract infection (CAUTI) are dangerous and costly to treat. Therefore, it is also important to develop a device surface coating which can prevent bacteria attachment. In this thesis, I took the catheter as a model medical device with a complicated surface and successfully developed a number of coating strategies which reduced bacteria adhesion on the surface by more than $4\log_{10}$ orders of magnitude.

A novel surface-initiated ozone-RAFT polymerization chemistry is developed and applied in a catheter coating procedure, which makes a surface-initiated block copolymer, combining the two functionalities of anti-fouling and antibacterial nitric oxide release. The antifouling layer and nitric oxide release layer work effectively together each other to produce more than 4 $\log_{10}$ inhibition of bacterial attachment in short-term (24hrs) and 3 $\log_{10}$ inhibition in long term (30 days) *in vitro* tests. The efficacy is also proved in *in vivo* studies, with >4 $\log_{10}$ inhibition of bacteria attachment when the catheter is tested in subcutaneous and urinary tract implantation.

In conclusion, this work develops several new potential antibacterial therapies. The antimicrobial mechanism of cationic nanoparticles based on the peptidopolysaccharide CSM5-K5is studied. Further, a new cationic polysaccharide 2,6-DAC is synthesized and found to synergize with multiple classes of antibiotics. For prevention of infection in medical devices, a novel and

highly effective antibiofilm/antibacterial surface coating technique is developed. The techniques and methods developed in this research may be useful in clinical therapy and can be applied in medical device modifications to prevent infection.

Chapter 2. Literature Review

2.1 Urgency of the need for novel antimicrobial therapy

'It is the end of the road for antibiotics unless we act urgently,' (Steele, 2016)as urged by Centers for Disease Control and Prevention, USA after report in 2016 of the first case bacteria with resistance to all antibiotics. Resistance to one or more antibiotics is now widespread in bacterial pathogens. For example, the ESKAPE pathogens *Enterococcus faecium, Staphylococcus aureus, Klebsiella pneumoniae, Acinetobacter baumannii, Pseudomonas aeruginosa, and Enterobacter* have developed resistance to antibiotics and are responsible to majority of nosocomial infections(Sirijan Santajit & Indrawattana, 2016). Therefore, development of new agents to which bacteria are not yet resistant a critical challenge. The most common mechanisms of antibiotics action on bacteria cells involve inhibition of cell wall synthesis and protein synthesis(Neu, 1973). The fundamental mechanisms of antimicrobial resistance are A) degradation of antibiotic, B) alteration of protein targeted by the antibiotic, and C) changing membrane permeability and antibiotic efflusing(Dever LA, 1991; Piddock, 2006). In antibiotics research, thousands of molecules are screened to overcome the above-mentioned mechanisms of antimicrobial resistance. However, the root of antimicrobial resistance mechanisms arises from gene expression and mutation(Nikaido, 2009). Bacteria can still evolve antimicrobial resistance even the new antibiotics are consistently invented. Therefore, it is necessary to explore alternative bactericidal mechanisms, to which bacteria will

not evolve resistance easily. Disruption of bacteria cytoplasmic membrane is a novel bactericidal mechanism of antimicrobial peptides (AMPs)(Berthony Deslouches et al., 2015; H.-G. S. Robert E W Hancock, 2006) and their analogues(Emilie A. Porter, Bernard Weisblum, & Gellman, 2002). The membrane targeting and disruption mechanism is thought to be more difficult for bacteria to develop resistance to.(H.-G. S. Robert E W Hancock, 2006) However, even though the antimicrobial polymers and peptides have good antimicrobial activities, they tend to have poor biocompatibility, which is problematic for therapy(David Andreu, 1998; Yuchong Yang, Zhengguo Cai, Zehuan Huang, Xiaoyan Tang, & Zhang, 2018).

2.2 Structure of bacteria

To improve the selectivity of therapy against pathogens over mammalian cells, the structure difference between mammalian cell and bacteria cell should be studied first. There are many differences in structure of bacteria cells and mammalian cells, and the most crucial two features are the absence of cell wall structure in mammalian cells and the negatively charged cytoplasmic membrane of bacterial cells(Nermina Malanovic, 2015).

The bacteria cell wall is a potential selective target for antimicrobial therapies. For example, teichoic acid anchored in cell wall is reported as a target for various antibiotics and antimicrobial therapies(Lincoln W Pasquina, John P Santa Maria, & Walker, 2013). Another major component in cell wall is the

peptidoglycan (PG), which is a polysaccharide of N-acetyl-glucosamine(Richard Wheeler, 2015), and N-acetyl-muramic acid conjugated with species-specific short peptides(KH, 1972). The cell wall in Gram-Negative bacteria consists of single layer of PG with thickness of 3-6nm, whereas in Gram-Positive bacteria, the thickness is 10-20nm with multiple layers of PG(Alexander J. F. Egan, Jacob Biboy, Inge van't Veer, Eefjan Breukink, & Waldemar Vollmer, 2015). The peptidoglycan(Koch, 2003; Michael F. Mesleh et al., 2015) and enzymes(Jun Cao et al., 2017) found in cell wall can be used as target. In recent research, peptidoglycan hydrolase found in bacterial cell wall(Heijenoort, 2011) can be used target for antibiotic binding.

In their review paper, Alexander *et al.* (Alexander J. F. Egan & Vollmer, 2013) gives a good summary of different enzymes involved in metabolism of peptidoglycan. Taking *E coli* as an example, enzymes from two procedures, peptidoglycan synthesis and hydrolysis, during the metabolism of bacteria are utilized for bacteria targeting: Peptidoglycan synthase and hydrolase are secreted and targeted towards different bonds in peptidoglycan, such as the peptide-sugar linker, amide bond between specific amino acid, as well as the different types of linkers between monosaccharides. Further, peptidoglycan synthase and hydrolase can form cytoplasm membrane-bound multi-enzyme complexes, which are regulated from cytoskeletal proteins inside the cell and interact with membrane bound molecules during cell division and growth(Errington, 2003). Peptidoglycan synthases include glycosyltransferase (GTase) and DD-transpeptidase (TPase). Peptide cross-links are formed by DD-transpeptidase

(TPase) reactions catalyzed by penicillin-binding proteins (PBPs), forming 4–3 cross-links.(Alexander J. F. Egan et al., 2015) Peptidoglycan hydrolases are a class of enzymes which can separate bacteria cell wall during cell division, modify the amide linkage(Emilisa Frirdich et al., 2012) (Sycuro, 2012) (Romeis T, 1994) on the peptide portion or the sugar linkage(Romeis, 1993) of newly synthesized peptidoglycan or act as a host defense tool(Waldemar Vollmer, 2008). These enzymes are found in periplasm and cell membrane for modification of cell wall(Heidrich, 2001)-(Frédéric Kerff et al., 2010).

Bacteria have negatively charged cytoplasmic membrane(Nermina Malanovic, 2015) (Table 2.1), which is a lipid bilayer with thickness less than 10 nm(Shu J. Lam et al., 2016). Gram-Negative bacteria have an additional outer membrane outside the cell wall, containing no glycerophospholipids, but highly ordered, quasi-crystalline Lipopolysaccharides (LPS)(Vaara, 1992). The outer membrane acts as a further barrier which is impermeable to large constituents such as polysaccharides and proteins(Beveridge, 1999). The thickness of outer membrane can be 7.5~10 nm in thickness(https://www.csun.edu/~hcbio027/biotechnology/lec4a/gram.html) , making a barrier of certain antibiotics such as vancomycin and polymyxins and novobiocin to reach bacteria(Miller, 2016).

Among the enzymes involve in bacteria cell wall synthesis and bacteria division, most of them located in the periplasmic region between cell wall and cell membrane, some enzymes anchor on the cytoplasmic membrane, and

cytoplasm membrane is important for transport of cell wall synthesis constituents(Wael Elhenawy, 2016). Therefore, bacterial cytoplasm membrane is important for cell wall synthesis and cell division. The disruption of cytoplasmic membrane will disrupt cell wall metabolism and therefore kill bacteria.

Table 2.1 Lipid contents found in cytoplasmic membrane of various kind of cells.(Nermina Malanovic, 2015)

	Gram-Negative		Gram-Positive		Fungi	Human	
	E. coli	*P. aeruginosa*	*S. aureus*	*B. subtilis*	*C. albicans*	RBC	Fibroblasts
PG	25	21	57	70			
LPG			38				
PE	75	60		12	26	27.5	31.8
LPE							
CL		11	5	4			
PS					21	14.8	5.9
PI					8	0.6	2.5
PC					15.5	29.2	43.7
LPC					5.5	1	
SP						26.2	13.8
PA					16.7		2.4
ERG/PL					0.66	0.8	0.16

CL, cardiolipin; PG, phosphatidylglycerol; ERG, ergosterol; LPC, Lysylphosphatidylcholine; LPG, lysylphosphatidylglycerol; LPE, lysylphosphatidylethanolamine; PA, phosphatidic acid; PC, phosphatidylcholine; PE, phosphatidylethanolamine; PC, phosphatidylcholine; PS, phosphatidylserine; PI, phosphatidylinositole; SP, sphingolipid.

As presented in Table 2.1, the anionic charged phosphatidylglycerol is present in both Gram-Negative and Gram-Positive bacteria plasma membrane but not in human plasma membrane, which contains zwitterionic lipids. Therefore, it is possible to utilize the anionic cytoplasmic membrane as a target for cationic antimicrobial polymers. Cytoplasmic membrane disruption is caused by electrostatic attraction of cationic charge and insertion of the hydrophobic part of the polymer causing damage to cytoplasmic membrane, inducing the leakage

of cytoplasm components (K^+, Na^+, RNA), and/or interruption of electron transport leading to death of bacteria.

2.3 Cationic antimicrobial polymer

2.3.1 Design of cationic polymer with balanced antimicrobial efficacy and biocompatibility

As previously noted, the anionic bacterial membrane can be used for targeted antimicrobial therapy, which has motivated study of cationic polymer agents for disruption of bacterial cytoplasmic membrane. The balanced cationic charge and hydrophobicity combination are reported: the cationic charge targets anionic cytoplasmic membrane, and the hydrophobic part will insert and disrupt the membrane(Yuchong Yang et al., 2018). King *et al.*(King et al., 2014) synthesized a series of grafted-copolymers consisting hydrophobic quaternary ammonium, grafted on hydrophobic poly-oxetanes main chains with low molecular weight (Mn of 4KDa) and found that with 50% grafting of alkyl C8 quaternary ammonium have optimized antimicrobial with minimum inhibitory concentration (MIC) against *E coli* as low as 4 μg/mL, and a therapeutic selectivity index (50% hemolytic concentration on RBC against MIC of *E. coil*) is 65. Punia *et al.*(Punia, Mancuso, Banerjee, & Yang, 2015) also synthesized grafted copolymer PM6-70-PEG300 with acrylic backbone, hexamethylene amine (30% grafting ratio) and PEG side chains (70% grafting ratio) and found very high selectivity for bacteria over red blood cells, with MIC against *E. coli* as 16 μg/mL and therapeutic selectivity index greater than 113. Other than the hydrophobic alkyl tail disruption of cell membrane, the aromatic heterocyclic

amines are also exhibit antimicrobial efficacy when quaternized. Rube *et al*.(Tejero， et al., 2015) reported polymethacrylate grafted with aromatic thiazole and bisheterocyclic thiazole-triazole derivatives (P(AN-*co*-MTA4)) as novel class of antimicrobial copolymer showing excellent antimicrobial function (MIC<10μg/mL against *P. aeruginosa, S. aureus* and *C. parapsilosis*) with low hemolysis (HC_{50}>5000μg/mL). Quaternized aromatic heterocyclic amines (triazole and thiazole) have better antimicrobial efficacy and biocompatibility compared with alkyl tails, indicating by therapeutic selectivity greater than 500.

Further the location of cationic charge on the polymer is also important(Jiangna Guo et al., 2018): polymers with cationic charges located in the main-chain or backbone of the polymer (Main-chain Polymers, Figure 2.1) are more effective (MIC of M-P[Im][Br] against *E. coli* is 26 μg/mL) than polymers with cationic charges located in the side-chains (Side-chain Polymers) (MIC of S-P[Im][Cl] against *E. coli* is 235 μg/mL) and definitely the main-chain charged polymers have better antimicrobial efficacy than the small molecule cationic compounds. This is due to the alternating arrangement of hydrophilic cationic charge and hydrophobic carbon chain which has a better accessibility to negatively charged bacteria surface, and better insertion of hydrophobic segment into cytoplasm membrane due to higher concentrated charge density(Jiangna Guo et al., 2018). In agreement with Rube, the aromatic imidazolium salt M-P[Im][Br] gives better antimicrobial efficacy compared with linear M-P[Qa][Br] or cyclic alkyl chains M-P[DABCO][Br] (Figure 2.1). The main chain cationic charged polymer also has better biocompatibility in terms of lower hemolysis.

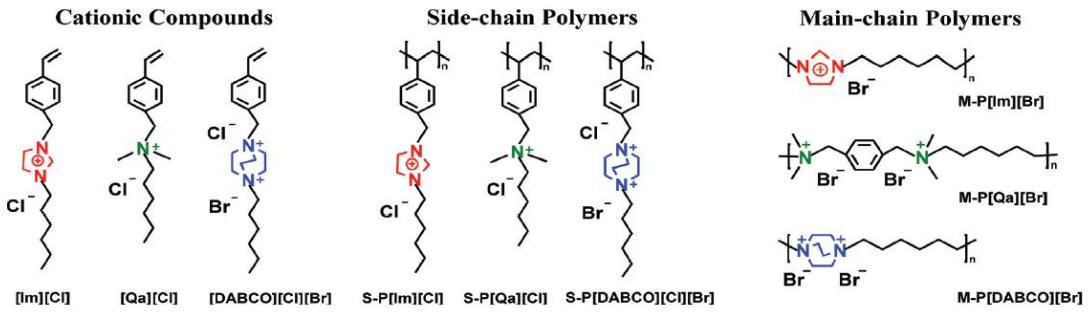

Figure 2.1 illustration of location of cationic charge in polymer(Jiangna Guo et al., 2018)

Some cationic charged (co)polymers can also form aggregates or particles which significantly affect the antimicrobial efficacy as well as biocompatibility. The colloidal behavior of cationic polymer aggregates can be tuned to shield the quaternary ammonium charge to make it less toxic to mammalian cells. In their paper Xinyuan Wan *et al.* designed micelles with poly-quaternary ammonium shielded by hydrophilic PEG(Xinyuan Wan, 2015). They optimized the quaternary ammonium with various long chain carbon (C=4,8,12) and mixed with hydrophilic PEG polymer to form a micelle structure. The positive charge on ammonium cation was shielded, and the cytotoxicity was reduced. Structures such as micelle(Chengcheng Zhou et al., 2016), core shell(Yongqiang Gao et al., 2018) or star shaped conformations with antimicrobial functions have been reported, which can either concentrate the cationic charge, or shield the toxic hydrophobic groups to reduce the toxicity towards mammalian cells.

These reported copolymers demonstrate some essential principles for design of synthetic antimicrobial polymers:

1) the cationic charge can selectively bind with anionic bacteria membrane;
2) the hydrophobic chain can insert and therefore disrupt the membrane; the aromatic tertiary amine is better choice in this case; and
3) combination of hydrophilic PEG or polysaccharide chain with the hydrophobic part can enhance and tune biocompatibility. Additionally, PEG or polysaccharide also have hydrogen bonding to bacteria cell wall, which might enhance the selectivity.

Recently, there are several synthetic cationic copolymers with balanced excellent antimicrobial activity and biocompatibility reported by using controlled polymerization techniques, such as Atomic Transfer Radical Polymerization (ATRP)(Yuji Pu et al., 2017) or Reversible Addition-Fragmentation Transfer (RAFT) polymerizations(Edgar HH Wong et al., 2016) (Figure 2.2). Copolymers with more complicated structures were synthesized and showed balanced antimicrobial efficacy and biocompatibility(Edgar HH Wong et al., 2016; Yuji Pu et al., 2017).

(A)

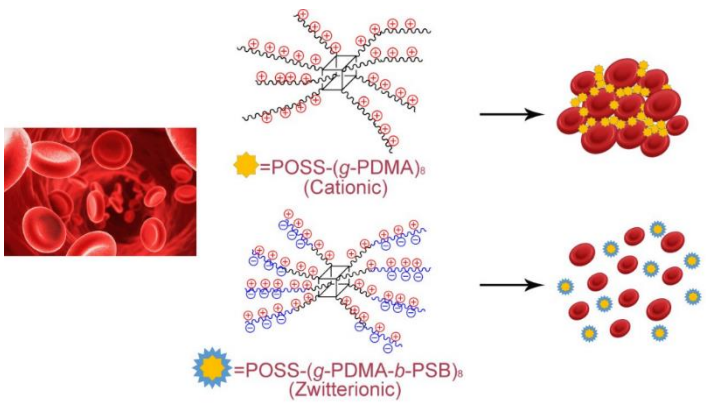

(B)

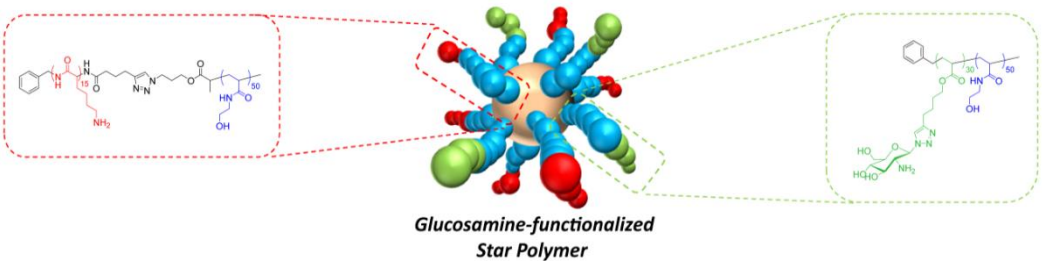

Figure 2.2 Illustration of cationic antimicrobial polymer with complicated structure synthesized by controlled polymerization techniques. (A) Branched cationic polymer synthesized by ATRP(Yuji Pu et al., 2017). (B) Star-shape cationic polymer synthesized by RAFT(Edgar HH Wong et al., 2016).

2.3.2 Cationic antimicrobial peptides and polysaccharides

Synthetic cationic polymers with carbon backbone such as polymethacrylate are usually non-biodegradable, which is hard for the human body to metabolize(Ana Maria Carmona-Ribeiro, 2013). Therefore, natural antimicrobial peptide and their modifications have attracted research attention, as they can be metabolized by proteolytic enzymes in the human body. In last one-two decades, more than 2000 AMPs(Nicole J. Afacan, 2012) have been reported. In spite of the large number and diversity of molecules that have been discovered, only a few AMPs have gone into clinical trials; amongst these are pexiganan, omiganan, and OP-145(Fox, 2013). Other AMPs in the pipeline against *P. aeruginosa* and *S. aureus* include peptides based on protegrin (Srinivas et al., 2010) and plectasin(Mygind et al., 2005) . The bactericidal mechanisms of membrane disruption by antimicrobial peptides are also well studied , and the following models are proposed(Brogden, 2005): A) barrel stave model; B) toroidal model and C) carpet model (Figure 2.3).

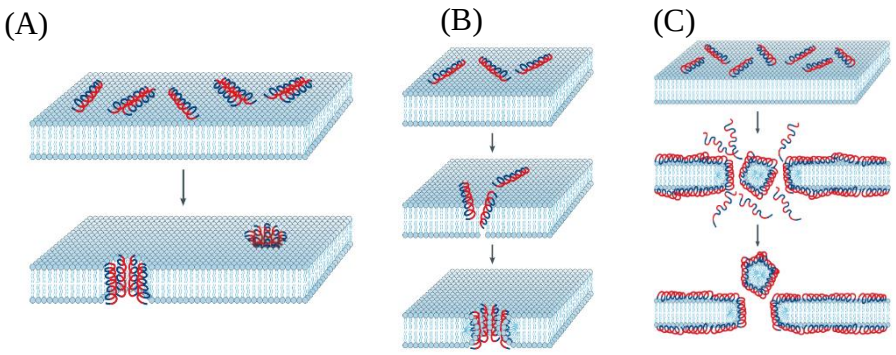

Figure 2.3 Illustration of membrane disruption mechanisms of antimicrobial peptide (AMP) (A) barrel stave model; (B) Toroidal model and (C) carpet model

The antimicrobial peptides that act via barrel stave and toroidal models forms around 2nm diameter pores on cytoplasm membrane; on the other hand, the carpet model involves detergent like-action to remove parts of the bilayer. Antimicrobial peptides that act via carpet model can kill Gram-Negative bacteria better due to total removal of outer cytoplasm membrane found in Gram-Negative bacteria and much larger pores formed on membrane. The limitation of the natural or synthesized antimicrobial peptide is they are usually hemolytic(Helio S. Sader, 2004; Kevin J. Hallock, 2003), for example omiganan and melittin. The toxicity is believed to be due to hydrophobic amino acids in the peptide chain, which also interact and disturb the zwitterionic lipids in human cytoplasmic membrane(Robert E W Hancock & Chapple, 1999; Yuxin Chen et al., 2007).

Table 2.2a summarizes the efficacy and biocompatibility of several reported cationic membrane interruption antimicrobial peptides. Therefore, it is important to redesign the amino acid sequence of antimicrobial peptides in order to enhance the selectivity. Inspired by the natural AMPs, it is possible to

synthesize similar biopolymers as analogues. Moreover, with advances in polymer synthesis techniques, the structure of synthetic polymers can be finely controlled and tuned to give a balance between antimicrobial activity and biocompatibility.

Other than the membrane interruption mechanism, the antimicrobial peptide can also be internalized into intracellular spaces with different modes of intracellular killing mechanisms (Table 2.2b). In following discussions, only membrane interrupting AMP and its analogues are focused.

Table 2.2a Summary of reported MIC and cytotoxicity and mechanism of promising membrane interrupting AMPs

Antimicrobial peptide	MIC (μg/mL)			Hemolysis/Cytotoxicity
	E. coli	*P. aeruginosa*	*S. aureus*	
omiganan(Helio S. Sader, 2004)	32	64-256	32	100μg/mL (HC10)(Hyung-Sik Won, 2011)
pexiganan(Lindsey M. Gottler, 2009)	16	16	64	40μg/mL (HC10)(Inna S Radzishevsky1, 2007)
plectasin(Per H. Mygind, 2005)	-	-	32	>512μg/mL (HC10)(Xintao Cao, 2015)
melittin	32	64	0	16 μg/mL (HC50)

Table 2.2b Summary of reported modes of intracellular killing AMPs

Modes of intracellular killing	Examples
Flocculation of intracellular contents	Anionic peptides

Alters cytoplasmic membrane septum formation	PR-39, PR-26, indolicidin and microcin
Inhibits cell-wall synthesis	Mersacidin
Binds nucleic acids	Buforin II and tachyplesin
Inhibits nucleic-acid synthesis	Pleurocidin, dermaseptin, PR-39, HNP-1, indolicidin
Inhibits protein synthesis	Pleurocidin, dermaseptin, PR-39, HNP-1, indolicidin
Inhibits enzymatic activity	Histatins, pyrrhocoricin, drosocin and apidaecin

N-Carboxyanhydride (NCA) Ring-Opening Polymerization (ROP) technique (Figure 2.4) is a versatile polymerization technique for synthesis of poly-peptide in large scale(David Huesmann et al., 2014). The NCA polymerization provides flexibility in design of antimicrobial peptides.

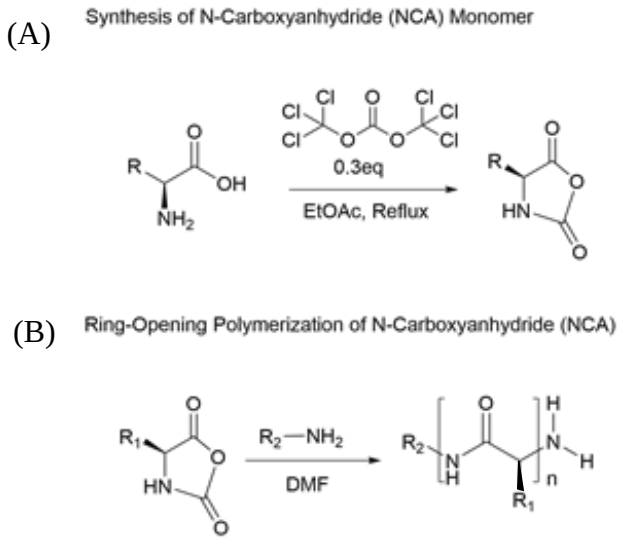

Figure 2.4 (A) Synthesis scheme of N-carboxyanhydride (NCA) monomer (B) Ring-Opening Polymerization of NCA monomer initiated by amine.

Chuncai Zhou et al,(Chuncai Zhou et al., 2010) have reported an AMP mimic simple linear cationic polypeptide which shows high potency and broad-spectrum antimicrobial activities. The antimicrobial polypeptide consists of both cationic lysine amino acid for bacterial targeting and hydrophobic amino acid for membrane disruption. However, even though the antimicrobial efficacy is

excellent with MIC against bacteria as low as 31μg/mL, the biocompatibility is very low, with HC50 as low as 16 μg/mL. More complex design of copolymers may be needed in order to achieve balanced antimicrobial activity and biocompatibility. Gerg Qiao's group has reported a cationic star-shape polypeptide (SNAPP) with excellent *in vivo* antimicrobial efficacy; the peptide is still hemolytic even though the therapeutic index is as high as 102~171 (measured by IC_{50}/MBC_{50})(Shu J. Lam et al., 2016). The star-shape peptide provides a novel cationic antimicrobial mechanism: the star-shape peptide with 7.7nm diameter acts as a proton sponge which destabilizes the cytoplasmic membrane by domain formation with the anionic phospholipids causing holes on cytoplasmic and outer membranes larger than the 2nm holes formed via toroidal and barrel stave models. The star-shape structure also concentrates the charge interrupting the ion exchange by making larger pores, disrupting ion segregation and collapsing the transmembrane potential. It suggests that aggregation of cationic peptide or their aggregations with larger diameter enhances antimicrobial efficacy (Figure 2.5).

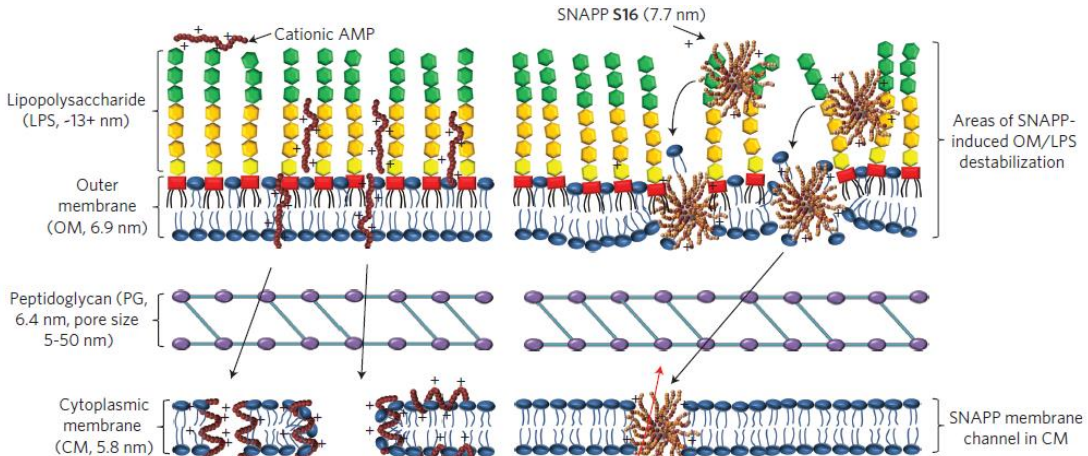

Figure 2.5 Antimicrobial mechanism of star-shape cationic peptide (SNAPP) compared with linear cationic peptide.

Dicky *et al.* (Dicky Pranantyo, Li Qun Xu, Zheng Hou, En-Tang Kang, & Chan-Park, 2017) reported a four-armed star shape polymer combining cationic poly-lysine and poly mannose which improved the biocompatibility measured by HC_{50} >8192 μg/mL, and kept the antimicrobial efficacy of poly cationic peptide. However, even though the polymer consists of a biodegradable peptide, the poly mannose chain of the star polymer is synthesized by ATRP polymerization. *i.e.* the backbone is still non-biodegradable. Nevertheless, the design of the polymer illustrates the usefulness of sugar units for improvement of the biocompatibility of antimicrobial polymers.

On the other hand, there are literature reports combining natural polysaccharide with synthetic polycationic polymer. Li *et al.*(Jianghua Li et al., 2018) reported block copolymer dextran-*block*-poly($AMPTMA_{95}$-r-BMA_5), which combine the natural hydrophilic poly-saccharide dextran with synthetic cationic antimicrobial polymer with repeat quaternary ammonium group. The presence of hydrophilic polysaccharide can help to tune the amphiphilicity the copolymer; therefore, the copolymer will assemble into nanoparticles with

desired morphology and functional groups to remove formed biofilms. Other than hydrophilicity adjustment, the sugar units can enhance bacteria targeting and binding. For example, branched poly-mannose is reported to target *E. coli* UTI89 by Surendra *et al.*(Surendra H. Mahadevegowda et al., 2018).

Cationic polysaccharides have also been reported as antimicrobial agents. Cationic derivatives of starch(Shrinivas Venkataraman et al., 2019) and alginate(Salah M. Tawfik & Hassan H. Hefni, 2016) are reported to have antimicrobial efficacy. Bacterial membrane disruption is still the major antimicrobial mechanism, similar to cationic polymers and peptides; however, the cationic polysaccharide are usually hydrophilic, which results in better biocompatibility, and are easily applied as antimicrobial hydrogels(Shrinivas Venkataraman et al., 2019) or in medical devices such as wound dressings(B.S.Anisha, RajaBiswas, K.P.Chennazhi, & R.Jayakumar, 2013). Cationic polysaccharides are bio-degradable, unlike common cationic polymers. Furthermore, the hydrogen bonding between sugar units within a cationic polysaccharide make the formation of aggregates possible; nanoparticles can be assembled from cationic polysaccharide for improved antimicrobial efficacy(Frans Ricardo Tamara, Chi Lin, Fwu-Long Mi, & Yi-Cheng Ho, 2018). Yammaura *et al.* modified cyclodextrin by grafting of cationic hydrophobic aliphatic or cyclohexyl rings and theses appear to be more bactericidal and less hemolytic than variants bearing aromatic or linear alkyl substitutions (Yamamura et al., 2014). The cyclic hydrophobic groups have smaller sizes than the aromatic amino hydrophobic groups and so are less hemolytic. However, the main

limitation for utilizing cationic polysaccharides as antimicrobial agents might be the difficulties in modification of sugar backbone, as normally polysaccharides can only dissolve in water, making chemical modifications difficult.

Chitosan is a cationic charged poly-saccharide derivative of chitin which is the main component in many natural materials. Chitosan is reported to have some of antimicrobial activity(Entsar I. Rabea, Mohamed E.-T. Badawy, Christian V. Stevens, Guy Smagghe, & Walter Steurbaut, 2003; M.S. Benhabiles et al., 2012). Various chemical modifications of chitosan have been reported(Keisuke Kurita, Hiroyuki Ikeda, Manabu Shimojoh, & Jin Yang, 2007; Ögmundur Vidar Rúnarsson, Clemens Malainer, Jukka Holappa, Snorri Th. Sigurdsson, & Már Másson, 2008). A unique property of chitosan is that it has a peptidoglycan-mimic structure due to its glucosamine building blocks; the presence of amino groups is a good platform for modification compared with other polysaccharides that are difficult to modify. Chitosan is a polysaccharide of glucosamine, the precursor building block of bacteria cell wall. Glucosamine is involved in many metabolism pathways(Dirk-Jan Scheffers & Mariana G. Pinho, 2005), including cell wall synthesis and bacteria division; therefore, glucosamine units might be utilized for specific binding towards bacteria. For example, it is reported that chitosan can target the teichoic acid found on bacteria cell wall(Dina Raafat & Sahl, 2009). Chitosan backbone tends to aggregate by hydrogen bond formation(K.Y. Lee, I.C. Kwon, Y.-H. Kim, W.H. Jo, & Jeong, 1998); the aggregated chitosan nanoparticle might function similar to a cationic proton sponge, can be utilized in gene transfection(Isabelle Richard, Marc

Thibault, Gregory De Crescenzo, Michael D. Buschmann, & Lavertu, 2013). Antimicrobial chitosan-based cationic polymers have been reported, such as the pure chitosan(Ming Kong, Xi Guang Chen, Ke Xing, & Park, 2010), quaternary ammonium chitosan(Jarmila Vinová, 2011), chitosan grafted with quaternary pyridinium(Warayuth Sajomsang, 2008) or quaternary phosphonium and sulphonamide groups(R. X. Zhimei Zhong, Song Liu, Lin Wang, Shengbao Cai, Pengcheng Lia, 2008) (Table 2.3). However, the toxicity of such chitosan derivative is still high due to introduction of hydrophobic cationic charge. Recently, chitosan grafted with hydrophilic cationic groups such as low molecular weight chitosan-*graft*-polylysine, has been reported with antimicrobial activities and balanced biocompatibility. In earlier work by Li Peng *et al.*(Peng Li, 2012), a peptidoglycan-mimic cationic copolymer was reported to have excellent antimicrobial activity and biocompatibility. The peptidoglycan mimic cationic co-polymer is synthesized via N-Carboxyanhydride (NCA) Ring-Opening Polymerization (ROP) of lysine initiated by chitosan macroinitiator, followed by acidic hydrolysis, which results in chitosan oligomer grafted with polylysine. By adjusting the polylysine chain length and overall molecular weight, the copolymer is optimized to give excellent antimicrobial activity against both Gram-Positive and Gram-Negative bacteria with good mammalian cell biocompatibility. Membrane disruption is still the antimicrobial mechanism for this antimicrobial copolymer. However, instead of hydrophobic moiety, such cationic copolymer breaks bacteria cytoplasm membrane via an aggregated proton sponge effect similar to SNAPP; it is achieved uniquely by chitosan

backbone hydrogen bonding(Zheng Hou et al., 2017). This unique class of cationic peptidopolysaccharide can also be synthesize by “grafting onto” route, with synthesized cationic polypeptide grafted onto the backbone via click chemistry(Priyanka Sahariah et al., 2015; Yajuan Su et al., 2017). Moreover, this cationic peptidopolysaccharide can be employed for antimicrobial surface modifications via layer-by-layer assembly(Dicky Pranantyo, Li Qun Xu, En-Tang Kang, & Chan-Park, 2018), suggesting a possible application of this cationic antimicrobial polymer.

Recently, polymers grafted with heterocyclic moieties such as triazole, diazole or thiazole are reported to have good antimicrobial activities via introducing hydrogen bond interaction between polymer and cell wall of bacteria (Anchalee, Shirui, Thomas, & Varaporn, 2008; Helio S. Sader, 2004; P. L. Zhimei Zhong, Ronge Xing, Song Liu, 2009; R. X. Zhimei Zhong, Song Liu, Lin Wang, Shengbao Cai, Pengcheng Lia, 2008). Also, the overall acid dissociation constant of the copolymer will be further tuned by introducing heterocyclic moieties. The electrostatic interaction can be tuned to responsive towards mild acidic micro-environment where bacteria survive. Hence, the selectivity of antimicrobial copolymer can be improved if some of the heterocyclic groups are also clicked onto the chitosan backbone with presence of polycations. Table 2.3 summarizes the efficacy of chitosan grafted with different chitosan derivatives including the backbone grafted with heterocyclic amines (CS-N-pyridinium).

Table 2.3 Summary of reported MIC and cytotoxicity of chitosan derivatives

Chitosan derivatives	MIC (μg/mL)			Hemolytic activity/Cytotoxicity
	E. coli	*P. aeruginosa*	*S. aureus*	
CS[$]-sulfate(P. L. Zhimei Zhong, Ronge Xing, Song Liu, 2009)	31.25	31.25	62.49	-
CS-Trimethyl ammonium(Warayuth Sajomsang, 2009)	16-64	-	8-64	10~1000μg/mL (IC_{50})
CS-N-pyridinium/ aryltrimethylammonium(Warayuth Sajomsang, 2008)	64	-	32	-
CS-thiourea(R. X. Zhimei Zhong, Song Liu, Lin Wang, Shengbao Cai, Pengcheng Lia, 2008)	15.62	62.49	62.46	-
Quaternized-CS(Warayuth Sajomsang, 2009)	16-64[*]	-	8-64	-

[$]CS=chitosan [ǂ]PHGH= polyhexamethylene guanidine hydrochloride *Depends on alkyl/aromatic tails used for quaternization(Warayuth Sajomsang, 2009)

2.3.3 Synergy between antibiotics and cationic polysaccharides

As discussed, bacteria have developed strategies to resist antibiotics, and have increasingly made antibiotics ineffective. The change on membrane pump is one of the major resistance mechanism where the bacteria membrane either prevents antibiotic from entering the cytoplasm or the efflux pumps on cytoplasmic membrane export antibiotics(Piddock, 2006). Figure 2.6 summarized the antibiotics which will be exported from bacteria via membrane efflux pumps. Those drugs will lose their antimicrobial efficacy. Antibiotic resistance is particularly problematic in Gram-Negative bacteria, which are

protected by an outer membrane, which is an additional barrier to drug penetration[35], especially by hydrophobic ones.

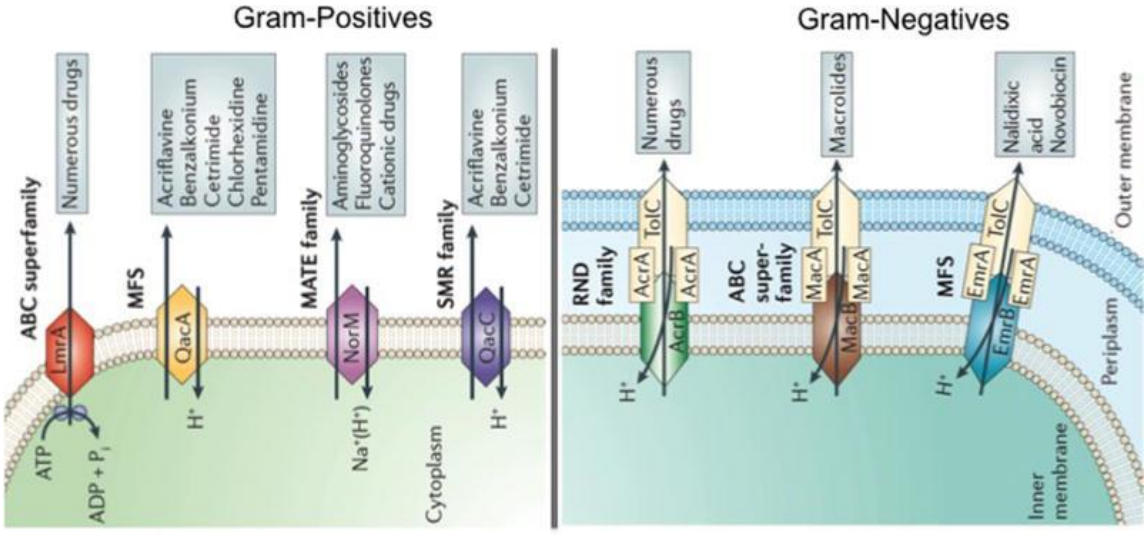

with and disruption of cytoplasm membrane and/or outer membrane of bacteria. By applying an antimicrobial copolymer together with antibiotic, the interaction of antimicrobial polymer with bacteria cytoplasmic membrane and/or outer membrane may make the membrane more permeable to the antibiotic; this could overcome bacterial resistance, re-sensitizing pathogens that have evolved resistance or sensitizing intrinsically resistant species. In other words, some antimicrobial polymers can synergize with antibiotics(Ng，, Xiyu Ke, Ashlynn L. Z. Lee, James L. Hedrick, & Yang, 2013).

The synergy between various cationic polymers and antibiotic is well-studied (Figure 2.7). Outer membrane disruption of Gram-Negative bacteria is one mechanism for synergy between cationic polymers and antibiotics. Taking

polyethyleneimine (PEI) as an example(Hayssam Khalil, Tao Chen, Rene´e Riffon, Rutao Wang, & Zhao Wang, 2008), PEI increases the permeability of the outer membrane of *P. aeruginosa* by formation of clusters with the outer membrane lipids; this improves penetration of hydrophobic antibiotics such as Novobiocin, chloramphenicol *etc.* Jingxiao Tian *et al.* have reported conjugated cationic polymer (CCP) synergy with antibiotics against Gram-Negative *E. coli* and Gram-Positive *B. subtilis* by penetration of both outer membrane and cytoplasmic membrane. However, the synergy is limited to hydrophilic polymyxin B (PLB) and polymyxin E (PLE)(Jingxiao Tian et al., 2017). Victor Ng *et al.* reported that poly-VitE-poly-cationic copolymer synergizes with a wide range of antibiotics such as doxycycline, streptomycin and penicillin; however, the biocompatibility of this polymer, measured by hemolytic activity, is poor(Ng ， et al., 2013). Synergy of cationic antimicrobial peptide (KFFKFFKFF) with antibiotics has also been reported(Martti Vaara & Porro, 1996). But the hydrophobic amino acid Phenylalanine (F) is essential for the synergy and reduces the biocompatibility of the cationic peptide.

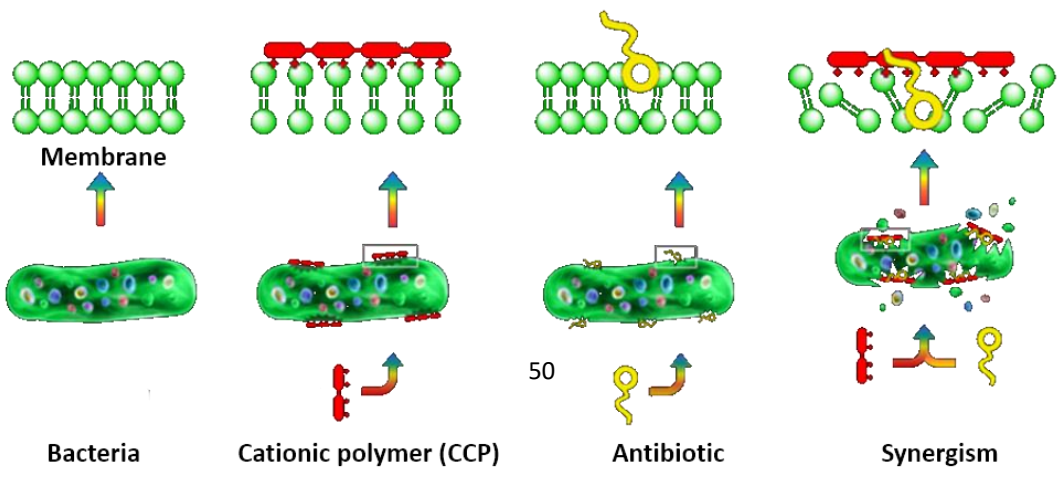

Figure 2.7 illustration of cationic polymer (CCP) synergizes with antibiotics(Jingxiao Tian et al., 2017)

Due to its unique cell wall mimic structure and membrane disruption ability, cationic polysaccharides based on chitosan and its derivatives are good candidates for synergy with antibiotics. The cationic polysaccharide is also hydrophilic and biodegradable, which improves biocompatibility. Chitosan is reported to synergize with a wide range of antibiotics such as gentamicin(Haibo Mu et al., 2014), ceftriaxone, sulfamethoxazole, tetracycline(San Tin, Chu Sing Lim, Meena Kishore Sakharkar, & Sakharkar, 2010) and caffeic acid(Ji-Hoon Kim et al., 2017) against a broad spectrum of Gram-Positive and Gram-Negative bacteria. San Tin *et al.* reported the synergy is affected by the molecular weight of chitosan, and chitosan oligomer shows the best synergy with various antibiotics(San Tin et al., 2010). This is due to the effect of chitosan molecular weight; chitosan oligomer is more soluble than heaver chitosan chains. On the other hand, modification of chitosan can further improve solubility(Shakeela Sayed, Tatiana Millard, & Jardine, 2018).

Further, chitosan backbones tend to self-assemble, providing more versatility for synergy of chitosan and antimicrobial nanoparticles(Zahra Assadia, Giti Emtiazib, & Zarrabia, 2018). Chitosan is also reported to have

synergy with essential oils such as clove bud oil, cinnamon oil and star anise oil against food pathogens such as *Aspergillus oryzae* and *Penicillium digitatum(Ng ， et al., 2013).* The synergy between pure chitosan and antibiotics are recently published, and possible synergies between modified chitosan derivatives or other cationic polysaccharides and antibiotics have not yet been reported.

2.4 Anti-infection surface coatings

2.4.1 Urgency of the need for antibacterial surface modification on medical devices

Nutrients in the body liquid such as protein, saccharide, and salts can attach on catheter surface and assist the formation of biofilm on the catheter surface(Flores-Mireles, Walker, Caparon, & Hultgren, 2015). Biofilm is a matrix formed by biomass (extracellular polymeric substances such as protein and polysaccharides as well as nucleic acids from the bacteria) in which bacteria is embedded and protected(Hans-Curt Flemming et al., 2016). Protein fouling is the first step in formation of biofilm(P. Stoodley, K. Sauer, D. G. Davies, & J.W. Costerton, 2002) (Figure 2.8), followed by contact or infection with bacteria. Bacteria adhere to the surface and develop into a biofilm, which when mature can release bacteria to spread the infection(Zachary K. Zander & Becker, 2018). Compared with planktonic bacteria, bacteria in a biofilm are more resistant to antibiotics, as drugs must penetrate through the hierarchical structure of the biofilm to reach and kill the bacteria(Thien-Fah C Mah & O'Toole, 2001), biofilm bacteria also tend to be less metabolically active than planktonic bacteria and this may contribute to reduced vulnerability to agents that target metabolically active

cells(Philip S Stewart & Costerton, 2001). As a result, the bactericidal efficacy is lowered and higher dosage (10~100 times of the MIC values)(Silvia Schwank, Zarko Rajacic, Werner Zimmerli, & Blaser, 1998) of antibiotics is needed to kill the biofilm bacteria. The antibiotic-resistant strains also generate during the antibiotic treatment process.

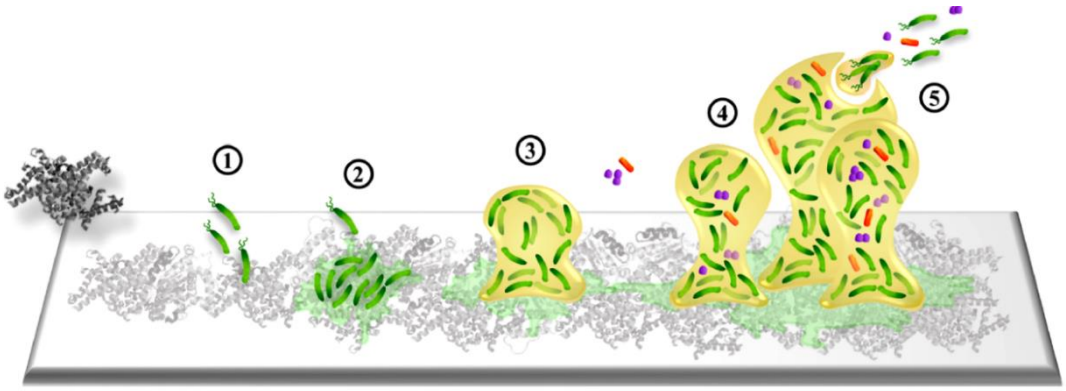

Figure 2.8 Development of biofilm on medical devices surface. After fouling of proteins (black and white), the following step happens (1) contact with bacteria happen, (2) bacteria adhere on surface (3) microcolony formation (4) microcolony maturation (5) Release of more bacteria as planktonic bacteria(Zachary K. Zander & Becker, 2018).

One of the most common applications for antimicrobial polymers is prevention of infections on medical devices. Implanted devices are exposed to pathogens during implantation and usage, and this led to infection. Prevention of infection is much preferable to treatment with antibacterial therapy or even device removal. This is due to the high cost in treatment and lethality of the healthcare associated infections (HAIs). Medical catheters are thin tubes made from medical grade materials serving a broad range of functions. They are routinely employed in in-patient settings for administration of medicines, provision of hydration and nutrition, collection of urine, blood sampling, hemodialysis, peritoneal dialysis and many other surgical procedures. Catheter-

related infections such as central line-associated bloodstream infection (CLABSI) and catheter-associated urinary tract infection (CAUTI) are major HAIs("Catheter-associated Urinary Tract Infections (CAUTI)," 2017; "Infection: Prevention and Control of Healthcare-Associated Infections in Primary and Community Care: Partial Update of NICE Clinical Guideline 2-Long term urinary catheters," 2012). Central line-associated bloodstream infections (CLABSI) are caused by bacterial contamination on catheters set in large veins for hemodialysis, intravenous medicine infusion, blood transfer and blood sampling("Central Venous Catheter," 2007). The cost of treatment of CLABSI is up to $36,000 per case in U.S with the estimation annual occurrence of CLABSI at 30,100(2017) in ICUs and above 60,000 cases(Shelley S. Magill et al., 2014) overall. The global annual occurrence is estimated at 250,000 cases(Yazan Haddadin & Regunath, 2019a). The incidence of CLABSI is higher in non-ICU than in ICU settings(Alexander J. Kallen, Priti R. Patel, & O'Grady, 2010; Crystal H. Son et al., 2012; Jonas Marschall et al., 2014). The rate of CLABSI in other countries (4.1 per 1000 central-line days) is much higher than in U.S(Jun Cao et al., 2017) (0.8 per 1000 central-line days) according to International Nosocomial Infection Control Consortium (INICC). Urinary tract infections (UTI) are among the most common bacterial infections, with 10.5 million cases each year in U.S. and 150 million cases worldwide; 70-80% of complicated UTIs are attributable to indwelling catheters(Ana L. Flores-Mireles, Jennifer N. Walker, Michael Caparon, & Scott J. Hultgren, 2015) as CAUTI. Further, 15% of all community-prescribed antibiotics in the U.S. are dispensed for UTI with total cost exceed

$1.6 billion(FME Wagenlehner & KG Naber) and the cost of treatment is up to $10,197 per case(Christopher S. Hollenbeak & Amber L. Schilling, 2018). Prolonged urinary tract infection can eventually lead to bloodstream infections (BSI) with 15% mortality(Nicolle, 2014b). Moreover, one of the major causes of peritoneal dialysis (PD) associated infection is tunnel infection from catheter use(Akoh, 2012), which is more serious than other infection route. The average rate of occurrence of peritonitis due to dialysis is 1 episode per 2 patient years and mortality due to peritonitis alone is 5%(Salzer, 2018); however, the peritonitis also triggers a cascading infections on peritoneal organs with 17.6% mortality and average cost of treatment is $73,533 per case(Bolin Niu et al., 2018). Repeated peritoneal infection eventually renders peritoneal dialysis ineffective, necessitating hemodialysis (which has its own catheter-associated risks) or kidney transplantation(Andrew M. Rizzi et al., 2018).

In most of the cases of catheter-associated infection, the contamination of the catheter that leads to the infection occurs during insertion of the catheter, through contact with pathogens on the patient's skin. Among the common pathogens in bloodstream infection (BSI), only *Staphylococcus* infection might be caused by blood-stream contamination; other major nosocomial infections with pathogens including *Stenorophomonas, Pseudomonas, Enterococci, Candida* arise by skin contact and contamination during hospitalization(Yazan Haddadin & Regunath, 2019b). Infections associated with central venous catheters usually happen within 7 to 10 days after placement(Yazan Haddadin & Regunath, 2019b) and in this case protein fouling is critical, as it makes the

surface vulnerable to pathogen adhesion and proliferation. The pathogens found in urinary tract infections are *E coli, Enterococci, Klebsiella, Pseudomonas, Enterobacter* and *Candida("Catheter-associated Urinary Tract Infections (CAUTI)," 2017)*. The traditional ways for prevention of bacterial infection related to catheter applications are coating or impregnation of the catheter with antibiotic(Michael Stenger et al., 2016); however, most of these pathogens have strains that are resistant to antibiotics(Nicolle, 2014a). The antibiotic treatment will not reliably prevent infection.

To avoid biofilm formation on catheters, many measures have been adopted in healthcare practice in recent decades(Phillips, 2014), such as shortening the implantation period, sterilization of surgery environment, and flushing the catheter lumen with antibiotic stock solution periodically *etc.*, and these have proved to be effective. However, the problem of drug resistant catheter infections is intractable with current methods and the rates of catheter-associated infection are not decreasing as predicated(Phillips, 2014).

The first approach to making catheters anti-infective was to load them with antibiotics; this shows excellent short-term inhibition of drug-sensitive bacteria but no long-term efficacy(Michael Stenger et al., 2016) . The antibiotics leaching works in individual clinical cases in short term use, but in long term use it fails because the drug leaches out completely, leaving the catheter without an antibacterial mechanism. Across the healthcare system, the antibiotics resistance developed easily in certain pathogens such as *S. aureus*, *Enterococcus* and *E.*

coli(David Roe, Balu Karandikar, Nathan Bonn-Savage, Bruce Gibbins, & Jean-Baptiste Roullet, 2008; T. Goto, Y. Nakame, M. Nishida, & Ohi, 1999); therefore, alternative antibacterial strategies other than antibiotics are urgently needed to control infections on medical devices. Contact-active antimicrobial efficacy and resistance to fouling by proteins are desired for coatings on medical devices to prevent infection and biofilm development during and after implantation of medical devices.

2.4.2 Common design concepts for surface modifications

Permanent surface modification techniques may be broadly divided into "grafting from" and "grafting onto" approaches for attaching surface functionalities. For anti-infection surface modifications, a further important concept is the idea of "bacteria responsive" design. These three approaches are discussed in the following sections.

Grafting-from strategy

"Grafting-from" strategy refers to introduction of initiator sites onto the surface followed by *in situ* polymerization process initiated from the surface. The initiator groups, such as peroxide, azo groups or bromide groups, may be formed on the target surface by a variety of means.

Plasma activation is a commonly used technique for introduction of peroxide initiator groups. Li Peng *et al.* employed this method for surface-initiated polymerization of cationic oligomer Polyhexanide (polyhexamethylene guanide, PHMG)(Zelun Zhi et al., 2017) with superior antibacterial efficacy

(99.9% killing). Further, the plasma treatment will also create hydroxyl groups on surface, making silane chemistry possible for introduction of initiator; however, the efficacy of hydroxyl group introduction is lower(Steve Edmondson, Vicky L. Osborne, & Huck, 2004). However, plasma activation is limited to only simple, relatively flat surfaces.

Other than plasma activation, there are few ways to introduce peroxide groups on polymeric surfaces. Solvent impregnation of peroxide compound or ozone initiated surface polymerization with hydrophilic modification of surface for long catheter was previously reported by Smith Roger(Smith et al., 2012) and Y. Yuan(Youling Yuan et al., 2004); but the stability of such method is low due to non-covalent linkage of the initiator with the substrate material.

Compared with other surface chemistry for introduction of initiator, ozone treatment can achieve much higher surface density of peroxide initiator (Figure 2.9). Keiji Fujimoto *et al.* reported up-to 378/nm^2 peroxide groups producing on polyurethane(Keiji Fujimoto, Yoshihiro Takebayashi, Hiroyuki Inoue, & Ikada, 1993). Surface activation by ozone treatment is much more effective than the alternatives. For example, plasma activation(Chiaki Yoshikawa et al., 2005; Keiji Fujimoto et al., 1993) can introduce 10-15 surface peroxide groups/nm^2. Polymerization initiated by solvent impregnation of the target substrate with peroxide compound results a non-durable coating(Wei Wang, Yang Lu, Jinbing Xie, Hui Zhu, & Cao, 2016). The high-density of peroxide groups introduced by ozone treatment results in a denser and/or more durable polymer brush coating

on surface than is achievable with alternative surface activation chemistries. Ozone being a gas, it also permits introduction of peroxide groups onto complex surfaces that would be difficult to functionalize with alternative methods.

Figure 2.9 Mechanism of peroxide formation induced by ozone(Criegee R, 1975)

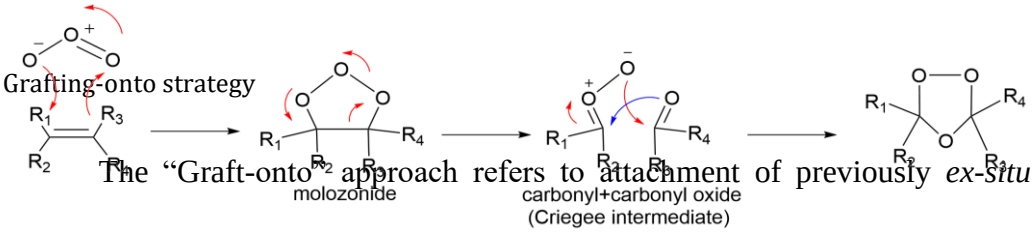

Grafting-onto strategy

The "Graft-onto" approach refers to attachment of previously *ex-situ* synthesized antibacterial polymer onto the surface. As with the "graft-from" approach, it may be necessary to pretreat or functionalize the substrate in order to provide sites for attachment of the antibacterial material.

Polyurethane (PU) can be activated by hexamethylene diisocyanate (HMDI) with further attachment of linear cationic polyethyleneimine (PEI) and shows 90%~99.9% bactericidal efficacy, depending on molecular weight and degree of alkylation of the PEI(Merve Gultekinoglu et al.). Azido-alkyne(Amanda C. Engler, Hyung-il Lee, & Hammond, 2009; Haifeng Gao & Matyjaszewski, 2007) or thiol-ene click(Pornpen Sae-ung et al., 2017), thiol-maleimide(Zhi Xiang Voo et al., 2016) and anhydride groups(Fabíola Costa, Isabel F. Carvalho, Ronald C. Montelaro, P. Gomes, & Martins, 2011) are also commonly used to attach antimicrobial polymers onto surfaces.

Layer-by-Layer approach is one of the most reported method for surface modification. Both natural and synthetic cationic polymers have been used in layer-by-layer approach. Commonly used cationic polymers include polyethyleneimine (PEI)(Fan Fan, Chunyu Zhou, Xu Wang, & Szpunar, 2015), poly (diallyldimethylaminonium chloride) (pDADMAC)(Baowei SU, Tingting Wang, Zongwen Wang, Xueli Gao, & Congjie Gao, 2012), and chitosan(Haiyong Ao et al., 2019). The cationic polymer is paired with an anionic polymer such as poly acrylic acid (PAA)(Fan Fan et al., 2015), polystyrene sulfonate (PSS)(Baowei SU et al., 2012) and hyaluronic acid(Jiezhao Zhan et al., 2015), *etc*. The layer-by-layer coated surface is antimicrobial as reported by Jiezhao Zhan(Jiezhao Zhan et al., 2015), and Dicky(Dicky Pranantyo et al., 2018). In addition to the simple assembly of alternative charged polyelectrolytes, bactericidal agents such as enzymes(Omar. S. Sakr & Borchard, 2013), silver ions(Xiaoying Zhu & Loh, 2015) and antibiotics(Xia-Chao Chen et al., 2015) can be incorporated into the coatings. However, the layer-by-layer fabrication of coatings is tedious, with repeated cycles of washing of unbonded polyelectrolytes. Complicated surfaces such as internal lumen is hard to coat due to surface tension.

The polymer can also be grafted onto surface utilizing catechol chemistry. Catechol chemistry is emerging from natural dopamine compound(Bruce P. Lee, P.B. Messersmith, J.N. Israelachvili, & Waite, 2011). Various surfaces can be coated using poly-dopamine chemistry(Bruce P. Lee et al., 2011). Polydopamine coating introduces imine (C=N), hydroxyl (OH), and amine (NH_2) groups(Bruce

P. Lee et al., 2011), facilitating further modification utilizing Michael addition or Schiff base chemistry(Kaiyang Lim et al., 2015). Further, dopamine can be copolymerized with other functional monomers and the resulting copolymer can be attached to surfaces via catechol adhesion.(Chuan Yang et al., 2014; Guozhu Li et al., 2008)

Bacteria-responsive strategy in design of medical device coatings

Bacterial infection prevention strategies such as cationic antimicrobial polymer, hydrated antifouling layer and nitric oxide release molecules are all passive methods: the exposure of cationic charge, the formation of hydrated layer or the release of NO is not controlled by the presence of bacteria. On the other hand, bacteria secrete many enzymes during metabolism(Saira Javed et al., 2018) and biofilm development at infection sites(Vasil ML, Graham LM, Ostroff RM, Shortridge VD, & Vasil AI, 1991). Some of these enzymes are unique to bacteria; glucuronidase, for example, has been used to trigger color change in synthetic polymer to indicates bacterial contamination of water(Mir-Morteza Sadat Ebrahimi, Yvonne Voss, & Schönherr, 2015). Bacteria-secreted enzymes could be used as a tool to trigger the action of antibacterial therapies. For example, lipase is overexpressed at infection sites of *P. aeruginosa*, *E. coli* and *S. aureus* The lipase enzyme can be used to release antimicrobial agents are; therefore, a smart polymer coating which respond to bacteria contact is reported as surface modifications on medical devices(Vitaly V. Komnatnyy, Wen-Chi Chiang, Tim Tolker-Nielsen, Michael Givskov, & Thomas E. Nielsen, 2014): the antibiotic ciprofloxacin is conjugated on top of PEG coating layer on medical device

(Figure 2.10); triclosan is encapsulated and coating onto medical devices using layer-by-layer approaches(Bailiang Wang, Huihua Liu, et al., 2017).

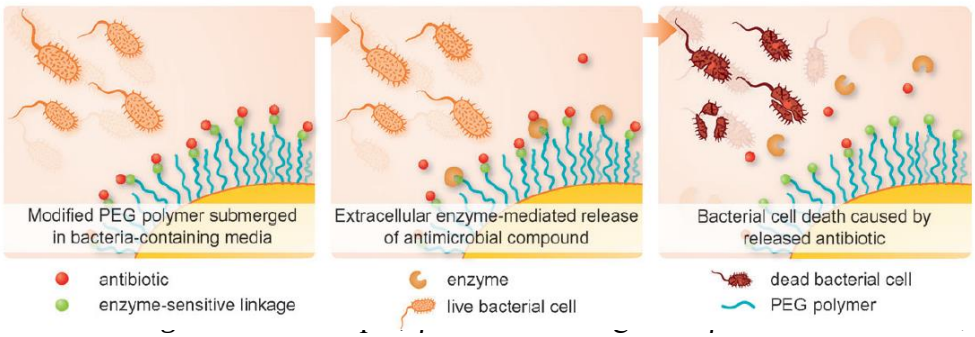

y V.
uch
eby
with
this

enzyme is utilized to trigger the release of Nitric oxide, which induces apoptosis of the bacteria(Nicolas Barraud et al., 2012), and Triclosan(Geoffrey W. Stone et al., 2004).

Bacteria-triggered strategies are a useful design principle for developing medical devices with improved and long-term antimicrobial efficacy, in which the antibacterial mechanism is activated and/or antimicrobial agents are released only when there is bacterial infection(Anna K. Winther et al., 2018; Jie Gao et al., 2013).

The “Grafting from”, “Grafting onto” and “bacteria-triggered” strategies provide frameworks for design of surface modifications. Specific surface modification antibacterial strategies are reviewed in following chapter.

2.4.3 Bactericidal modifications of medical devices

Cationic antimicrobial coatings

Cationic antimicrobial polymers, as discussed previously, can be coated onto medical devices to prevent infection, and can achieve superior bactericidal efficacy. Cationic poly-allylamine and p(DADMAC) (Figure 2.11A) can be grafted onto the surface of various medical devices. However, the primary amine from poly-allylamine only shows 98% killing of attached bacteria(Dmitri D. Iarikov et al., 2014). The p(DADMAC) coating with permanent quaternary ammonium charge shows 6 log reduction against *K. pneumoniae* and *S. aureus*(Maryam Mazloumpour, Priya Malshe, Ahmed El-Shafei, & Hauser, 2013). However, the coating with cationic charge causes protein fouling(Jean-Luc Dewez, Aurora Doren, Yves-Jacques Schneider, & Rouxhet, 1999; Zheng Zhang et al., 2008) and consequently does not have good antibiofilm effect, with less than $2\log_{10}$ *in vivo* biofilm inhibition(Chao Zhou et al., 2017). Therefore, despite the high bactericidal efficacy achieved by cationic modification of surface, the long term biofilm inhibitory efficacy is not good enough(Zhi Xiang Voo et al., 2016). As reported by ZX Voo *et al.*(Zhi Xiang Voo et al., 2016), even though the grafted-onto cationic quaternary ammonium polycarbonate shows bactericidal activity with 96% inhibition of *E. coli*, the cationic part needs to be

covered with hydrophilic high molecular weight PEG (10kDa) (Figure 2.11B) in order to get long-term bacteria adhesion resistance. To overcome the fouling problem, cationic-zwitterionic switchable approach is also presented by Gang Cheng *et al*,(Gang Cheng, Hong Xue, Zheng Zhang, Shengfu Chen, & Jiang, 2008). Also, the cationic charged monomers can be copolymerized with hydrophilic monomers (Figure 2.11C)(Zelun Zhi et al., 2017). However, the cationic charge and hydrophilic monomers may work antagonistically, resulting in reduced bactericidal and antibiofilm effect(Chao Zhou et al., 2017).

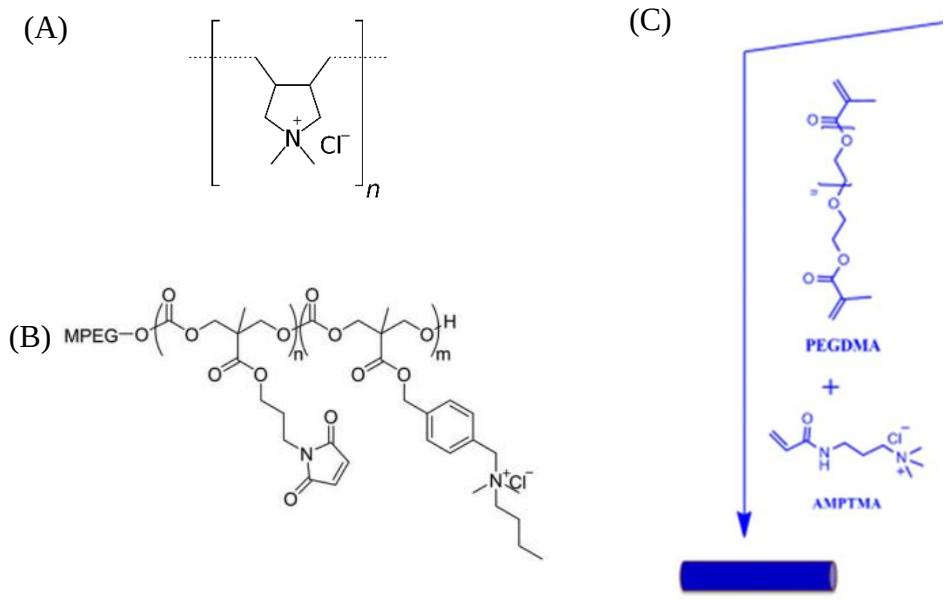

Figure 2.11 Illustration of various cationic coatings (A) purely cationic coating (pDADMAC) (B) Cationic-hydrophilic block copolymer for coating (C) cationic monomer co-coating with hydrophilic monomers

Reactive-Oxygen Species (ROS) release coatings

Reactive oxygen species (ROS) are reactive chemical species containing oxygen. Examples include peroxides, superoxide, hydroxyl radical, and singlet oxygen(Maan Hayyan, Mohd Ali Hashim, & AlNashef, 2016). The antibacterial efficacy of ROS (H_2O_2) release coating is reported by CZ Wu(Changzhu Wu et al., 2017) who encapsulated glucose oxidase with glucose in surface hydrogel; however, the release is uncontrollable. Chao Ding(Chao Ding, Zhengqing Yan, Jinsong Ren, & Qu, 2017) reported H^+ triggered release of H_2O_2 utilizing the same enzyme with glucose chemically bonded onto acid labile poly boronic acid. The release of H_2O_2 is only activated under acidic pH. In both cases, H_2O_2 release declines as the glucose "charge" in the coating is depleted, which limits the application of such modifications in medical devices that require sustained release of antibacterial agent. Bruce Lee *et al.* report dopamine hydrogel and microgel for sustained release of H_2O_2 ; these materials have the property that the release can be recycled and regenerated by tuning of pH(Hao Meng et al., 2019). However, the surface attachment of their materials is difficult, and the impracticality of *in vivo* pH tuning hinders the application of this approach in implantable medical devices.

Nitric oxide release modifications

Nitric oxide (NO) is a small, reactive but biocompatible molecule produced in epithelial cells(Bogdan, 2001) in human vascular lumen(Yingzi Zhao, Paul M. Vanhoutte, & Leung, 2015), with broad spectrum antimicrobial activity and good diffusivity, which can regulate biofilm formation by dispersing various bacteria to planktonic state(Bibhuti B. Mishra et al., 2017; Dhruv P.

Arora, Sajjad Hossain, Yueming Xu, & Boon, 2015; Qiaohong Liu, Priyadarshini Singha, Hitesh Handa, & Locklin, 2017; Regev-Shoshani Gilly, Ko Mary, Miller Chris, & Av-Gay Yossef, 2010; Zhou & Meyerhoff, 2005). Diazeniumdiolates (NONOate)(Elizabeth J. Brisbois et al., 2016) and S-nitrosothiols (RSNO)(Yaqi Wo et al., 2015) are commonly used NO release precursors for modification of catheters (Figure 2.12A and B).

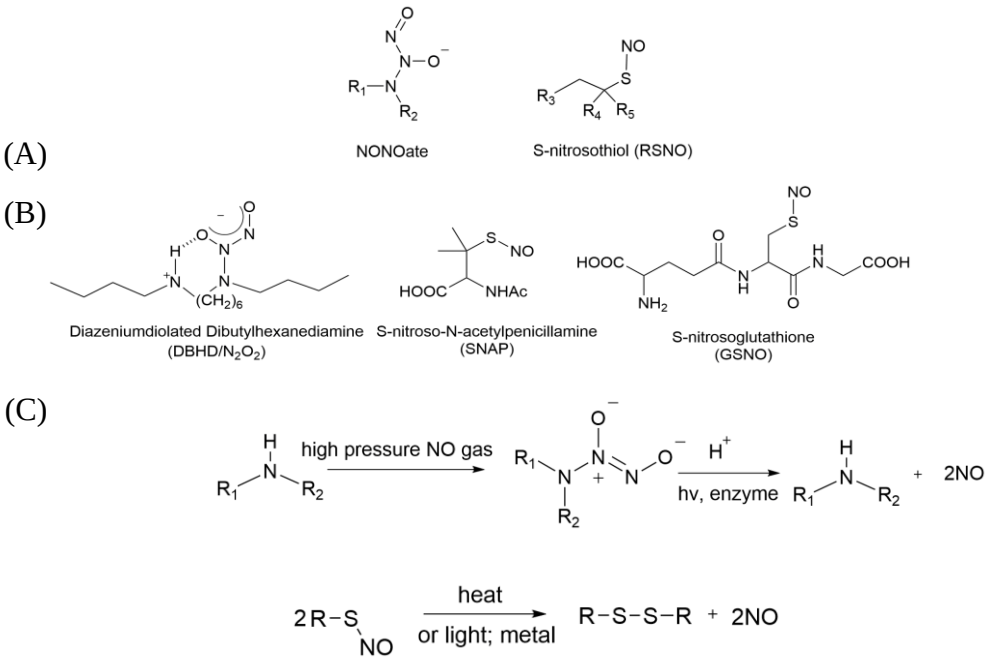

Figure 2.12 (A) Chemical structure of NO release precursors. (B) Examples of common small molecule NO release precursors (C) NO release mechanism from RSNO and NONOate

Usually, the NO release from NONOate is triggered by (H^+) proton from water; and the NO release from RSNO is triggered by heat. (Figure 2.12C)

The NONOate precursor is carcinogenic and releases nitric oxide in a burst. Upon exposure to oxygen, NONOates can be converted to carcinogenic nitrosamine(Keefer, 2011). After the nitric oxide is released from NONOate, it can be oxidized by oxygen to nitrous oxide, which further converts the secondary

amine residue from NONOate to nitrosamine(Keefer, 2011). The NONOate can also be further oxidized directly to nitrosamine by oxygen(Keefer, 2011) (Figure 2.13A). To counter the problem of carcinogenic nitrosamine generation, the NONOate precursor can be covalently bonded with a macromolecular scaffold such as polymer(Ho-Wook Jun, Lakeshia J. Taite, & West, 2005), polysaccharide(Ajun Wan, Yan Sun, & Li, 2008), dendrimers(Nathan A. Stasko & Schoenfisch, 2006) and nanoparticles(Robert J. Soto, Lei Yang, & Schoenfisch, 2016). Even though in this way the possible carcinogenic nitrosamine will not be released, the burst release of nitric oxide is still not controlled upon contact with physiological fluids. In contrast, the release kinetics of RSNO can be easily tuned by choice of the primary, secondary or tertiary thiol group in preparation of nitrosothiol(Caihong Zhang et al., 2017). The tertiary nitrosothiol will result in prolonged gradual, rather than burst, release of nitric oxide(Tuanwei Liu, Wei Zhang, Xinlin Yang, & Li, 2015; Yan Li & Lee, 2009). Normally, due to the water sensitivity of NONOate and the temperature, light and catalyst sensitivity of RSNO(Caihong Zhang et al., 2017), the incorporation of NO release precursor into polymer coatings are limited to solvent impregnation or blending with the raw materials(Yaqi Wo et al., 2015) without covalent bonding to the polymer scaffold. Under this strategy, the NONOate incorporated catheter shows 95% *in vivo* efficacy for 9 days in a rabbit hemodialysis model(Elizabeth J. Brisbois et al., 2016), and the RSNO impregnated silicone catheter shows *in vitro* antibiofilm efficacy above $3\log_{10}$ reduction for 21days(Alex R. Ketchum, Michael P. Kappler, Jianfeng Wu, Chuanwu Xi, &

Mark E. Meyerhoff, 2016) which is the best antibiofilm modification yet reported. The excellent antibacterial and antibiofilm efficacy shows great potential for the use of NO release precursor for modification of medical devices. However, incorporation of NO release precursor without covalent linkage will result in release of the precursor from the device. The released NONOate is carcinogenic(Keefer, 2011) and nitrosothiol disturbs the normal NO signaling (Figure 2.13B) (Brian C Smith & Marletta, 2012)

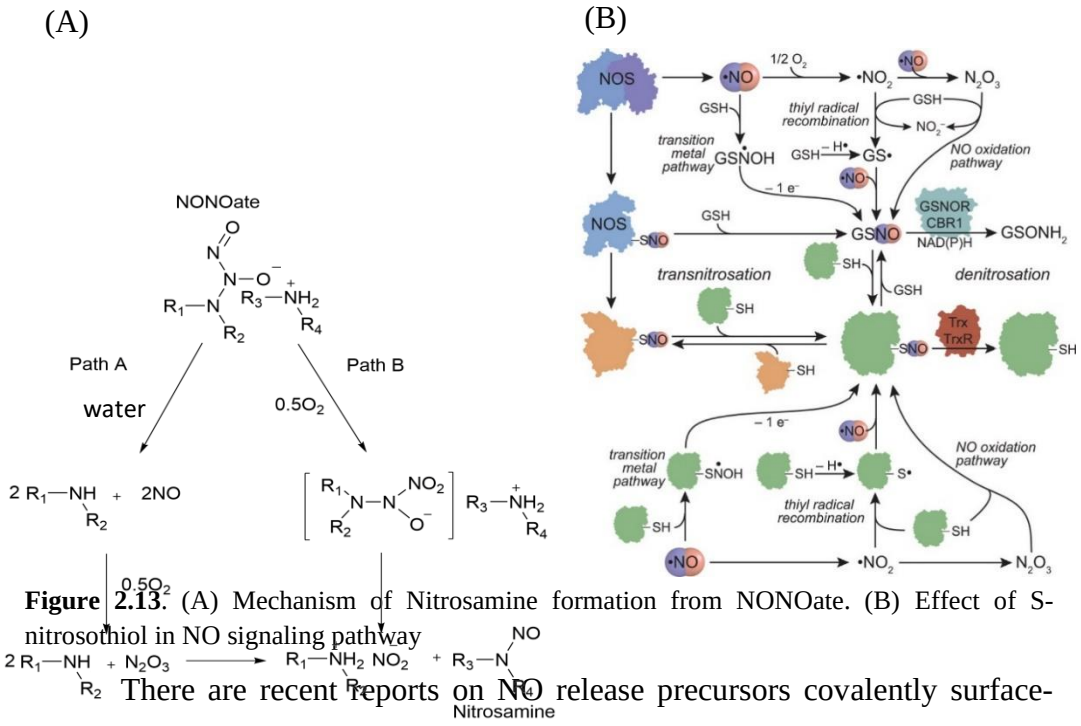

Figure 2.13. (A) Mechanism of Nitrosamine formation from NONOate. (B) Effect of S-nitrosothiol in NO signaling pathway

There are recent reports on NO release precursors covalently surface-bonded instead of blended with raw materials. For example, George Fleming(George Fleming et al., 2017) and Zahra Sadrearhami(Zahra Sadrearhami et al., 2019) report the surface attachment of NO release precursor, NONOate, on poly(ethylene terephthalate) (PET), Silicone elastomer (SE), glass and polyester via plasma and dopamine chemistry. However, the antibacterial/antibiofilm efficacy is low due to the rapid release of nitric oxide.

There is a report of covalent bonding of RSNO release precursor with polyphosphazene polymer backbone(Alec Lutzke, Jesus B. Tapia, Megan J. Neufeld, & Reynolds, 2017), and the sustained release of nitric oxide is demonstrated, but the labile SNO bond limits further modification of the polymer or device. The material must be specially synthesized rather than applied as a modification to the materials commonly employed in medical devices(Alec Lutzke et al., 2017).

In recent reports, the NO release functionalities are synergized with antifouling hydrophilic coatings, and in some of the reports the antibiofilm efficacy is much improved(Kagya A. Amoako, Harihara S. Sundaram, Ahmed Suhaib, Shaoyi Jiang, & Cook, 2016; Qiaohong Liu et al., 2017). However, in their paper, Zahra Sadrearhami combined hydrophilic PEG with NO release precursor by dopamine chemistry, but the antibiofilm efficacy of the NO release coating was not much improved after hydrophilic PEG was introduced onto the coating(Zahra Sadrearhami et al., 2019). The possibility of additive combinations of NO-release precursor and antifouling polymer suggests a novel direction for design of effective antibiofilm modifications for medical devices; however, the swiftest route to clinical applications is to develop post-modifications of materials, such as polyurethane (PU), that are currently employed in the manufacture of medical devices. New methods to control the interaction (and, it is hoped, synergy) between NO-release and hydrophilic functions may need to be developed.

Even though the bactericidal strategies are well-studied, these strategies do not prevent protein fouling on device surfaces, which is the first step for initiation of bacterial biofilm, as discussed above. Resistance to protein fouling is a highly desirable property for device surface modification. The hydrophilic modification of surface is reported to have protein fouling resistance. Therefore, it is discussed in next section.

2.4.4 Antifouling coatings on medical devices

Hydration layer

The principle by which hydrophilic polymer coatings resist attachment of bacteria is the formation of hydration layers(Shenfu Chen, Lingyan Li, Chao Zhao, & Zheng, 2010). The hydration layer formed on a substrate surface prevents direct contact with proteins; thermodynamically, the Gibbs energy increases ($\Delta G_{Ads}>0$) during protein penetration of the hydration layer, which hinder the adsorption process(Mingrui He et al., 2016). Steric hindrance from polymer chains is another mechanism for protein fouling resistance. During protein fouling on surface, the protein penetrates the hydration layer and compress the polymer chains of the surface coating, causing the decrease of entropy ($\Delta S_{polymer}<0$), which is unfavorable thermodynamically(Mingrui He et al., 2016)(Figure 2.14). The surface brush density is another factor in protein resistance efficacy(Wufang Yang & Zhou, 2017). As surface brush density increases, the morphology changes from “pancake” and “mushroom” to “high-density brush” (Figure 2.14). In both pancake and mushroom morphologies, the

surface polymers are collapsed, *i.e.* the monomer units within each chain interact with other units in the same chain and are less available for formation of a hydration layer. Therefore, the high-density brush morphology is preferred for surface coatings with high protein resistance. This requires a high surface density of attachment sites for the polymer molecules. As previously noted, ozone surface treatment is the most useful approach for introduction of very high surface density of initiation sites, which is required for high-density brush coating(O'Neill, 1972).

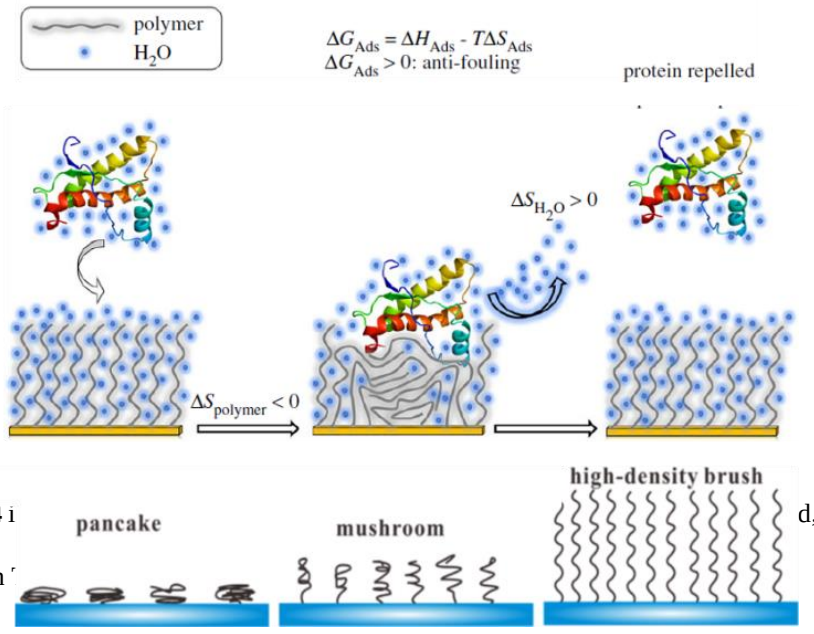

Figure 2.14 i d, Dhyani , , & Anish ´

Synthetic surface polymer brush

Zwitterionic polymers contain the same numbers of cationic and anionic charges(Laschewsky, 2014). Much effort has been put into development of hydrophilic surface coatings(Hong Chen et al., 2016; Nana Cai et al., 2017), among which surface-initiated hydrophilic zwitterionic polymer coatings have been extensively studied due to their non-leachability and long-lasting anti-biofilm activity(Mi & Jiang, 2014; Smith et al., 2012). Both hydroxyl-terminated monomers (HEMA, OEGMA, PEGMA) and zwitterionic monomers are used for antifouling coatings, as such coatings in complex physiological environments are able to form a hydration layer making the surface stealth and non-fouling (Bernards, Cheng, Zhang, Chen, & Jiang, 2008; Chang et al., 2009; Dobbins, McGrath, & Bernards, 2012; Herzberg et al., 2011; Holmlin, Chen, Chapman, Takayama, & Whitesides, 2001; Shih et al., 2014). Poly-zwitterionic coatings have better antifouling efficacy compared with polymer coatings with hydroxyl-terminated monomers(Jon Ladd, Zheng Zhang, Shengfu Chen, Jason C. Hower, & Shaoyi Jiang, 2008). While both hydroxyl-terminated polymers such as polysaccharide and PEG and zwitterionic polymer coatings can form hydration layers upon contact with water, mechanism is different. Hydrogen bonding is the driving force for hydration layer formation of hydroxyl-terminated monomers (Figure 2.15A). On the other hand, within the zwitterionic coating, both cationic and anionic charges can form electrostatically attract water molecules (Figure 2.15B). In a fully formed hydration layer, each repeat unit of zwitterionic polymer is integrated with 8 water molecules, whereas each OH-terminated repeat unit is integrated with only one water molecule(Jon Ladd et al., 2008). The electrostatic

interaction is stronger and more stable than hydrogen bonding. Therefore, the hydration layer formation on a zwitterionic polymer coating is more robust than that on a hydroxyl-terminated polymer coating(Shenfu Chen et al., 2010).

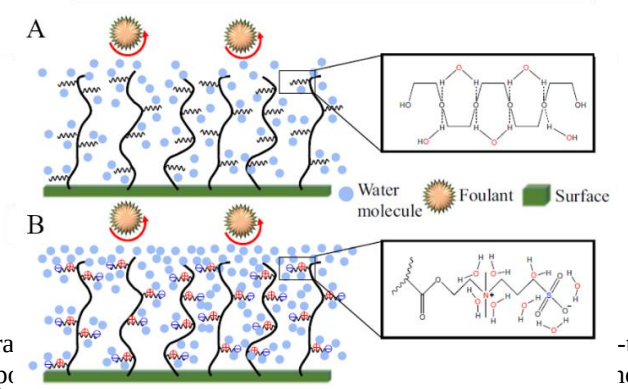

Figure 2.15 Illustra -terminated coating (B) zwitterionic pc ıonspecific protein adsorption in different ways.

The commonly used zwitterionic monomers are carboxybetaine methacrylate (CBMA)(2015), sulfobetaine methacrylate (SBMA)(Guozhu Li et al., 2008) and methacrylate phosphorylcholine (MPC)(2015) with coatings on polyurethane(Youling Yuan et al., 2004), PDMS(Hongbin Zhang & Mu Chiao, 2015) and other materials used in medical devices; these zwitterionic polymers exhibit some degree of *in vitro* inhibition of bacterial biofilm formation ($2\log_{10}$ orders of inhibition). Smith *et al.*(S et al., 2012) and Wang *et al.* (Wei Wang, Yang Lu, Jinbing Xie, Hui Zhu, & Cao, 2016) used solvent impregnation of peroxide initiator into the PU catheter followed by redox polymerization of a zwitterionic SBMA coating. Subcutaneous study of pure hydrophilic coating shows 1.5 $\log_{10}$ biofilm inhibition in 24hrs against *S. aureus*(S et al., 2012), which is low due to negligible bactericidal efficacy of hydrophilic-only coatings. Further, this modification lacks long-term stability and loses its hydrophilicity in

2 weeks, as reported by Wang *et al.*(Wei Wang, Yang Lu, Jinbing Xie, Hui Zhu, & Cao, 2016) due to the introduction of the initiator by solvent impregnation rather than covalent bonding.

Antifouling hydrogels

Hydrophilic crosslinked or hydrogel polymer coatings are reported to be antifouling. The zwitterionic hydrogel DURA-Z is reported by Wang *et al.* to retain antifouling efficacy after 30 days of water flushing(Wei Wang, Yang Lu, Hui Zhu, & Cao, 2017). Zwitterionic macro-crosslinker is also reported for modification of polyurethane(Wei Wang, Yang Lu, Jinbing Xie, Hui Zhu, & Cao, 2016). Crosslinked coating with hydroxyl-terminated poly(glycidol), produced by radiation initiated surface polymerization, is reported to show excellent antibiofilm efficacy(Jacob N. Lockhart et al., 2018).

Hydrophilic coatings are useful for their ability to slow bacterial attachment, but their lack of bactericidal properties renders them unable to prevent acute infections and can result in low antibiofilm efficacy in long term usage.

2.4.5 Advanced surface modification using controlled polymerization

To overcome the limitations of single-function surface modifications, modifications combining multiple functional components have been reported. For example, Zhi *et al.* combined antifouling PEG with cationic antimicrobial PHMB in their coating(Zelun Zhi et al., 2017). NO-release precursor impregnation can be combined with antifouling poly-MPC coating to achieve

antibacterial adhesion efficacy(Qiaohong Liu et al., 2017). Further, surface-initiated controlled polymerizations such as SI-ATRP and SI-RAFT provide the versatility for control of the structure and composition of coatings.

Surface-initiated atomic transfer radical polymerizations (SI-ATRP) has been applied on various surfaces such as PDMS(Yuanzi Wu, Yanyi Huang, & Hongwei Ma, 2007), PU(Wenjie Yuan et al., 2013) and metals(Xiaowu Fan, Lijun Lin, Jeffrey L. Dalsin, & Phillip B. Messersmith, 2005; Yuanzi Wu et al., 2007). The chemical bonding of bromide initiator group is achieved by isocyanate chemistry(Wenjie Yuan et al., 2013), silane chemistry(Fan Zhang, F. J. Xu, E. T. Kang, & Neoh, 2006) and dopamine attachment(Xiaowu Fan et al., 2005)-(Xingxing Jin, Jiang Yuan, & Shen, 2016). Among these reports, Fan Zhang *et al.* have demonstrated a P(PEGMA)-*block*-P(DMAEMA) copolymer coating formed by SI-ATRP on titanium(Fan Zhang et al., 2006) after bromide group attachment via silane chemistry. These reports demonstrate the great potential of SI-ATRP for controlled formation of polymer coatings. However, SI-ATRP requires copper (I) ions as catalyst, which is highly toxic, highly sensitive to oxygen and hard to be remove from coatings. Further, the detailed chemistries of adhesion of poly-dopamine onto different surfaces are as yet not well understood. In most of the cases, the poly-dopamine is unstable under acidic conditions(Wei Yang, Chanjuan Liu, & Chen, 2018) resulting in detachment of the coating. SI-ATRP does not appear to be a highly suitable technique by which to form durable antifouling and antibacterial device coatings.

Reversible addition−fragmentation chain-transfer polymerization (RAFT) is a versatile living polymerization technique which provides the flexibility for design and synthesis of block copolymers combining different classes of monomers such as hydroxyl-terminated and zwitterionic monomer(Kay E. B. Doncom, Nicholas J. Warren, & Armes, 2015). Surface-initiated block copolymers synthesized by RAFT have been reported by a few groups(Chunmiao Bo & Yinmao Wei, 2017; Jong-Bum Kim, Wenxi Huang, Merlin L. Bruening, & Gregory L. Baker, 2002). Block copolymer brush provides additional functional design flexibility in comparison with random copolymer brush in that the physical arrangement of the blocks can be designed to promote the designed functions of the copolymer coating There are usually two strategies used in surface-initiated RAFT polymerization(Justin O. Zoppe et al., 2017): (i) grafting the initiator on surface first, followed by polymerization with chain transfer agents in solution (Figure 2.16A)(W. H. Yu, E. T. Kang, & Neoh, 2005) or (ii) grafting the chain transfer agents and polymerizing with initiator in solution (Figure 2.16B) (Bailiang Wang, Zi Ye, et al., 2017). B. Wang(Bailiang Wang, Zi Ye, et al., 2017) reported a block copolymer coating with a tertiary amine DMAEMA at bottom and antifouling monomer on top. The underlying P(DMAEMA) block is quaternized after polymerization and becomes the cationic bactericidal block. These reports demonstrate the possibility of use of novel surface-initiated RAFT chemistries to activate surfaces with complex shapes and then perform living polymerization to fabricate smart coatings combining complementary or synergistic functions.

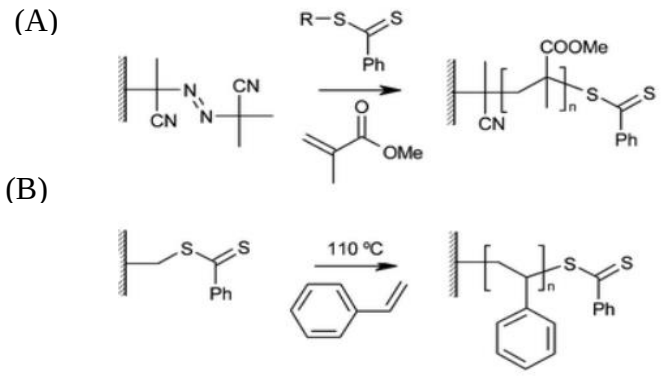

Figure 2.16 (A) Surface initiated RAFT polymerization based on surface peroxide. (B) comparison of SI-RAFT polymerization designs (i) introduction of initiator site on surface (ii) introduction of chain-transfer agents on surface

In a nutshell, the antibacterial and antifouling strategies reviewed have both advantages and disadvantages. The cationic coatings will have superior short-term bactericidal efficacy, but it will cause fouling of proteins tend to facilitate bacterial attachment and biofilm formation in long-term use. The ROS generation coating is less bactericidal than cationic coating and is also complicated or requires glucose to be effective, limiting its utility as medical device coating. The NO-release modification can have excellent and long term antibiofilm efficacy, but the methods of covalent linkage of the precursor onto medical devices are still under development. The hydrophilic coatings have antifouling efficacy, but negligible bactericidal efficacy, which results in lower *in vivo* antibiofilm efficacy compared with NO release modification. However, the development of surface initiated controlled living free-radical polymerization chemistry provides more versatility in combining of different surface functions and achieving synergism which can overcome the limitations of each individual modification.

2.5 Conclusion

Several antimicrobial strategies have been presented and discussed. Those strategies can be applied in both killing of planktonic bacteria and prevention of infection on medical device surfaces. Direct contact killing of bacteria is achievable by cationic antimicrobial polymers, which kill bacteria by membrane perturbation. The ROS and NO induce bacterial apoptosis and inhibit biofilm formation. Anti-protein-fouling hydration layer can prevent nutrient fouling and delay pathogen attachment onto the modified surface. With suitable chemistry and copolymer design, multifunctional surfaces can be formed which combine in complementary or even synergistic ways these different approaches to control of infection.

Chapter 3. Methodology

This chapter describes the commonly used experimental and characterization techniques in this thesis to avoid repeating the same experimental details in later chapters. All other relevant experimental details for each study are described in Chapters 4-6.

3.1 Culture of bacteria and fungus

The bacteria or fungus strains used in this thesis were purchased from American Type Culture Collection (ATCC): *Pseudomonas aeruginosa* PAO1, *S. aureus* ATCC 29213, *Methicillin-resistant Staphylococcus aureus* BAA38, *Escherichia coli* 8739, *Escherichia coli* K12, *Escherichia coli* UTI89, Vancomycin-Resistant *Enterococci* (VRE) V583, *Acinetobacter baumannii* ATCC19606, *Acinetobacter baumannii* (Pan sensitive), *Acinetobacter baumannii* AB-1 (MDR), Methicillin-Resistant *Staphylococcus epidermidis* 35984 and *Candida albicans* 90028.

All broths or agar media were purchased from Becton Dickinson Company. All bacteria and fungus were stored in 15% v/v aqueous glycerol at -80 °C. To recover cells from frozen storage, for bacteria a single colony was inoculated in Muller Hinton (MH) broth at 37 °C for 4 to 8 hours, with shaking at 200 rpm. *C. albicans* was inoculated in Yeast Malt (YM) broth at 28 °C for 24 to 48 hours, with shaking at 200 rpm. After centrifugation (6,000 rpm) for 10 min and PBS washing, the bacterial/fungal cells were diluted to the desired concentration.

For antibiofilm test, all bacteria were incubated in TSB at 37 °C for 24hrs and *C. albicans* was incubated in YM broth at 28 °C for 24 to 48 hours.

3.2 Antimicrobial assays

3.2.1 Minimum inhibitory concentrations (MICs)

Bacteria cells were grown overnight at 37 ºC in LB broth (YM broth and 28 ºC for fungus) to a mid-log phase and diluted to 10^4 to 10^5 CFU/ml in PBS. A two-fold dilution series of 100 µl antimicrobial polymer solution in the broth (LB broth for bacteria and YM broth for fungus) was made in a 96-well microplate, followed by the addition of 100µl bacterial/fungal suspension (10^4 to 10^5 CFU/mL). The plates were incubated at 37 ºC for 18-24h (28 ºC, 36-48h for fungi), and the absorbance at 600nm was measured with a microplate reader (BIO-RAD Benchmark Plus, US). Positive control was without product, and negative control was without bacteria/fungi inoculum. MICs were determined as the lowest concentration that inhibited cell growth by more than 90%.

3.3 Biocompatibility assays

3.3.1 MTT assay

Methyl tetrazolium (MTT) assay was used to examine cell viability and proliferation. After specified cell culture time periods, MTT solution (5 mg/ml, 100 µL), formed from MTT solids pre-dissolved in PBS and filter sterilized, was introduced to each sample in a 96-well TCPS plate. The plate was then incubated at 37 °C for 4 h. After this time, DMSO (200 µL) was added. The plate was then

placed in a shaking incubator for 30 min before measurement of the absorbance at wavelength 490 nm using a microplate spectrophotometer (Benchmark Plus, BIO-RAD).

3.4 Characterization techniques

3.4.1 Proton nuclear magnetic resonance (1H NMR)

Proton nuclear magnetic resonance (1H-NMR) spectroscopy was performed on a Bruker DMX-300 instrument. The products were first dissolved in deuterated solvents, then characterized under a resonance frequency of 300 MHz.

3.4.2 Fourier transform infrared (FTIR) spectra

Fourier transform infrared (FTIR) spectra analysis was performed on a Nicolet™ 5700 FTIR Spectrometer (Thermo Electron Corporation, US) equipped with a single reflection diamond attenuated total reflection (ATR) unit, over the wavenumber range between 400-4000 cm^{-1}, at a resolution of 2 cm^{-1} and each FTIR spectrum was produced from 64 scans over the studied wavenumber range.

3.4.3 Gel permeation chromatography (GPC)

Polymer molecular weight and polydispersity were measured using a Waters GPC instrument equipped with a refractive index detector (RID), using a ultrahydrogel GPC column and sodium acetate buffer (0.5 M, pH 4.5). Samples were analyzed at 40°C with an eluent flow rate of 0.5 ml/min.

Chapter 4. Nanoparticles of Short Cationic Peptidopolysaccharide with Antibacterial Effect

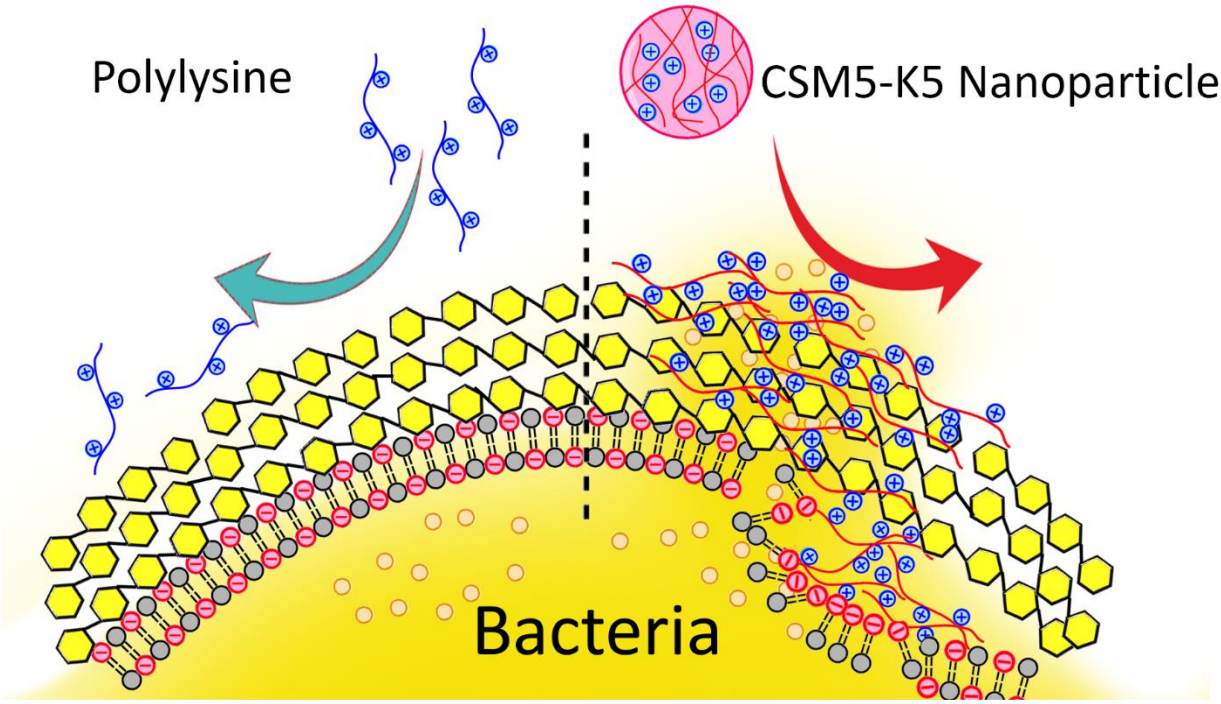

Cationic antimicrobial peptides (AMPs) and polymers are active against many multi-drug resistant (MDR) bacteria but only a limited number of these compounds are in clinical use due to their unselective toxicity. The typical strategy for achieving selective antibacterial efficacy with low mammalian cell toxicity is through balancing the ratio of cationicity to hydrophobicity. Herein, we report a cationic nanoparticle self-assembled from chitosan-*graft*-oligolysine (CSM5-K5) chains with ultra-low molecular weight (1450 Daltons) that selectively kills bacteria. Further, hydrogen bonding and not the typical hydrophobic interaction causes the polymer chains to be aggregated together in

water into small nanoparticles (with R_H = 37nm) to concentrate the cationic charge of the lysine. When complexed with bacterial membrane, these cationic nanoparticles cluster anionic membrane lipids and produce greater membrane perturbation and antibacterial effect than would be achievable by the same quantity of charge if dispersed in individual copolymer molecules in solution. The small zeta potential (+15 mV) and lack of hydrophobicity of the nanoparticles impedes the insertion of the copolymer into the cell bilayer to improve biocompatibility. *In vivo* study (using a murine excisional wound model) shows that CSM5-K5 suppresses the growth of methicillin-resistant *Staphylococcus aureus* (MRSA) bacteria by 4.0 orders of magnitude, an efficacy comparable to that of the last resort MRSA antibiotic vancomycin; it is also non-inflammatory with little/no activation of neutrophils (CD11b and Ly6G immune cells). This study demonstrates a promising new class of cationic polymers -- short cationic peptidopolysaccharides -- that effectively attack MDR bacteria due to the synergistic clustering of, rather than insertion into, bacterial anionic lipids by the concentrated polymers in the resulting hydrogen bonding-stabilized cationic nanoparticles.

4.1 Materials

Low molecular weight chitosan (200 KDa), Nε-benzyloxycarbonyl-L-lysine, triphosgene, ethyl acetate (anhydrous), hexane, phthalic anhydride, triphenylchloromethane, hydrazine solution, hydrochloride acid (37 v/v% in water), hydrogen bromide (33% in acetic acid), N,N- dimethylformamide (DMF

dried on CaH_2 and freshly distilled before use), pyridine, trifluoracetic acid (TFA), Lisamine rhodamine B sulfonyl chloride, sodium hydroxide, Lipopolysaccharide (LPS) (extracted from Pseudomonas aeruginosa 10 and Escherichia coli 0111: B4) are purchased from Sigma-Aldrich Corp. 1-palmitoyl-2-oleoyl-sn-glycero-3-phosphocholine (POPC); palmitoyl-oleoyl phosphatidylglycerol (POPG) and are purchased from Avanti Polar Lipid

4.2 Experiments

4.2.1 Synthesis

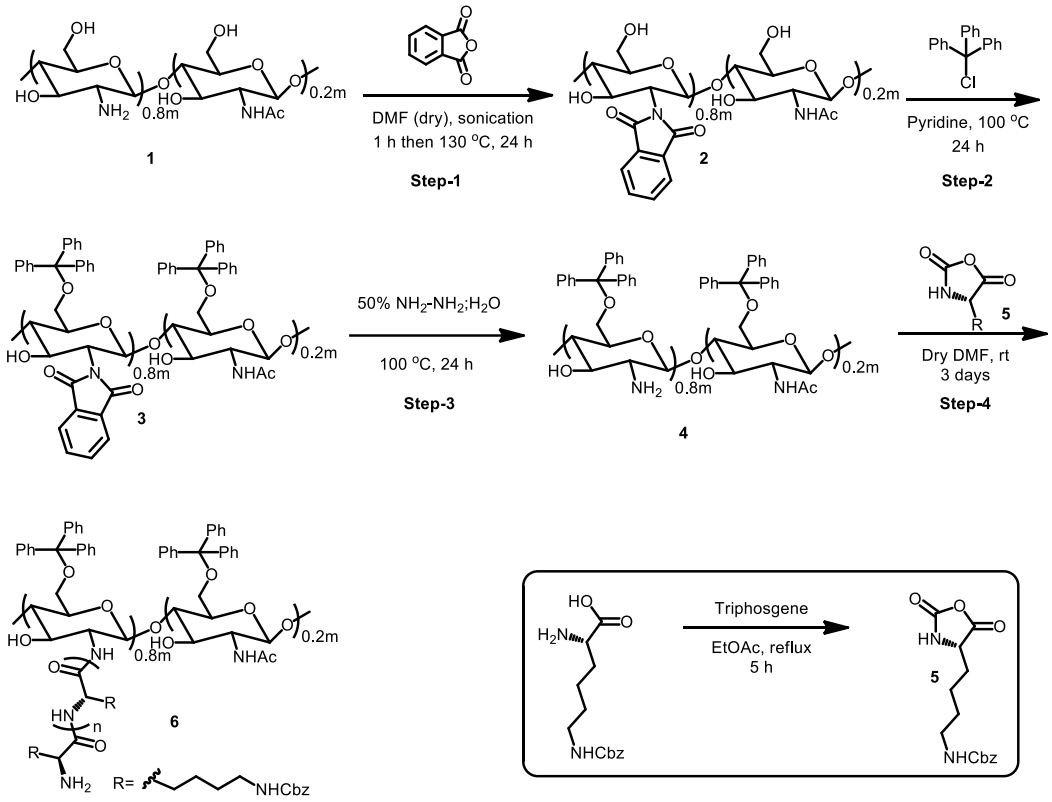

Scheme 4.1 Synthesis scheme for protected CSM5-K5 copolymer (CS-Kn(Cbz)) (CBz is Benzyl carbamates protection group for side chain amine of lysine)

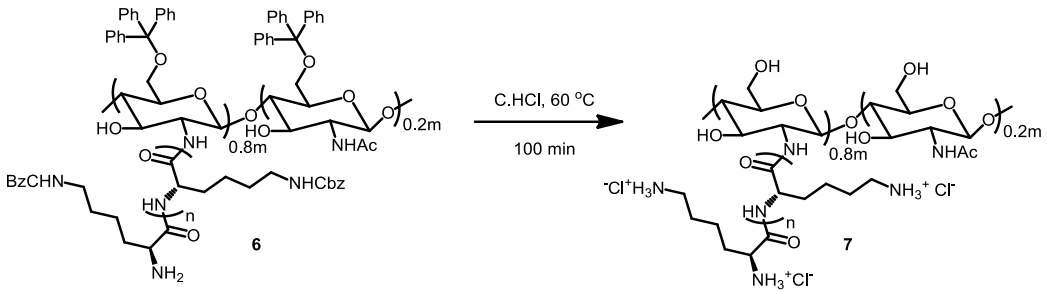

Scheme 4.2 Deprotection of CSM5-K5(Cbz) (**6**) using concentrated HCl.

Ultrashort Chitosan-grafted-polylysine (CSM5-K5) is synthesized via NCA polymerization initiating from protected chitosan (**Scheme 4.1**) followed by acidic hydrolysis (**Scheme 4.2**). The 5g of low molecular weight chitosan (M.W 200KDa) is firstly dispersed in 100mL anhydrous DMF and sonicated at 80C for 1hrs under Ar protection. The protection of amine group on chitosan is carried by further adding of 13.8g of phthalic anhydride under 130°C and reacting for 24hrs. The further protection of 6-hydroxyl group is carried by reacting of 8g phthalic protected chitosan with 24g of trityl chloride in 100mL anhydrous pyridine at 100°C for 24hrs. Then, the chitosan macroinitiator is obtained by deprotection of phthalic group using hydrazine. Typically, 5g of protected chitosan is deprotected by 100mL of 50% hydrazine at 100°C for 24hrs. The protected chitosan-grafted-polylysine is synthesized by ring-opening polymerization of lysine N-carboxyanhydride (NCA) monomer initiated by chitosan macroinitiator. Briefly, 1.32g of lysine-NCA monomer is dissolved in 8mL of anhydrous DMF and 112mg of chitosan macroinitiator is dissolved in 3mL of anhydrous DMF, the chitosan macroinitiator solution is added into lysine-NCA monomer solution under Ar protection to initiate polymerization.

The polymerization is carried at room temperature for 3 days. Ultra-short CSM5-K5 cationic peptidopolysaccharide is obtained by acidic deprotection and hydrolysis of 1g protected chitosan-grafted-polylysine with 10mL of concentrated hydrochloride solution (37%) at 60°C for 100mins. The crude deprotected product was neutralized by NaOH solution (1M) and dialyzed with 1000 Da cut-off cellulose membrane against DI water for 5 days. The residue was lyophilized to obtain a white solid with molecular weight at 1450 Da (determined by Maldi-Tof analysis).

The reaction intermediates and product are characterized by NMR spectrum (Figure 4.1-2.6).

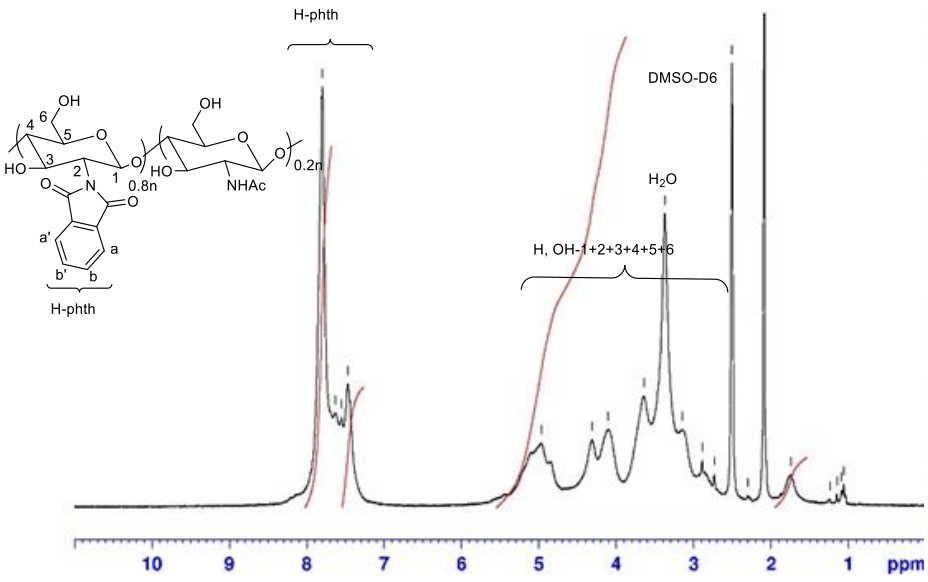

Figure 4.1 NMR spectrum of N-Phthaloyl Chitosan (compound **2**)

$$\text{Phthaloylation percentage} = \frac{(intergation\ from\ 7.5\ to\ 8)/4}{(intergration\ from\ 4\ to\ 5.5)/4} \times 100$$

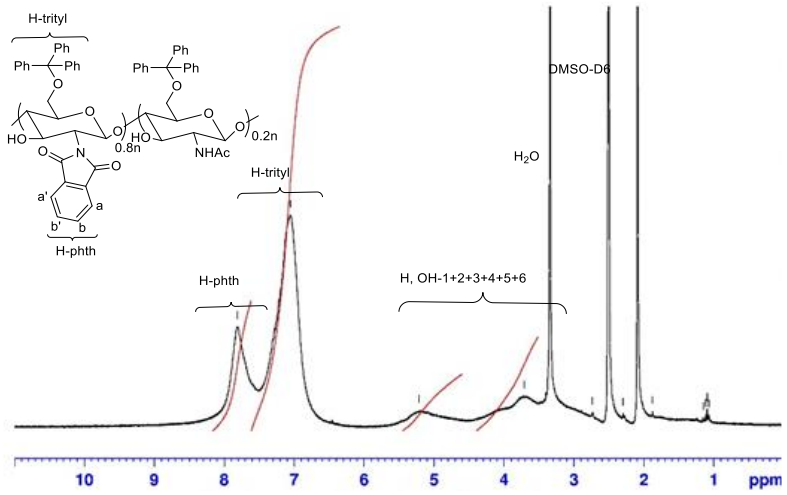

Figure 4.2 NMR spectrum of N-Phthaloyl-*6*-O-triphenylmethyl chitosan (compound **3**)

$$\text{Trityl Percentage} = \frac{(integration\ from\ 6.5\ to\ 7.5)/15}{(integration\ from\ 3.5\ to\ 5.5)/5} \times 100\%$$

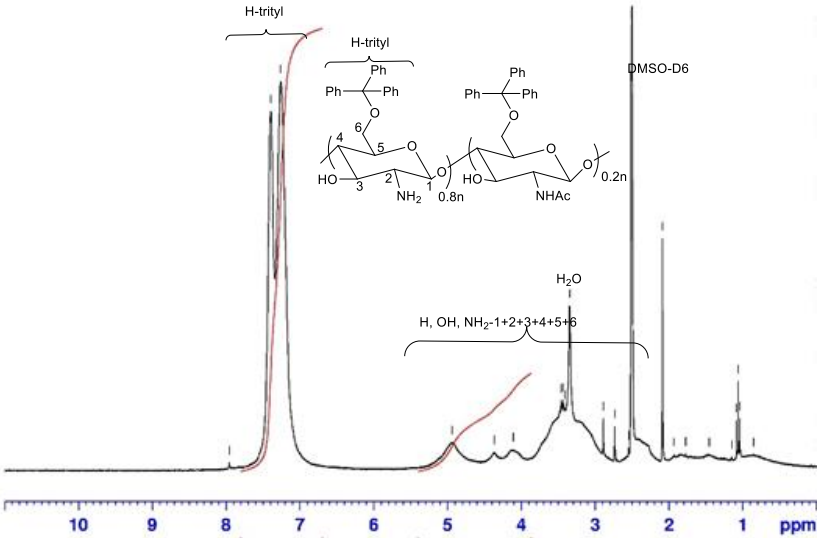

Figure 4.3 NMR spectrum of *6*-O-triphenylmethyl chitosan (compound **4**):

$$\text{Trityl Percentage} = \frac{(integration\ from\ 7\ to\ 8)/15}{(integration\ from\ 4\ to\ 5)/3} \times 100\%$$

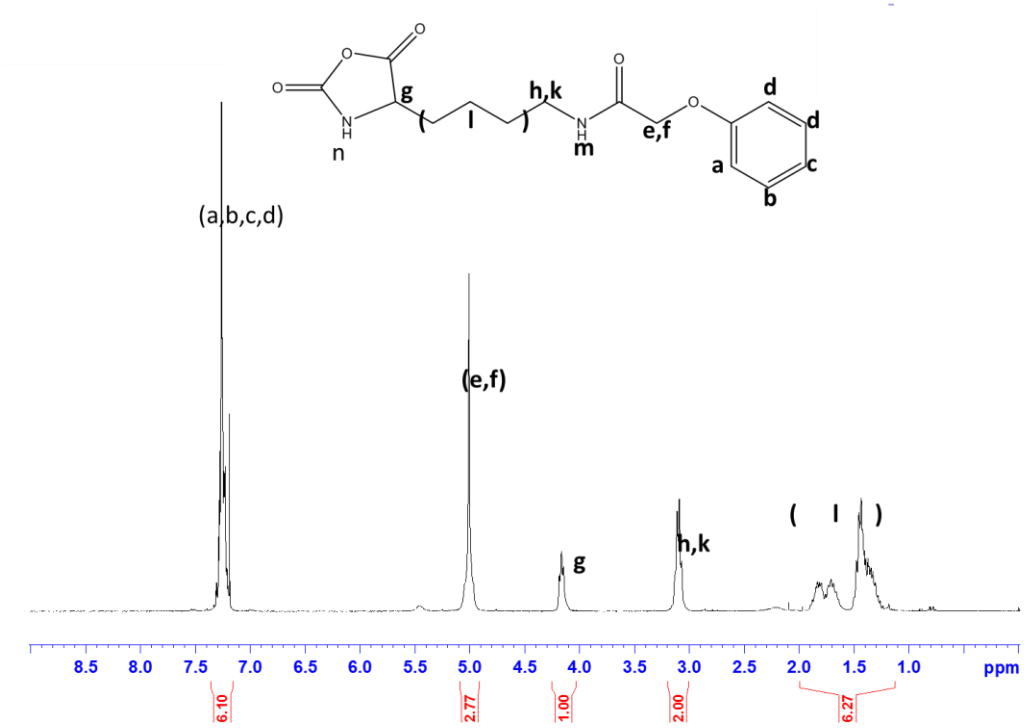

Figure 4.4 NMR spectrum Lysine NCA monomers (compound **5**)

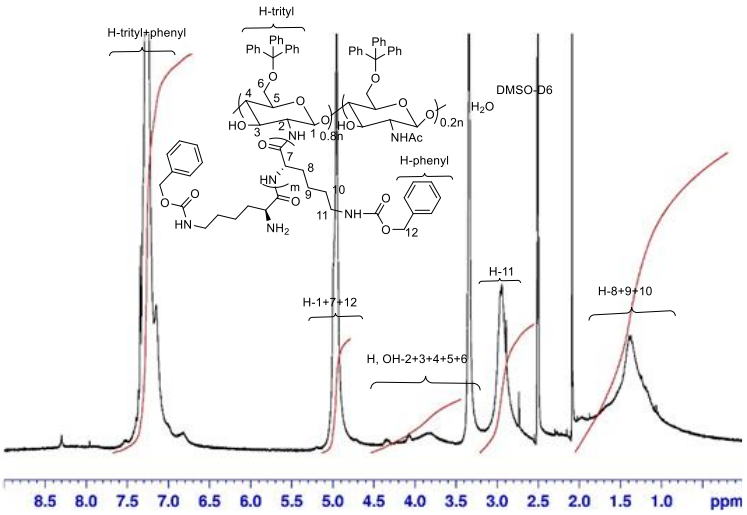

Figure 4.5 NMR spectrum of Protected CSM5-K5 copolymers (compound **6**);

$$\text{N of protected polymer} = \frac{(integration\ at\ 5)/3}{(integration\ from\ 3.5\ to\ 5.5)/5}$$

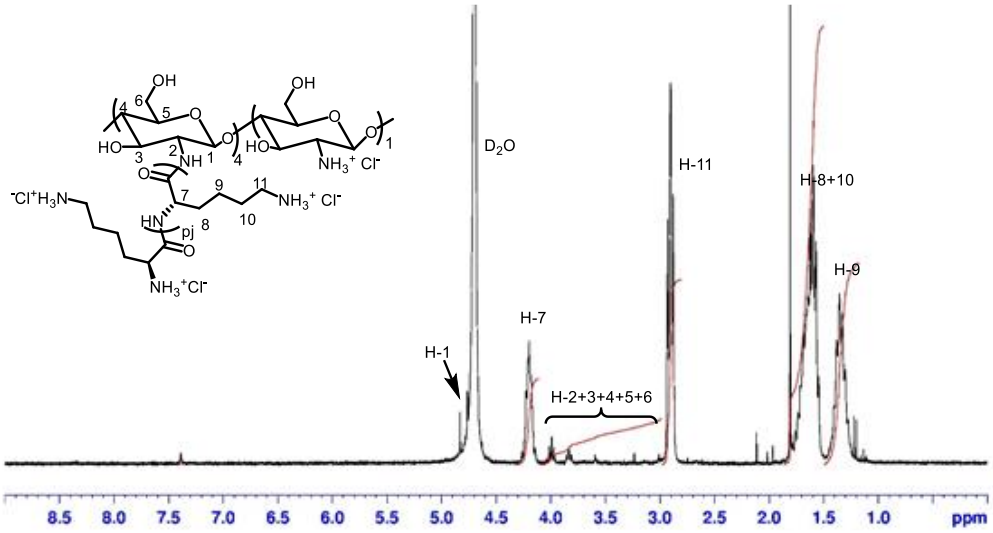

Figure 4.6 NMR spectrum of Deprotected CSM5-K5

$$\text{polysine chain length per glucosamine units} = \frac{(integration\ form\ 4.1\ to\ 4.3)}{(integration\ from\ 3\ to\ 4)/6}$$

$$Degree\ of\ Deprotection = \frac{(integration\ from\ 7.3\ to\ 7.4)/5}{(intergation\ from\ 4.1\ to\ 4.3)} \times 100\%$$

The series of L-polylysine (K10, 20, 30, 40 and 100) (**10**) are synthesized from the compound **5**. The Methyl amine is used as initiator for polymerization of NCA monomer **5** gave compound **9** with good yield. The salts of compound **10** is obtained from **9** by using either HCl or HBr/TFA deprotection.

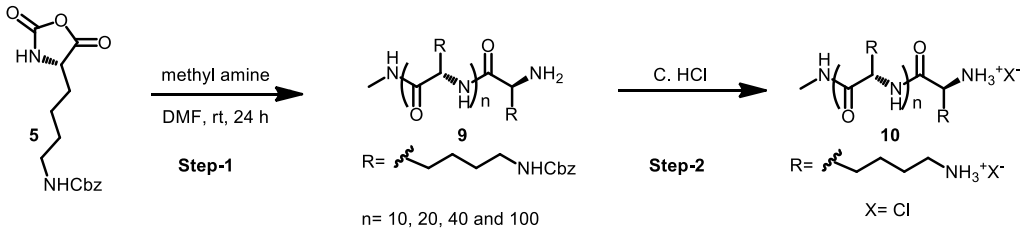

Scheme 4.3 Synthesis of linear polylysine

Synthesis of Lisamine Rhodamine B dye attached CSM5-K5 (12); To a solution of CSM5-K5 (20 mg) in 0.1 M sodium carbonate/bicarbonate buffer (4

mL, pH 9.0) (5 mg/mL) is added Lisamine Rhodamine B sulfonyl chloride (200 µL, 1 mg/mL in DMF) solution under dark envoirnment. The solution is stirred at room temperature for 1 h and dialyzed with cellulose membrane (spectrum chemicals M.W. 1000 Da.) for 2 days and then freeze-dried. (Scheme 4.4)

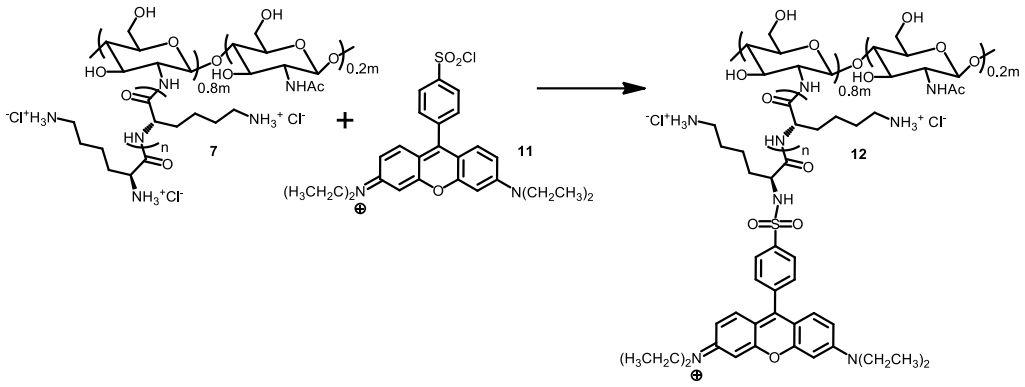

Scheme 4.4 Conjugation of Lisamine Rhodamine B dye on CSM5-K5

Gel Permeation Chromatography (GPC) study of molecular weight; The molecular weight of protected product 4 is measured using HPLC grade dimethylformamide (DMF) with 1mg/mL LiBr addition is used as effluent, with Agilent Polar Gel column. Molecular weight of deprotected product 5 is determined using water phase GPC with acidic buffer (0.5M Sodium acetate and 0.5M Acetic acid, with pH=4.5), with Waters Ultrahydrogel column.

4.2.2 *In vitro* biological activity test

Anti-microbial activity assay

Minimum Inhibitory Concentration (MIC) determination

Bacteria cells are grown overnight at 37 ^{0}C in MHB to a mid-log phase and diluted to 10^5 CFU/ml in PBS. A twofold dilution series of 50µl product solution in the broth is made on 96-well microplate, followed by the addition of 50µl

bacterial/fungal suspension (10^4 to 10^5 CFU/mL). The plates are incubated at 37 ºC for 18-24h (28 ºC, 36-48h for fungi), and the absorbance at 600nm is measured with a microplate reader (BIO-RAD Benchmark Plus, US). Positive control is without product, and negative control is without bacteria/fungi inoculum. MICs are determined as the lowest concentration that inhibited cell growth by more than 90%.

Cytotoxicity assay

a) Mammalian Cell Biocompatibility test via MTT cell proliferation assay; The mammalian cell biocompatibility test is done according to the published protocol using 3T3 cells. In a 96-well plate, 3T3 cells are co-cultured with polymer at cell concentration of 1×10^5 cell per well. The viability cell co-cultured with polymer at concentration 100µg/mL and 200µg/mL are tested via incubation with the polymer at 37C for 24h. The culture medium is then removed. The well is washed by PBS followed by addition of MTT solution and incubated for 4 h. The MTT medium is then removed. 100µL of DMSO is added to the well. The plate is shaken at 100rpm for 15mins. The cell viability is measured as absorbance at 570 nm for each well.

b) Hemolytic activity test; Fresh human blood is collected from a healthy donor (age 23, Male). 1mL blood is mixed with 9mL Tris buffer (10 mM Tris, 150 mM NaCl, pH 7.2) and centrifuged at 1000 rpm for 5 min. Red blood cell (RBC) pellet is collected and subsequently washed with Tris buffer three times and diluted to a final concentration of 5% v/v. 50µL of antimicrobial solution at different concentrations mixed with 50µL red blood cell stock are added to a 96-well

microplate and incubated for 1 h at 37 ℃ with 150 rpm shaking. The microplate is centrifuged at 1,000 rpm for 10 min. 80 mL aliquots of the supernatant are then transferred to a new 96-well microplate and diluted with another 80 mL of Tris buffer. Hemolytic activity is determined at 540 nm with a 96-wells plate spectrophotometer (Benchmark Plus, BIO-RAD). Triton X-100 (0.1% in Tris buffer) which is able to lyse RBCs completely is used as positive control, while Tris buffer is used as negative control. The hemolysis percentage (H) is calculated from the following equation:

$$hemolysis\% = \frac{[(O_p - O_b)]}{[(O_t - O_b)]} \times 100\% \qquad (1)$$

where Op is the absorbance for the antimicrobial agent, Ob is the absorbance for the negative control (Tris buffer), and Ot is the absorbance for the positive control of Triton X-100.

4.2.3 *In vivo* biological test

In vivo Toxicity test to determine LD_{50}

Six- to eight-week-old male wildtype BALB/c mice purchased from the *In Vivos* Pte Ltd, Singapore are used in all *in vivo* study, with five animals per group. Mice are allowed to acclimatize to laboratory conditions for a week before starting the experiment. Drinking water and food are provided throughout the experiment, except for the short fasting period where the drinking water is still in free access, but no food supply is provided 12 h prior to treatment. The toxicity of polymers is evaluated in mice according to the procedures outlined by the Organization for Economic Co-operation and Development (OECD). Two different doses 50 and

100 mg polymer/kg body weight respectively (dissolved in sterile PBS) are administered by the intraperitoneal route (IP) mice in the treatment group while the control group are received sterile PBS. The mice are observed in detail for any indications of toxicity effect within the first four hours after the treatment period, and daily further for a period of 14 days. Surviving animals are weighed and visual observations for mortality, behavioral pattern, changes in physical appearance, injury, pain and signs of illness are conducted daily during the period. The dosage that killed 50% of the experimental animals within 24 h is taken as the LD50 value.(Lorke, 1983)

Incisional Wound Model

The C57BL/6 female mice with 6-8 weeks' old are anaesthetized, depilated and full thickness incision wounds (1-1.5 cm length) will be inflicted on the dorsal area. This is most easily done using a curve scalpel. Approximately 1 x 10^7 CFU of S. aureus in 20 µL PBS will be topically inoculated. The wounds will be treated topically with antimicrobial compounds (8×MIC, 12×MIC, and 20×MIC), while the control mice are treated with saline/vehicle. The wounds will be covered using Tegaderm transparent film. The mice will be placed carefully into the cages. You can clip the ear for easier subsequent identification. After 24h post injury, animals are euthanized with CO_2. The wound skin tissues, including 5 mm of the peripheral region, will be excised. The skin tissue will either be bisected or trisected. .

1) **Bacterial count**: The skin will be placed in PBS and then vortexed at maximum speed for 5 min. Samples are serially diluted and plated on LB agar plates. CFU are enumerated after 24 h of incubation at 37°C.
2) **Fluorescence-activated cell sorting (FACS)**: One end of the skin section will be subjected to tissue dissociation. Single-cell suspensions from wound samples will be obtained using MACS Dissociator (Miltenyi Biotec). The digested tissue solution will be gently filtered through a 40µm nylon filter cup by gravity. The single cell suspension is pelleted and transferred to a 1.5 mL microfuge tube. It is then resuspended and blocked in 1 mL of 3% BSA (in PBS) on ice for 30 minutes. Cells are then probed with the fluorescence-labelled antibodies CD11b and Ly6G (Miltenyi Biotec) in the dark for 30 minutes on ice, followed by wishing using PBS buffer. The washed pellet is then re-suspended in 300µL of PBS for flow cytometry using Accuri C6 flow cytometer (BD Biosciences). Data analysis is performed using Flowjo software version 7.6.5 (Tree Star).

4.2.4 Characterizations

Light Scattering study of polymer aggregation; The Light Scattering study of polymer aggregation as well as interaction with liposome are both carried out using BI-200SM light scattering system, Brookhaven instrument. Detailed methods are summarized in Appendix A1-A4

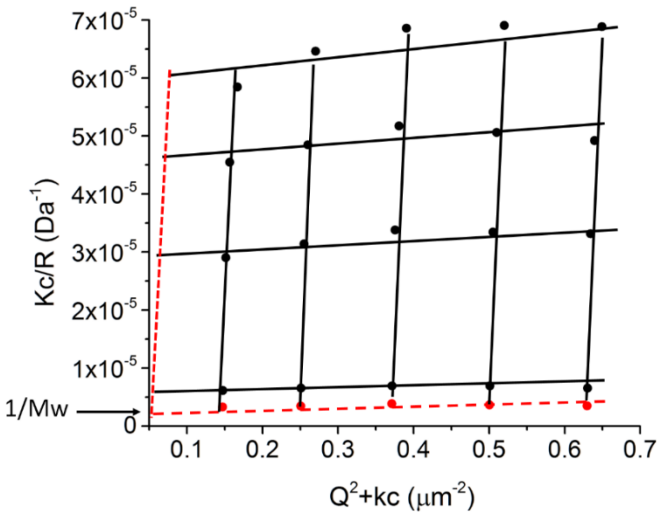

Figure 4.7: Zimm plot of CSM5-K5

The average molecular weight of CSM5-K5 nanoparticle is:

$$Mw = \frac{1}{0.248 \times 10^{-5}} = 403325Da$$

Therefore, the average aggregation number of CSM5-K5 nanoparticle is:

$$N = \frac{Molecular\ weight\ of\ CSM5-K5\ nanoparticle}{Molecular\ weight\ of\ CSM5-K5} = \frac{403325Da}{3648Da} = 110$$

The molecular weight of CSM5-K5 is based on GPC study.

Determination of (R_h) Hydrodynamic Radius using Correlation functions measured by dynamic light scattering:

The intensity autocorrelation functions of light scattered by the copolymer were measured at angles: 45, 60, 75, 90, 105,120, 135 and 150.

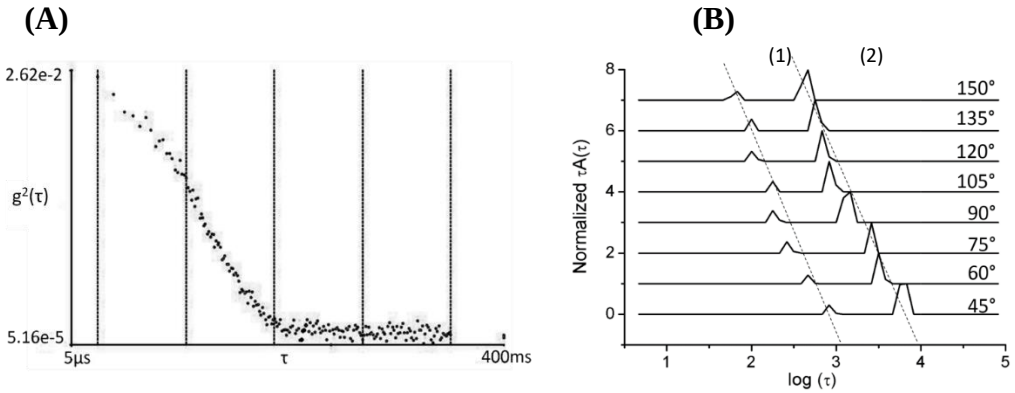

Figure 4.8 The mathematical analysis of dynamic light scattering followed method presented by Schillen *et al*(Karin, Wyn, & Robert, 1994): (A) Autocorrelation function of scattered light ($g^2(\tau)$ vs τ) measured at 90 degrees. The τ scale is logarithmic; (B) Normalized relaxation time distribution function $\tau A(\tau)$ $vs.\log(\tau)$ at different angles (θ) (45, 60, 75, 90, 105,120, 135 and 150)

The autocorrelation functions (Figure 4.8A) were processed using GENDIST package. The autocorrelation function was firstly processed by Regularized Inverse Laplace Transformation (RILT), to obtain relaxation time distribution functions ($\tau A(\tau)$ $vs.\log(\tau)$) at different angles (Figure 4.8B).(Karin et al., 1994)

Circular Dichroism Measurement; Far-UV Circular Dichroism measurement is done at 298.13K in DI water solution, with 0.4mM concentration based on amine unit. The wavelength measured is 190nm to 260nm.

Surface charge characterization of polymer; The surface charge of polymers is characterized in solution in PBS buffer, which provides a constant pH environment (pH=7.4, physiological pH) using Malvern Nano ZS sizer. The polymers are prepared based on 1mM amine concentration.

pH-potentiometric titration; pH titration is performed according to this reference (C. Wang, 2000)with modification. A polymer solution of 5mM actual

amine repeat unit in the polymer is prepared in 0.01M NaOH solution (with pH=12). 15 mL of the prepared solution is titrated with 10μL droplets of 0.1M HCl until pH reached 2. The pH potentiometer used is 809 Titrando, Metrohm. The pH and conductivity of the solution in the beaker changed with addition of HCl and is plotted. The protonation degree of amine groups on polymer is calculated by the conductivity curve between 2 inflexion points where the onset of the plateau is denoted as 0% protonation (α=0), and the onset of the rise of conductivity with further acid addition as as 100% protonation (α=1)

The acidic dissociation constant (pKa) value is calculated based on the pH value corresponding to each degree of protonation via Henderson-Hasselbalch Equation:

$$pK_a = pH + \log\left(\frac{1-\alpha}{\alpha}\right) \qquad (2)$$

The pK_α values at α=0 and α=1 cannot calculated directly from Henderson-Hasselbalch equation; therefore, are estimated by graphic extrapolation of the curve pK_α against α.

Inner cytoplasmic membrane depolarization

The inner cytoplasmic membrane depolarization activity of polymer is determined by using the membrane potential-sensitive fluorescent dye 3,3'-Dipropylthiadicarbocyanine Iodide(diSC3-5). *E.coli* K12 and *S.Aureus*29213 bacteria are harvested at mid-log phase, washed three times with HEPES buffer (20 mM glucose and 5 mM HEPES, pH 7.4). The bacteria are re-suspended to O.D 600 of 0.2 in the HEPES buffer with additional 0.1 M KCl to equilibrate the

cytoplasmic and external K^+, For Gram-negative bacteria, additional 0.2mM of EDTA solution is added to remove the outer cytoplasmic membrane. Subsequently the bacterial suspensions are diluted to 10^6 CFU/mL and incubated with DiSC3(5) (20nM) until the dye is incorporated into the cell membranes. Fluorescence is recorded for subtraction with Perkin Elmer LS-55 luminescence spectrometer (excitation λ = 620 nm, emission λ = 670 nm, High stirring speed), then polymers are added at a concentration of 100μg/ml, and the fluorescence is also recorded. Triton X-100 solution is used as positive control to completely depolarize the inner cytoplasmic membrane.

ATP bioluminescence assay of cytoplasm membrane interruption

The overnight culture of E. coli K12 and MRSA BAA-40 were firstly prepared by picking a few colonies from bacteria streaked plate into 10mL of fresh MHB broth. The MHB broth were incubated overnight at 37oC, 200rpm in an incubator. The subculture was prepared by diluting overnight culture to 0.01 in fresh MHB media and grown until OD600 of 0.2 reached. Bacteria were washed at 3800rpm for 10mins and resuspend the bacteria pellet with fresh MHB and adjust the starting OD of bacteria inoculum, OD600: 0.2 (108cfu/mL). Aliquot 200uL of bacteria suspension into each well of 96-well flat bottom clear plate incubated with corresponding antibiotics. After 1hour of incubation, transfer 50uL of bacteria suspension into each well of 96-well black clear bottom plate. Add 50uL of Luciferase reagent and take the luminescence readings immediately at 135 gains.

Outer cytoplasmic membrane depolarization

The outer cytoplasmic membrane depolarization activity of polymer is determined by using the membrane potential-sensitive fluorescent dye 1-N-Phenylnaphthylamine (NPN). *E.coli* K12 and *P aeruginosa* O1 bacteria are harvested at mid-log phase, washed three times with HEPES buffer (5 mM HEPES, pH 7.4). The bacteria are resuspended to a O.D 600 of 0.2 in the HEPES buffer. Subsequently the bacterial suspensions are 10^6 CFU/mL and incubated with NPN (20nM). Fluorescence is recorded for subtraction with Perkin Elmer LS-55 luminescence spectrometer (excitation λ = 350 nm, emission λ = 420 nm, high stirring speed), then polymers are added at a concentration of 100µg/ml, and the fluorescence is also recorded. Polymyxin B with same concentration as polymer (100µg/ml) is used as positive control.

Stimulated emission depletion microscopy (STED)

To prepare samples for super resolution STED microscopy, cells from logarithmic phase cultures are pelleted by centrifugation at 3,000 X *g* for 10 min, suspended in culture media at a concentration of 10^8 CFU ml^{-1} and incubated for 1 h in the dark with the chitosan grafted copolymer (CSM5-K5). Membrane stain FM1-43FX (5 µg/ml; Life Technologies) is added to the samples for 5 min, as suggested by the manufacturer, before wishing the cells three times with PBS and resuspending in a fixative solution of 2% paraformaldehyde in PBS [pH 7.0]. Cells are fixed for 2 h at room temperature, washed three times in PBS and applied to a sterile glass bottom collagen coated dish (MatTek Corporation).

STED super resolution microscopy is performed on a Leica TCS SP8 STED-3X (Leica Microsystems, Wetzlar, Germany) at SingHealth Advanced Biomaging Core. Further image processing required deconvolution, which is done using Huygens Professional software (Scientific Volume Imaging, Hilversum, Netherlands). ImageJ is utilized for further image processing.

Preparation of Liposome models; The combinations of different lipids such as 1-palmitoyl-2-oleoyl-sn-glycero-3-phosphocholine (POPC); palmitoyloleoyl phosphatidylglycerol (POPG) and Lipopolysaccharide (LPS) are used to model the cell membrane from different class of cells. The cell membrane from mammalian cell is modeled by pure POPC lipid. The outer cell membrane of Gram-negative bacteria is modeled by combined POPC to LPS ratio at mass ratio 4:1. The cell membrane of Gram-positive bacteria is modeled by combined POPC with POPG as mass ratio 4:1 also.

Typically, the preparation of liposome model is carried in scale of 10mg. 10mg of lipid is dissolved in methanol/chloroform (v/v=3:1). The solution is then evaporated. The residue is re-suspended in 1ml of 10mM potassium phosphate buffer solution. The suspension is sonicated for 2hrs for more evenly dispersed in buffer. After sonication, the suspension is frozen in liquid nitrogen and thaw in 40C water. The freeze-thaw process is repeated for 5 times. The suspension is filtered using 200nm polycarbonate membrane for 10 times. The prepared liposome suspension is kept in 4C. Liposome suspension is diluted 100 times when used for light scattering measurements.

Isothermal Titration Calorimetry

Isothermal titrations are performed using PEAQ-ITC from MicroCal Malvern. Both polymer and liposome are dispersed in MES buffer at pH=6.5. The background Gibbs energy change is firstly tested using 2μL of polymer solution titrated against MES buffer (Supplementary). Then, 2μL of polymer solutions are added from syringe to 270μL liposome solutions in the cell at 150s interval with 750rpm stirring speed. Overall, 19 injections are performed. The temperature is kept at 37C with reference power set at 10μcal/s. The concentrations of polymer and lipid are adjustable parameters. Thermodynamic parameters are determined from Gibbs free energy equation:

$$\Delta G = \Delta H - T\Delta S = -RT\ln K_D \qquad (3)$$

Where ΔG is Gibbs free energy for binding, ΔH is enthalpy change of binding, ΔS is entropy change of binding. K_D is the association constant.

Light Scattering of polymer binding with different liposome model; The different liposome suspension is firstly prepared as described. 100μg/mL of polymer solution is then mixed with liposome suspension; the mixture is allowed to stabilize for 20mins. Dynamic Light Scattering is then carried out.

4.3 Results and Discussion

4.3.1 Synthesis

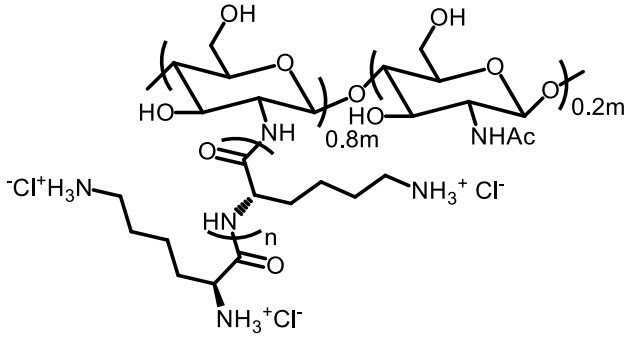

Figure 4.9 Schematic of CSM5-K5 (the design structure, unless otherwise stated, where n is repeat units of lysine of side chain polylysine, m is repeat unites of glucosamine in chitosan backbone)

CSM5-K5 (Figure 4.9) is synthesized via a several step reactions involving the protection of CS, N-Carboxyanhydride (NCA) polymerization from the $–NH_2$ group on the CS backbone followed by deprotection. The molecular weight of CSM5-K5 measured by water phase GPC and MALDI-TOF is 3648/4084 Daltons (Mn/Mw) and 1450 Daltons respectively (Table 4.1, Figure 4.10 and Figures 3.11). The actual structure obtained is likely to be $(GlcN\text{-}K5)_1$-$(GlcN)_4$ (where GlcN is a glucosamine repeat unit) with totally 5 repeat units of glucosamine (Figure 4.11) and is presented by the short name: **CSM5-K5**.

(A) (B)

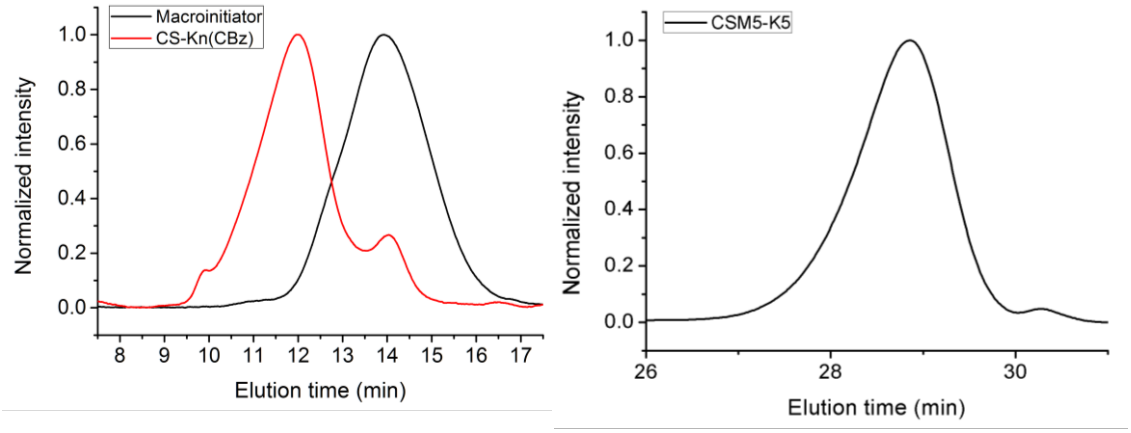

Figure 4.10 (A) Summary of DMF phase GPC spectrums for the protected chitosan-grafted polylysine. (B) Summary of water phase GPC spectrums for deprotected chitosan-grafted polylysine via HCl deprotection method

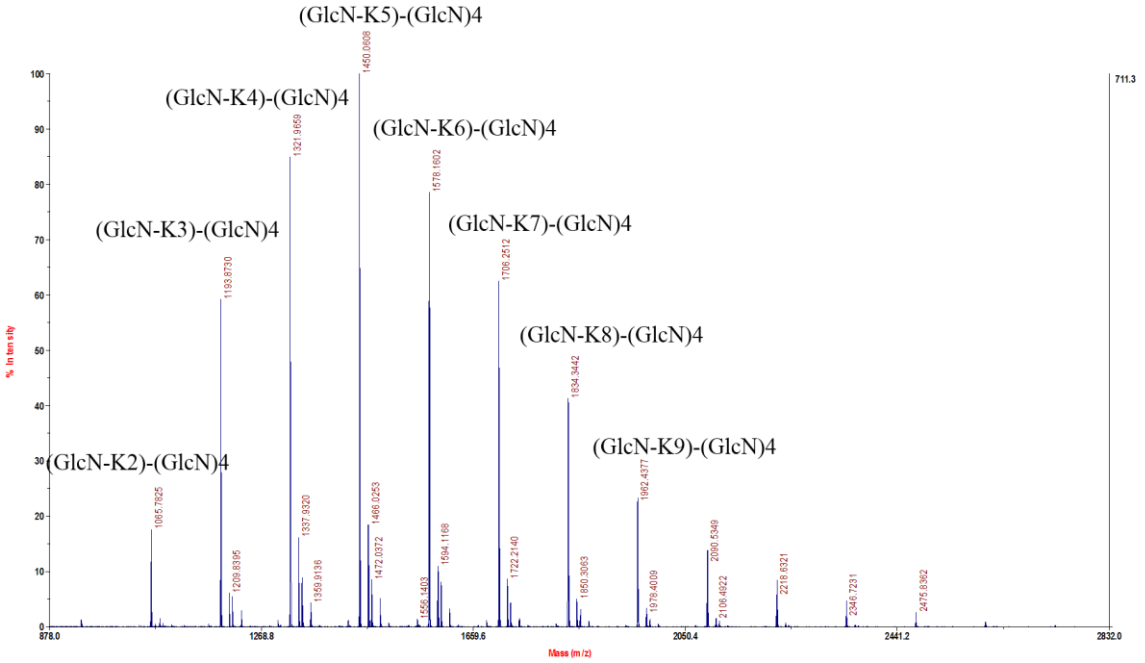

Figure 4.11 Maldi-Tof Spectrum of CSM5-K5

Table 4.1 Molecular weight and Light scattering study of CSM5-K5, and K100

Polymer	M_n[†]	M_w[†]	R_h for individual polymer (nm)	Polymer aggregates (DI water, pH=7)		
				R_g (nm)	R_h (nm)	Aggregation number
CSM5-K5	3648Da	4084Da	7.75	42.7± 3.4	36.5± 3.5	110[$]
K100	10947 Da	12522 Da	9.25	No aggregation		

[†]Using GPC

[$]Based on M_n from GPC

4.3.2 Antimicrobial Efficacy

From Table 4.2, we see that CSM5-K5 is broad spectrum active with bactericidal activity even against various pathogenic strains; the MIC against Gram-positive multi-drug resistant S. aures and Gram-negative *E. coli K12* and *P. aeruginosa* PA01 (Table 4.2 series 1) are 16, 16 and 64 μg/mL respectively. The cytotoxicity of CSM5-K5 series against 3T3 fibroblast cells as well as human red blood cell hemolysis test are also measured (Table 4.2 series 1). The 3T3 cell viability with 100μg/mL co-polymer is above 70% which is biocompatible. The CSM5-K5 co-polymer also has 10% hemolytic concentration (HC10) above 5000μg/mL (Table 4.2 series 1) indicating that it is relatively non-hemolytic compared to most AMPs(Helio S. Sader, 2004; Kevin J. Hallock, 2003). A series of linear poly(L-lysine) (denoted by K10, 20, 30, 40 and 100) is also synthesized by NCA polymerization (Scheme 4.3) for comparison with CSM5-K5; this series shows poor bactericidal activity, though good fibroblast cell compatibility (Table

4.2 Series 2). This series also have low hemolytic activity, suggesting good hemocompatibility.

The *in vitro* cytotoxicity against 3T3 fibroblasts and human red blood cell hemolysis were also measured; the 3T3 cell viability with 100 μg/mL CSM5-K5 is 83.4% indicating good biocompatibility. The CSM5-K5 copolymer has 10% hemolytic concentration (HC10) above 5000 μg/mL (1hr and 8hr treatment) indicating that it is highly non-hemolytic compared to most AMPs. The *in vitro* immunomodulatory ability of CSM5-K5 to prevent LPS/LTA-mediated activation of TLR4/TLR2 is proved by measurement of pro-inflammatory cytokines secretion (IL-6, IL-8 and TNF-α) from cultured macrophage cells. We see that LPS and CSM5-K5 both individually induce the secretion of IL-6, IL-8 and TNF-α secretion by the macrophages (Figure 4.12). With LPS mixed with CSM5-K5 at 1:1 weight ratio, the cytokines secretions are lower compared with only LPS or CSM5-K5, suggesting that CSM5-K5 nanoparticle can suppress the cytokines secretion caused by LPS, which is a common endotoxin found in bacterial infection.

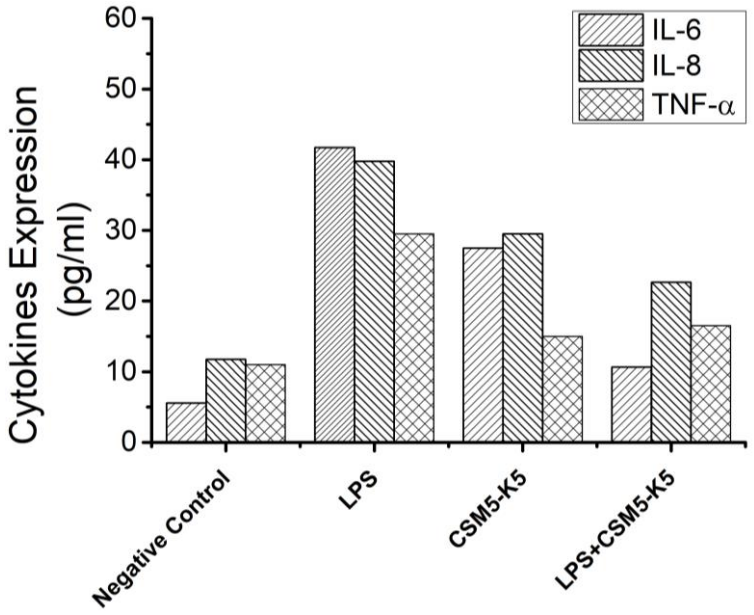

Figure 4.12 *In vitro* cytokines secretion from macrophages by LPS, CSM5-K5 nanoparticle and their combination; negative control is macrophage cells without addition of LPS or CSM5-K5.

Compared with other common antimicrobial peptides such as Magainin-2, LL-37, melittin, and polymyxin B (Table 4.2 series 3), CSM5-K5 shows better antimicrobial activities. CSM5-K5 has comparable MIC against Gram-negative bacteria than melittin but the latter is rather hemolytic. CSM5-K5 has better MICs than Maginin-2 and LL-37 and these latter two peptides show no antimicrobial activity against Gram-positive bacteria, such as *S. aureus*; the biocompatibility with fibroblasts of CSM5-K5 is comparable to LL-37, a peptide from the human immune system. Furthermore, all the reported AMPs are Gram-selective or hemolytic, unlike CSM5-K5. We also determined the MIC of CSM5-K5 copolymer in human blood. The MIC of CSM5-K5 in blood against MRSA is increased a little (1-2-fold) but with E. coli. it is quite drastically increased by 3-fold.

After the balanced antimicrobial activity and biocompatibility is proved, more bacteria strains were tested and summarized in Table 4.3. The CSM5-K5 has excellent antimicrobial activity against clinically found *S. aureus* bacteria.

Table 4.2 Antimicrobial Activity, mammalian cell biocompatibility and hemolysis of Chitosan-grafted Kn series and their comparison to polylysine as well as other published antimicrobial peptides

	Entry	MIC[a] (μg/mL)				[b] %Cell Viability Test with 100μg/mL of compound	Hemolytic Activity (HC10, RBC) (μg/mL)	[c]Selectivity based on HC50
		Gram-negative		Gram-positive				
		E coli K12	P. aeruginosa PAO1	S.aureus 29213	MRSA BAA-40			
1(a)	CS-K2	32	512	32	64	74.32	>5000	>156.25
1(b)	CS-K4	32	512	32	64	75.54	>5000	>156.25
1(c)	CS-K8	16	256	32	64	96.85	>5000	>312.5
1(d)	**CSM5-K5**	**16**	**64-128**	**32**	**32**	**83.34**	**>5000**	**>312.5**
1(e)	CS-K24	16-64	64-128	32	32	64.37	>5000	>312.5
2(a)	K10	>512	>512	>512	>512	96.26	>5000	
2(b)	K20	>512	>512	>512	>512	97.4	>5000	-
2(c)	K40	512	512	>512	>512	86.7	>5000	
2(d)	K100	256	>512	128	128	82.12	>5000	
3(a)	Magainin-2	64	512	512	512	98.22	>500	>7.8125
3(b)	LL-37	512	64	512	512	75.8	-	-
3(c)	Melittin	32	64	8	8	2.16	16	0.5
3(d)	polymyxin B	2	1	32	64	99.64	>2500	>1250

[a] The strains used in this study are: *E. coli* (K12), *P. aeruginosa* (PA01), *S. aureus* (ATCC 29213), *E. faecalis* (ATCC 8739), methicillin-resistant *Staphylococcus aureus* (MRSA, BAA-40), as well as oxacillin resistant *Staphylococcus aureus* (ORSA, USA-300). The MIC value may vary for different strains even same bacteria is tested. [b] Cell Viability is tested against 3T3 cells at 100000 cells per well. [c]Selectivity is HC50/MIC of *E coli* K12. [d]More strains: *E. coli* (ATCC 8730, K12, W3110, UTI89, EC958, and PTR3), *P. aeruginosa* (PA01, and D25), *S. aureus* (ATCC 29213), *E. faecalis* (OG1RF, and V583) are test against CSM5-K5 (Table 4.3).

Table 4.3 MIC (in μg/mL) of CSM5-K5 (and K100) against Gram-positive and Gram-negative bacteria

	CSM5-K5	K100
Gram-positive Strains		
S. aureus 29213	32	128
S. aureus BAA-40 (MRSA)	16	
S. aureus USA-300 (ORSA)	16	
S. aureus MRSA-1	32	
S. aureus MRSA-2	32	
S. aureus MRSA-3	16	
S. aureus MRSA-4	32	
S. aureus MRSA-5	32	
S. aureus MRSA-6	32	
S. aureus MRSA-7	32	
Bacillus subtilis	8	
Enterococcus faecium 19434	128	
Enterococcus faecalis OG1RF	256	
Enterococcus faecalis V583	128	
Gram-negative strains		
E. coli K12	32	256
E. coli W3110	32	
E. coli UTI89	64	
E. coli EC958	64	
E. coli PTR3	64	
E. coli 8739	16	
E. coli 25922	32	
P. aeruginosa PAO1	64	512
P. aeurginosa PAD1	64	
P. aeruginosa PAD25	64	
P. aeruginosa PAW238	64	
P. aeruginosa PAES	128	
P. aeruginosa PAER	128	

Aeromonas salmonicida 33658	16
Salmonella enterica subsp. enterica 13076	64
Vibrio parahaemolyticus 17802	64

The *in vivo* study of CSM5-K5 is firstly carried on toxicity, the lethality of high dosage of CSM5-K5 (50 mg/kg and 100 mg/kg) is examined in an intraperitoneal (IP) injection model. All the mice are alive at these two dosages (Table 4.4), suggesting the good biocompatibility of CSM5-K5 copolymer.

Table 4.4 Summary of symptoms for Lethal Dosage test, Intraperitoneal injection model

Symptoms	CSM5-K5 50mg/kg (2 mice)		CSM5-K5 100mg/kg (2 mice)	
	24 hrs	48 hrs	24 hrs	48 hrs
Alive	Yes	Yes	Yes	Yes
Heartbeat	Normal	Normal	Increased	Back to normal
Hair/weight loss	No	No	No	No
Activity	ok	ok	Reduced activity	Activity recovered
Weakness (e.g. shaking body)	No	No	Yes	Recovered
Swelling	No	No	Yes	Recovered

The *in vivo* antimicrobial efficacy of CSM5-K5 against MRSA (BAA-40) was measured using a murine excisional wound model. The CSM5-K5 treated wounds resulted in significantly lower MRSA bacteria concentration. With a dosage of 2.5 mg/kg of CSM5-K5 applied to the murine wound, the

MRSA burden has a statistical significant lowering of 4.0 orders compared to that of the control without treatment, making it comparable in efficacy to that with vancomycin which is a last resort antibiotic against MRSA (**Figure 4.13A**).

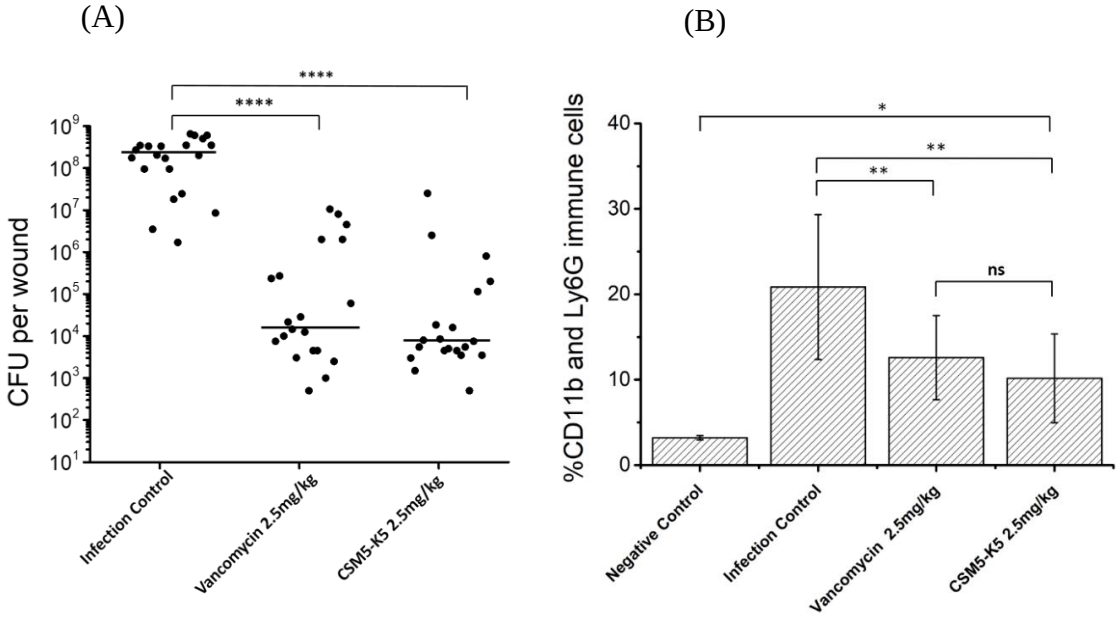

Figure 4.13 (A) *In vivo* test of antibacterial activity of CSM5-K5 in a murine excisional wound model. Bacteria (MRSA BAA-40) concentration (CFU per wound) of control mice is compared with treated mice (the median is presented by the horizontal line for each group). The values are obtained from 3 experimental replicates with **** P≤0.0001, Mann-Whitney test compared to infection control (with bacteria and no treatment). **(B)** The FACS analysis of *in vivo* immune cell neutrophils characterized by positive expression of both CD11b and Ly6G antibody. The values are obtained based on 3 experimental replicates, with **p≤0.01 Mann-Whitney test compared to infection control (CSM5-K5 treated group) and *p<0.1 Mann-Whitney test compared to negative control (negative control is wound without bacteria and without any treatment).

The immune response of the infected skin was also quantified by fluorescence activated cell sorting (FACS) of Lymphocyte antigen 6 complex locus G6D (Ly6G) and CD11b immune cells (neutrophils) (**Figure 4.13B**), where Ly6G is a marker on the surface of neutrophils and may be used for neutrophil detection and quantification, regardless of the cause for neutrophil increase(Joon-Il, Ki-Hyun, & Lester, 2015); CD11b expression of wound tissues

is a marker for leukocytes such as monocytes, neutrophils, natural killer cells, granulocytes and macrophages. The negative control group (*i.e.* wound without bacterial infection and without polymer addition) gives a 3.2% expression of CD11b and Ly6G immune cells, while the MRSA infection group gives 21% expression of CD11b and Ly6G immune cells, suggesting that inflammatory response is caused by bacteria infection. The immune cell expressions were 13 % and 10% for vancomycin and CSM5-K5 respectively, showing statistically insignificant difference between these 2 treatment groups. Comparing CSM5-K5 with the negative control, there was still significant activation of immune cells (*$p<0.1$); however, as compared with infection control mice, CSM5-K5 treated mice shows lower immune cell expression suggesting CSM5-K5 reduces inflammation compared with the untreated wound.

Though research on AMPs in the last one to two decades has been intense(H.-G. S. Robert E W Hancock, 2006), only several AMPs have gone into clinical trials and amongst them are pexiganan, omiganan and OP-145(Fox, 2013). Other promising AMPs in the pipeline against *P. aeruginosa* and *S. aureus* include peptides based on protegrin (Srinivas et al., 2010) and plectasin (Mygind et al., 2005) The antimicrobial activities of these most promising AMPs are comparable to CSM5-K5 but these peptides like omiganan and pexiganan are much hemolytic (HC 10 for omiganan is 100μg/mL(Hyung-Sik Won, 2011) and for pexiganan is 40μg/mL). The high hemolytic tendency of these AMPs is due to the hydrophobic component which is necessary for facilitating the peptide insertion into the bacterial lipid bilayer. Using the liposome model study(Dong-

Kuk Lee, 2013), pexiganan has been shown to cause even more percentage leakage of zwitterionic liposome (POPC, palmitoyloleoylglycero-phosphocholine) which models the human cell membrane than negatively charged liposome (POPG, palmitoyloleoylglycero-phosphoglycerol) which models bacteria membrane due to its hydrophobic component in the peptide chain. On the other hand, CSM5-K5 based on chitosan and lysine has no hydrophobic component and so possesses extremely high hemolytic concentration.

4.3.3 Nanoparticle Formation and Hydrogen Bonding Effect

Using a Dynamic Light Scattering (DLS) setup (where intensity changes with time), we can determine the particle hydrodynamic radius (R_h) from the Stokes-Einstein Equation (1) In an aqueous environment with neutral pH, CSM5-K5 aggregates into nanoparticles with R_h of 36.5±3.5 nm, (**Figure 4.14A**).

From a Static Light Scattering (SLS) setup (where intensity is measured over a short time) to get the plot of intensity reciprocal (I^{-1}) versus wave factor (q^2) and applying the Rayleigh-Debye-Zimm formulism(Cao, 2003), the radius of gyration (R_g) of CSM5-K5 can be obtained; the Rg of CSM5-K5 is measured to be 42.7±5.6nm. The aggregated molecular weight of CSM5-K5 is measured to be 4.03×10^5 g/mol using via a Zimm plot with different polymer concentrations. (The calculation procedure of R_g and R_h follows those of references.(Bahattin & Cigdem, 2013; Yury, Valentina, Olga, Irina, & Ekaterina, 2016)). The nanoparticles are in equilibrium with individual polymer chains with R_h smaller

than 10 nm. The average radius of the polymer nanoparticle determined by TEM is 27.4 nm (**Figure 4.14B**), qualitatively corroborating the size distribution determined by light scattering. The dynamic light scattering studies of CSM5-K5 nanoparticle were also done at different fluids to confirm the stability of the nanoparticle (**Table 4.5**).

Table 4.5 DLS study of CSM5-K5 in different solvent and different concentrations

Concentration (µg/mL)	Hydrodynamic Radius (R_h) in nm			
	DI water (pH=7)	PBS buffer (pH=7.4)	Urea (8M)	Acidic condition (pH=3.5)
1000	36.5±3.5	48.7±5.5	122±3	6.5±0.4
100	34.8±2.6	30.4±2.4	6.4±0.8	5.1±0.4
10	6.1±0.5	8.1±0.7	6.1±0.9	3.5±0.7

From the light scattering study, if the Rg/Rh greater than 1, we can infer that the polymer forms a Gaussian's chain aggregation(Burkhard, Dirk, Martin, & Kurt) . The CSM5-K5 has R_g/R_h ratio of 1.17 combined with average aggregation number of 110 indicate that our nanoparticle is probably a Gaussian's chain aggregation(Shinpei Yamamoto, Muhammad Ejaz, Yoshinobu Tsujii, & Fukuda, 2000). As the solution pH value was reduced below 3.5, the aggregates disappeared probably due to increased repulsion of the more protonated CSM5-K5 and then only individual CSM5-K5 polymer chains with R_h of 7.75nm were detected by DLS (**Figure 4.14A**). In contrast, linear K100 does not aggregate in solution but rather exists as individual polymer chains with hydrodynamic radius (R_h) less than 10 nm (**Figure 4.14A**).

The circular dichroism (CD) spectra of CSM5-K5 and linear K100 in DI water were also measured (**Figure 4.14C**). CSM5-K5 exhibits a positive band appearing at 218 nm that resembles that of collagen(Norma, 2007; Xinhua, Weihua, Haiyan, Nianhua, & Juxia, 2015) suggesting aggregation of rigid rod-like chitosan backbone which corroborates the particle aggregation detected by DLS.

The computer simulation was performed to understand the interaction forces causing the CSM5-K5 nanoparticle formation. The simulation shows that pairs of the CSM5-K5 copolymer molecules aggregate in solution because of hydrogen bonding between two –NHC(=O) groups, as well as two –OH groups. It appears that dimerization maximizes the hydrogen bonding interaction between 2 chitosan backbones and minimizes the energy of unfavorable side chain Kn-Kn contacts. The computer simulation corroborates the light scattering observation of nanoparticle formation from CSM5-K5.

CSM5-K5 exists as nanoparticles because of hydrogen bonding between two –NHC(=O), as well as between two –OH groups on two chitosan backbones.

pH-potentiometric titration of CSM5-K5 and linear K100 with pH varying from 12 to 2 were performed to track the protonation process. From the pH-potentiometric titration curve, the degree of protonation (α) can be estimated from the plateau region of the conductivity curve (**Figure 4.14D**). The apparent

dissociation constant (pK_α) can also be calculated from the pH-potentiometric curves by the Henderson-Hasselbalch equation (**Figure 4.14D**).

The variation of the apparent dissociation constant (pK_α) with the degree of protonation (α) for both CSM5-K5 and K100 is shown in **Figure 4.14E** and they are quite different. Unlike linear K100, CSM5-K5 is only partially protonated: for example, at neutral pH, the latter is only 46 % protonated. For the linear K100, the apparent pK_α varies linearly with α, suggesting that protonation is a simple one-stage process in which addition of H^+ leads to incremental protonation of the amine groups. In contrast, the plot of pK_α against α for CSM5-K5 shows two regions, one (from pK_α of 13 to around 3) at the initial protonation stage in which pK_α decreases rapidly with increasing α, and a second (for $\alpha > 0.6$, pKa<3) regime in which the pKa change is much slower and the slope of $\Delta pK_\alpha/\Delta\alpha$ becomes much more negative and similar to that of K100 (**Figure 4.14E**). This suggests that there are two mechanisms of protonation for the graft CSM5-K5 copolymer compared to the linear K100 polymer(Michal & Ger, 1997; Stefano, Luigi, Giorgio, & Luciano, 2012): in the first stage, H^+ enters the spaces between the polylysine side chains and in the second stage, protonation of the amine groups on polylysine side chain occurs. At physiological pH (around 7), the CSM5-K5 copolymer aggregates into nanoparticles which can absorb more protons into the interior but when pKa<3, the free protons cause the sharp in the degree of protonation (α) (**Figure 4.14E**); the absorption of protons by CSM5-K5 which is probably due to the branched cationic copolymer structure makes it behave like a “proton sponge” (Michal & Ger, 1997). Additionally, the surface

charges of CSM5-K5 at different pH values were measured in water; protonation of nanoparticle also occurs at the basic pH of 9 indicated by a positive zeta potential of +15mV and increases (to +26.5mV) as pH decreases to 4 and plateaus off, which is consistent with the pH-potentiometric trend (Figure 4.14F).

The surface charges of CSM5-K5 and linear K100 in PBS buffer solution (pH=7.4, *i.e.* physiological pH) and DI water at 3 concentrations (1000, 100 and 10 μg/mL) were determined by zeta potential measurements (**Figure 4.14F**). In both media, CSM5-K5 copolymer possesses higher zeta potential than K100 (**Figure 4.14F**), indicating greater surface cationic charge. The zeta potential values, as well as particle size, in PBS with the 2 higher concentrations were quite close to each other (Table 4.5), suggesting their stabilities under these conditions. The difference in cationic surface charge may be attributable to the aggregated structure of CSM-K5 nanoparticles and to its higher amine concentration density per unit mass. Based on the pH-potentiometric titration, CSM5-K5 has about 2.6 times more amine groups on the polymer backbone than linear K100 (0.121 mole/g versus 0.047 mole/g) (**Table 4.6**). Since there are more amines on CSM5-K5 and it tends to aggregate, whereas K100 remains in the form of individual polymer chains, the overall surface charge density of CSM5-K5 nanoparticle is higher.

Table 4.6 Calculated results of moles of amine per unit weight (mole/g) of polymer

	Moles of HCl used for amine neutralization	Moles of amine/g

K100	0.34	0.047
CSM5-K5	0.91	0.121

The “proton sponge” character with “free” protons within the nanoparticles, together with higher cationic zeta potential (a surface charge measure), would favor the interaction of the copolymer with negatively charged bacteria cell membrane compared to the linear K100 that lacks the “proton sponge” effect(Chuanbao, Jianyuan, Xianmo, & Yu, 2008). Upon binding with the cytoplasm membrane, the excess protons can increase the local osmotic pressure, eventually leading to membrane rupture(Akin, Mini, Alexander, & Robert, 2005). This may be the cause for the higher potency of antimicrobial efficacies of CSM5-K5 versus K100 (**Table 4.2**)

(A)

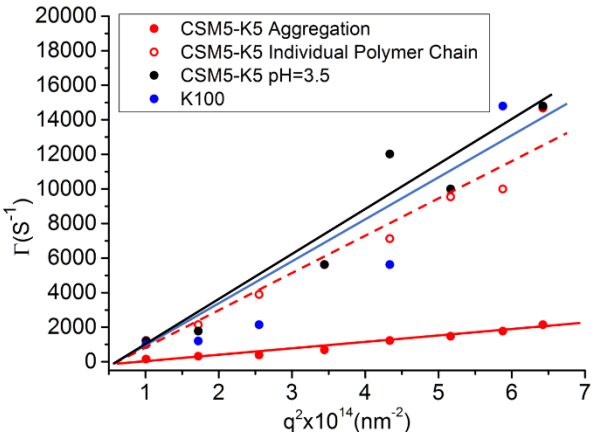

(B)

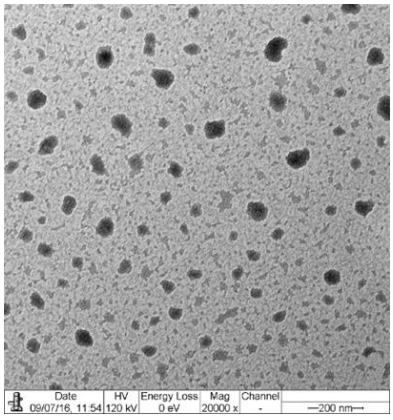

(C)

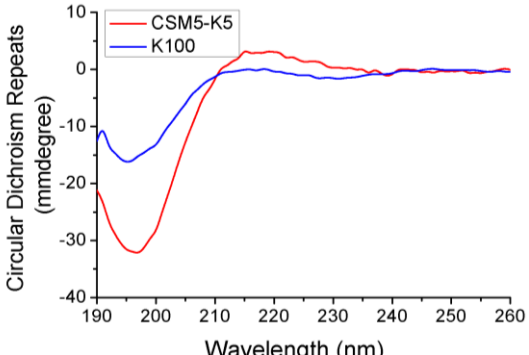

(D)

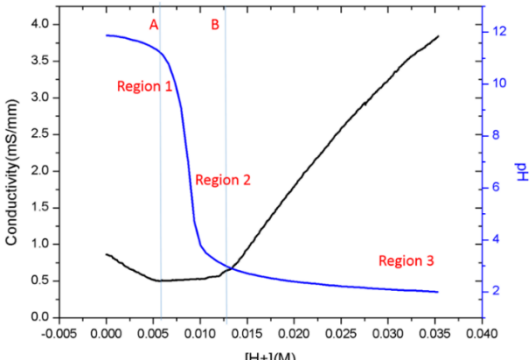

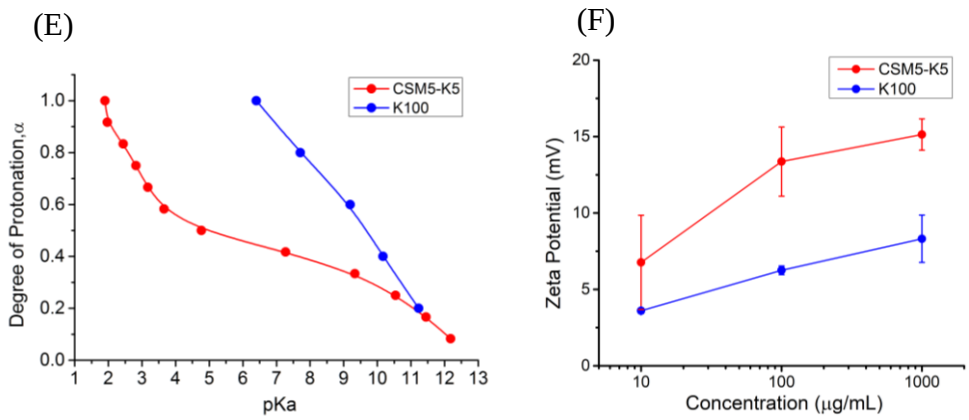

Figure 4.14 Solution properties of CSM5-K5 compared with K100: (A) Dynamic light scattering (DLS) : decay rate (Γ) versus wave vector (q2) for CSM5-K5 suspension at pH=7 (red), CSM5-K5 suspension at acidic pH (pH=3.5) (black) and K100 (blue). The decay rate (Γ) and wave vector (q2) were evaluated based on relaxation function measured at specific angles (B) TEM image of CSM5-K5 at pH=7. (C) CD spectrum of CSM5-K5 vs K100 (D)pH-potentiometric titration of CSM5-K5 (E) Degree of protonation (α) of CSM5-K5 and K100 change versus pKa. (F) Zeta-potential of CSM5-K5 and K100 measured at different concentrations at physiological pH (PBS, pH=7.4).

4.3.4 Proposed Mechanism with membrane assays, TEM and confocal microscopy with bacteria

To further understand the penetration of CSM5-K5 or K100 on bacteria cell membrane, 1-N-phenylnaphthylamine (NPN) and 3,3′-Dipropylthiadicarbocyanine iodide [DiSC3(5)] dye leakage fluorescence assays are performed (Figure 4.14) to study the extent of penetration into the bacterial outer membrane and inner cytoplasm membrane respectively.

The sharp rise of NPN fluorescence intensity shows that CSM5-K5 effectively penetrates the outer membrane of Gram-negative bacteria E. coli K12 (Figure 4.15A) and to a limited extent that of P. aeruginosa PAO1 (Figure 4.15B) but the linear polylysine K100 is ineffective to do so. The DiSC3(5) dye leakage test shows that CSM5-K5 only poorly penetrates the inner membrane of Gram-negative bacteria E. coli K12 (Figure 4.15C) and Gram-positive bacteria S. aureus 29213 (Figure 4.15D) compared to the Triton X100 control. (For P. aeruginosa, the interaction detected by DISC35 is even weaker – data not shown.) Also, CSM5-K5 shows relatively better penetration compared with linear K100. Taken together, CSM5-K5 is membrane-active; it is more effective than K100 in penetrating the outer cytoplasmic membrane of E coli and P. aeruginosa and the inner cytoplasmic membrane of S. aureus. The ATP bioluminescence assays were performed (Figure 4.15E, F) to study the extent of permeabilization into the bacterial inner membrane respectively. The intracellular ATP release test shows that there were only increase of intracellular ATP detected, when both E. coli K12 and MRSA BAA-40 were treated with polymer concentration greater than the MIC values; suggesting the antimicrobial activity of CSM5-K5 nanoparticle is strongly related to cytoplasm membrane interruption. Taken together, CSM5-K5 is membrane-active and is more effective than K100 in permeabilizing the OM of E. coli and P. aeruginosa and the cytoplasm membrane (IM) of E. coli and S. aureus.

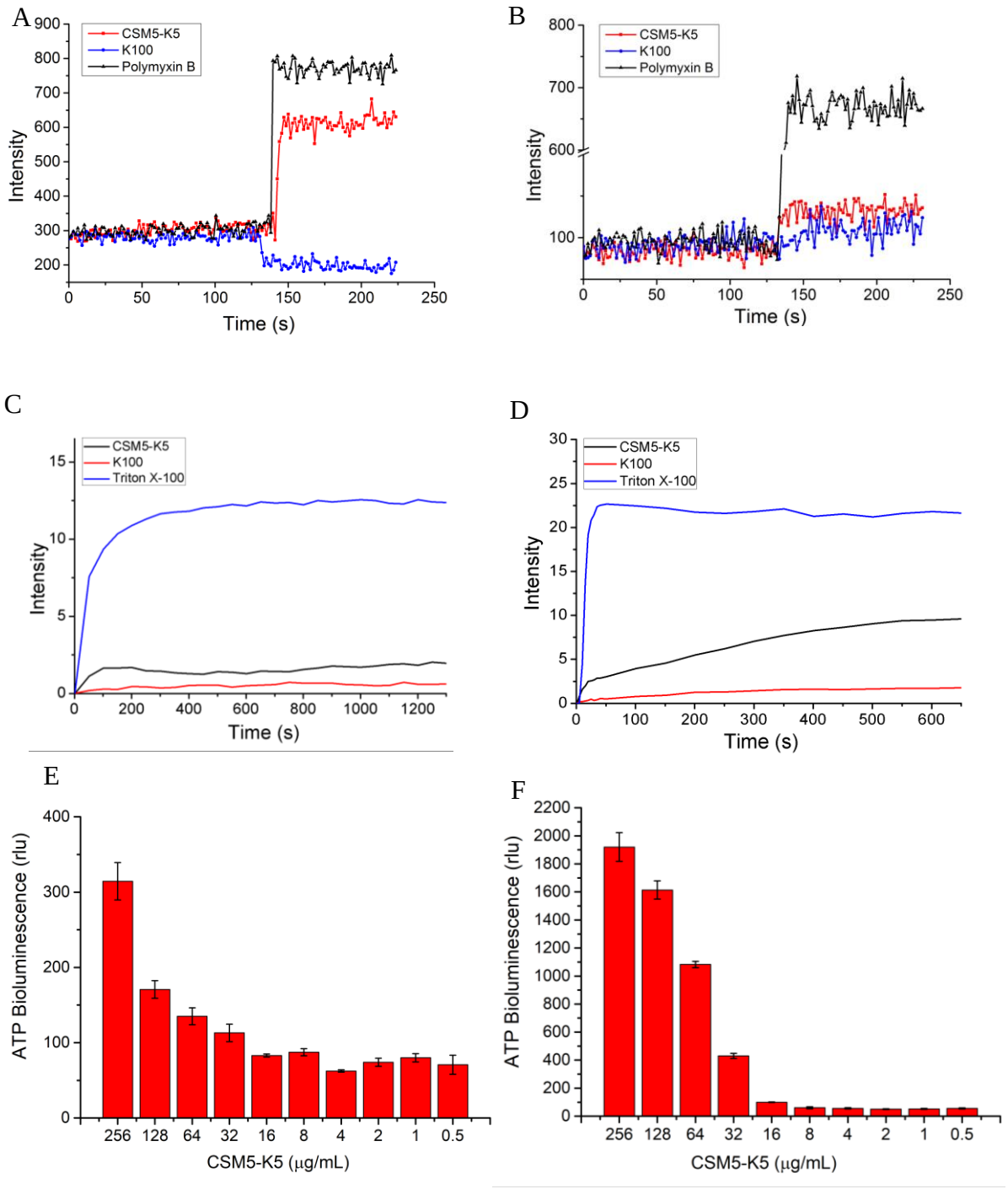

Figure 4.15 NPN dye leakage assay of (A) *E. coli* K12, and (B) *P. aeruginosa* PA01, DISC3(5) dye leakage assay of (C) *E. coli* K12, and (D) *S. aureus* 29213. For DISC3(5) dye leakage assay, triton is used as control to break inner cell membrane completely; for NPN dye leakage assay, Polymyxin B is used as control with same concentration as polymer (100μg/mL) ATPase assay of (E) *E. coli* K12, and (F) MRSA BAA-40.

Super resolution STED microscopy experiments of polymer-treated bacteria are also performed. Lissamine rhodamine B sulfonyl chloride fluorescent dye is used to label CSM5-K5 copolymer (Scheme 4.4) for conducting and studying the localization of the compound within different strains of bacteria treated with it. Two Gram-positive bacteria (*E. faecalis* V583 and MRSA BAA-40) and one Gram-negative strain (*E. coli K12*) are incubated for 1 hour with 50 µg/ml of rhodamine-labeled CSM5-K5 (in red) and the plasma membrane is stained using FM1-43FX probe (in green). For the three strains tested, we observed localization of the rhodamine-labeled copolymer with the bacteria membrane as well as internalization of the compound into the cell cytoplasm (Figure 4.16). MRSA BAA-40 showed the best compound uptake of the three tested bacteria, and the polymer probably enters the disrupted membrane bacteria. Altogether, it is observed that CSM5-K5 copolymer binds to the bacteria membrane and gets internalized into their cytoplasm.

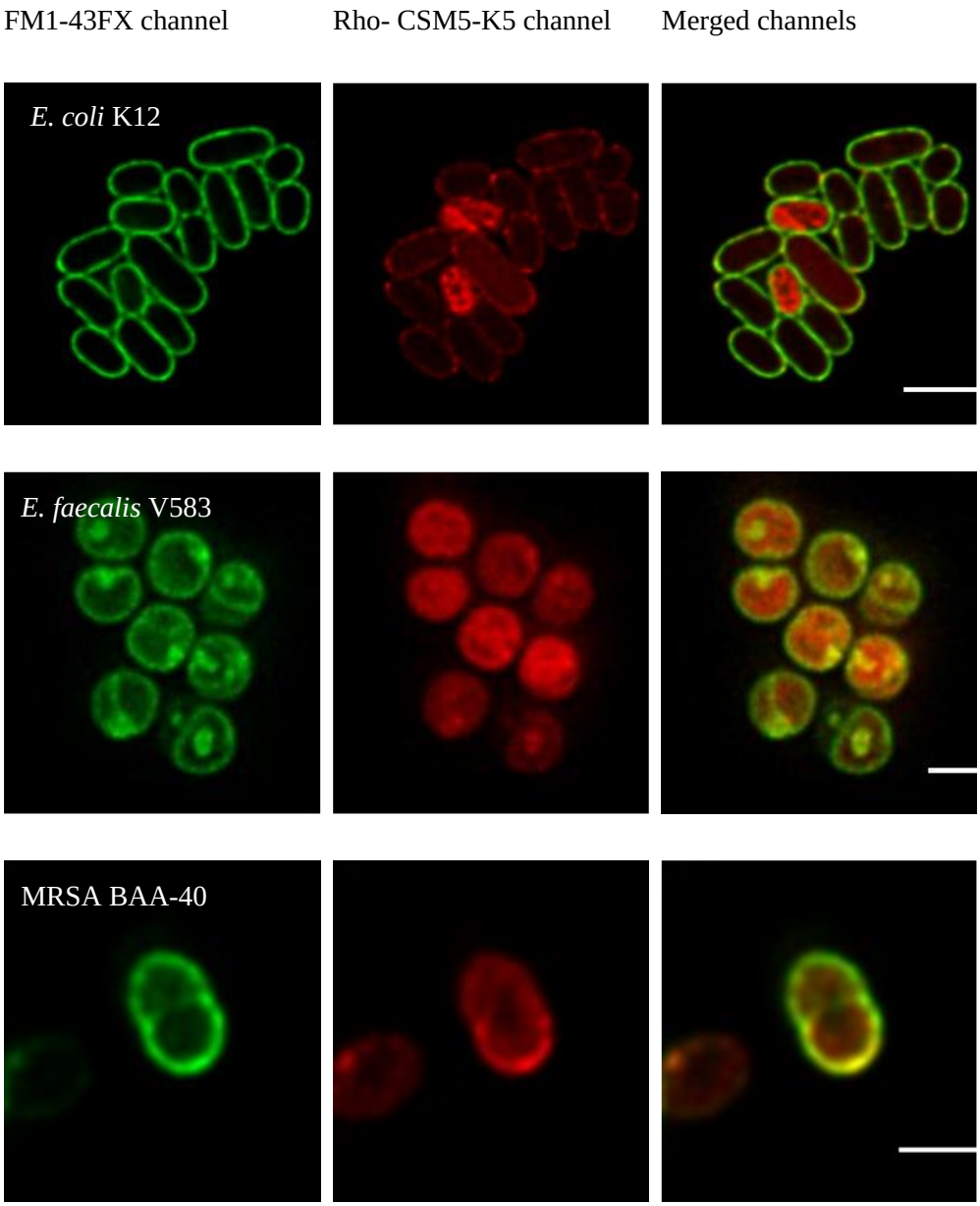

Figure 4.16 Fluorescence microscopy images of *E. coli* K12, MRSA BAA-40 and *E. faecalis* V583 incubated with Rho-CSM5-K5 (first column is the FM1-43FX membrane dye; second column is CSM5-K5 conjugated with Rhodamine dye; third column is the merging of both channels). *E. coli* K12 scale bar = 2 µm. MRSA BAA-40 and *E. faecalis* V583 scale bars = 1 µm.

Next, cryo-TEM is utilized to visualize the effect of CSM5-K5 copolymer on the cytoplasmic membrane of the Gram-positive MRSA BAA-40. Without treatment, the bacterial cell membrane and cell wall are intact (Figure 4.17A);

also, the cell wall is thin and of defined and regular thickness. Figure 4.17B (red circle) shows that after treatment with CSM5-K5, large vesicle space formed between cell membrane and cell wall, suggesting the separation of cell membrane from cell wall(G.W Richter, 1967; Vale´rio R. F. Matias, 2006). The vesicle may be caused by breakage of cytoplasm membrane by CSM5-K5, resulting in leakage and accumulating of low density constituents from the cytoplasm(Vale´rio R. F. Matias, 2006). Also, the damaged cytoplasmic membrane can separate from protoplasm (cell wall) during sample preparation(Vale´rio R. F. Matias, 2006). Membrane ripples are also observed (Figure 4.17C Blue circle), suggesting cell membrane shrinking from cell wall, due to leakage of cytoplasm from dead bacteria (G.W Richter, 1967) caused by CSM5-K5.

We also observed other interesting phenomena with CSM5-K5 treated MRSA that the cell wall become irregular in thickness and generally thicker, and the septum growth is inhibited and cell division is inhibited (Benoıˆt Zuber, 2006) (Figure 4.17D Yellow circle). In untreated cells, we found 17 cases (out of 57 images taken) of cell division whilst in treated cells, we found only 2 cases of cell division (out of 83 images taken). We hypothesize that CSM5-K5 may be "mistaken" by bacterial cells to be lipid II as they are similar in backbone and so it gets incorporated into the cell wall which became thicker(Tsung-Shing Andrew Wang, 2011). We postulate that cell division is impeded by CSM5-K5 due to the thicker cell wall and this has been observed by others(Gaurav Misra, 2013). Also, the disruption of cytoplasm membrane may interrupt the cell division (Figure

4.17D) which requires the invagination of membrane(Wael Elhenawy, 2016) . Further, after treatment with CSM5-K5, the cationic polymer may bind and disrupt the cytoplasmic membrane and possibly the proteins in periplasmic space.(Wael Elhenawy, 2016) It has been reported that *staphylococcus aureus* possess a periplasmic space (termed as inner wall zone, IWZ) between cytoplasm membrane and peptidoglycan (Benoıˆt Zuber, 2006) of cell wall. The periplasmic space is crucial for cell wall synthesis and bacteria cell division, as various enzymes and proteins found in periplasmic space are involved in peptidoglycan synthesis pathway, such as penicillin binding proteins (PBP) which cross-link the glucosamine units in peptidoglycan synthesis. (Benoıˆt Zuber, 2006) Also, in cell wall synthesis pathway, the Lipid II needs to bind to and be modified by the MurJ flippase (Wael Elhenawy, 2016) of PBP anchored on cytoplasmic membrane but this process may be interrupted by the disrupted membrane to prevent cell wall synthesis and septum formation. This type of mechanism has been observed in daptomycin (Anna Müllera, 2016).

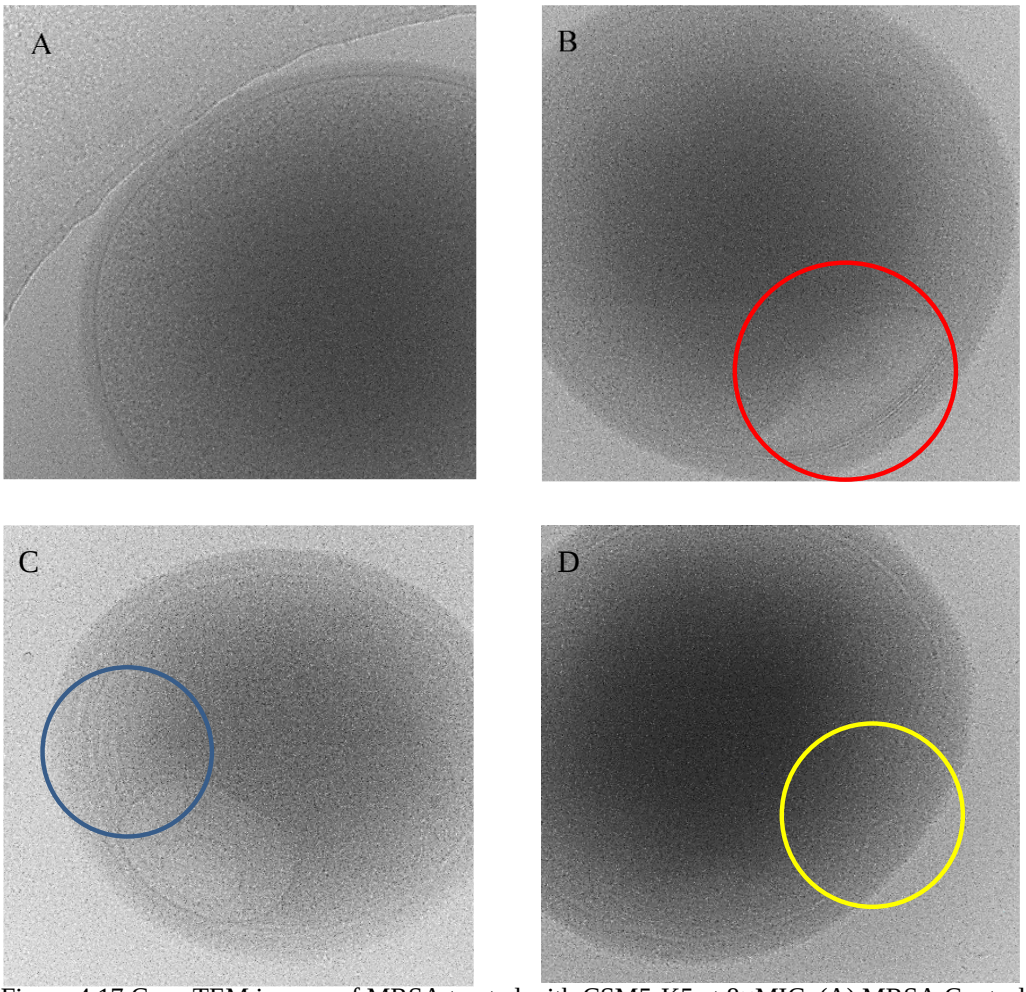

Figure 4.17 Cryo-TEM images of MRSA treated with CSM5-K5 at 8×MIC. (A) MRSA Control without treatment by CSM5-K5; (B) Separation of Cell membrane from cell wall after treatment of CSM5-K5; (C) Shrinking of cell membrane after treatment of CSM5-K5; (D) Irregular cell wall after treatment of CSM5-K5; Scale bar=500nm.

Combining the results from membrane test, confocal microscopy as well as cryo-TEM visualization, CSM5-K5 copolymer can disrupt the cytoplasm membrane of both Gram-negative and Gram-positive bacteria and get internalized into bacteria cytoplasm. Additionally, CSM5-K5 copolymer causes the bacteria cell wall to become thicker and cell division is retarded when observed by cryo-TEM, due possibly to thicker cell wall and disrupted

membrane. The cationic peptidopolysaccharide also causes separation between cell wall and cytoplasmic membrane of bacteria(Hyyryla, ¨inen‡, & Colin R. Harwood§, 2000), possibly contributing to erratic thicker growth of bacteria cell wall, and inhibition of cell division. The peptidoglycan mimic copolymer CSM5-K5 has similar structure and components compared with Lipid II, the peptidoglycan precursor; it may be mistaken as Lipid II and participate in the synthesis route of peptidoglycan cell wall of bacteria(Matthew A. Jorgenson, 2016) (Tsung-Shing Andrew Wang, 2011) as an intermediate compound.

4.3.5 Liposome model of bacteria with CSM5-K5 and K100

a) Isothermal Titration Calorimetry

CSM5-K5 does not have any hydrophobic component unlike many AMPs and we applied Isothermal Titration Calorimetry (ITC) and Dynamic light scattering (DLS) to model membranes for studying the nature of the interaction. Three kinds of liposome models are prepared in this study: the POPC (4): POPG (1) model which represents bacterial inner membrane and POPC (4): LPS (1) model which represents the outer membrane of Gram-negative bacteria. In both models, the liposome is made of 80% of zwitterionic POPC by weight, and either anionic LPS or POPG make-up the rest of weight ratio. As a control, pure POPC liposome is also prepared. To mimic the outer membrane of the Gram-negative bacteria, i.e. E. coli and P. aeruginosa, the respective LPS is used. For both POPC: LPS and POPC: POPG liposomes, ITC shows that the binding is favorable as the Gibbs energy change is negative (Table 4.6). In contrast, pure

POPC liposome shows no change in Gibbs energy hence no interaction with CSM5-K5 copolymer.

Table 4.7 Summary of thermodynamic parameters determined by isothermal titration calorimetry (ITC)

Components	ΔG(Kcal/mol)	ΔH(Kcal/mol)	TΔS(Kcal/mol)	$K_D(10^{-6}M)$	*Binding Site, n
LPS from E coli	-6.21	-0.21	6.00	42	0.392
LPS from P. aeruginosa	-5.20	-1.10	4.10	217	0.296
POPG	-5.86	-8.96	-3.76	75	0.173

*Binding Site, n is determined based on no. of moles of CSM5-K5 polymer binding with no. of moles of liposome.

We see that the favorable interaction of CSM5-K5 with POPC: LPS of E. coli or P. aeruginosa is entropic driven (ΔS is positive) (Table 4.7). The entropic interaction is probably due to attraction of the polyglucosamine backbone of CSM5-K5 to the Lipid A portion of LPS to expel water molecules to cause entropy rise(Jianhui Tian, 2013), suggesting the chitosan backbone is essential for LPS binding. LPS from E coli shows slightly stronger binding affinity (with Ka=23752.97 M^{-1}) as compared with LPS from P. aeruginosa (Ka=4608.29 M^{-1}) probably because E coli has stronger Lipid A interaction because of hydrogen interaction. The overall surface charge on POPC: LPS liposome is -4.5mv determined by zeta-potential measurement; therefore, electrostatic interaction also contributes to the binding with CSM5-K5 corroborated by the enthalpy decrease of the interaction, but it is not the significant interaction. Also, the lower

affinity towards LPS from P. aeruginosa explained the poorer bactericidal activity against P. aeruginosa compared with E coli (Table 4.2 and Table 4.3).

To mimic the Gram-positive bacteria inner membrane (IM), ITC titration of POPC: POPG liposomes show that interaction of the liposomes with CSM5-K5 is enthalpy (electrostatic) driven (Figure 4.18 and Table 4.6), rather than entropic-driven. The proposed electrostatic binding of CSM5-K5 with the IM seems to corroborate the DISC35 test results indicating that the binding does not involve penetrating the IM as indicated by relatively lower fluorescence signal compared with control (Triton X100) which completely remove the IM. The electrostatic basis of binding of CSM5-K5 with IM is also consistent with the trend of larger zeta potential values of CSM5-K5 versus that of linear polylysine. Also, S. aureus has a more anionic IM and hence has a stronger DISC35 interaction with CSM5-K5 than with E. coli.

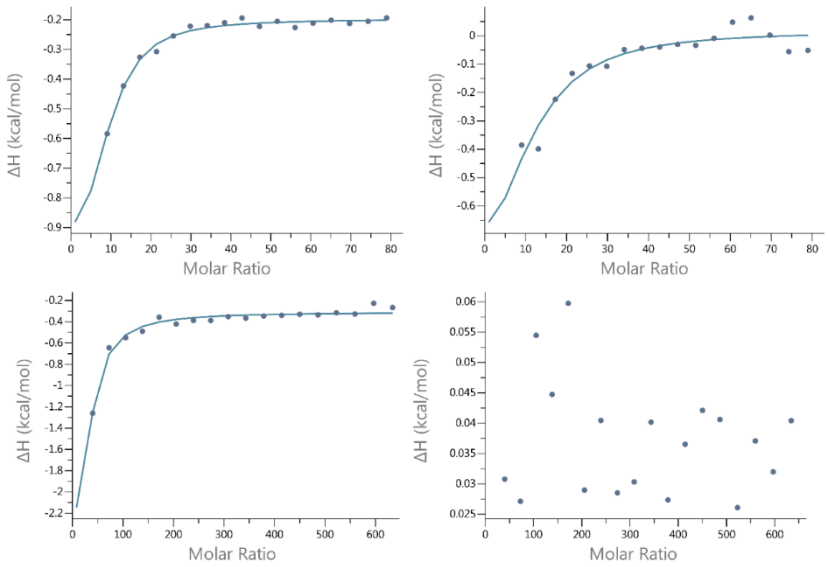

Figure 4.18 Summary of enthalpy profile (kcal/mol) change with mole ratio of polymer added into liposomes determined by isothermal titration calorimetry study of CSM5-K5 interaction with (i) POPC: LPS liposome with LPS from *E coli*; (ii) POPC: LPS liposome with LPS from *P. aeruginosa* PAO1; (iii) POPC: POPG liposome; (iv) Pure POPC liposome

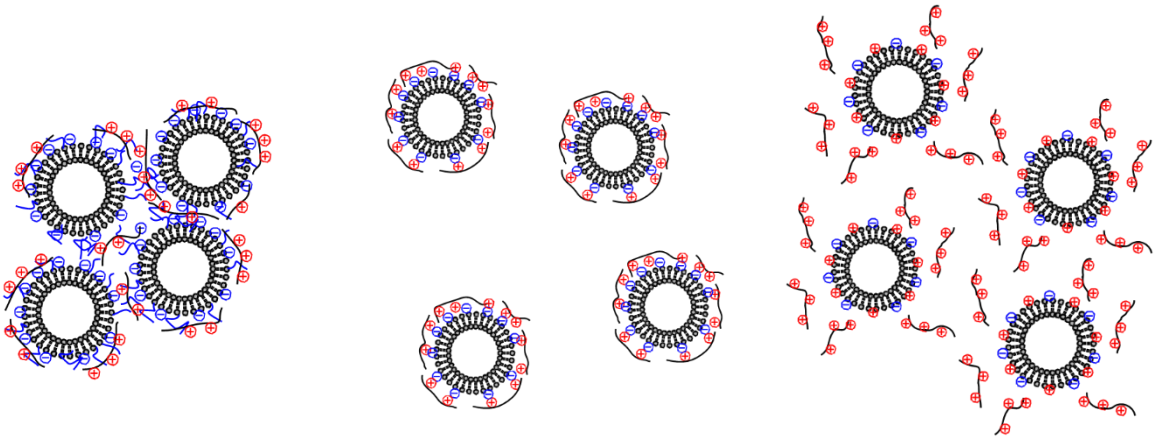

(A) POPC: LPS (B)POPC: POPG (C)Pure POPC

Figure 4.19 illustration of cationic copolymer binding on Liposome models: (A) the polymer has very strong interaction with liposome and cause the aggregation of liposome (POPC: LPS), (B) the polymer can bind with liposome (POPC: POPG), (C) the polymer has no interaction with liposome (Pure POPC).

We also applied dynamic light scattering (DLS) to study the interaction of different liposome models with CSM5-K5. Pristine chitosan (3kDa molecular weight) and linear K100 salt are used as comparison (Table 4.8). Pristine chitosan 3KDa or linear polylysine individually did not cause any change in hydrodynamic radius, indicating negligible interaction. However, CSM5-K5 copolymers show strong binding interaction with POPC: LPS liposome model: the hydrodynamic radii of POPC: LPS liposome incubated with the CSM5-K5 series increase dramatically from around 75nm to 682nm, suggesting strong interaction between the LPS liposome and the copolymer (Figure 4.19A). This result is consistent with the ITC finding that the binding of LPS with CSM5-K5 is thermodynamically favorable. CSM5-K5 also shows some interaction with POPC: POPG liposome model, as the size slightly increase. The polymers might

be absorbed on the surface of liposome (Figure 4.19B). For the pure POPC model, which represent mammalian cells, the interaction with CSM5-K5 copolymer is not significant as the size of liposome shows almost no changes from DLS (Figure 4.19C). Therefore, from DLS interaction mechanism study based on liposome models, CSM5-K5 can selectively targeting cytoplasmic components from both Gram-positive and Gram-negative bacteria.

Table 4.8 Hydrodynamic Radius (Rh) of different liposome interacted with polymer

	POPC: LPS	POPC: POPG	POPC
Control[a]	75.0	60.1	70.0
CSM5-K5	682.0	81.4	70.6
Chitosan 3kDa	75.9	70.0	64.5
K100	69.2	66.2	68.0

[a]Control is pure Liposome only

CSM5-K5 is a unique cationic peptide since it has polysaccharide backbone (chitosan) that determines the aggregation and interacts strongly with bacterial membrane through hydrogen bonding as shown by ITC studies. AMPs, on the other hand, in general destabilize bacteria membrane through hydrophobic interaction and via various models, such as the toroidal model and carpet model. From our biophysical study and computational simulation, CSM5-K5 penetrates bacteria membrane via carpet model. Hyung-Sik et al.(Hyung-Sik Won, 2011) pointed out antimicrobial peptide with carpet model has some advantages in penetrating the outer membrane, of Gram-negative bacteria, as the outer membrane may be a barrier for the toroidal model antimicrobial peptide to penetrate; however, the antimicrobial peptide with carpet model behave similar to detergent and can form micelles with lipid from outer membrane, then

completely remove outer membrane(Yi He, 2013). With this, they explained the better antimicrobial activity of pexiganan compared with omiganan. The carpet model also corroborates that fact that CSM5-K5 has better antimicrobial activity on Gram-negative bacteria than omiganan which is based toroidal model.

4.4 Conclusion

In conclusion, short CSM5-K5 peptidopolysaccharide with only a few (about 5) repeats of chitosan monomer in the backbone can effectively reduce the MRSA bacterial burden in a murine excisional wound model by 4.0 orders of magnitude and can eradicate clinically important MDR MRSA and Gram-negative *E. coli* and *P. aeruginosa* in *in vitro* studies. CSM5-K5 spontaneously self-assembles in water and the consequent concentration of multiple charged polymer chains in a single nanoparticle causes high localized charge density and enhanced bactericidal activity. Hence, the good bactericidal activity of CSM5-K5 is due to hydrogen bonding between chitosan chains and electrostatic interaction with bacteria, and not due to hydrophobic interaction as in most other AMPs. When complexed with bacterial membrane, these highly charged nanoparticles cluster anionic membrane lipids and result in greater membrane perturbation and antibacterial effect than would be achievable by the same quantity of charge if dispersed in individual copolymer molecules in solution. CSM5-K5 does not rely on membrane insertion for its kill mechanism – indeed its lack of hydrophobic content makes such insertion energetically unfavorable –

and so by design it is intrinsically more biocompatible than agents which are able to insert into lipid bilayers. Due to its concentrated charge, it more strongly interacts with anionic lipids than zwitterionic lipids; therefore, by design, more strongly interacts with bacterial membrane than with mammalian membrane.

CSM5-K5 represents a novel approach to rational design of selective peptide-based antimicrobial nanoparticles totally based on hydrogen bonding, rather than hydrophobic interaction, for particle assembly and based on electrostatic interaction without bilayer insertion for membrane perturbation effects. This new approach may accelerate the development of a wide range of next-generation membrane-targeting anti-microbial therapies.

Chapter 5. Synergism between Antibiotics with Cationic Antimicrobial Polysaccharide

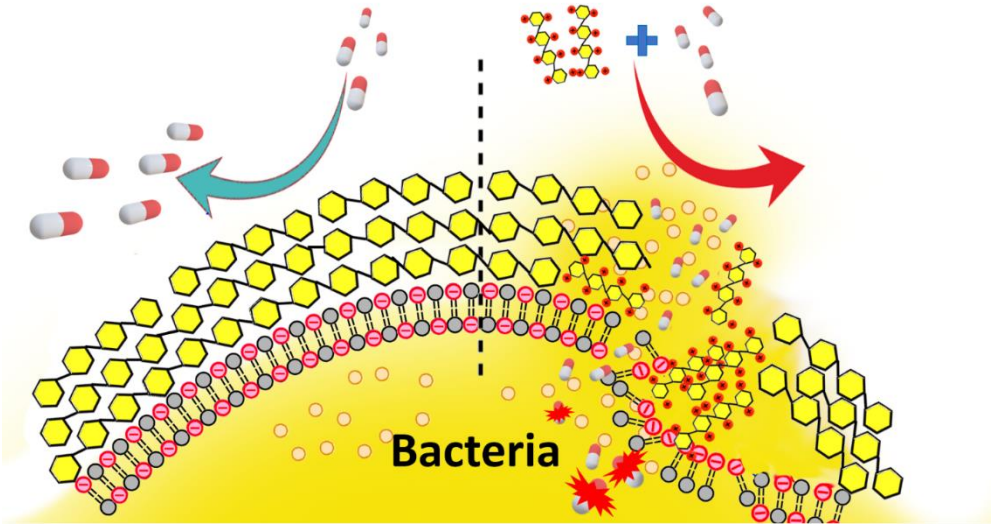

Cationic polymers are attractive as antibacterial agents since they have low propensity for resistance evolution, but they usually have low biocompatibility due to their hydrophobic and cationic moieties. Herein, we reported a new series of antibacterial biodegradable chitosan-derived polymer, 2,6-Diamino Chitosan (2,6-DAC) with excellent broad-spectrum antimicrobial activity, and balanced biocompatibilities due to the absence of hydrophobic moieties. 2,6-DAC shows an excellent antimicrobial activity with minimum inhibitory concentrations (MICs) of 8-32 μg/mL against clinically relevant bacteria including *Staphylococcus aureus, Listeria, E. coli, Pseudomonas aeruginosa* and *A. baumannii*. Further, 2,6-DAC shows excellent synergistic effect with various classes of clinically relevant antibiotics such as DNA gyrase inhibitor (amikacin and Tobramycin), protein synthesis inhibitor (novobiocin) and β-lactamase

inhibitor (Tazobactam) by bringing down their minimum inhibitory concentrations against *A. baumannii* to less than 1µg/mL. Single dose of 100 mg/kg via the oral route to mice does not cause any weight change and a single dose of 25 mg/kg via intraperitoneal injection did not cause any change to the mice liver and kidney biomarkers nor the important electrolyte. A combination of 2,6-DAC (at 25 mg/kg) together with novobiocin (10 mg/kg) and rifampicin (10mg/kg) showed > 2.5 log10 reduction of *A. baumannii* with a murine intraperitoneal and lung infection model. The novel chitosan derivative 2,6-DAC can be utilized as more biocompatible cationic and degradable antimicrobial against broad spectrum of Gram-positive and Gram-negative bacteria, including WHO's CRE-gram-negative bacteria. It has great potential as food rinse or assembled as layer-by-layer surface coating of medical devices.

5.1 Materials

Low molecular weight chitosan (200 KDa), phthalic anhydride, N-methyl pyrrolidinone, N-bromosuccinimide, triphenylphosphine, sodium azide, hydrazine solution, anhydrous *N*,*N*- dimethylformamide, Lisamine rhodamine B sulfonyl chloride, sodium hydroxide, 3,5-amino 1,2,4 triazole, 3-amino 1,2,4 triazole, 5-amino imidazole 4-carbonitrile, spermine, ethylene diamine, diethylenetriamine, Tris(2-aminoethyl)amine, ethylene glycol bis (2-aminoethyl)ether, 1-(3-aminopropyl)imidazole are purchased from Sigma-Aldrich Corp and used without further purification.

Bacteria: *Pseudomonas aeruginosa* PAO1, *S. aureus* ATCC 29213, MRSA BAA-40, *Escherichia coli* 8739, *Escherichia coli* K12, *Enterococcus faecalis* ATCC 29212*Acinetobacter baumannii* ATCC19606, *Acinetobacter baumannii* (Pan sensitive), and *Acinetobacter baumannii* AB-1(MDR) are from ATCC

5.2 Experiment

5.2.1 Characterizations

1H NMR spectra are recorded at 25°C on a Bruker AV300 NMR spectrometer at 300 MHz Chemical shifts (δ) are reported in parts per million (ppm) with reference to the internal standard protons of tetramethyl silane (TMS). The molecular weight of deprotected product 5 is determined by water phase GPC using a Waters Ultrahydrogel column with acidic buffer (0.5M Sodium acetate and 0.5M Acetic acid, with pH=4.5) as eluent.

5.2.2 Synthesis

Synthesis of N-Phthaloyl Chitosan (2): (N-Phthaloyl chitosan prepare same as reference 1) To 5 g (27.93 mmol) chitosan 1 is added 100 mL anhydrous DMF and the mixture is bath sonicated (bath preheated at 80^{o}C) for 1 h under Ar atmosphere. Then the mixture is stirred at 80^{o}C for 1h to fully dissolve the chitosan. The solution is reacted with 13.8 g (93.2 mmol) phthalic anhydride at 130^{o}C for 24 h under Ar atmosphere, then cooled to room temperature, precipitated into of DI water (500 mL) and filtered. The product is washed repeatedly with water, ethanol and acetone, and vacuum dried for overnight at 60^{o}C. The NMR analysis shows that >96% of chitosan amine groups are

phthaloyl-protected. 1H NMR (300MHz) DMSO-D_6, 25C: δH (ppm) 8-7.5 (m, 5H, phthalic) 5-3.5 (m, overlap, 7H chitosan backbone) (Figure 5.1A).

Synthesis of 6-deoxy-6-bromo-N-phthaloyl-chitosans (3): Compounds 3-5 are synthesized as reference 2. N-bromosuccinimide and triphenylphosphine (226.34 mmol each) are added to a solution of 2 (7 g, 22.63 mmol of sugar unit) and NMP (700 mL) in an ice/ water bath, and then the mixture stirred at 80^{o}C for 8 h under nitrogen. The dark brown reaction mixture is poured into EtOH (2 L), and the resulting precipitate is collected by centrifugation and filtration, and then washed with EtOH, acetone-water, and then acetone. After drying under reduced pressure at 60^{o}C, the bromo-deoxy derivative 3 is obtained as dark brown powder. 1H NMR (300MHz) DMSO-D_6: δH (ppm) 8-7.5 (m, 5H, phthalic), 5.27 (1H, anomeric ring proton), 4.35-3.0 (m, overlap, 6H chitosan backbone) (Figure 5.1B).

Synthesis of 6-azido-6-deoxy-N-phthaloyl-chitosan (4): Sodium Azide (8.73 g, 134.34 mmol) is added to a solution of 3 (5 g, 13.43 mmol of sugar unit) in NMP (500 mL), and the mixture is stirred at 80^{o}C for 8 h under nitrogen. The mixture is filtered through cotton to remove the salts and the filtrate is poured into EtOH (1.5 L). The resultant precipitate is collected by centrifugation and washed with EtOH–water, then acetone. After drying under a reduced pressure at 60^{o}C, 6-azido-6-deoxy- N-phthaloyl-chitosan 4 is obtained as a dark brown powder. 1H NMR (300MHz) DMSO-D_6: δH (ppm) 8-7.5 (m, 5H, phthalic), 5.27 (1H, anomeric ring proton), 4.35-2.90 (m, overlap, 6H chitosan backbone) (Figure 5.1C).

Synthesis of 2,6-Diamino Chitosan (5a): Triphenylphosphine (7.06 g, 26.92 mmol) is added to a solution of 4 (3 g, 8.97 mmol of sugar unit) in NMP (200 mL), and the reaction solution is stirred at rt for 12 h under nitrogen. The reaction mixture is then treated with 4 M aqueous hydrazine monohydrate (200 mL) and stirred at 100 ^{o}C for 12 h. Following evaporation of the water, the suspended reaction mixture is poured into EtOH (2 L). The resultant precipitate formed is collected by centrifugation and washed with EtOH and acetone repeatedly to give 5 as a brown powder. 1H NMR (300MHz) D_2O: δH (ppm) 5.2-4.9 (1H, anomeric ring proton), 4.35 (1H, C-4 proton), 4.1-2.5 (5H, C-2, 3, 5, 6 and -NH2 protons) (Figure 5.1D).

General Procedure for Synthesis of 6-substituted-6-deoxy- chitosan derivatives 5b-j: Amines a-i (1.61 mmol) are added to a solution of 3 (200 mg, 0.537 mmol of sugar unit, d.s. bromo 0.95) in NMP (5 mL), and the reaction solution is stirred at 80^{o}C for 12 h under nitrogen atmosphere. The reaction mixture is then treated with 4 M aqueous hydrazine monohydrate (5 mL) and stirred at 100^{o}C for 12 h. Then reaction mixture is cooled to room temperature and dialyzed (1 KDa cut-off dialysis membrane) against DI-water for four days. The polymers 5b-j are obtained via lyophilization.

After the amination reaction of 6g, 2 equivalence of hydrogen peroxide and 2M NaOH solution is added to the solution and stirred for 4 h. Then phthalimide deprotecting reagent is added to the solution.

5.2.3 Antimicrobial Efficacy

Minimum Inhibitory Concentration (MIC) determination

MIC values are determined using a broth micro dilution method. Bacteria cells are grown overnight at 37°C in MHB to a mid-log phase (OD_{600} between 0.4-0.5 for each organism) and diluted in MHB to 10^5 CFU/ml. The polymer is dissolved in water to a stock concentration of 10 mg/ml. The antibiotics listed in Table 5.2 are dissolved and prepared stock concentrations according to CLSI guidelines. 50 µl of the 1-5×10^5 CFU/ml bacterial cultures (final concentration) is aliquoted into 96-well microtiter plates and mixed with 50 µl of two-fold dilutions of the peptide polymer or antibiotics and incubated for 16-18 h at 37 ^{0}C with shaking at 200 rpm. Growth inhibition is determined by measuring the optical density at 600 nm (OD600) of each well using a TECAN M200 microplate reader; the lowest peptide concentration which exhibited no bacterial growth is defined as the MIC.

Time Killing assay:

Bacteria cells are grown, diluted, and aliquoted into 96 well plates as described for the MIC assay, and then mixed with 50 µl volume containing 0.5× and 1× MIC of the polymer and/or antibiotics. The plates are sealed and incubated at 37 ^{0}C with shaking at 200 rpm.

At 0, 0.5, 1, 2, 3, 5, and 24h post-inoculation, each well thoroughly mixed with a multi-channel pipette and 20µl of sample is removed, serially diluted in sterile phosphate buffered saline (PBS), plated on MH agar plates, and incubated at 37 ^{0}C for 12 hrs. Colonies are counted to determine the CFU/ml at each time point.

5.2.4 Measurement of Synergy

Synergy is measured by time killing assay and checkerboard assy. Time killing assay is performed as described like above. Checkerboard susceptibility assays to measure combinations of antimicrobials are performed in MHB at 37°C as previously described. The fractional inhibitory concentration (FIC) indices are calculated according to the following formula:

$$\text{FIC index} = FIC_A + FIC_B$$

Where

$$FIC_A = \frac{MIC\ of\ drug\ A\ in\ combination}{MIC\ of\ drug\ A\ alone}$$

$$FIC_B = \frac{MIC\ of\ drug\ B\ in\ combination}{MIC\ of\ drug\ B\ alone}$$

Conservative interpretation of the FIC index has traditionally defined synergism as a FIC index ≤0.5 and FIC index range from 0.5~1 as additive or partial synergy. And FIC index greater than 1 shows no synergism.

5.2.5 *In vitro* Cytotoxicity assay

Mammalian Cell Biocompatibility test via MTT cell proliferation assay;

The mammalian cell biocompatibility test is done according to the published protocol using 3T3 cells. In a 96-well plate, 3T3 cells are co-cultured for 24 h at 37 ^{o}C with polymer (100 µg/mL and 200 µg/mL) at initial cell density of 1×10^5 cells per well. At the end of the incubation period the culture medium is removed, each well is washed with PBS followed by addition of MTT solution, and the plate is incubated for 4 h at 37 ^{o}C. The MTT medium is then removed, 100 µL of DMSO is added to each well, the plate is shaken at 100 rpm for 15 mins and the

absorbance at 570 nm is measured with plated reader (BIO-RAD Benchmark Plus, US).

5.2.6 *In vivo* Toxicity and Antimicrobial efficacy assay

In vivo oral and sepsis toxicity determination

A single high dose of 100 mg/kg of 2,6-DAC is administered by the oral route for Balb/c mice. The body weight of the mice is determined. The mice are observed in detail for any indications of toxicity effect within the first six hours after the treatment period, and daily further for a period of 7 days. Surviving animals are weighed and visual observations for mortality, behavioral pattern, changes in physical appearance, injury, pain and signs of illness are conducted daily during the period.

Further, a signal dosage of 25 mg/kg DAC is injected by intraperitoneal injection, the biomarkers, the biomarkers are determined at day 1 and day 7 after treatment.

In vivo synergism of 2,6-DAC with antibiotics

Intraperitoneal infection model

Bacterial cultures of MDR A. baumannii (AB-1) are prepared and used to infect 8-week-old female BALB/c mice. 300µL of 10^6cfu/mL of AB-1 is injected into the intraperitoneal cavity to introduce the infection. After 2hrs of infection, specific dosage of antibiotic, 2,6-DAC or the combination of antibiotic and 2,6-DAC are injected into the intraperitoneal cavity. PBS is used as a control. Mice authorization at indicated time points (24hrs) is achieved by CO_2 asphyxiation followed by cervical dislocation. The intraperitoneal fluid, kidney, spleen and liver are recovered, and counted for bacteria concentration.

Lung infection model

Bacterial cultures of MDR A. baumannii (AB-1) are prepared and used to infect 8-week-old female BALB/c mice. 30µL of 10^6cfu/mL of AB-1 is inhaled by the mouse to introduce the infection via intranasal route. After 2hrs of infection, specific dosage of antibiotic, 2,6-DAC or the combination of antibiotic and 2,6-DAC are inhaled trough intranasal route. Mice authorization at indicated time points (24hrs) is achieved by CO_2 asphyxiation followed by cervical dislocation. The lung is recovered and counted for bacteria concentration.

5.3 Results and Discussion

5.3.1 Synthesis and Biological Characterization of 2,6-Diamino Chitosan Derivatives

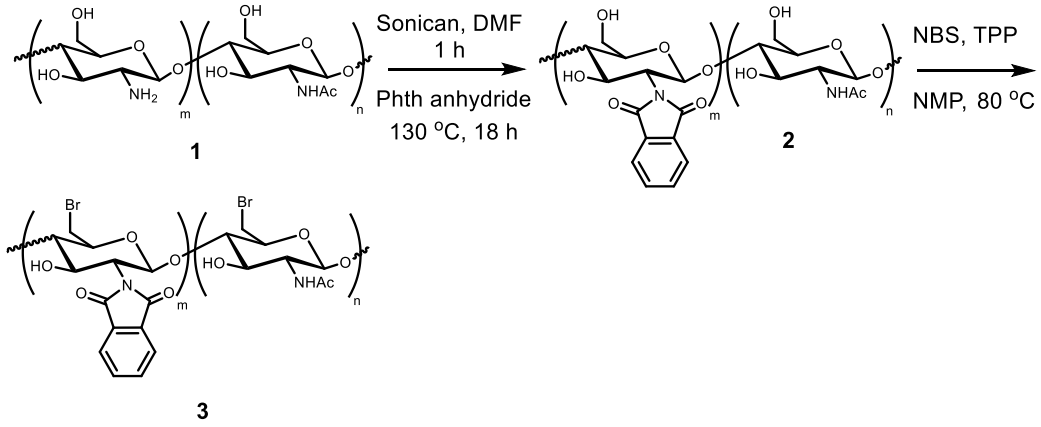

Scheme 5.1a Synthesis of Chitosan Intermediates

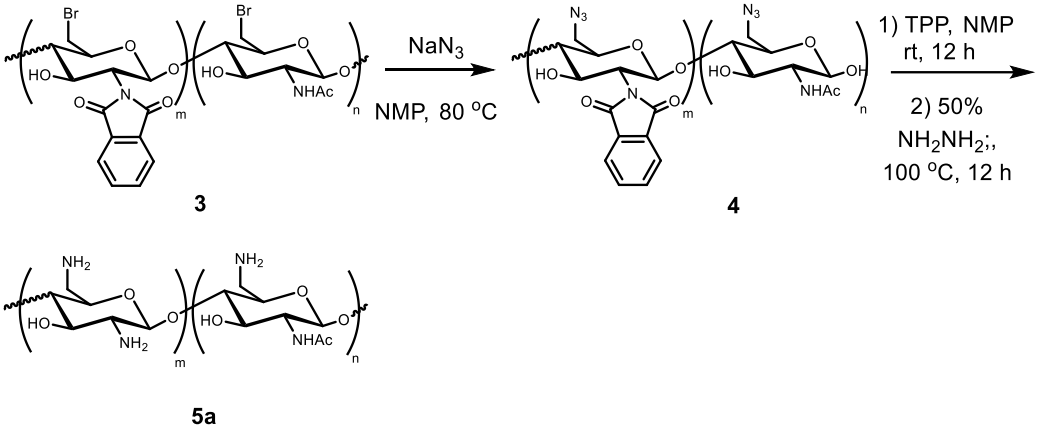

Scheme 5.1b Synthesis of 2,6-DAC

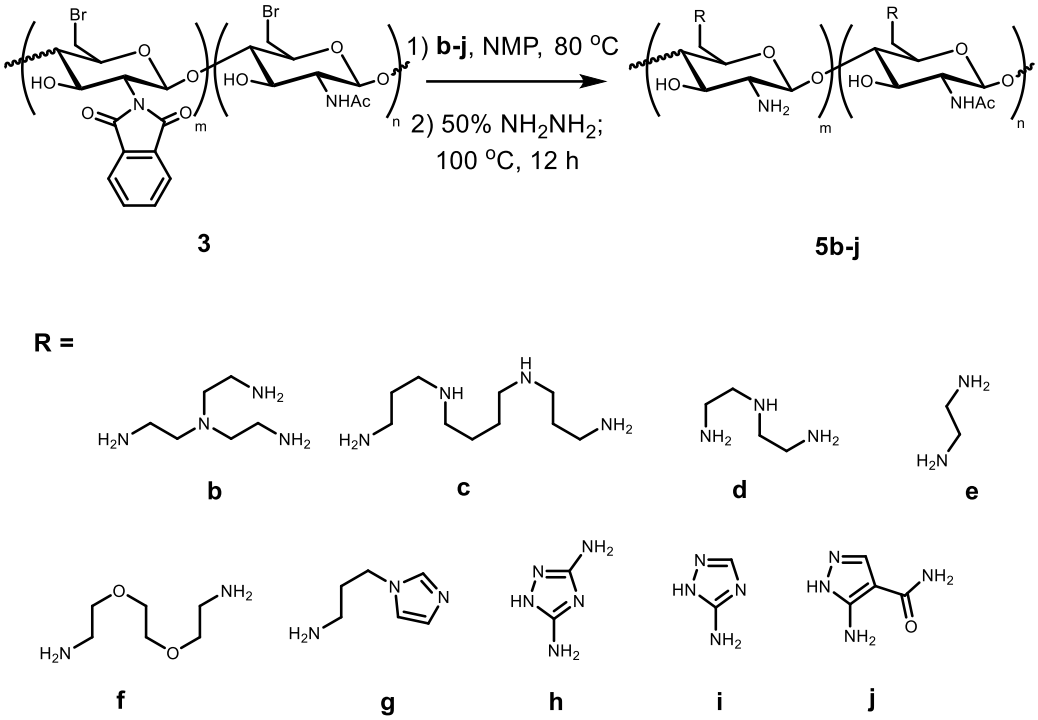

Scheme 5.1c Synthesis of chitosan derivatives:

The synthesis schemes of 2,6-Diamino Chitosan is summarized in Scheme 5.1a an b. Other amino-/imidazole/triazole chitosan derivatives are synthesized as in Scheme 5.1c. Briefly, the intermediate 6-deoxy-6-bromo-N-

phthaloyl chitosan (Compound 3) is synthesized by phthalic protection of the amino group on chitosan followed by replacement of the hydroxyl group on the 6-position of chitosan to bromide by N-bromosuccinimide (Scheme 5.1a). The bromide group in Compound 3 is converted to the azido group (N_3) and further reduced to amino group (Scheme 5.1b). Similarly, various functional groups are used to substitute the bromide group on chitosan, resulting a library of chitosan derivatives (Scheme 5.1c)

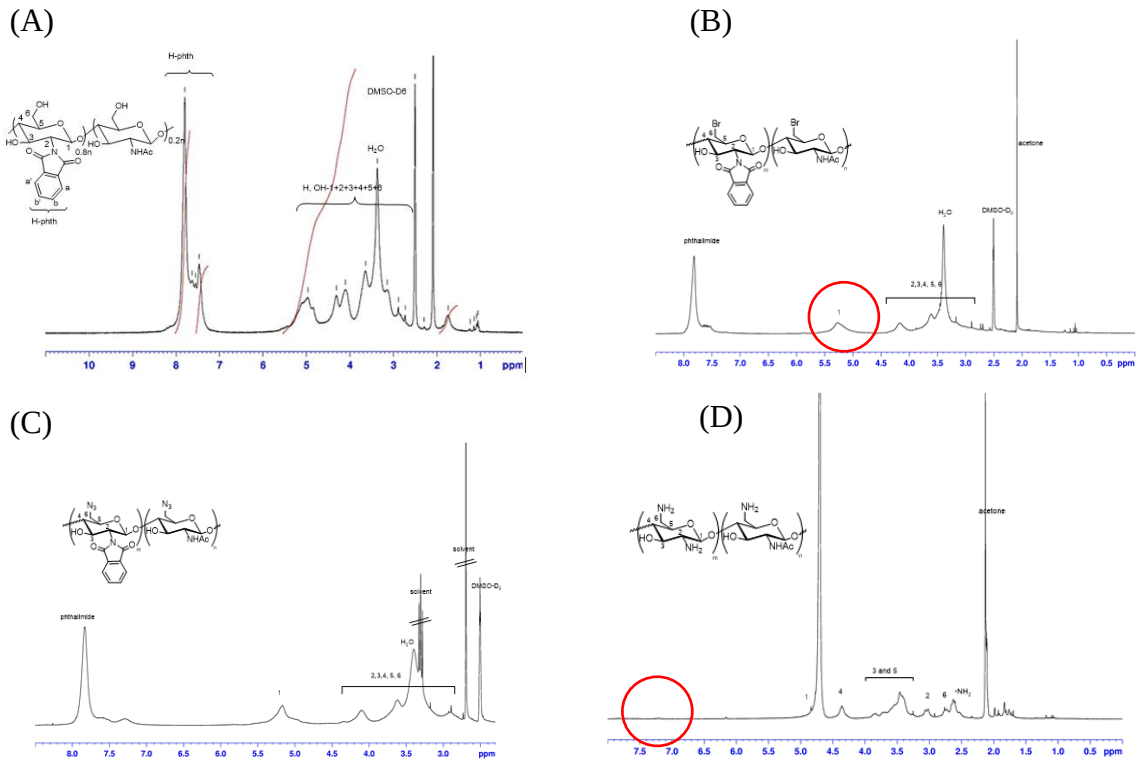

Figure 5.1 NMR spectrum of 2,6-DAC synthesis(A) N-Phthaloyl Chitosan (B) 6-deoxy-6-bromo-N-phthaloyl-chitosans (C) 6-azido-6-deoxy-N-phthaloyl-chitosan (D) 2,6-Diamino Chitosan

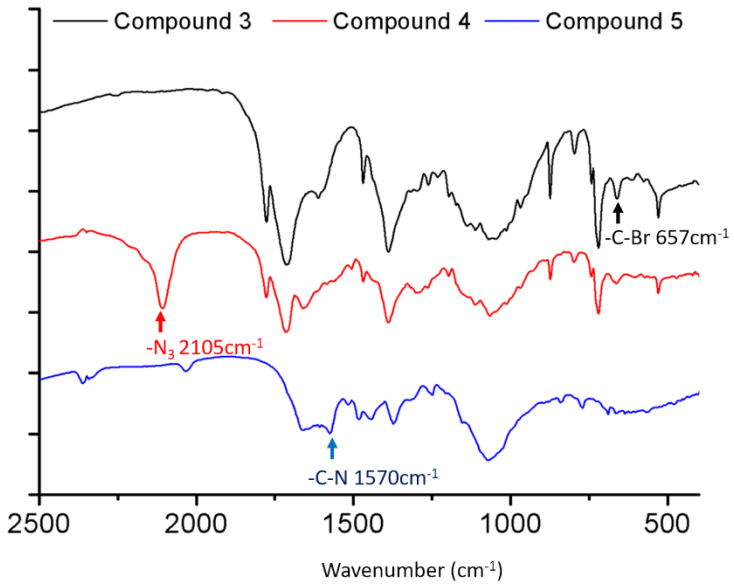

Figure 5.2 FTIR characterization of synthesis of 2,6-Diamino Chitosan (3) 6-deoxy-6-bromo-N-phthaloyl-chitosans (4) 6-azido-6-deoxy-N-phthaloyl-chitosan (5) 2,6-Diamino Chitosan

The synthesis of 2,6-Diamino-chitosan is tracked by NMR (Figure 5.1) and FTIR (Figure 5.2) characterization. For the Compound 2, the 1H NMR peak at 7.5-8.0ppm is due to the phthalic aromatic H, corroborating the successful phthalic anhydride protection (Figure 5.1A). For Compound 3, the new 1H NMR peak from 5.0-5.5ppm (Figure 5.1B) and the new FTIR peak at 657cm^{-1} (Figure 5.2, compound 3) indicate the successful grafting of Br at the 6-position of glucosamine. The substitution of bromo group by the azido group (Compound 4) is not trackable by NMR. However, the azido group on compound 4 is corroborated by the FTIR signal at 2105cm^{-1} (Figure 5.2, Compound 4). For compound 5a, the final deprotection of the phthalic group is confirmed by the disappearing of 7.5-8.0ppm in the 1H NMR (Figure 5.1D red circle) and the

reduction of azido group is confirmed by the disappearing of the FTIR 2105cm^{-1} peak (Figure 5.2, Compound 5a); there is further increase of the FTIR C-N bond signal at 1570cm^{-1}, indicating the conversion of C-N_3 to C-NH_2 group at the 6-position of glucosamine.

(5b)

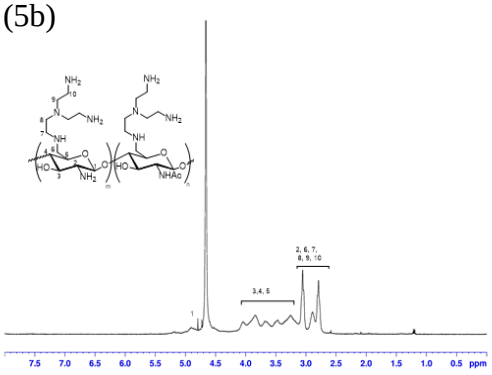

(5c)

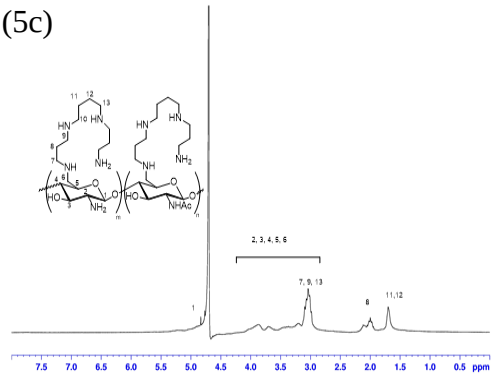

(5d)

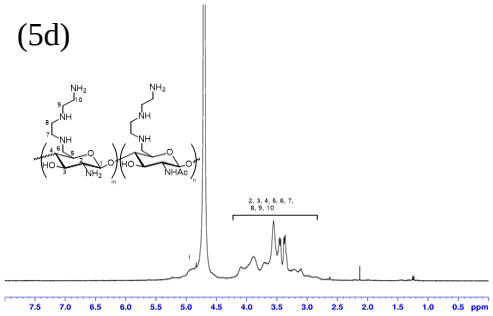

(5e)

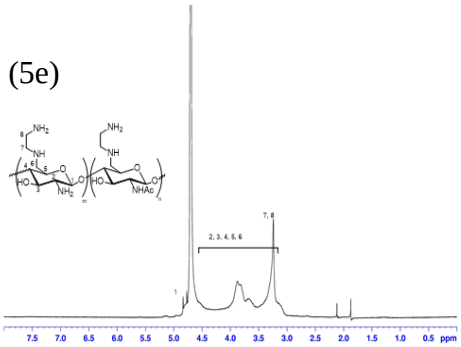

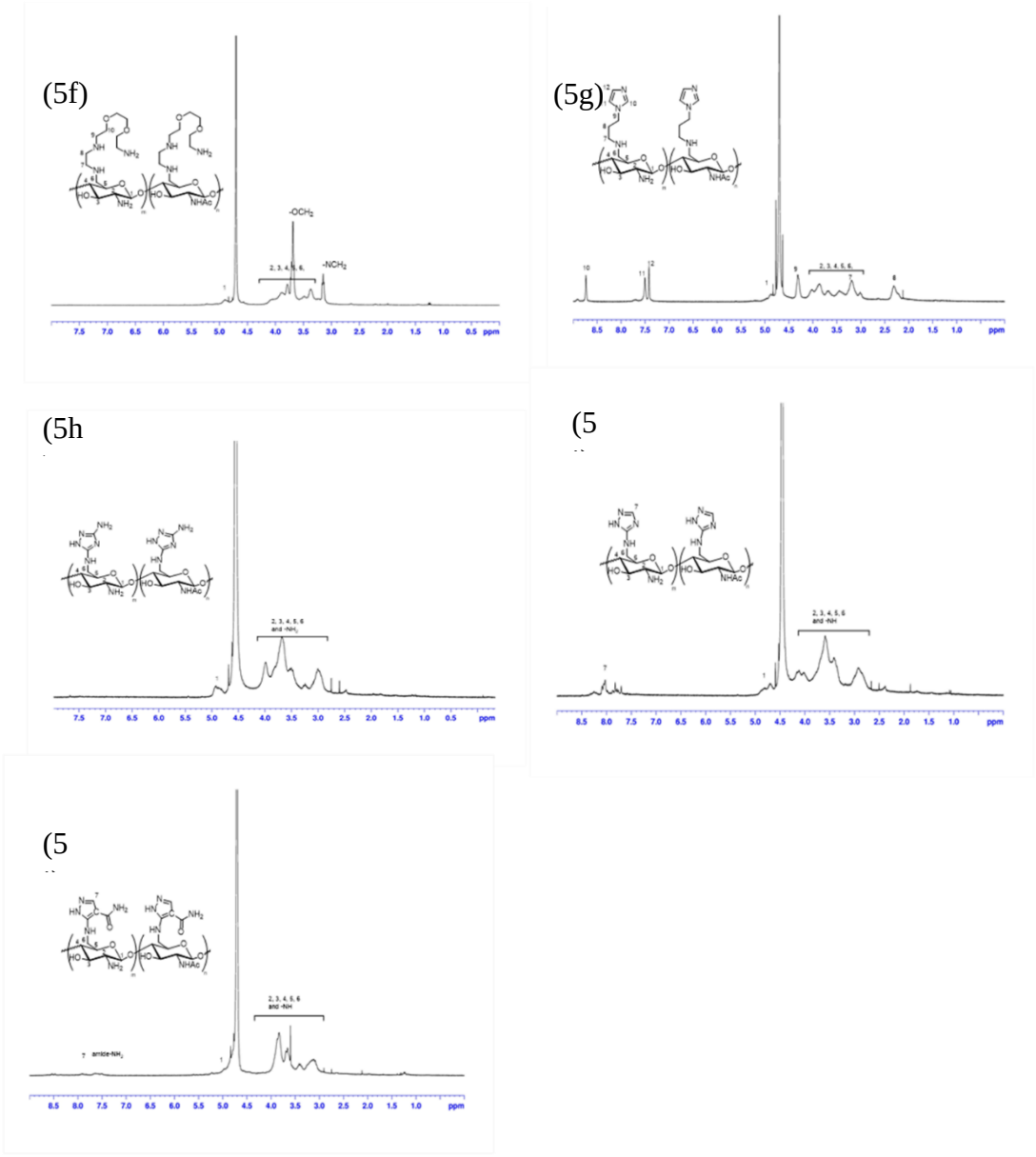

Figure 5.3 NMR spectrum of other chitosan derivatives (5b) 6-EG Diamine Chitosan, (5c) 6-Spermine Chitosan, (5d) 6-DET Chitosan, (5e) 6-EDA Chitosan, (5f) 6-Triamine Chitosan, (5g) 6-Aminopropyl imidazole Chitosan, (5h) 6-Diamino Triazole Chitosan, (5i) 6-Amino Triazole Chitosan, (5j) 6-3 Amino 4-Carboxamide Imidazole Chitosan

The NMR spectrum of other chitosan derivatives are summarized in Figure 5.3. Compared with raw material chitosan, 6-Triamine chitosan, 6-Spermine Chitosan, 6-DET-chitosan, 6-EDA-chitosan, 6-EG-Diamine chitosan

shows alky group signal at 2.5-3.0ppm. However, the peaks are overlapping with the sugar signal. For 6-Aminopropyl imidazole chitosan, 6-diamino triazole chitosan, 6-amino triazole chitosan and 6,3-amino 4-carboxamide imidazole chitosan, the synthesis is confirmed by appearing of imidazole group at 7.5-8.0ppm

5.3.2 *In vitro* Antimicrobial Efficacy Test

Table 5.1 summarizes the antimicrobial efficacy and cytotoxicity of 2,6-DAC and other chitosan derivatives. 2,6-DAC (Compound 5a) and 6-Triamine Chitosan (Compound 5b) show broad antimicrobial activity against both Gram-Positive and Gram-Negative bacteria. Additionally, 6-Spermine Chitosan (Compound 5c), 6-DET Chitosan (Compound 5d) and 6-EDA Chitosan (Compound 5e) also shows selective antimicrobial activity against Gram-Positive bacteria. However, only 2,6-DAC, 6-DET Chitosan and 6-EDA Chitosan show good biocompatibility as measured using the 3T3 fibroblast cells (Table 5.1). Comparing the antibacterial activity with their cytotoxicity, only 2,6-DAC shows excellent broad antimicrobial activity with good biocompatibility.

Table 5.1 and 2 shows that 2,6-DAC displays broad-spectrum antimicrobial activity against various laboratory strains of multiple Gram-negative and Gram-positive bacteria, including *P. aeruginosa*, *E. coli*, *A. baumanii* and *S. aureus*. We further tested 2,6-DAC against a panel of clinically relevant antibiotic-susceptible and multidrug resistant (MDR) clinical isolates of *Acinetobacter baumannii* (AB-1, BAA 2803), *P. aeruginosa* BAA 2797, and *K.*

pneumoniae BAA 2784. We found that 2,6-DAC demonstrates good antibacterial activity with minimum inhibitory concentrations (MICs) range of 8 to 32 μg/ml against *Acinetobacter baumannii* strains (Table 5.2). The MIC of 2,6-DAC against *P. aeruginosa* and *K. pneumoniae* is also low (8-16 μg/ml) except against *Salmonella enterica* (128 μg/ml). The MICs of various common antibiotics against the various bacteria *Acinetobacter baumannii-1* are also listed in Table 5.3. We can see that some of the common antibiotics are not possible to be eradicated *Acinetobacter baumannii-1* (MIC>128 μg/ml), compared with 2,6-DAC.

Table 5.1, Summary of antimicrobial efficacy and cytotoxicity of 2,6-DAC and its derivatives

Sample		Minimum Inhibitory Concentration (MIC) (μg/mL)					%Cell viability	
		Gram Negative Bacteria			Gram Positive Bacteria		100μg/mL	200μg/mL
		PA01	*E. Coli*	*A. baumannii*	*S.aureus*	*MRSA*		
5a	**2,6-Diamino Chitosan (2,6-DAC)**	**8**	**16-32**	**8-32**	**16**	**16**	**98.63**	**94.25**
5b	6-Triamine Chitosan	8	16	-	16	16	5.8	5.7
5c	6-Spermine Chitosan	256	512	-	16	32	10.0	5.6
5d	6-DET Chitosan	8	256	-	16	64	87.9	23.3
5e	6-EDA Chitosan	>512	>512	-	32	32	85.1	70.2
5f	6-EG Diamine Chitosan	128	512	-	16	512	47.6	12.7
5g	6-Aminopropyl imidazole Chitosan	>512	512	-	>512	>512	79.2	47.8

5 h	6-Diamino Triazole Chitosan	>512	>512	-	>512	>512	89.4	45.8
5i	6-Amino Triazole Chitosan	>512	>512	-	>512	512	83.1	79.0
5j	6-3 Amino 4-Carboxamide Imidazole Chitosan	>512	>512	-	>512	>512	91.2	52.1

Table 5.2. Antimicrobial efficacy of 2,6-DAC against more bacteria

Gram-Negative	Minimum Inhibitory Concentration (MIC) (µg/mL)
Salmonella enterica (human pathogen)	128
A. baumannii BAA 2803	8
A. baumannii 17978	32 or 16
P. aeruginosa BAA 2797	8
K. pneumoniae 43826	16
K. pneumoniae BAA 2784	16
E. coli BAA 2774	16

Gram-Positive	Minimum Inhibitory Concentration (MIC) (µg/mL)
Listeria monocytogenes	16

The antimicrobial activity on *Acinetobacter baumannii-1* is further confirmed by the time-kill essay, 2,6-DAC treated *Acinetobacter baumannii-1* (AB-1) rapidly stops growth and displayed $4\log_{10}$ orders of killing. (Figure 5.4).

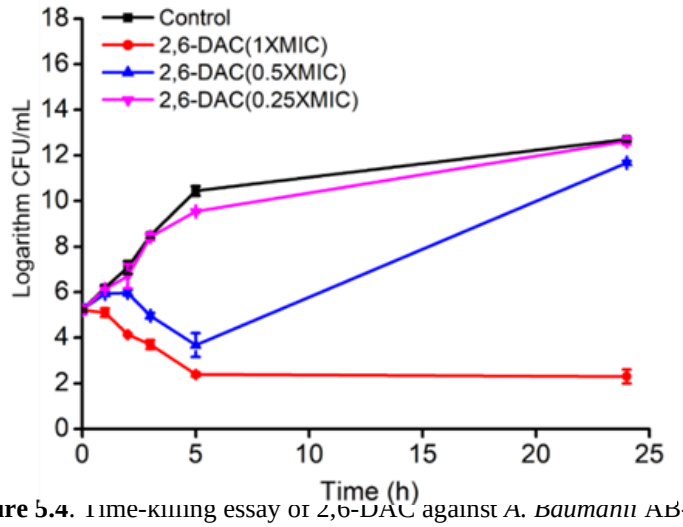

Figure 5.4. Time-killing essay of 2,6-DAC against *A. Baumanii* AB-1

5.3.3 Synergistic Study of 2,6-Diamino Chitosan with antibiotics

We also screened 2,6-DAC as a potentiating agent for antibiotics for synergistic combinations against both MRSA USA300 and *Acinetobacter baumannii* AB-1.

Before the synergistic tests, the MIC values of antibiotics are tested against MDR *Acinetobacter baumannii* AB-1 and MRSA USA 300 (Table 5.3 for AB-1, Table 5.5 for MRSA USA 300). Then, the presence (or absence) of synergy of combinations of 2,6-DAC with antibiotics is determined using the checkerboard assay. As shown from Table 5.3, 2,6-DAC displayed potent synergy with antibiotics that function as protein synthesis inhibitor (Tobramycin and Amikacin) against MDR pathogen AB-1. The fractional inhibitory concentration (FIC) index is less than 0.5. Combining 2,6-DAC at a combination MIC of 8 and 16 µg/ml, the MICs of both Amikacin and Tobramycin are reduced greatly from greater than 128 µg/ml to 1~2 µg/ml. Furthermore, 2,6-DAC demonstrated synergy with Novobiocin, a DNA gyrase inhibitor. The MIC value of Novobiocin alone against AB-1 is 8 µg/ml. Combining of 2,6-DAC at a combination MIC of 8 and 16 µg/ml with Novobiocin restored sensitivity as the antibiotic MICs

become 0.5 and 0.25µg/ml respectively (Table 3). Additionally, 2,6-DAC also displays synergistic interaction with Tazobactam, a β-lactamase inhibitor (Table 5.3). However, combination of 2,6-DAC with other antibiotics demonstrated only partial synergistic activity (0.5<FIC<1) against MDR AB-1 (Table 5.4).

Table 5.3 Summary of synergistic study of 2,6-DAC with various antibiotics against AB-1

Antibiotics	Antimicrobial mechanisms	MIC µg/ml			FIC
		Without 2,6-DAC	+ 16 µg/ml 2,6-DAC	+ 8 µg/ml 2,6-DAC	
Amikacin	Protein synthesis inhibitor	>128	1	2	<0.5
Tobramycin	Protein synthesis inhibitor	>128	1	2	<0.5
Novobiocin	DNA gyrase inhibitor	8	0.25	0.5	<0.5
Tazobactam	β-lactamase inhibitor	64	1	16	<0.5

Table 5.4, FIC indices of antibiotics in combination with 2,6-DAC against *Acinetobacter baumannii* AB-1(MDR) with partial synergistic effect

Antibiotics	Antimicrobial mechanisms	MIC µg/ml			FIC
		Without 2,6-DAC	+ 32 µg/ml 2,6-DAC	+16 µg/ml 2,6-DAC	
Ofloxacin	DNA Gyrase inhibitor	8	4	8	> 0.5 <1
Levofloxacin	DNA Gyrase inhibitor	4	≤1	2	> 0.5 <1
Azithromycin	Protein synthesis inhibitor	128	1	64	> 0.5 <1
Erythromycin	Protein synthesis inhibitor	>128	4	64	> 0.5 <1
Meropenem	Cell wall synthesis inhibitor	64	1	4	> 0.5 <1
Imipenem	Cell wall synthesis inhibitor	64	1	8	> 0.5 <1
Ertapenem	Cell wall synthesis inhibitor	>128	2	4	> 0.5 <1
Doripenem	Cell wall synthesis inhibitor	32	≤2	4	> 0.5 <1
Cephalothins	Cell wall synthesis inhibitor	>128	2	128	> 0.5 <1
Cefoxitin	Cell wall synthesis inhibitor	>128	8	128	> 0.5 <1
Ceftazidime	Cell wall synthesis inhibitor	>128	2	128	> 0.5 <1
Ceftriaxone	Cell wall synthesis inhibitor	>128	2	128	> 0.5 <1

Ramoplanin	Cell wall synthesis inhibitor	>128	2	128	> 0.5 <1
Amoxicillin	Cell wall synthesis inhibitor	>128	16	128	> 0.5 <1

2,6-DAC also shows synergistic activity with Carbenicillin (β-lactamase inhibitor), Novobiocin (DNA gyrase inhibitor) and Tobramycin (protein synthesis inhibitor) (Table 5.5) against MRSA USA-300. The synergism of 2,6-DAC with antibiotics depend on the action mechanism of antibiotics. It appears 2,6-DAC synergizes better with protein synthesis inhibitor, DNA gyrase inhibitor and β-lactamase inhibitor. However, it only shows partial synergism with cell wall synthesis inhibitor (Table 5.5).

Table 5.5 FIC indices of antibiotics in combination with 2,6-DAC against MRSA USA300

Antibiotics	Antimicrobial mechanisms	MIC µg/ml			FIC
		Without 2,6-DAC	Antibiotic in combination (µg/ml)	2,6-DAC in combination (µg/ml)	
Meropenem	β-lactamase inhibitor	1	0.5	0.25	<0.5
Carbenicillin	β-lactamase inhibitor	8	2	4	<0.5
Tobramycin	Protein synthesis inhibitor	1	0.25	1	<0.5
Novobiocin	DNA gyrase inhibitor	0.125	0.03125	1	<0.5

Moreover, synergistic effects of 2,6-DAC with antibiotics are demonstrated by time-killing curves. Combinations of sub-inhibitory concentrations of 2,6-DAC (0.5×MIC) with sub-inhibitory concentrations of Novobiocin (0.06 To 0.25×MIC) against MDR AB-1 (Figure 5.2A) is found to be synergistic and bactericidal, and achieving up-to $4\log_{10}$ orders of bacteria killing. Similarly, combination of 2,6-DAC with Tazobactam (0.06×MIC) and Amikacin

(0.0019×MIC), demonstrated synergistic and 4log$_{10}$ bactericidal efficacy (Figure 5.2 B, C). The overall bactericidal efficacy of Tobramycin (0.0019×MIC) and 2,6-DAC is poor with 2log$_{10}$ orders against AB-1.

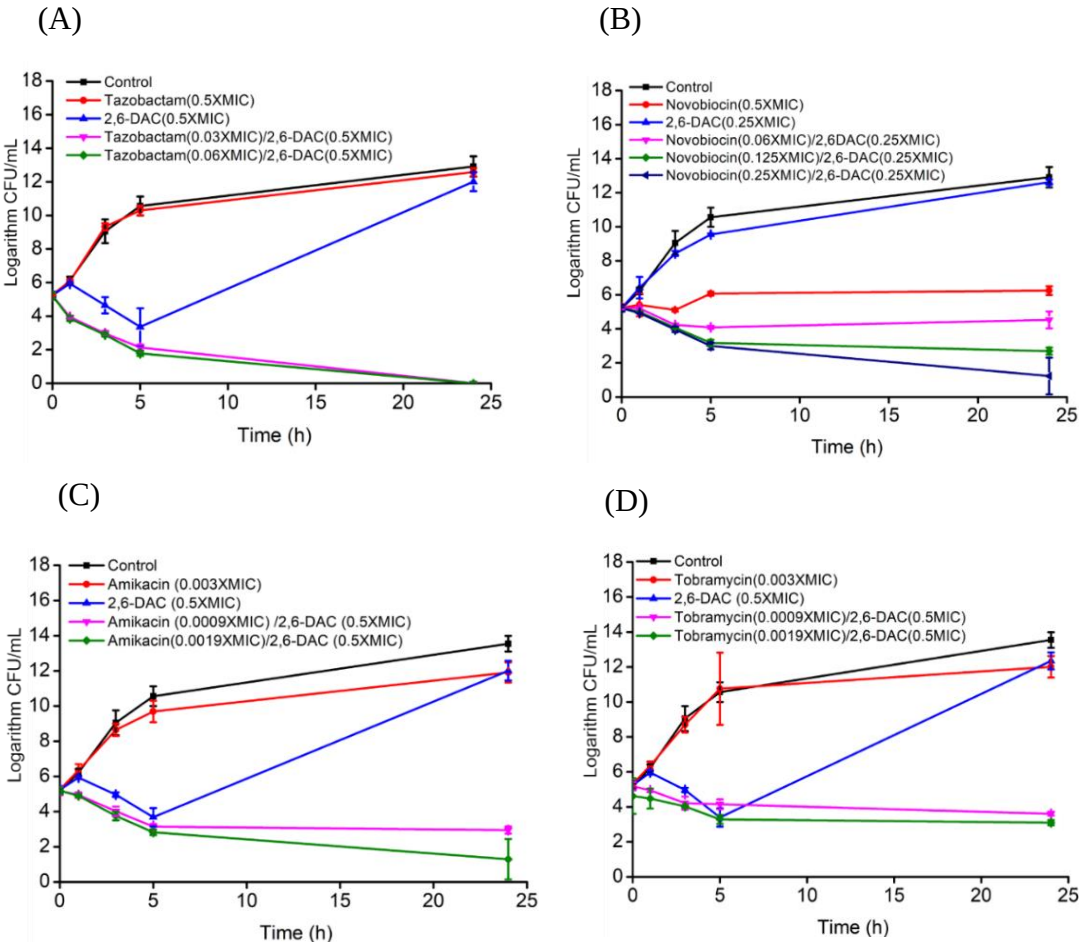

Figure 5.5 Time-killing essay of 2,6-DAC with various antibiotic against AB-1, A) Novobiocin; B) Amikacin; C) Tobramycin; D) Tazobactam.

5.3.4 *In vivo* toxicity and antimicrobial test

The systemic toxicity of DAC is measured by injecting 25mg/kg DAC solution into the intraperitoneal space of mice and through oral gavage (100 mg/kg); the systemic toxicity and oral toxicity measured by monitoring the liver and kidney biomarkers and body weight. A single dosage of 25 mg/kg DAC by

intraperitoneal injection didn't cause significant change in the blood levels of kidney and liver biomarkers (such as alanine transaminase, aspartate aminotransferase and total bilirubin) (Table 5), indicating it didn't cause any liver and kidney toxicity or influence the electrolyte such as Creatinine, Urea, K^+ and Na^+ (Table 5.6). More interesting, a single dosage of 100 mg/kg DAC didn't cause any decrease of body weight, supporting a good biocompatibility of DAC treatment by oral (Figure 5.6A).

Table 5.6 *In vivo* toxicity of DAC, effect on liver and kidney functions as well as balance of electrolytes in the blood.

	ALT*(Ul^{-1})	AST** (Ul^{-1})	TBIL*** (μmol^{-1})	Creatinine (μmol^{-1})	Urea nitrogen ($mmol^{-1}$)	Potassium ($mmol^{-1}$)	Sodium ($mmol^{-1}$)
0 day	44.00±7.07	99.80±23.52	3.72±1.10	53.20±27.67	8.27±0.72	5.46±0.22	147.2±5.45
1 day	55.80±9.88	106.8±17.02	3.60±1.17	42.40±14.47	7.58±0.76	5.31±0.24	144.2±2.05
7 days	54.20±24.08	92.80±24.90	4.27±0.81	57.40±18.39	10.65±0.96	5.79±1.78	143.2±1.10

*ALT: Alanine transaminase **AST: Aspartate aminotransferase ***TBIL: Total Bilirubin

The *in vivo* synergism against MDR *A. baumannii* (AB-1) is also established in the intraperitoneal and lung infection models. In the intraperitoneal model, bacteria is firstly introduced by IP injection, followed by injection of combination dosages, Figure 5.6 B-E shows that DAC (25 mg/kg) or novobiocin (10 mg/kg) had no influence on the bacterial survival in both intraperitoneal fluid and intraperitoneal organs such as liver, kidney and spleen. However, Figure 5.6B shows a combination treatment of them led to 99.76% (2.626 log) eradiation of bacteria in the intraperitoneal cavity. Moreover, reduction of bacteria is also found in the distal organs, including kidneys (97%, 1.5 log) (Figure 5.6C), spleen

(98%, 1.8 log) (Figure 5.6D) and liver (96.45%, 1.45 log) (Figure 5.6E). Furthermore, the proof of efficacy of combination treatment is further demonstrated in a neutropenic lung infection model. Rifampicin (10mg/kg) alone has around 1.7 log reduction on the lung bacteria while DAC (20 mg/kg) didn't have any protection effect (Figure 5.6F). However, the combination treatment further improves the rifampicin efficacy from around 1.7 log to 2.85 $\log_{10}$ of bacteria reduction (Figure 5.6F).

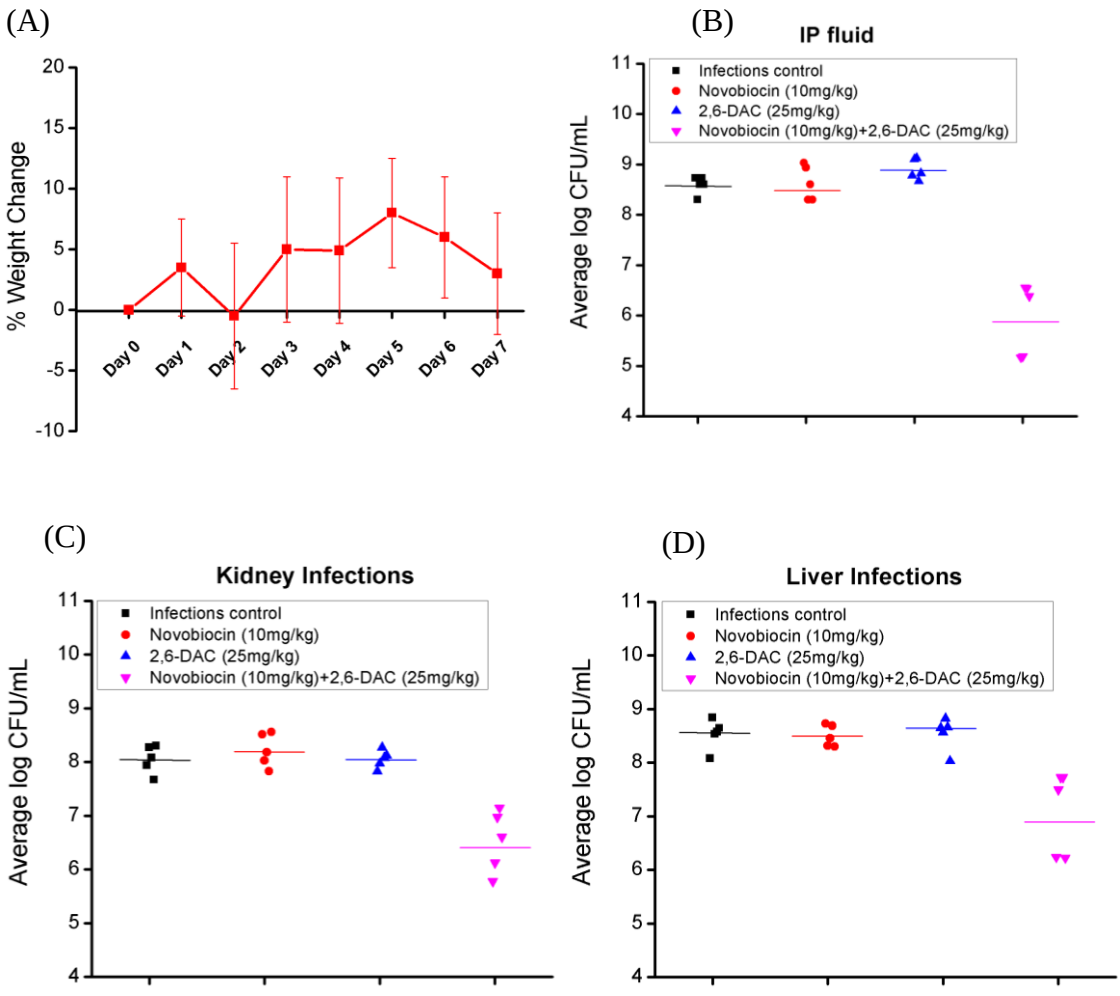

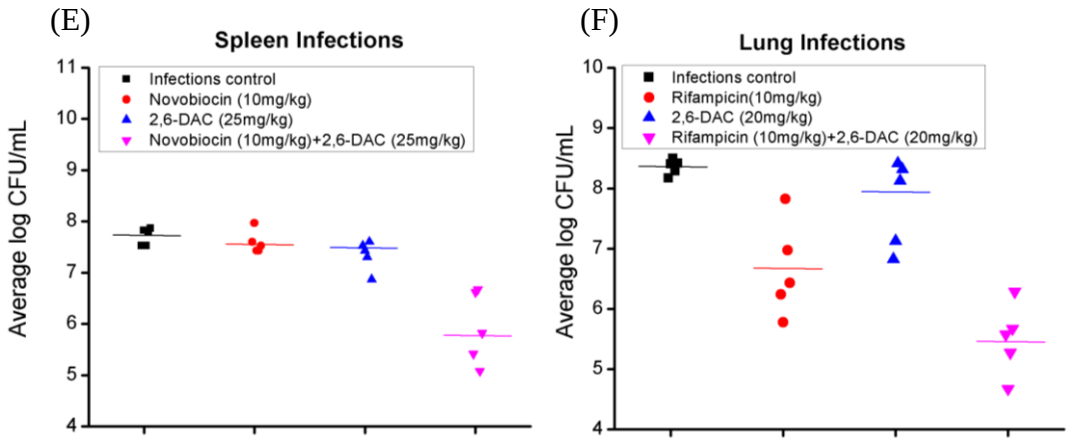

Figure 5.6 (A) Weight change of mice in *in vivo* oral toxicity test with 100mg/kg dosage. (b-e) *in vivo* efficacy of sepsis model (b)IP fluid (c)Kidney infection (d)Liver infections (e) Spleen infections. (f) Lung infection model Sepsis infection of MDR *A. baumannii* (AB-1) into intraperitoneal distal organs

5.4 Conclusion

The 6' position on glucosamine units was modified into various groups amine/imidazole/triazole groups via the nucleophilic substitution reactions of the bromide group attached on 6 position. However, despite the reported antimicrobial efficacy of heterocycles, the amino group shows better antimicrobial efficacy. This might be due to the introduction of amino groups enhance hydrogen bonding between sugar backbones; therefore the 2,6-DAC are more likely to aggregate and have better antimicrobial efficacy. The simple amino groups are also more hydrophilic, which have better biocompatibility compared with imidazole and triazole groups.

2,6-Diamino Chitosan shows a balanced antimicrobial efficacy and biocompatibility. DAC shows broad bactericidal efficacy towards both Gram-Positive and Gram-Negative bacteria with minimum inhibitory concentration

(MIC) of 8~32μg/mL, especially against the clinically important MDR *A. Baumannii* (MIC of 2,6-DAC is 8~32 μg/mL).

2,6-DAC also shows synergistic activity with various kinds of antibiotics, including ?? what antibiotics which are protein synthesis inhibitor, DNA gyrase inhibitor and β-lactamase inhibitor respectively. The synergistic activity of 2,6-DAC and Novobiocin and rifampicin is also shown by the *in vivo* intraperitoneal or long infection/treatment model. This is the first reported 6 position modified cationic polysaccharide synergized with antibiotics. The antimicrobial synergisms between antibiotics and cationic polymers or peptides are reported as discussed in literature review; however, the synergism is limited to cationic/hydrophobic copolymers or peptides which have lower biocompatibility or only apply to limited kinds of antibiotics. In this chapter, the 2,6-DAC is hydrophilic and biodegradable cationic polysaccharide, which show synergism with various classes of antibiotics. The *in vivo* synergism is also proved. This 2,6-DAC can be further applied in antimicrobial therapies such as fabrication of nanoparticle with antibiotics or layer-by-layer assembled antimicrobial coatings.

Chapter 6. Precisely linked NO-donor catheter coating with *in vivo* antibacterial, antibiofilm and non-thrombogenic functions

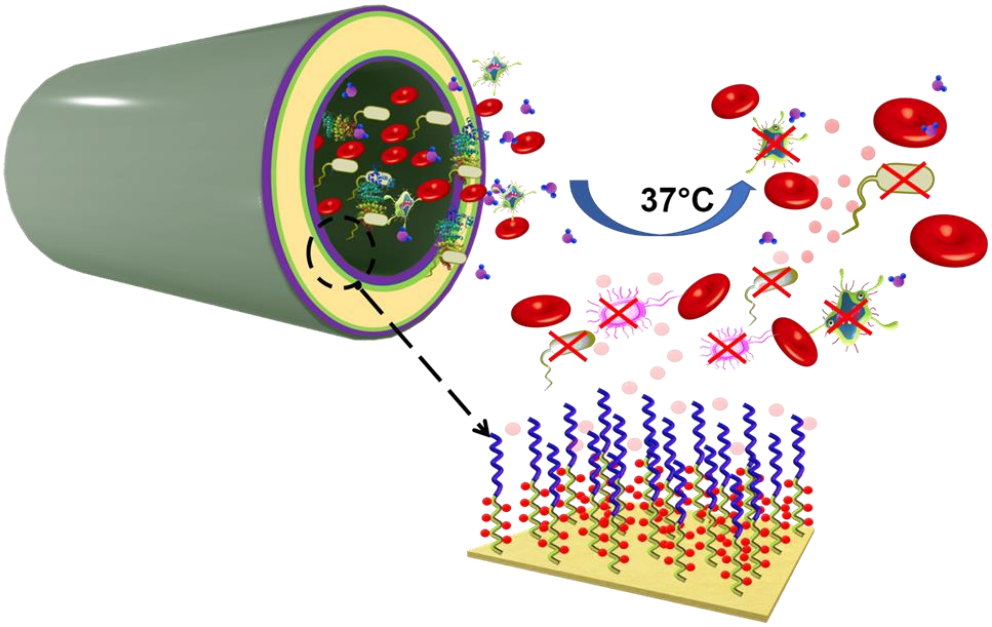

Catheter-associated infections (CAI), particularly bloodstream-related, cause a huge healthcare burden and significant mortality. Various strategies involving antibiotics, silver or hydrophilic coatings cannot effectively inhibit biofilm nor thrombus formation. We invented a high-density surface-initiated controlled block copolymerization strategy by "grafting from" the ozone gas pretreated catheter surface via RAFT (Reversible Addition−Fragmentation Chain-Transfer) polymerization. Further, we found that a diblock copolymer brush composed an outer hydrophilic block made from hydrophilic zwitterionic sulfobetaine (S) methacrylate and an inner hydrophilic functionalizable hydroxyethyl methacrylate (H) which is covalently post-linked to a tertiary S-

nitrosothiol (a nitric oxide, NO-donor) shows outstanding antibacterial and antibiofilm activities. The other arrangements of S and H/N monomers via the random copolymers and hydrogels showed inferior performance. The H(N)-*b*-S diblock brush achieves a >4.00$\log_{10}$ eradication of *in vitro* biofilm formed by various clinically important Gram-negative and Gram-positive bacteria and *Candida albicans* (a fungus), compared with (less than 1.50$\log_{10}$) of a commercially available silver-hydrogel coated catheter. The diblock-coated catheter also shows >2.5$\log_{10}$ inhibition against both *Staphylococcus aureus* and *Pseudomonas aeruginosa* biofilm formation for 30 days, while the silver-hydrogel coated catheter shows no efficacy. The coating is found to be non-toxic to mammalian cells. The H(N)-b-S catheter also significantly reduces thrombus formation and the blood immune cell immunological response compared with unmodified catheters. Further, the modified catheter shows >3.00$\log_{10}$ *in vivo* inhibition of *S. aureus* and *P. aeruginosa* biofilm formation in an *in vivo* subcutaneous implantation model. We show that high density hydrophilic brushes with prolonged transient NO gas emitting from non-leachable donors that kills bacteria at a distance is a promising platform to achieve antibacterial, antibiofilm and non-thrombogenic effects without toxicity.

6.1 Materials

Polyurethane catheters (Micro-Renathane Tubing) with specific sizes are purchased from Braintree Science. 2-Hydroxyethyl methacrylate (>99%) (HEMA), [2-(Methacryloyloxy) ethyl] dimethyl-(3-sulfopropyl) ammonium hydroxide (SBMA), 4-Cyano-4-(phenylcarbonothioylthio) pentanoic acid (CPCPA), 4,4′-Azobis(4-cyanovaleric acid) (ACVA), butylamine, oxalyl chloride, tert-butyl nitrite, 3-Mercapto-3-methylbutan-1-ol, and Ethanol are purchased from Sigma-Aldrich and used without further purification. Ozone is generated by Arzocon RMU16-K3 using air as inlet.

Bacteria: *Methicillin-resistant Staphylococcus aureus* BAA38, Vancomycin-Resistant *Enterococci* (VRE) V583, Methicillin-Resistant *Staphylococcus epidermidis* 35984, *Pseudomonas aeruginosa* PAO1, *Escherichia coli* UTI89, *Acinetobacter baumannii* 19606 and *Klebsiella pneumoniae* 13883 are obtained from ATCC.

6.2 Experiment

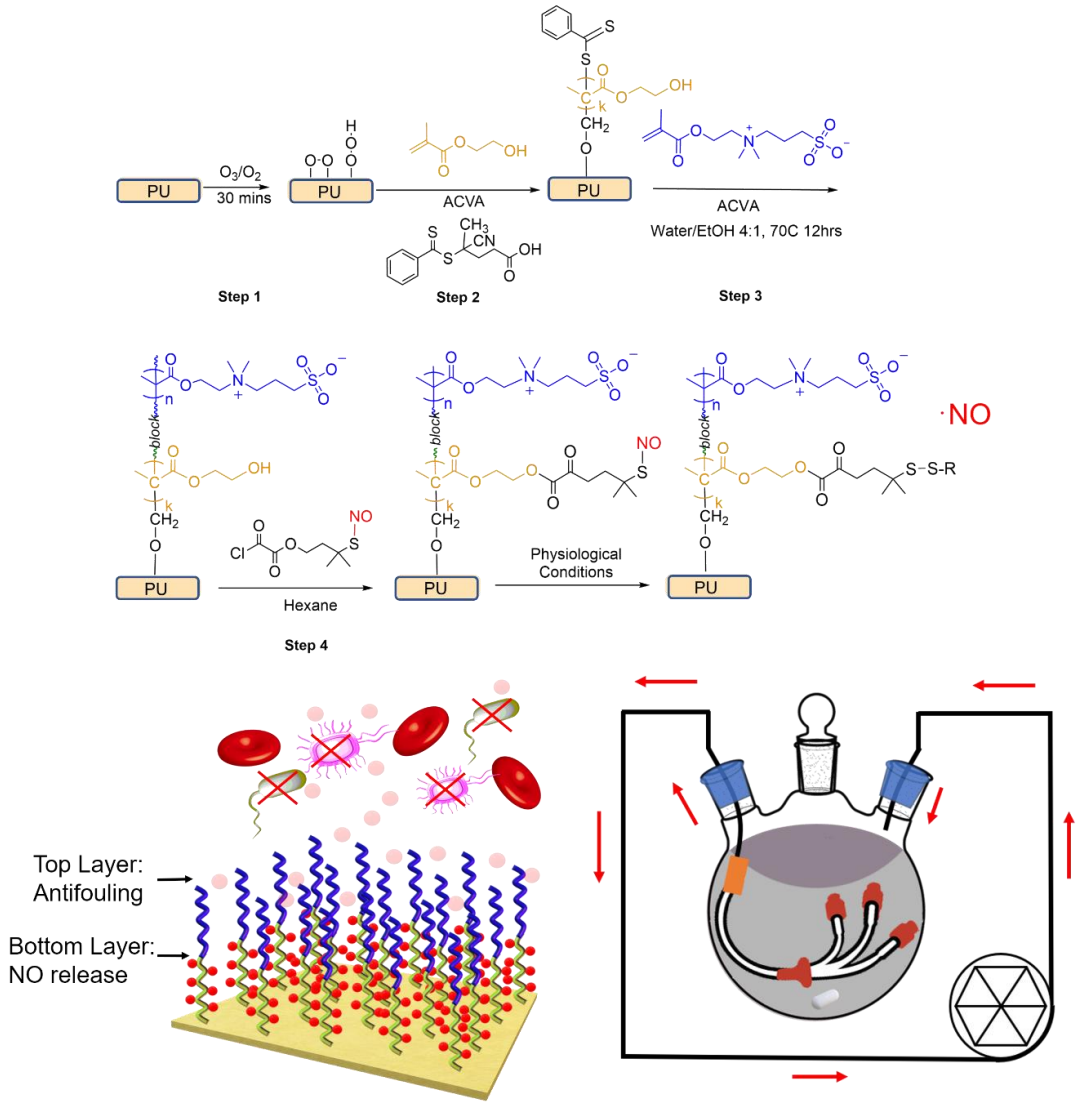

Scheme 6.1: Synthesis of surface-initiated Ozone-RAFT polymerization and grafting of tertiary nitrosothiol NO releasing precursor.

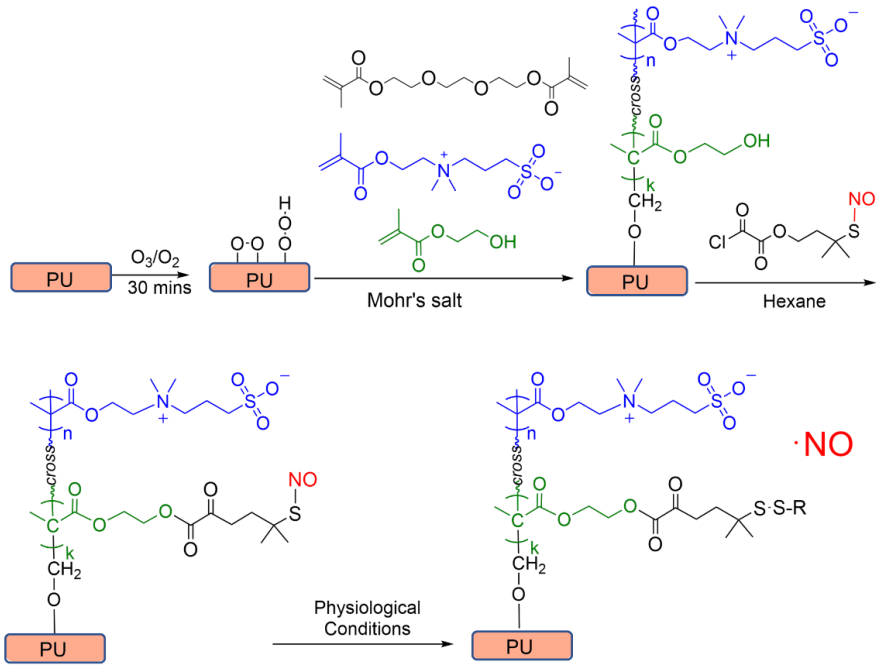

Scheme 6.2 Synthesis of cross-linked coating (#8 H(N)-x-S)

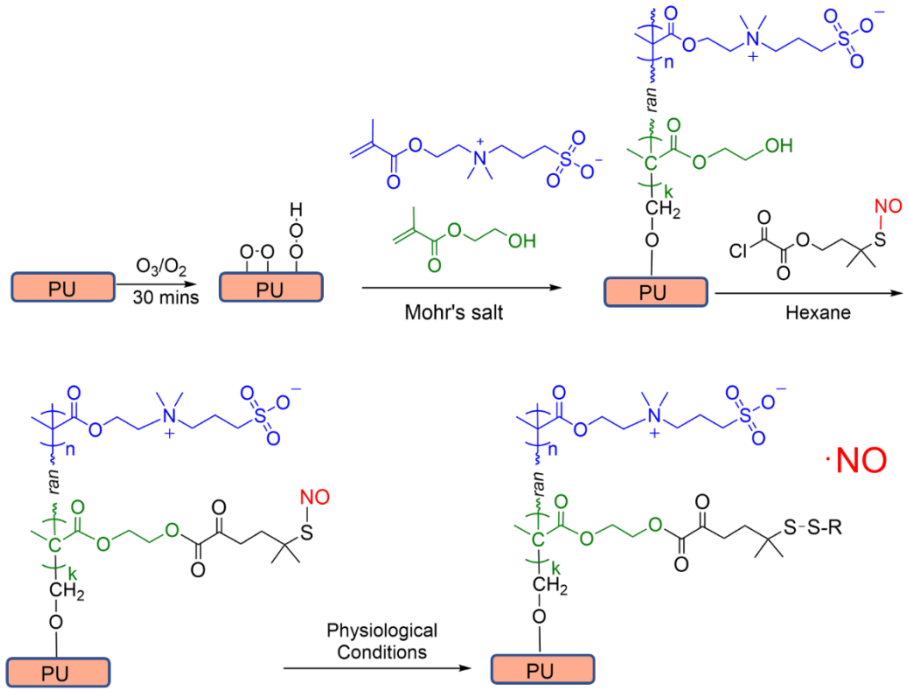

Scheme 6.3 Synthesis of random copolymer coating (#9 H(N)-r-S)

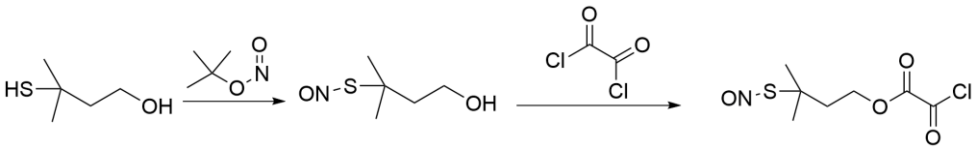

Scheme 6.4 Synthesis of tertiary nitrosothiol chloride S-nitroso-3-mercapto-3-methylbutyl oxalate chloride (abbreviation: SNO-Cl)

6.2.1 Characterization

Surface analysis

The surface functional groups of modified catheters were characterized using Fourier-transform infrared spectrometer (FTIR) with ATR accessory at an incident angle of 90°(Nicolet 5700, Thermo Fisher Scientific, U.S.A. Contact angle and morphologies of the catheters were studied with Goniometer (DSA 25, Kruss Scientific, Germany) and Scanning Electron Microscopy (JEOL JSM-6701F, Japan), respectively.

Measurement of NO release profile

The release of Nitric Oxide from catheter is triggered by raising the temperature to specific values. 0.5cm of catheter sample is soaked in 1mL of PBS and incubated under specific temperature. Both acute and long- term release of NO is measured using Apollo 1000 NO detector from world precision instrument.

Surface Antifouling Test

Catheter pieces were sterilized using 75% ethanol and soaked in PBS overnight before testing. The catheters were then introduced in 50% human serum, 1% Fibrinogen or 10% Albumin and incubated at 37°C for 24hrs. The catheters were

then removed and washed thrice using PBS. The washed catheters were put in 1mL of 1% SDS shake under 110rpm for 2hrs and sonicated for 10mins. The 1% SDS solutions were incubated with BCA protein assay kit solution for 30mins under 60°C. The OD values of the SDS solutions were then measure under wavelength 562nm. The protein concentrations were calculated according to the calibration curve provided in the kit.

6.2.2 Synthesis

Ozone Treatment of Poly-urethane catheter

The polyurethane catheter pieces are cleaned by methanol followed by deionized water. Air was used as inlet for ozone generator and the outlet ozone is purified by passing a 15cm sodium hydroxide column. The peroxide group was introduced by ozone treatment of PU catheter for 30mins. The ozone treated PU catheters were put under vacuum treatment (<10 Pa) for 1hr to remove the oxygen/ozone diffused into PU catheter surface.

The concentration of surface peroxide group is titrated against sodium thiosulfate. Total of 25 ml isopropanol was added to the sample, followed by 1 ml of saturated potassium iodide and 1 ml of glacial acid. The mixture was heated almost to boiling, kept at incipient boiling for 5 min with occasional swirling and without cooling, titrated with standard sodium thiosulfate (0.01mM) until the disappearance of the yellow color.

Surface-Initiated Ozone-Raft Polymerization

Grafting of Chain-Transfer agent terminated poly (hydroxyethyl methacrylate) layer

10% weight percentage of HEMA solutions in 10mL water and ethanol (1:1) mixture was prepared. 10mg of thermal initiator ACVA and 40mg of CPCPA were then dissolved in the solution. The solution was purged in Schlenk Tube using Ar for 30mins. The ozone treated catheters were then put into the monomer solution, the solution is purged for further 5mins, and sealed. The surface Ozone-Raft polymerization is initiated by heat-up at 70˚C. The polymerization reaction was carried for 24hrs. The polymerization is then quenched by ice-bath. The coated PU catheter was washed and sonicated in pure ethanol to remove homopolymer formed.

Surface-Initiated Raft Polymerization of poly (zwitterionic) polymer. (#7 H-b-S)

For Surface initiated Raft polymerization of poly (zwitterionic) polymer, 10% weight percentage of SBMA is dissolved in methanol and water mixture (1:1). 10mg of thermal initiator ACVA was dissolved in the solution. The chain-transfer agent grafted catheter prepared in step i) was placed in the solution. The solution was purged in Schlenk Tube using Ar for 30mins. The polymerization is then initiated by heat-up at 70°C and carried for 12hrs. The polymerization is then quenched by ice-bath. The coated PU catheter was washed and sonicated in pure ethanol to remove homopolymer formed. The terminal chain transfer agent

is removed by heat the catheter in 10% butylamine in methanol solution at 40°C for 1hr.

Preparation of Longer (30cm) PU catheter

30cm of PU catheter was cleaned using methanol and deionized water; and undergoes same ozone treatment as small pieces of PU catheters. The polymerization reactions and further modifications were done using a Plug-Flow reactor (Scheme 6.1).

General Surface Grafting of Nitric Oxide precursor onto Catheters

The S-nitroso-3-Mercapto-3-methylbutan-1-chloride (SNO-Chloride) was firstly prepared. Briefly, 1.2g of 3-Mercapto-3-methylbutan-1-ol was dissolved in 10ml cold ether, 1.03g of tert-butyl nitrite is added dropwise. The reaction carried for 30mins for fully conversion of nitroso group. The reaction solution was then purified by reduce pressure to remove by-product and ether. The S-nitroso-3-mercapto-3-methylbutan-1-ol was then quickly dissolved in 10mL hexane, with addition of 1.39mL of Triethylamine, the solution is then kept in 0˚C. 0.84mL of Oxalyl chloride was firstly dissolved in 5mL of hexane and added drop wisely in the S-nitroso-3-mercapto-3-methylbutan-1-ol solution. The reaction is kept in 0°C for further 2hrs and raised to room temperature. The surface grafted catheter was then added into the solution and kept the reaction for further 12hrs. The modified catheters were washed in methanol and water for 1hrs under 0°C to remove unreacted S-nitroso-3-Mercapto-3-methylbutan-1-chloride.

6.2.3 *In vitro* test of catheters

General procedure for Bacteria inoculum preparation: microbe suspension was prepared by scratching the colonies from plate and dipped in protein rich medium (Tryptic Soy Broth, TSB for bacteria and yeast mold broth for fungus). The inoculum is incubated with shaking at 225rpm at 37°C (28°C for fungus) to obtain the overnight culture.

General procedure for preparation of catheters for testing: catheter samples including control sample are sterilized with 75% ethanol, and then soaked in PBS before testing.

Surface antimicrobial assay: The bacteria or fungus overnight cultures are washed by PBS and resuspended into 10^8 cfu/mL in PBS. 10µL of the suspension is spread onto the catheter piece. The catheter piece is then incubated at 37°C for 3hrs with humidity not less than 90%. After the incubation, the catheter piece is washed throughout using 100µL of PBS, to recover the microbes. CFU number was counted by serial dilution of the bacteria suspension and culture on Lysogeny Broth Agar Plate (YM Agar for fungus)

Static Biofilm Growth Test: catheter pieces are immersed in 1mL TSB in a 24 well plate (YM medium for fungus). 10^6 CFU/ml microbe suspension was made by diluting in 10 mM phosphate buffer saline (PBS, PH 7.4) from overnight culture; 8 µl of this diluted bacteria suspension was added to each well. The plate was incubated at 37^{o}C for 24 hours. Catheter samples were then removed and washed gently thrice with PBS buffer to remove unattached bacteria. Each catheter sample was then placed in an Eppendorf tube with 1 ml PBS buffer. The

tube was placed in ultra-sonicator bath for 15 minutes at 0 ^{o}C and vortexed for 5 minutes to strip and remove the attached biofilm from the surface. CFU number was counted by dilution of the stripped bacteria suspension in PBS and culture on Lysogeny Broth Agar (LB Agar) plate. (YM Agar for fungus)

Intraluminal Biofilm Growth Test (For 30cm PU catheter): The antibiofilm efficacy of longer catheter is tested using an In-vitro catheterization model. The catheters are then incubated in human serum for 30min to mimic blood contacting. The catheter samples are incubated in PBS suspension of bacteria MRSA BAA-38 with 10^{8}cfu/mL for 2hrs. The catheter samples relate to peristaltic pump. The BHI medium is flowing through catheter and recycled at 0.7mL/min, 37^{o}C for specific time interval using peristaltic pump. Catheter samples were then removed from the medium and cut into 5mm pieces. The catheter pieces were washed gently thrice with PBS buffer to remove unattached bacteria. Each catheter sample was then placed in an Eppendorf tube with 1 ml PBS buffer. The tube was placed in ultra-sonicator bath for 15 minutes at 0 ^{o}C and vortexed for 5 minutes to strip and remove the attached biofilm from the surface. CFU number was counted by dilution of the stripped bacteria suspension in PBS and culture on Lysogeny Broth Agar (LB Agar) plate.

For all *in vitro* catheter antibiofilm efficacy tests, the Log reduction of modified catheter compared with unmodified control catheters was calculated as following:

$$Number\ of\ Log\ Reduction = log_{10}\left(\frac{CFU\ of\ control}{CFU\ of\ coated\ catheter}\right)$$

In vitro Biocompatibility assay

Cytotoxicity assay

The cytotoxicity assay is an extraction model adapted from ISO 10993-5 protocol.

Cell lines preparation:

The fibroblasts 3T3, Human embryonic kidney 293 cells (HEK), Human Dermal Fibroblasts (HDF) and HepG2 cell lines obtained from ATCC were cultured in DMEM medium supplemented with 10% fetal bovine serum (FBS) and antibiotics (glutamine (2 raM), penicillin (100 units/mL), and streptomycin (100 µg/mL). The cells were maintained at 37°C in a humidified incubator with 5% CO_2 until a monolayer, with greater than 80% confluence, was obtained.

Extraction method:

The 0.5cm sterilized catheters were incubated in DMEM complete medium. The plates were incubated at 37°C in a humidified with 5% CO_2 incubator for specific time, this to extract the material from the catheter.

Cytotoxicity assay of the extraction:

After 24hr, the cell line culture medium was discarded, and the cells were rinsed with PBS and the extraction was added into the wells and incubate for 24hr at 37°C in a humidified with 5% CO_2. Then, MTT (200 µl of 5mg/ml) was added into each well and the plates were incubated in a CO_2 incubator for 4h. The MTT was aspirated and dimethyl sulfoxide (DMSO) was added into each well and the

plates were kept in the shaker (at 150rpm). The absorbance of each well was measured at 570 nm using microplate reader spectrophotometer (BIO-RAD, Benchmark Plus). All the assays were performed in triplicate. The percentage of the cell viability was calculated by the formula:

$$\%\ Cell\ viability\ = \frac{Average\ absorbance\ from\ treated\ cells\ X\ 100\%}{Average\ absorbance\ from\ control\ cells}$$

Immunostaining of activated cells in blood

Rabbit whole blood is used to test the blood immunological response triggered by catheters. The blood is freshly collected from the jugular vein of female New Zealand white rabbit and used immediately.

The 0.5cm sterilized catheters were incubated with 100µL of Rabbit whole blood for 30mins. The blood is then fixed with 4% paraformaldehyde for 10mins under room temperature. The excess paraformaldehyde is then removed and washed twice with PBS. Specific antibodies were dissolved in PBS and incubated with blood samples for 1hr. (lymphocytes: CD3-APC and CD25-FTIC; monocytes: CD14-APC, CD11b-FTIC; platelets: CD41-FTIC, CD62p-APC; Polymorphs: CD66b-APC, CD11-FTIC). The labelled blood cells were then washed twice with PBS. Cell counts were performed using Attune NxT Acoustic Focusing Cytometer. Blood without any treatment is used as negative control.

Thrombus activation and formation test

The 0.5cm sterilized catheters were incubated with 100µL of Rabbit whole blood for 2hrs in 96well plate. The catheter is then washed with PBS thrice to remove

unattached protein or blood cells. For quantification of thrombus by ADP assay, the catheter pieces are incubated with 100µL of 5% Disodium 4-Nitrophenyl Phosphate for 2hr. The catheter is removed and 100µL of 1M sodium hydroxide is added. The intensity of each well is measured under wavelength of 405nm. For Scanning Electronic Microscopy observation of surface thrombus on catheter pieces, the catheter pieces are fix with 4% paraformaldehyde in PBS solution overnight at 4°C. The fixed catheter pieces are dehydrated by soaking in 25%, 50%, 75% and 100% ethanol. The ethanol from dehydrated samples are removed by Argon gas follow. The dried samples are observed under Scanning Electronic Microscope.

6.2.4 *In vivo* test of catheters

***In vivo* Mice Subcutaneous Implantation Model(Jagath L. Kadurugamuwa et al., 2003):** Overnight culture of bacteria were diluted in 1% TSB in PBS to give a final concentration of about 10^7 cfu/mL. Both control catheter and modified catheters were incubated with the bacteria inoculum at 37°C for 2hr. 7 to 8 weeks old female Balb/c mice were anesthetized by injection of Ketamine and shaved. 5mm of wounds were made on the back of the mice. The bacteria infected catheters were then inserted into the subcutaneous part of the wound. The wounds were then sealed with 3M Tegaderm. At the 24h time point, mice were euthanized with CO_2. The implanted catheters were then removed and observed the blood coagulation. The samples were then sonicated to remove the adhered bacteria and serially diluted and plated on LB agar plates. CFU were enumerated after 24h of incubation at 37°C.

6.3 Results and discussion

The zwitterionic (with SBMA monomer, labelled as "S") and hydroxyl terminated (HEMA, "H") monomers are polymerized into 3 structural arrangements： block copolymerized (#7 H-b-S), crosslinked into hydrogels (#5 H-x-S) or randomly copolymerized (#6 H-r-S). Then, the 3 differently-structured polymer coatings were further modified via the hydroxyl group to attach the NO-precursor to result in crosslinked NO-release coating (#8 H(N)-x-S) (Scheme 2) random copolymer with NO-release coating (#9 H(N)-r-S) (Scheme 3), and block copolymer with NO-release coating (#10 H(N)-b-S); in these designations, the 'N' indicates the presence of covalently bonded NO release precursor. In addition, controls were also made to evaluate the efficacy of the modified catheters and to provide references to changes caused by attachment of the NO release precursor: the neat (zwitterionic) poly-SBMA coating (S) and the (neutral) poly-HEMA coated PU catheter with covalent attachment of NO-release precursor (Poly-HEMA-*graft*-RSNO, *i.e.* #4 H(N)) and commercially available silver coated catheter (#2 Silver).

6.3.1 Surface characterization

Figure 6.1A (1) exhibits the gross visual appearance of (30 cm) long unmodified PU and H(N)-b-S catheters. The color is changed from transparent to dark green due to the presence of the tertiary nitrosothiol group. The scanning electron microscopy cross-section (Figure 6.1A (2)) shows that the #10H(N)-b-S coating is about 10μm thick; the thickness is due mainly to addition of the

hydroxyl base layer (PU-H-raft) and the hydrophilic top layer (#3 S) . The 3D AFM image for #3 H(N)-b-S indicates that block copolymer coating is very dense and thick with full coverage of PU substrate (Figure 6.1A (3)).

Quantification of the surface peroxide groups generated by ozone treatment of the PU substrate, indicates 169 peroxide initiators/nm^2 (Equation 1), which is consistent with previous literature(Keiji Fujimoto et al., 1993), We compared the chemical structures of different coatings using ATR-FTIR: comparing the poly-HEMA-coated PU (PU-H) surface with unmodified PU control (Figure 6.1Bii,i), the poly-HEMA (Figure 5.1Bii) first block shows increased peak intensity and new peaks appearing at 1750cm^{-1} and 1020cm^{-1} respectively, corroborating the addition of ester carbonyl group and hydroxyl (C-O-H) group from HEMA. The success of the second copolymerization step, of the poly-SBMA block, is proved by appearance in the H-b-S coating spectrum (Figure 6.1Biii) of the sulfonyl signal at 1040cm^{-1} and further increase of the ester carbonyl signal (1750cm^{-1}) from the methacrylate group. The C-O-H group signal (1020 cm^{-1}) from the poly-(HEMA) underlying block (H) is still detectable. After grafting of NO-release precursor (Figure 6.1B-iv), the signal of C-O-H groups (1020cm^{-1}) disappear, indicating successful reaction between surface C-O-H group with chloride group from (RSNO-Cl, the NO release precursor). Also, the ester carbonyl signal (1750cm^{-1}) in the #10 H(N)-b-S spectrum is further increased, indicating increase of ester linkages due to chloride group reactions with hydroxyl groups in the poly-(HEMA) layer.

The modification process was also tracked by water contact angle changes (Figure 6.1C). The contact angle of the catheter declined from 82.3±0.1° (#1 Unmodified PU) to 45.4±0.1° (H) after grafting the first layer of poly-HEMA. A single layer of poly-SBMA makes the surface even more hydrophilic, with contact angle reduced to 4.7±0.1° (#3 S), but poly-(SBMA) does not have any functional groups for further modification. Grafting of the NO-precursor to poly-(HEMA) coating increases the contact angle to 87.8±0.1° (#4 H(N)). The random (#5 H-r-S) and crosslinked (#6 H-x-S) coatings have smaller contact angles of 47.3° and 45.4o for #5 H-r-S and #6 H-x-S respectively and are much less hydrophilic than the block copolymer coating (#7 H-b-S) which has the contact angle of 5.4±0.1° which is almost similar in hydrophilicity to the homo poly-(SBMA) coating (#3 S, 4.7±0.1°). Further, after grafting of the random and cross-linked coatings with NO-release precursor, the contact angles increase substantially, to 80.8° (#8 H(N)-r-S) and 70.1° (#9 H(N)-x-S) respectively, and the hydrophilicity is lost (Figure 6.1C). However, grafting of NO-release precursor (R-SNO-Cl) to the diblock only slightly increases the water contact angle (to 8.0° for #10 H(N)-b-S), which indicates the intrinsic hydrophilicity of the surface zwitterionic polymer layer is preserved.

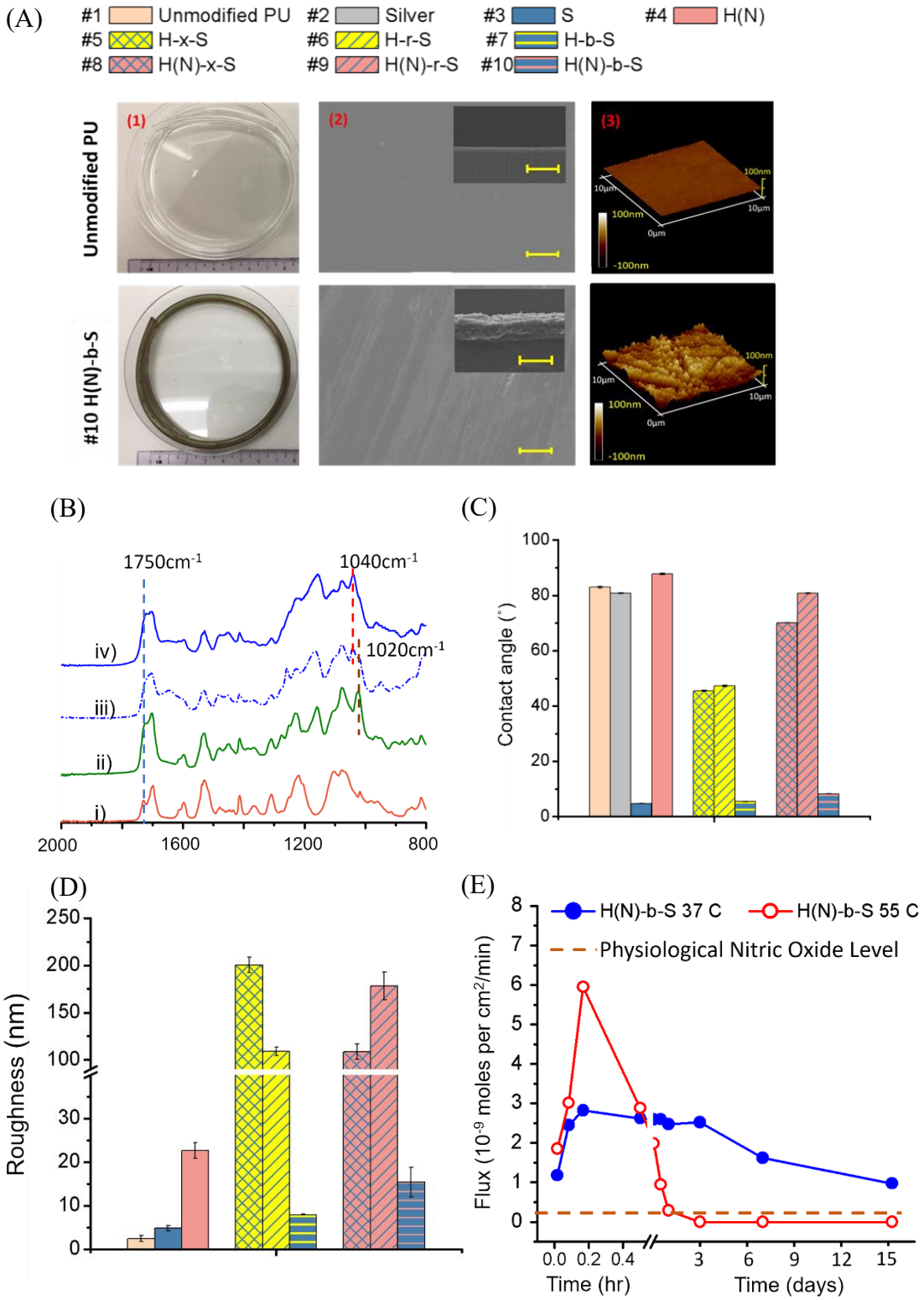

Figure 6.1. Characterizations surface coatings. (A) surface characterizations. (1) photograph of long H(N)-b-S coated catheter compared with unmodified catheter (2) SEM images of surface and cross-sections of unmodified catheter and H(N)-b-S catheter. Scale bar =10μm (3) Surface morphologies of unmodified catheters and H(N)-b-S catheter measured by AFM. (B) FTIR

characterization of block copolymer coating by surface-initiated Ozone-RAFT polymerization. (i) unmodified PU control. (ii) Polymerization of first block (PU-H), (iii) Polymerization of second block (#10 H(N)-*b*-S). (iv) After covalently grafting of SNO-chloride NO release precursor. (C) Change of contact angles for different modifications. (D) Change of roughness for different modifications. (E) Long term NO release flux.

Figure 6.1D shows that compared to the unmodified PU (RMS=2.4nm), #5 H-r-S and #6 H-x-S have much higher surface roughness (RMS >100nm). The surface roughness of #7 H-b-S (RMS=7.9nm) is not much larger than that of unmodified PU, similarly, the #10 H(N)-b-S (RMS = 15.4nm). The stability of ozone-initiated coatings is proved by incubating the modified catheters (#3 S and #10 H(N)-b-S) with water (Figure 6.2A) and PBS (Figure 6.2B), serum (Figure 6.2C) and bacteria inoculum (Figure 6.2D and E). The water contact angles of these catheters remain to be low (<20°) even after 30-day incubation in various fluids, indicating long-term stability of the hydrophilicity properties of #3 S and #10 H(N)-b-S.

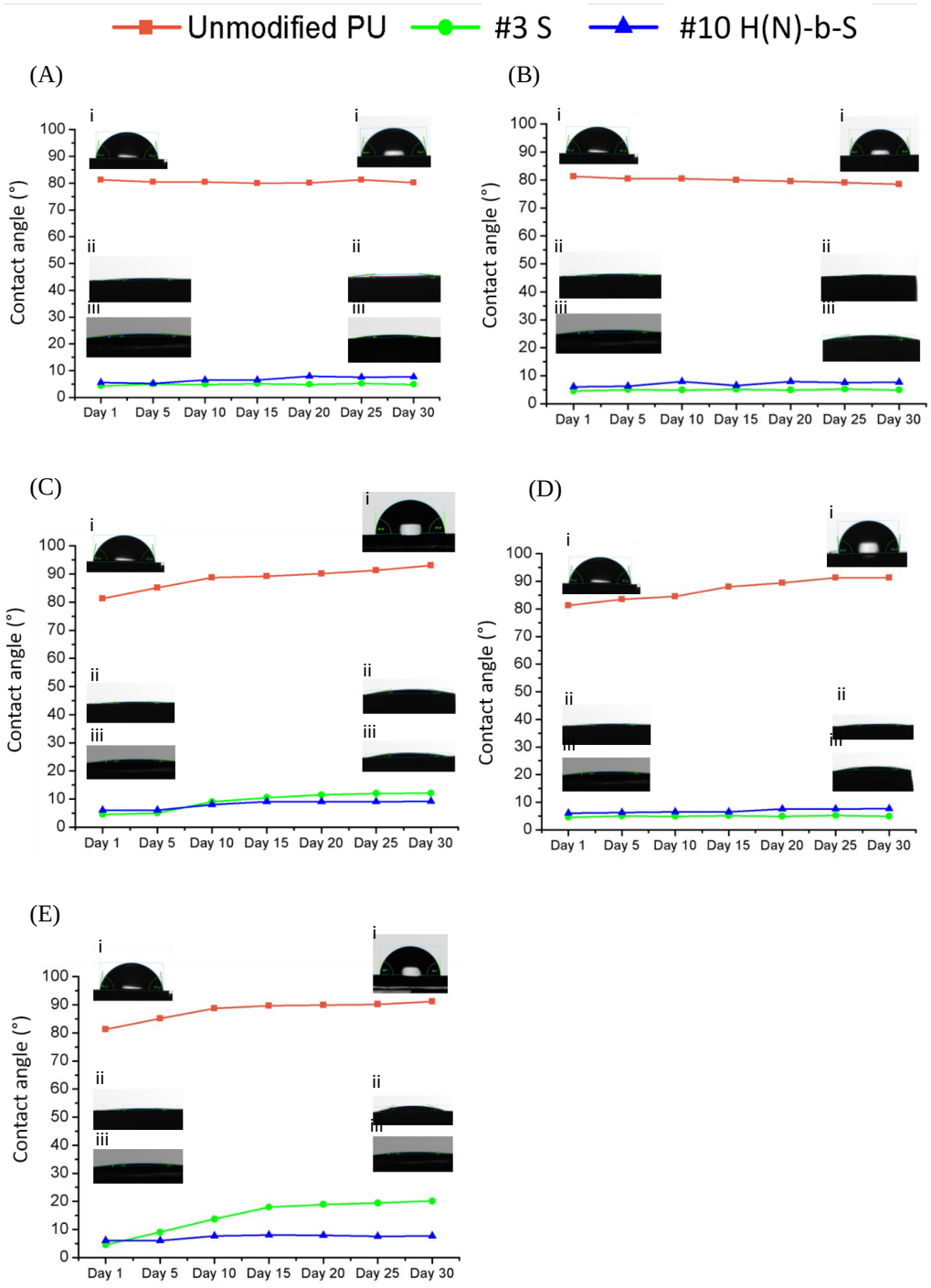

Figure 6.2 Long term hydrophilic test under various conditions. Simple fluid: (A) Water (B)PBS saline (C) Serum (D) S. aureus inoculum (E) P. aeruginosa inoculum. The contact angle on catheters are photographed: (i) unmodified PU (ii) #3 S (iii) #10 H(N)-b-S

The #10 H(N)-b-S catheter was extracted with polar (methanol) and nonpolar (hexane) solvents and with PBS solution for 24H-r-S (Figure 6.3A) and 1 week (Figure 6.3B); no leaching of NO precursor was detected in any of the experiments. The flux of released Nitric Oxide from the #10 H(N)-b-S catheter was measured with an Apollo 1000 NO detector with the catheter immersed in PBS at 37°C to mimic physiological conditions (Figure 6.1E). The NO release flux reaches the maximum (2.45×10^{-9} mol/cm^2/min) in 10 mins and remains at that level until 72H-r-S (3days), after which it declines slightly but is still higher than the natural NO flux from epithelial cells (0.5×10^{-10}mol/cm^2/min)(Alessandro Colletta et al., 2015). (At higher temperature (55°C), the early-time release is faster, which exhausts the NO precursor within 2-3 days (Figure 6.1E).)

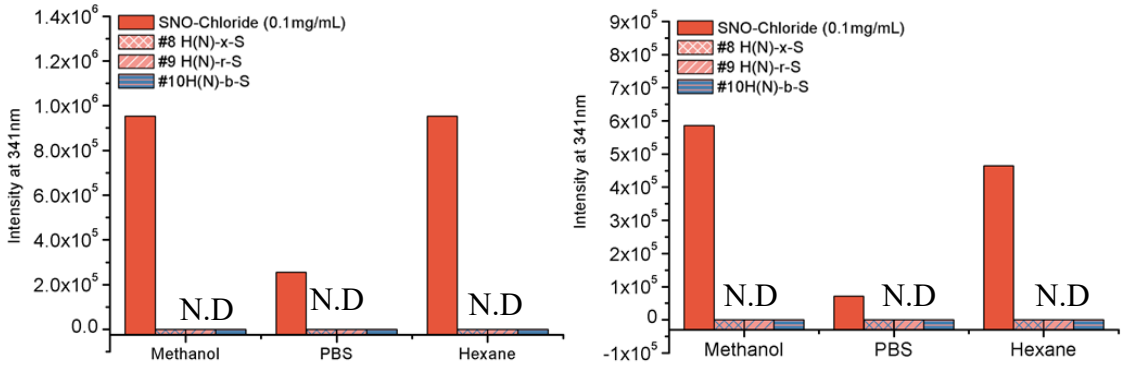

Figure 6.3. HPLC detection of NO release precursor leaching to different solvents. N.D refers to no detection of leaching (intensity = 0). (A) 24hrs extraction (B) 1-week extractions

6.3.2 Excellent antimicrobial and antibiofilm efficacy of the block brush coating

The purely hydrophilic coatings (#3S, #5H-r-S, #6H-x-S and #7H-b-S) show no bactericidal efficacy (Figure 6.4A, B and C). The bacteria were loaded directly on the catheter surface for 2h before counting. After attachment of R-SNO, all the NO-emitting coatings, whether homopolymer or copolymer derived (#4H-N, #8H(N)-r-S, #9H(N)-x-S and #10H(N)-b-S), show significant antibacterial effect (>3$\log_{10}$) against Gram-negative and Gram-positive bacteria and a fungus, (specifically *E.coli* UTI89, *K. pneumoniae* 13883, *P. aeruginosa* PAO1, *A. baumannii* 19606, Methicillin-resistant *Staphylococcus aureus* (MRSA) BAA38, Vancomycin-Resistant *Enterococci* (VRE) V583, Methicillin-Resistant *Staphylococcus epidermidi*s (MRSE) 35984; and Candida albicans 90028), which is comparable to the commercial silver coated catheter(#2 Silver). More interestingly, the structure of the copolymer coating (i.e., random, cross-linked or block, #8-#10) has little effect on the bactericidal and fungicidal efficacy.

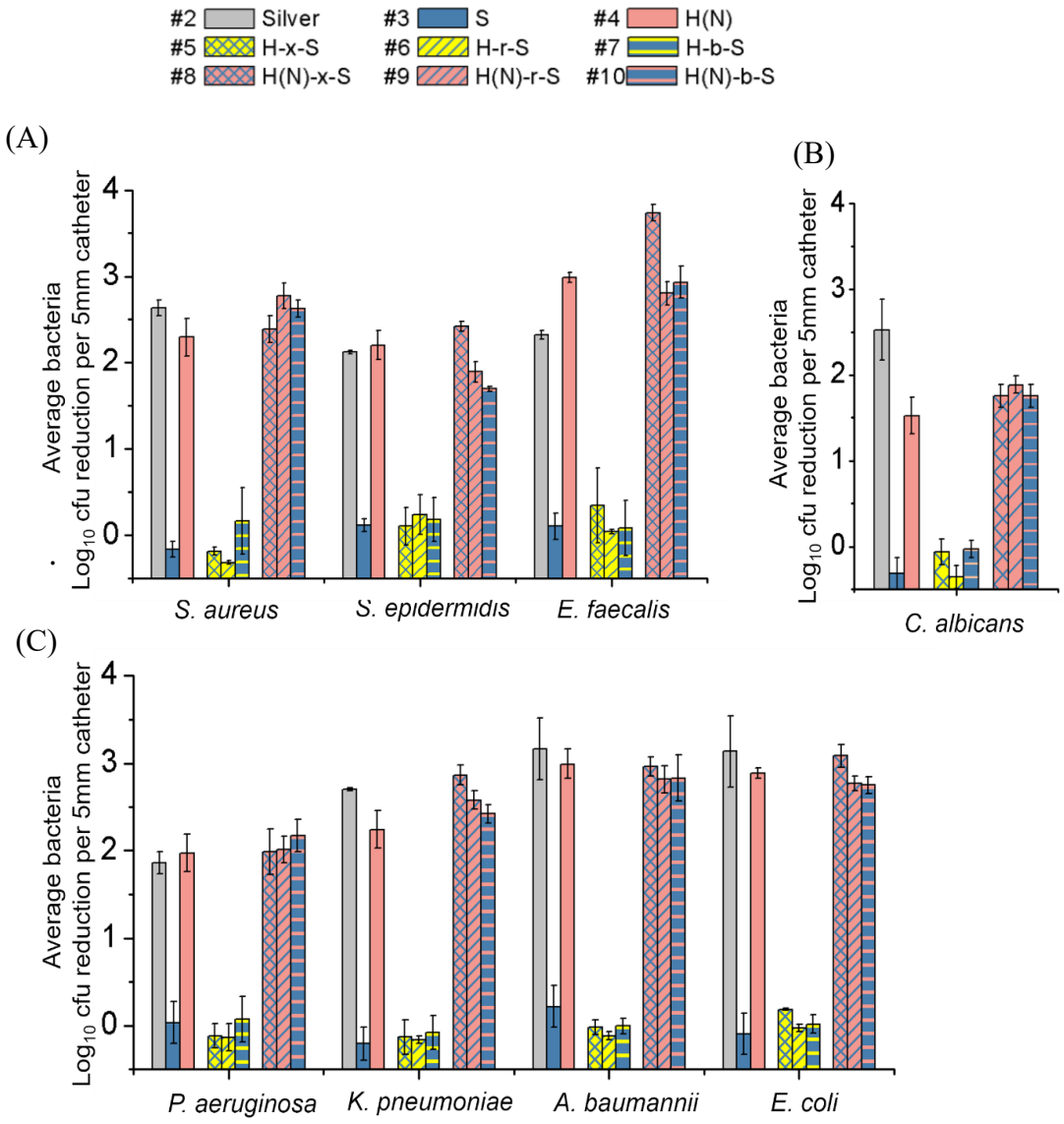

Figure 6.4. Acute surface antimicrobial efficacy measured by contact killing (A) Antibacterial efficacy against Gram-Positive bacteria. (B) Antifungal efficacy against *Candida albicans.* (C) Antibacterial efficacy against Gram-Negative bacteria.

The catheters were also tested for antibiofilm efficacy in a protein rich (Tryptic Soy Broth) medium in the presence of bacteria with a fairly long (24h) incubation period to promote biofilm formation (Figure 6.5A, B and C). The silver coated control catheter (#2) shows insignificant inhibition of biofilm

growth (<1.5log$_{10}$). The hydrophilic coatings (#3S, (#5H-r-S, #6H-x-S, and #7H-b-S) reduce the biofilm by 1.5-2.5 log$_{10}$ for all the pathogens.

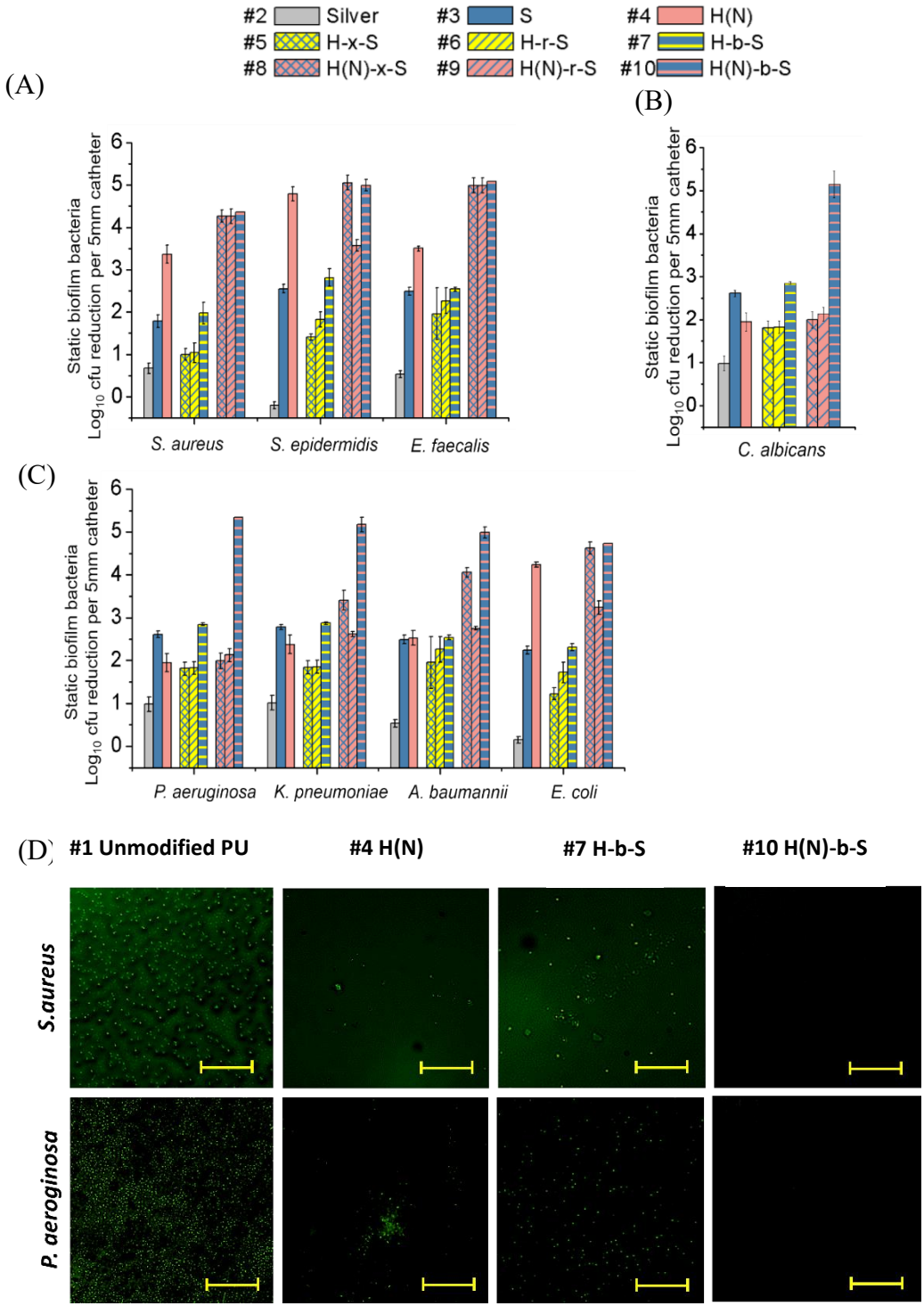

Figure 6.5 Biofilm bacteria attachment inhibition efficacy of the coatings measured by both static and long-term intraluminal models. (A) Biofilm bacteria inhibition efficacy against Gram-

Positive bacteria. (B) Biofilm fungi inhibition efficacy against *Candida albicans*. (C) Biofilm bacteria inhibition efficacy against Gram-Negative bacteria. (D)Fluorescence Microscopy of catheter incubated with bacteria. bar=20μm

With Gram-positive bacteria (Figure 6.5A), the introduction of NO-release precursor into the coating (#4H-N, #8H(N)-r-S, #9H(N)-x-S, and #10H(N)-b-S) greatly improves the biofilm inhibition efficacy as compared to purely hydrophilic coatings without NO (#3S, #5H-r-S, #6H-x-S and #7H-b-S) . For example, with S. aureus (Figure 6.5A), the biofilm bacterial reduction of the 3 NO-containing coatings (#8H(N)-r-S, #9H(N)-x-S, and #10H(N)-b-S) are 4.2 to 4.5 $\log_{10}$ compared with 1.2 to 2.0$\log_{10}$ for the no NO-containing coatings (#5H-r-S, #6H-x-S, and #7H-b-S). However, with Fungus and Gram-negative bacteria (Figure 6.5B and C), only the block copolymer brush containing the NO precursor (#10) is superior in biofilm reduction compared to the parent hydrophilic coating without NO-release (#7); the NO-emission in other brush structures (#8, #9), i.e. random brush and hydrogel coating, do not seem to improve the biofilm reduction compared to their parent structures (#5, #6) except *E. coli*. With Candid which has the same trend as the Gram-negative bacteria, only the combination of block copolymer brush with NO release (#10), but not #9 and #8, can have significantly high antibiofilm effect of >4.5$\log_{10}$. The improved antibiofilm efficacy of #10H(N)-b-S compared with #5H-b-S and #4H-N indicates the importance of the spatial organization of the coating components for optimization of the respective contributions of the NO-release and antifouling components. Our optimization shows that #10 gives the superior antibiofilm and antibacterial effect against all pathogens tested (Figure 6.4 and Figure 6.5).

The bacteria adhesion inhibition of the catheters was observed with fluorescence microscopy (Figure 6.5D). For the unmodified PU control, the surface was fully covered with *S. aureus* (MRSA BAA-38) and *P. aeruginosa* (PAO1), the H-b-S and H(N) coated catheter show significant reduction of bacteria adhesion; however, small numbers of bacteria can still be found on the surfaces. For the #10 H(N)-b-S coating, no bacteria were found adhered on the surface.

Further, 30cm-long H(N)-b-S (#10) catheters were surface-modified using the scaled-up Ozone-RAFT technique. The coated catheter #10 was tested under a circulatory intraluminal contact condition mimicking blood vessel circulation, together with controls of unmodified PU catheter (#1), silver coated catheter (#2), and hydrophilic coated catheter (#3). The catheters were loaded with bacteria (MRSA (BAA-38) or *Pseudomonas aeruginosa* (PAO1)), and then biofilm promoting medium (Brain heart infusion) was circulated through the catheter for 30 days. For both bacteria (Figure 6.6), silver coated catheter shows limited initial antibiofilm efficacy at Day 1 but became totally non-antibacterial from Day 5 onwards. With MRSA, the #3S and #10H(N)-b-S initially (at day 1) shows 2.5$\log_{10}$ and >4$\log_{10}$ inhibition but at Day 15, the bacterial reduction is about 1.5$\log_{10}$ and 3$\log_{10}$ respectively for the 2 catheters. Comparing with Figure 6.1E (NO release profile), the bacteria count starts to grow from Day 15 as the nitric oxide release declines. At Day 30, the bacterial reduction is 3$\log_{10}$ for #10H(N)-b-S but 1.5$\log_{10}$ for #3S.

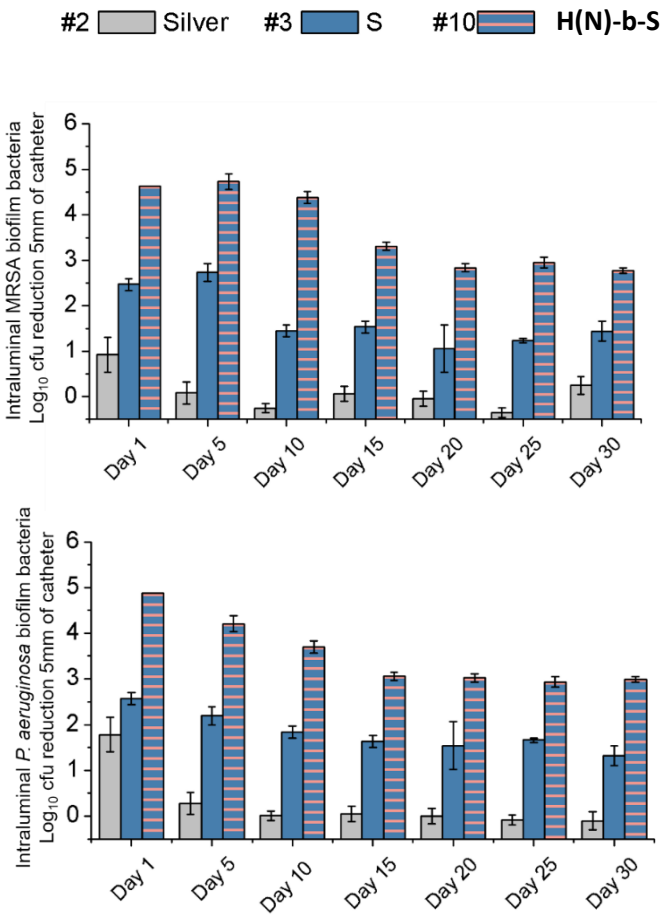

Figure 6.6 Long-term (30 Days) intraluminal biofilm inhibition against MRSA and *P. aeruginosa* biofilm formation

6.3.3 Excellent Biocompatibility

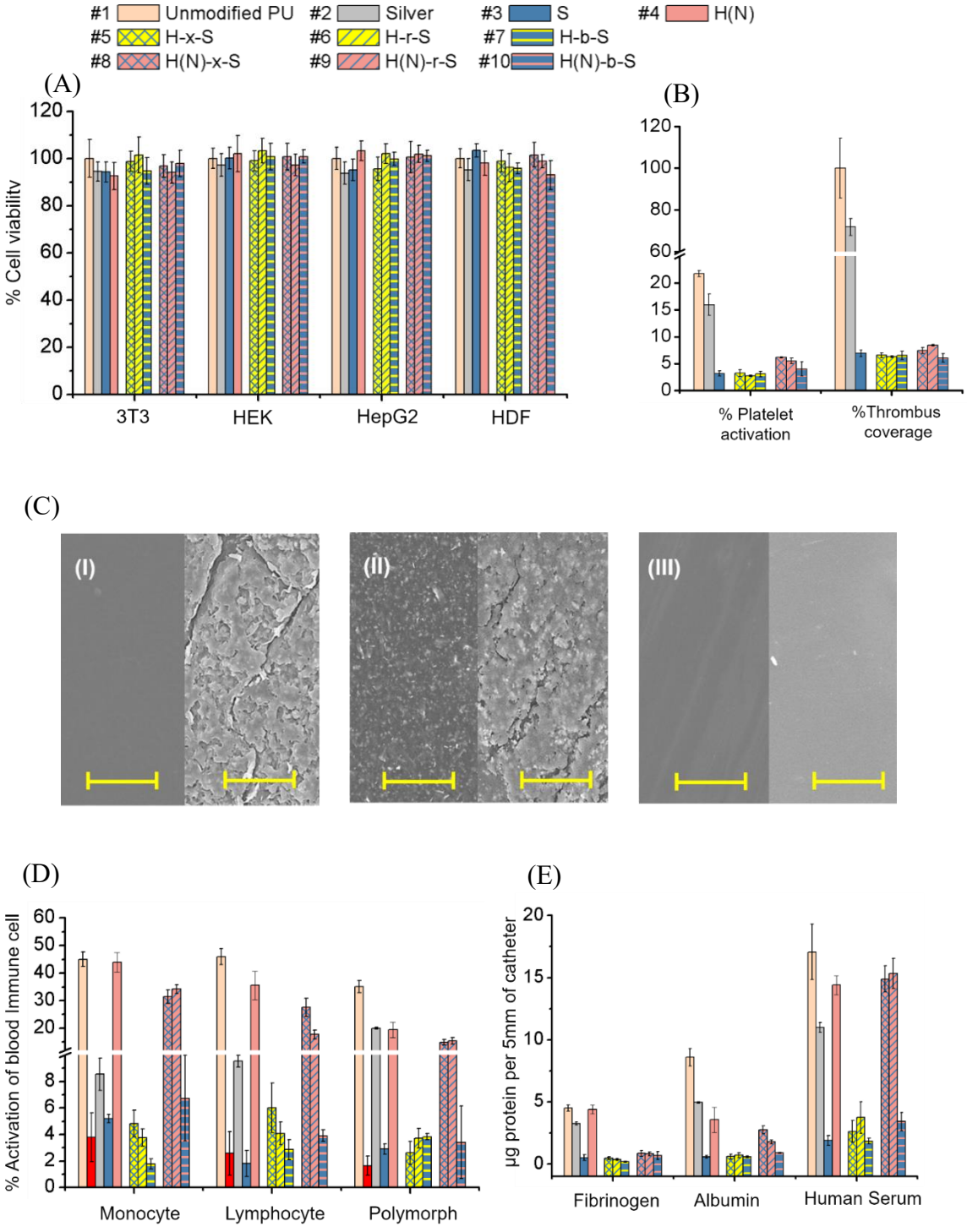

Figure 6.7. Biocompatibility against mammalian cells, blood immune cells and antithrombogenic efficacy of the coatings. (A) Mammalian cell compatibility of extractants from soaking modified catheters in DMEM for 24hrs. (B). Antithrombogenic efficacy of the coatings measured by platelet activation and surface thrombus formation. (C) Scanning Electronic Microscopy images of thrombus formed on catheters, Left: before incubation with rabbit whole blood. Right: after

2hrs incubation with rabbit whole blood: (i) unmodified PU catheter. (ii) commercial silver coated catheter. (iii) #10 H(N)-b-S Scale bar=10μm. (D) Activation of blood immune cells red bar endogenous level of immune cell activation. (E) Blood protein fouling on catheters.

The modified catheters were extracted with DMEM medium. The cytotoxicity of the extracts was tested against multiple mammalian cell lines (3T3 fibroblasts, HDF human vascular cells, HepG2 liver cells and HEK kidney cells) (Figure 6.7A). Extractants from all catheter coatings, including the NO-emitting coated catheters (#4, #8-#10) show >80% cell viability for all cell lines, indicating good biocompatibility of the coating.

Catheter-triggered platelet activation and thrombus formation were measured by *in vitro* incubation of the catheter with whole rabbit blood. The activated platelets were labelled with antibodies and tracked by Fluorescence-Activated Cell Sorting (FACS) analysis; thrombus formation on the surface was quantified by measuring Adenosine 5'-diphosphate (ADP) trapped in thrombi using 4-Nitrophenyl phosphate disodium salt hexahydrate (Figure 6.7B). The unmodified catheters (Figure 6.7B, #1) produced activation of 22.5% platelets and were densely covered with thrombi (that we set as 100%). The silver coated catheter shows 15.1% platelet activation and 73.2% thrombus coverage. With purely NO-emitting coating (Figure 6.7B, #4), significant thrombus formation (58.6%) was measured because this coating is hydrophobic with contact angle of 87.8 (Figure 6.1C #4) as it lacks the zwitterionic component (S), indicating the importance of hydrophilicity for non-thrombogenicity. All the purely hydrophilic (#3, #5-#7, Figure 6.7B), and hydrophilic-NO coated catheters (#8-10, Figure

6.7B) showed low platelet activation (<10% activation) and thrombus coverage (<10% coverage of thrombus).The thrombi formed on catheter surfaces were imaged with scanning electronic microscopy (Figure 6.7C). High coverage with thrombi was seen on unmodified catheter (#1, Figure 6.7C and Figure 6.8). No thrombi were found for the block copolymer NO-release coating (#10, Figure 6.7C-iii,). Similarly, no thrombi were found for the random copolymer or the cross-linked with/without NO (Coating 5-#10, Figure 6.8). SEM imaging also corroborates that coating #4, i.e. the NO release catheter without zwitterionic monomers (H-N), shows some thrombus formation (Figure 6.8 red circle).

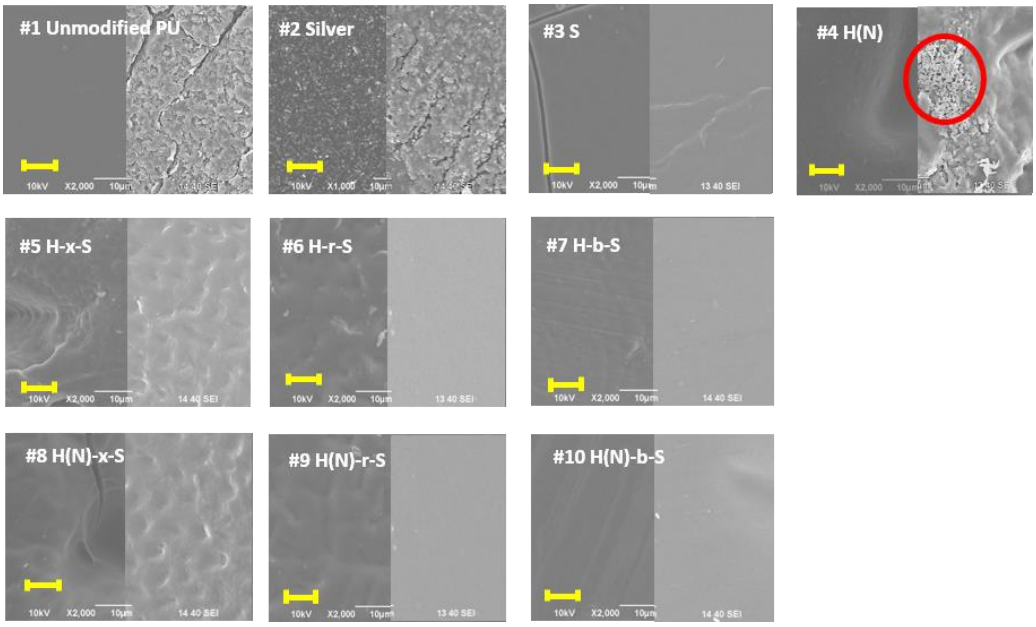

Figure 6.8. SEM images of thrombus formation on catheter samples. Red circle: partially coverage of thrombus

Figure 6.7D shows that the unmodified PU catheter (#1) triggers the immune activation of monocytes (45% activation), lymphocytes (48% activation), and polymorphs (34% activation) as measured by FACS. The silver

coated catheter (#2, Figure 6.7D) also triggers the immune activation of polymorphs (8.2% activation), monocytes (9.5% activation) and lymphocyte (20.0% activation). With purely hydrophilic modification (#3, #5-#7), the immune cell activation is significantly reduced to 2~6% for all immune cells, which is only slightly higher than the endogenous level (1~4%, red bar, Figure 6.7D) of blood immune cell activation in the absence of trigger (negative control). With the random and crosslinked copolymer with NO-release coating (#8 and #9, Figure 6.7D), significant (20-30%) activation of the immune cells was observed. On the other hand, the block copolymer NO-release coating (#10, Figure 6.7C), H(N)-b-S, shows insignificant activation of lymphocytes (6.4%), monocytes (3.9%) and polymorphs (3.7%), which is comparable to the endogenous levels (red bar, Figure 6.7D).

The protein fouling resistance of the coated catheters was evaluated by incubating the catheters with both defined proteins such as fibrinogen and albumin, and with serum, which contains a complex mixture of blood proteins (Figure 6.7E). The unmodified catheter (#1) experienced high protein fouling (5μg/cm^2 for fibrinogen, 9.6μg/cm^2 for albumin and 17.25μg/cm^2 for human serum); the protein fouling on silver catheter was also high (4μg/cm^2 for fibrinogen, 5.5μg/ cm^2 for albumin and 11.2μg/ cm^2 for human serum) due to the hydrophobic nature of the surface (contact angle of 82.3°, Figure 6.1C). All the purely hydrophilic coatings (#3, #5-#7, S, H-r-S, H-x-S and H-b-S) reduced fouling, to <0.5μg cm^2 for fibrinogen, <1μg/ cm^2 for albumin and <4μg/ cm^2 for human serum. After covalent attachment of NO-release precursor, the H(N)-r-S

(#8) and H(N)-x-S (#9) lost the protein fouling resistance in human serum (>15 µg/ cm^2). However, the H(N)-b-S (#10) catheter preserved the intrinsic protein fouling resistance of the parent hydrophilic H-b-S coating.

6.3.4 *In vivo* inhibition of pathogen adhesion of modified PU catheter

(A)

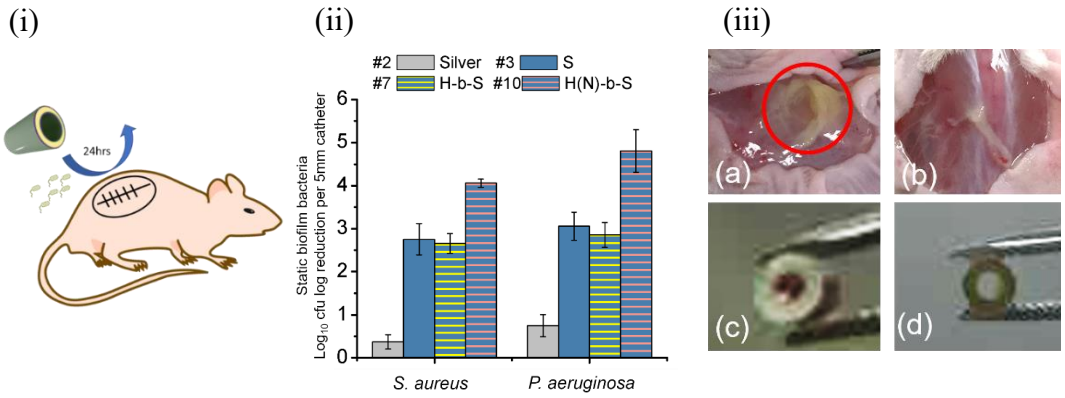

Figure 6.9. *In vivo* antibacterial efficacy (A) Murine subcutaneous model (i) illustration of subcutaneous implantation and infection. (ii) *In vivo* antibacterial efficacy for subcutaneous infection model. (iii) Images of infected subcutaneous pocket and recovered catheter after 24hrs implantation. (a) Serious sign of infection found in the subcutaneous pocket implanted with unmodified catheter (b) Minimal sign of infection found in the subcutaneous pocket implanted with #10 H(N)-b-S catheter. (c) Clotted blood found on unmodified catheter. (d) No blood clotting found on #10 H(N)-b-S catheter.

Subcutaneous antibiofilm experiments (Figure 6.9A) were performed on best coated (#10) and control (#2, #3, #7) catheters. Catheters were firstly infected with high concentrations of MRSA-BAA38 and PAO1 (10^8cfu/mL) and implanted into a subcutaneous pocket created on mice (Figure 6Ai). After 24H-r-S of implantation, the catheters were removed. The bacteria adhered on the #10 H(N)-b-S catheter surface achieved an excellent (>4log_{10}) bacteria reduction compared with the unmodified PU control catheter (Figure 6.9A iii), compared with less than 1 log_{10}, 3log10 orders, and 3log10 orders with silver, #3, and #7 controls against both *S. aureus* and *P. aeruginosa*. The pocket implanted with

unmodified PU-control catheter shows yellowish mass which is indicative of infection/inflammation (Figure 6.9A iia), and the intraluminal space is filled with clotted subcutaneous blood (Figure 6.9A iic). The pocket implanted with H(N)-b-S catheters (#10) is almost clean and without inflammation (Figure 6A iib) and no clotted blood was observed in the intraluminal space (Figure 6.9A iid).

6.4 Discussion

Although NO has very attractive antibacterial antibiofilm and antithrombogenic properties, challenges in using it practically in catheters revolve around overcoming its toxicity, localized sustained delivery(Lei Yang, Evan S. Feura, Mona Jasmine R. Ahonen, & Schoenfisch, 2018). The toxicity stems from leaching and increased hydrophobicity due to the NO-donor, particularly for the RSNO donor which is organic (unlike NONOates which normally exist as sodium salts). Our works shows that only with the block copolymer brush with covalent attachment of the NO-donor to the inner layer leaving the outer layer hydrophilic (#10H(N)-b-S), then only is the antibiofilm effect and the anti-thrombogenic effect excellent. Further, with this covalent attachment of the NO donor to the coating, the biocompatibility is excellent (MTT Figure 6.7A). Many catheter-works involving NO release involve impregnation of the NO donor into the catheter itself, but this will release in the donor leaching and toxicity. Sadrearhami et al has used dopamine to covalently react with NO gas at high pressure (5 atm) with methanol and base (NaOMe) for glass slides, but these conditions will be feasible for plastic catheter(Zahra

Sadrearhami et al., 2019). In our project, a Surface Initiated Ozone-RAFT polymerization was developed which can be applied on various plastics.

Surface ozone treatment can introduce high density of peroxide initiator groups as 169 peroxide initiators/nm^2 (Supporting Info, Equation 1), which is agreeable with previous literature(Keiji Fujimoto et al., 1993). The O_3 treatment results in significantly denser initiating points compared with other chemistries such as thiol-Au linkage(Zhiyi Bao, Merlin L. Bruening, & Baker, 2006), silane chemistry(Shinpei Yamamoto et al., 2000) and plasma activation. For example, plasma activation(Chiaki Yoshikawa et al., 2005; Keiji Fujimoto et al., 1993) can introduce 10-15 surface peroxide groups/nm^2. Silane chemistry typically achieves 0.04~4 group/nm^2,(Kohji Ohno et al., 2011; Shinpei Yamamoto et al., 2000).The high-density peroxide/ hydroperoxide is probably not to a single layer but a multi-layer structure as O_3 gas diffuses through. It can also be applied on different kinds of substrates, including different plastic such as Silicone, PU, PMMA and PE(Keiji Fujimoto et al., 1993) which can usually be attacked by common organic solvents. The high-density peroxide groups introduced by ozone treatment results a dense polymer brush coating with fully coverage on surface compared with other surface activation chemistries which is important for the antibacterial/antibiofilm effect. The surface-initiated polymer brush is chemically bonded onto catheter surface compared with the initiator impregnation method, which shows unstable brush coating(Wei Wang, Yang Lu, Jinbing Xie, Hui Zhu, & Zhiqiang Cao, 2016). Reversible addition−fragmentation chain-transfer polymerization (RAFT) is a versatile

living polymerization technique which provides the flexibility of designing and synthesizing various block copolymers combining different classes of monomers such as hydroxyl-terminated monomers and zwitterionic monomers(Kay E. B. Doncom et al., 2015). For catheters with small luminal space, where surface tension between solvent and surface and the complex shape of the substrate dominates, RAFT has not been reported.

We have shown that #10 H(N)-b-S coated catheter by surface initiated Ozone-RAFT chemistry can achieve excellent antibiofilm (>4.0 log_{10} orders) and antibacterial (~3.0log_{10}) effect against the clinically important Gram-positive and Gram-negative ESKAPE bacteria and Fungi, with good biocompatibility (Figure 6.4-Figure 6.5). Further, our *in vivo* mice experiment shows that #10 H(N)-b-S catheter achieves >4log_{10} orders of reduction of MRSA and *P. aeruginosa*. Of the 3 structures of coatings combining zwitterionic monomer and NO-release component, i.e. random copolymer coating (#9 H(N)-r-S), crosslinked coating (#8 H(N)-x-S), and block copolymer coating (#10 H(N)-b-S), only the precisely structured block copolymer brush which is hydrophilic and having embedded covalently linked NO-donor has good antibacterial/antibiofilm properties. The different arrangement of NO-release precursor and zwitterionic monomers further affect synergism between the two functionalities.

After introduction of NO release precursor, both the random copolymer coating and crosslinked coating become more hydrophobic (Figure 6.2C) due to exposure of NO release precursor. More than hydrophobicity increases, the

disulphide bond formed after NO released is still bio-active towards thiol containing proteins(Xiaona Yang, Dawei Chen, & Zhao, 2016), which results in additional attachment of protein contained thiol groups. The advantage of the block copolymer coating (#10 H(N)-b-S) is the hydrophobic NO-release precursor fully covered under a hydrophilic zwitterionic block as proved by little water contact change after grafting of NO-release precursor. Further, the uncontrolled random or crosslinking polymerizations results a much higher roughness coating compared with controlled block copolymer coating (Figure 6.2D). The increases in hydrophobicity and surface roughness will induce more surface contacting area with blood protein and cells, the fouling of blood protein such as fibrinogen, albumin and other proteins in serum might eventually cause attachment of pathogen, immune response(Jae Kyu Ryu et al., 2015) and cascading thrombus formation(Yaqi Wo, Elizabeth J. Brisbois, Robert H. Bartlett, & Mark E. Meyerhoff, 2016).

6.5 Conclusion

We have successfully developed a novel Ozone-RAFT approach to "graft from" small but long bores of a PU catheter high density brushes of a diblock copolymer which are post-polymerization covalently linked with a RSNO-donor. The diblock brush with covalent linked NO-donor (H(N)-b-S) achieves excellent antibacterial (> $3\log_{10}$ orders) and antibiofilm effect (>$4\log_{10}$ orders) against clinically relevant Gram negative and Gram-positive bacteria (list), while the random copolymer (H(N)-r-S) or hydrogel (H(N)-x-S) has poor antibiofilm efficacy at around $2\log_{10}$ orders against Gram Negative bacteria such as *P.*

aeruginosa and K. pneumonia respectively. The coating synergizes anti-fouling resistance of the zwitterionic layer with the anti-biofilm/-bacterial activity of the inner NO-releasing layer, achieving an outstanding *in vivo* and *in vitro* inhibition of bacteria biofilm formation on the inner surface of the catheter. Both the *in vivo* and *in vitro* antibiofilm testing show greater than $4\log_{10}$ of short-term inhibition of a broad-spectrum bacteria biofilm formation on catheter surface.

The biocompatibility of the H(N)-b-S modified catheter is also improved as seen from the reduced immunological response from blood immune cells, reduced surface thrombus formation and negligible toxicity toward various mammalian cell lines, as compared with unmodified and random copolymer/hydrogel-modified catheters, which show serious blood protein fouling and possible cause failures of catheter in long term.

Further, a long (30cm) polyurethane catheter coated with H(N)-*b*-S show greater than $2.5\log_{10}$ orders of inhibition of bacteria biofilm formation even after 30 days of dynamic circulation of a rich medium mimicking the real vascular mimic condition (compared with commercial silver catheter ~0 orders and with the hydrophilic catheter $1.5\log_{10}$ orders). It demonstrates the feasibility of the Ozone-RAFT approach on modification of medical devices with complicated shape and inner surface, which might be hard to modified by conventional chemistry.

The method develop from this work has a great potential to applied on surface modification of catheters as well as other medical devices in industrial applications.

Chapter 7. Conclusion

Thesis reports synthesis of novel antimicrobial cationic polysaccharides and novel medical device surface modification for prevention of bacterial infections. A novel biocompatible cationic peptidopolysaccharide and polysaccharide are synthesized with antimicrobial efficacy and synergy with commercial antibiotics. And an antibacterial adhesion surface coating is developed which can prevent medical device infections.

The peptidopolysaccharide CSM5-K5 has good broad-spectrum antimicrobial activity against “super bugs” with antimicrobial resistance, such as MRSA and ORSA and possesses good mammalian cell (fibroblast) compatibility. CSM5-K5 also shows outstanding hemocompatibility with human red blood cells (with HC10 >5000 μg/mL), which is much superior to most AMPs which due to the absence of hydrophobic amino acids groups in CSM5-K5.

The glucosamine units of the chitosan backbone are crucial for antimicrobial activity as it causes nano-scale aggregates of the polymer which concentrates surface charge and improves bactericidal efficacy compared to linear K100. The aggregated CSM5-K5 polymer particle can selectively bind with bacteria cells cytoplasmic membrane over mammalian cells via electrostatic

interaction reinforced by hydrogen bonding, as shown by ITC and membrane assays. Once the copolymer is attached onto the cell membrane via electrostatic interaction, the local lipid bilayer is destabilized by cationic charge, as well as the proton sponge effect of the nanoparticles, which leads to leakage of cytoplasm. The bactericidal activity of CSM5-K5 is likely due to membrane disruption, as well as decreased cell division due to cell wall thickening and detachment of cell membrane from cell wall as seen by TEM. The similarity of CSM5-K5 compared with Lipid II may be the reason for the cell wall thickening and decrease of septum formation in treated bacterial cells. We show that CSM5-K5 can be applied *in vivo* as a cure for infection with MRSA USA-300 in a murine infected wound model.

To further explore the antimicrobial and antibacterial potential of polysaccharide, the cationic polysaccharide 2,6-Diamino-chitosan (2,6-DAC) is synthesized and is found to exhibit antimicrobial efficacy comparable to CSM5-K5 (32μg/mL towards MRSA). 2,6-DAC synergizes with various bacterial cell wall targeting antibiotics against the important Gram-Negative pathogen AB-1, which is very difficult to be eradicate with antibiotics.

Bacterial adhesion on medical device surfaces is an important cause of infections. Such infections can be difficult to treat and may require removal of the infected device. In this work, the catheter is chosen as the model device to be modified. The surface of catheter is complicated, and the internal surface is difficult to modify in large scale. I have firstly explored a synthesis procedure

using ozone-initiated surface polymerization, which can coat catheters in large scale. The modified catheter shows good bacterial biofilm inhibition due to its antifouling surface, and this synergizes with the antibacterial nitric oxide release precursor which is covalently attached to the coating polymer structure.

I have successfully developed a novel Ozone-RAFT approach of synthesizing surface-initiated di-block copolymer biofilm inhibited coating on complicated medical device surfaces. The coating synergizes the protein fouling resistance property of the luminal surface hydrophilic layer with the antibacterial effect of a sub-surface nitric oxide release layer, achieving an outstanding *in vivo* and *in vitro* inhibition of bacteria biofilm formation on all surfaces of the catheter. Both the *in vivo* and *in vitro* antibiofilm testing show greater than $4\log_{10}$ inhibition of formation of biofilms of a broad-spectrum of bacteria. The biocompatibility of this modified catheter is also superior to comparison devices in terms of reduced immunological response from blood immune cells and negligible toxicity toward various mammalian cell lines. To demonstrate the feasibility of scaling the surface modification process, a long (30cm) polyurethane catheter piece is coated using the technique developed in this project. The modified polyurethane catheters (#10 H(N)-b-S) show more than $3\log_{10}$ inhibition of bacteria biofilm formation, compared with the unmodified PU control, under *in vitro* vascular simulation conditions after 30 days of exposure to a protein-rich biofilm promoting medium continuously circulated through the lumen of the catheter. These studies demonstrate the feasibility of the ozone-initiated Ozone-RAFT approach for modification of medical devices with

complicated shapes and internal surfaces, which may be difficult to modify with conventional chemistry. The method developed in this work has great potential for application to surface modification of catheters as well as other medical devices.

The research presented in this thesis has potential applications in topical and systemic anti-infection therapy as well as in prevention of medical device infections.

Chapter 8. Future studies

In this thesis, the proton sponge mechanism of cationic antimicrobial peptidoglycan was studied in detail: the cationic polysaccharide (2,6-DAC) was synthesized, its synergies with various antibiotics were evaluated, and a process for precisely controlled coating of medical devices was developed.

The cationic polysaccharide 2,6-DAC may be further modified to improve the antimicrobial efficacy and biocompatibility. For example, conversion of amine groups to guanidine groups is reported to improve antimicrobial efficacy in other polymers containing amine groups. This substitution has not been reported for chitosan.

Based on the synergism and hydrogen bonding between sugar backbone, synergistic combinations of 2,6-DAC with antibiotics can be made into nanoparticles using techniques such as layer-by-layer assembly and electrostatic complexation. The 2,6-DAC and antibiotics nanoparticles will have wider application than the cationic polysaccharide sugar alone.

The essential oils such as eugenol, cymene and carvacrol also have antibacterial efficacy. Research on synergies between 2,6-DAC and essential oils could lead to combination therapies that avoid use of antibiotics. This is desirable since employment of antibiotics can lead to resistance and they cannot be used in certain applications such as food preservation and prolonged applications of wound dressings.

The ozone-initiated modification process of medical device surface was further developed to achieve precisely controlled copolymer brush coatings. However, the release of NO therapy gas is still passive, and is triggered simply by temperature increase. Release mechanisms which permit better control could improve the long-term storage stability precise antimicrobial efficacy of the coatings. Surface coatings with bacteria- triggered release of antimicrobial agents should be developed in future works.

The cationic antimicrobial polymer could be combined with antibiofilm materials to form a bacteria-triggered responsive multifunctional antimicrobial/antifouling coating. Such a coating could achieve more than inhibition of bacteria attachment and biofilm development on the device surface; the device would act as a drug-delivery vehicle, releasing antimicrobial polymer from the implantation site to prevent infection at distal organs.

Appendix

A1. Calculation of Radius of Gyration (R_g)

The Radius of Gyration of nanoparticles can be obtained by static light scattering interpreted by Zimm plot at specific concentration:

The basic static light scattering principle equation is Rayleigh-Debye-Zimm Formulism:

$$\frac{Kc}{R_\theta} = (\frac{1}{M_W} + 2A_2c)\frac{1}{P_\theta}$$

where M_w is the aggregated molecular weight of nanoparticle; c is the concentration of solution.

The constant K is calculated from:

$$K = \frac{2\pi^2}{\lambda_o^4 N_A}(n_0 \frac{dn}{dc})^2$$

where λ_0 is laser wavelength; N_A is Avogadro's Number; n_0 is refractive index number of solvents; and $\frac{dn}{dc}$ is the differential refractive index number of solvent increments.

The P_θ is calculated from:

$$P_\theta = 1 + \frac{16\pi^2 {n_0}^2 R_g^2}{3\lambda_0^2} sin^2(\frac{\theta}{2})$$

where R_g is Radius of Gyration, and θ is the angle of measurement.

The R_θ can be calculated based on average light scattering intensity of solution over time:

$$R_\theta = \frac{I_A n_0^2}{I_T n_T^2} R_T$$

where I_A is the average intensity of solution over time, I_T is the intensity of standard (Toluene); n_T is refractive index of standard (Toluene); and R_T is Rayleigh ratio of standard (Toluene).

The Rayleigh-Debye-Zimm Formulism can be further simplified into:

$$\frac{Kc}{\Delta R_{(\theta,c)}} = \frac{1}{M_W}\left(1 + \frac{R_g^2}{3}q^2\right) + 2A_2c$$

where A_2 is the second coefficient, and $\Delta R(\theta,c)$ is measured on specific angle of measurement (θ) and concentration of solution (c); and wave factor q2 is calculated as:

$$q = \frac{4\pi n_0}{\lambda} \sin\left(\frac{\theta}{2}\right)$$

The Radius of gyration (R_g) at specific concentration can be then calculated out by plotting of measured I_A^{-1} against wave factors q^2 at different angles,

$$\frac{Kc}{I_A} = \frac{R_T n_0^2 R_g^2}{3 I_T n_T^2 M_W} q^2 + \left(\frac{R_T n_0^2}{M_W I_T n_T^2} + \frac{2 R_T n_0^2 A_2 c}{I_T n_T^2}\right)$$

A2. Zimm plot and aggregation number:

The Zimm plot also utilizes the equation:

$$\frac{Kc}{\Delta R_{(\theta,c)}} = \frac{1}{M_W}\left(1 + \frac{R_g^2}{3} q^2\right) + 2A_2 c$$

With different concentration of solution measured at different angles (Figures 2.7), the extrapolated Y-intercept at $(\theta,c)=(0,0)$ is the aggregated molecular weight.

A3. Calculation of hydrodynamic radius (R_h)

The hydrodynamic radius (R_h) is calculated based on Stokes-Einstein Equation:

$$R_h = \frac{k_B T}{6\pi\eta D_T}$$

where k_B is the Boltzmann constant, η is the viscosity of the polymer solution and T is absolute temperature in Kelvin (K).

To obtain the diffusion coefficient (D_T) of the polymer suspension, the wave vector q at different angles (θ) are firstly calculated via:

$$q = \frac{4\pi n_0}{\lambda} \sin\left(\frac{\theta}{2}\right)$$

where n_0 is the refractive index of copolymer solution, and λ is incident wavelength, 637 nm.

Then, the decay rates (Γ) at different angles are obtained from relaxation time distribution function, with respect of τ:

$$\Gamma = 1/\tau$$

The decay rates (Γ) at different angles are then plotted against square of wave vector (q^2) as a straight-line passing origin point (0,0). The diffusion coefficient (D_T) is the gradient of the of decay rate Γ variation with q^2:

$$D_T = \frac{\Delta\Gamma}{\Delta q^2}$$

Finally, the hydrodynamic radius R_H was calculated using this diffusion coefficient in the Stokes-Einstein Equation, giving:

$$R_h = \frac{k_B T}{6\pi\eta D_T}$$

A4. Correlation of Rg/Rh to the morphology of a nanoparticle

The structure information can be understood by studying the shape factor, which is calculated via Rg/Rh(Cao, 2003):

Rg/Rh	Structure
< 0.6	Core-shell
~ 0.774	Hard Sphere
~ 1	Vesicle
~ 1.5	Gaussian Chain
>2	Long Rod

A5. Calculation of surface peroxide group after ozone treatment

Volume of Sodium thiosulfate solution (0.01mM) used:3.30mL

Moles of peroxide=moles of thiosulfate titrated:

$$0.01 \times 10^{-3} \times 3.30 \times 10^{-3} = 3.3 \times 10^{-8} mole\ of\ peroxide\ per\ 5mm\ of\ catheter$$

Calculation of Surface peroxide group density:

$$\sigma = \frac{No.\ of\ peroxide\ group\ on\ 5mm\ of\ cateter}{Surface\ area\ of\ 5mm\ cathter}$$

$$\sigma = \frac{3.3 \times 10^{-8} \times 6.023 \times 10^{23}}{0.25 \times 0.5 \times 3.14 + 0.4 \times 0.5 \times 3.14 + 3.14((0.5 \times 0.4)^2 - (0.5 \times 0.25)^2) \times 2}$$

$$\sigma = \frac{1.98 \times 10^{16}}{1.17 cm^2}$$

$$\sigma = 1.69 \times 10^{16} / cm^2$$

$$\sigma = 169 / nm^2$$

Reference

Ajun Wan, Yan Sun, & Li, H. (2008). Characterization of folate-graft-chitosan as a scaffold for nitric oxide release. *International Journal of Biological Macromolecules, 43*, 415-421.

Akin, A., Mini, T., Alexander, M., Klibanov; , & Robert, L. (2005). Exploring Polyethylenimine-Mediated DNA Transfection and the Proton Sponge Hypothesis. *The Journal of gene medicine, 7*, 657-663.

Akoh, J. A. (2012). Peritoneal dialysis associated infections: An update on diagnosis and management. *World Journal of Nephrology, 1*(4), 106-122.

Alec Lutzke, Jesus B. Tapia, Megan J. Neufeld, & Reynolds, M. M. (2017). Sustained Nitric Oxide Release from a Tertiary S-Nitrosothiol-based Polyphosphazene Coating. *ACS Applied Materials & Interfaces, 9*, 2104-2113.

Alessandro Colletta, Jianfeng Wu, Yaqi Wo, Michael Kappler, Hao Chen, Chuanwu Xi, & Meyerhoff, M. E. (2015). S-Nitroso-N-acetylpenicillamine (SNAP) Impregnated Silicone Foley Catheters: A Potential Biomaterial/Device To Prevent Catheter-Associated Urinary Tract Infections. *ACS Biomaterials Science & Engineering, 1*, 416-424.

Alex Kate Halvey, Brian Macdonald, Dhyani，, A., & Anish Tuteja. (2018). Design of surfaces for controlling hard and soft fouling. *Philosophical Transactions of the Royal Society A, 377*.

Alex R. Ketchum, Michael P. Kappler, Jianfeng Wu, Chuanwu Xi, & Mark E. Meyerhoff. (2016). The preparation and characterization of nitric oxide releasing silicone rubber materials impregnated with S-nitroso-tertdodecyl mercaptan. *Journal of Materials Chemistry B, 4*(3), 422-430.

Alexander J. F. Egan, Jacob Biboy, Inge van't Veer, Eefjan Breukink, & Waldemar Vollmer. (2015). Activities and regulation of peptidoglycan synthases. *Philosophical Transactions B, 370*.

Alexander J. F. Egan, & Vollmer, W. (2013). The physiology of bacterial cell division. *Annals of the New York Academy of Sciences*(Antimicrobial Therapeutics Reviews).

Alexander J. Kallen, Priti R. Patel, & O'Grady, N. P. (2010). Preventing Catheter-Related Bloodstream Infections outside the Intensive Care Unit: Expanding Prevention to New Settings. *Clinical Infectious Diseases, 51*(3), 335-341.

Amanda C. Engler, Hyung-il Lee, & Hammond, P. T. (2009). Highly Efficient "Grafting onto" a Polypeptide Backbone Using Click Chemistry. *Angewandte Chemie International Edition, 48*, 9334-9338.

Ana L. Flores-Mireles, Jennifer N. Walker, Michael Caparon, & Scott J. Hultgren. (2015). Urinary tract infections: epidemiology, mechanisms of infection and treatment options. *Nature Reviews Microbiology, 13*, 269-284.

Ana Maria Carmona-Ribeiro, L. D. d. M. C. (2013). Cationic antimicrobial polymers and their assemblies. *International journal of molecular sciences, 14*(5), 9906.

Anchalee, J., Shirui, M., Thomas, K., & Varaporn, B., Junyaprasert; . (2008). Physicochemical properties and biocompatibility of N-trimethyl chitosan: Effect of quaternization and dimethylation. *European Journal of Pharmaceutics and Biopharmaceutics, 70*, 563-571.

Andrew M. Rizzi, Stephen D. Riutta, Joshua M. Peterson, Galina Gagin, Danielle M. Fritze, Meredith Barrett, . . . Lu, Y. (2018). Risk of peritoneal dialysis catheter-associated peritonitis following kidney transplant. *Clinical Transplantation, 32*.

Anna K. Winther, Betina Fejerskov, Marja ter Meer, Najah B.S. Jensen, Ross Dillion, Jeremy E. Schaffer, . . . Zelikin, A. N. (2018). Enzyme Prodrug Therapy Achieves Site-Specific, Personalized Physiological Responses to the Locally Produced Nitric Oxide. *ACS Applied Materials & Interfaces, 10*(13), 10741-10751.

Anna Müllera, M. W., Henrik Strahl, Fabian Grein, Terrens N. V. Saaki, Bastian Kohl, Tjalling Siersm, Julia E. Bandow, Hans-Georg Sahl, Tanja Schneider, Leendert W. Hamoen. (2016). Daptomycin inhibits cell envelope synthesis by interfering with fluid membrane microdomains. *PNAS*.

Audrey Beaussart, T. R., Marie-Cle´mence Duchene, Sofiane El-Kirat-Chatel, Guillaume Andre, Pascal Hols, Yves F. Dufrene. (2013). Binding Mechanism of the Peptidoglycan Hydrolase Acm2: Low Affinity, Broad Specificity. *Biophysical Journal, 105*, 620-629.

B.S.Anisha, RajaBiswas, K.P.Chennazhi, & R.Jayakumar. (2013). Chitosan–hyaluronic acid/nano silver composite sponges for drug resistant bacteria infected diabetic wounds. *International Journal of Biological Macromolecules, 62*, 310-320.

Bahattin, B., & Cigdem, K. (2013). Quasielastic Light Scattering Studies of Polypeptides: Evidence for Chain Extension in Solution. *Turkish Journal of Chemistry, 37*(4), 480-491.

Bailiang Wang, Huihua Liu, Zefeng Wang, Shuai Shi, Kaihui Nan, Qingwen Xu, . . . Hao Chen. (2017). A self-defensive antibacterial coating acting through the bacteria-triggered release of a hydrophobic antibiotic from layer-by-layer films. *Journal of Materials Chemistry B, 5*.

Bailiang Wang, Zi Ye, Yihong Tang, Yuemei Han, Quankui Lin, Huihua Liu, . . . Kaihui Nan. (2017). Fabrication of nonfouling, bactericidal, and bacteria corpse release multifunctional surface through surface-initiated RAFT polymerization. *International Journal of Nanomedicine, 12*, 111-125.

Baowei SU, Tingting Wang, Zongwen Wang, Xueli Gao, & Congjie Gao. (2012). Preparation and performance of dynamic layer-by-layerPDADMAC/PSS nanofiltration membrane. *Journal of Membrane Science, 423*, 324-331.

Benoıˆt Zuber, M. H., Taˆnia Ribeiro, Kathrin Minnig, Fa´tima Lopes, Philippe Moreillon, Jacques Dubochet. (2006). Granular Layer in the Periplasmic Space of Gram-Positive Bacteria and Fine Structures of Enterococcus gallinarum and Streptococcus gordonii Septa Revealed by Cryo-Electron Microscopy of Vitreous Sections. *Journal of bacteriology, 188*(18), 6652–6660.

Bernards, M. T., Cheng, G., Zhang, Z., Chen, S., & Jiang, S. (2008). Nonfouling polymer brushes via surface-initiated, two-component atom transfer radical polymerization. *Macromolecules, 41*(12), 4216-4219.

Berthony Deslouches, Jonathan D. Steckbeck, Jodi K. Craigo, Yohei Doi, Jane L. Burns, & Montelaro, R. C. (2015). Engineered Cationic Antimicrobial Peptides To Overcome Multidrug Resistance by ESKAPE Pathogens. *Antimicrobial agents and chemotherapy, 59*(2), 1329-1333.

Beveridge, T. J. (1999). Structures of Gram-Negative Cell Walls and Their Derived Membrane Vesicles. *Journal of bacteriology, 181*(16), 4725-4733.

Bibhuti B. Mishra, Rustin R. Lovewell, Andrew J. Olive, Guoliang Zhang, Wenfei Wang, Eliseo Eugenin, . . . Christopher M. Sassetti. (2017). Nitric oxide prevents a pathogen-permissive granulocytic inflammation during tuberculosis. *Nature Microbiology, 2*, 17072.

Bogdan, C. (2001). Nitric oxide and the immune response. *Nature Immunology, 2*, 907-916.

Bolin Niu, Brian Kim, Berkeley N. Limketkai, Jing Sun, Zhiping Li, Tinsay Woreta, & Chen, P.-H. (2018). Mortality from Spontaneous Bacterial Peritonitis Among Hospitalized Patients in the USA. *Digestive Diseases and Sciences, 63*, 1327-1333.

Brian C Smith, & Marletta, M. A. (2012). Mechanisms of S-nitrosothiol formation and selectivity in nitric oxide signaling. *Current Opinion in Chemical Biology, 16*, 498-506.

Brogden, K. A. (2005). Antimicrobial peptides: pore formers or metabolic inhibitors in bacteria? *Nature Reviews Microbiology, 3*(3), 238-250.

Bruce P. Lee, P.B. Messersmith, J.N. Israelachvili, & Waite, J. H. (2011). Mussel-Inspired Adhesives and Coatings. *Annual Reviews of Materials Research, 41*, 99-132.

Burkhard, D., Dirk, R., Martin, S., & Kurt, K. Corrections to Scaling in the Hydrodynamic Properties of Dilute Polymer Solutions. *Journal of Chemical Physics, 117*(2).

C. Wang, K. C. T., R. D. Jenkins, D. R. Bassett. (2000). Potentiometric titration and dynamic light scattering of hydrophobically modiÐed alkali soluble emulsion (HASE) polymer solutions. *Physical chemistry chemical physics, 2*(9).

Caihong Zhang, Tyler D. Biggs, Nelmi O. Devarie-Baez, Shaomin Shuang, Chuan Dong, & Xian, M. (2017). S-Nitrosothiols: chemistry and reactions. *Chemistry Commnunications, 53*,

11266-11277.
Cao, A. (2003). Light Scattering. Recent Applications. *Analytical Letters, 36*(15), 3185-3225.
Catheter-associated Urinary Tract Infections (CAUTI). (2017). Retrieved from https://www.cdc.gov/hai/ca_uti/uti.html
Central Venous Catheter. (2007). *American Journal of Respiratory and Critical Care Medicine, 176*, 3-4.
Chang, Y., Shu, S.-H., Shih, Y.-J., Chu, C.-W., Ruaan, R.-C., & Chen, W.-Y. (2009). Hemocompatible mixed-charge copolymer brushes of pseudozwitterionic surfaces resistant to nonspecific plasma protein fouling. *Langmuir, 26*(5), 3522-3530.
Changzhu Wu, Schwibbert, K., Katharina Achazi, Petra Landsberger, Anna Gorbushina, & Haag, R. (2017). Active Antibacterial and Antifouling Surface Coating via a Facile One-Step Enzymatic Cross-Linking. *Biomacromolecules, 18*, 210-216.
Chao Ding, Zhengqing Yan, Jinsong Ren, & Qu, X. (2017). Autonomous and Continuous Stimuli-Responsive Polymer Surface for Antibacterial Application through Enzymatic Self-Propagating Reactions. *Chemistry: A European Journal, 23*, 14883-14888.
Chao Zhou, Yang Wu, Kishore Reddy Venkata Thappeta, Jo Thy Lachumy Subramanian, Dicky Pranantyo, En-Tang Kang, . . . Chan-Park, M. B. (2017). In Vivo Anti-Biofilm and Anti-Bacterial Non-Leachable Coating Thermally Polymerized on Cylindrical Catheter. *ACS Applied Materials & Interfaces, 9*, 36269-36280.
Chengcheng Zhou, Fengyan Wang, Hui Chen, Meng Li, Fulin Qiao, Zhang Liu, . . . Wang, Y. (2016). Selective Antimicrobial Activities and Action Mechanism of Micelles Self-Assembled by Cationic Oligomeric Surfactants. *ACS Applied Materials & Interfaces, 8*(6), 4242-4249.
Chiaki Yoshikawa, Atsushi Goto, Yoshinobu Tsujii, Takeshi Fukuda, Kazuya Yamamoto, & Kishida, A. (2005). Fabrication of High-Density Polymer Brush on Polymer Substrate by Surface-Initiated Living Radical Polymerization. *Macromolecules, 38*, 4604-4610.
Christopher S. Hollenbeak, & Amber L. Schilling. (2018). The attributable cost of catheter-associated urinary tract infections in the United States: A systematic review. *American Journal of Infection Control, 46*(7), 751-757.
Chuan Yang, Xin Ding, Robert J. Ono, Haeshin Lee, Li Yang Hsu, Yen Wah Tong , . . . Yang, Y. Y. (2014). Brush-Like Polycarbonates Containing Dopamine, Cations, and PEG Providing a Broad-Spectrum, Antibacterial, and Antifouling Surface via One-Step Coating. *Advanced Materials, 26*, 7346-7351.
Chuanbao, W., Jianyuan, H., Xianmo, D., & Yu, L. (2008). Random Branched Poly(hydroxyetheramine): a Novel Polycation with Proton Sponge Effect and High Density of Discrete Charge. *Polymer Bulletin, 60*, 635–645.
Chuncai Zhou, Xiaobao Qi, Peng Li, Wei Ning Chen, Lamrani Mouad, Matthew W. Chang, . . . Chan-Park, M. B. (2010). High Potency and Broad-Spectrum Antimicrobial Peptides Synthesized via Ring-Opening Polymerization of alpha-Aminoacid-N-carboxyanhydrides. *Biomacromolecules, 11*, 60-67.
Chunmiao Bo, & Yinmao Wei. (2017). Preparation and evaluation of surface-grafted block copolymers and random copolymers via surface-initiated atom transfer radical polymerization for hydrophilic/ion-exchange stationary phases. *RSC Advances, 7*.
Criegee R. (1975). Mechanism of Ozonolysis. *Angewandte Chemie International Edition, 14*(11), 745-752.
Crystal H. Son, Titus L. Daniels, Janet A. Eagan, Michael B. Edmond, Neil O. Fishman, Thomas G. Fraser, . . . Kent A. Sepkowitz. (2012). Central Line–Associated Bloodstream Infection Surveillance outside the Intensive Care Unit: A Multicenter Survey. *Infection Control & Hospital Epidemiology, 33*(9), 869-874.
David Andreu, L. R. (1998). Animal Antimicrobial Peptides: An Overview. *BIopolymers(Peptide Science), 47*, 415-433.
David Huesmann, Alexander Birke, Kristina Klinker, Stephan Turk, Hans Joachim Rader, & Barz, M. (2014). Revisiting Secondary Structures in NCA Polymerization: Influences on the Analysis of Protected Polylysines. *Macromolecules, 47*, 928-936.

David Roe, Balu Karandikar, Nathan Bonn-Savage, Bruce Gibbins, & Jean-Baptiste Roullet. (2008). Antimicrobial surface functionalization of plastic catheters by silver nanoparticles. *Journal of Antimicrobial Chemotherapy, 61*, 867-876.

Dever LA, D. T. (1991). Mechanisms of bacterial resistance to antibiotics. *Archives of Internal Medicine, 151*(5), 886-895.

Dhruv P. Arora, Sajjad Hossain, Yueming Xu, & Boon, E. M. (2015). Nitric Oxide Regulation of Bacterial Biofilms. *Biochemistry, 54*(24), 3717-3728.

Dicky Pranantyo, Li Qun Xu, En-Tang Kang, & Chan-Park, M. B. (2018). Chitosan-Based Peptidopolysaccharides as Cationic Antimicrobial Agents and Antibacterial Coatings. *Biomacromolecules, 19*, 2156-2165.

Dicky Pranantyo, Li Qun Xu, Zheng Hou, En-Tang Kang, & Chan-Park, M. B. (2017). Increasing bacterial affinity and cytocompatibility with four-arm star glycopolymers and antimicrobial α-polylysine. *Polymer Chemistry, 8*.

Dina Raafat, & Sahl, H.-G. (2009). Chitosan and its antimicrobial potential – a critical literature survey. *Microbial biotechnology, 2*(2), 186-201.

Dirk-Jan Scheffers, & Mariana G. Pinho. (2005). Bacterial Cell Wall Synthesis: New Insights from Localization Studies. *Microbiology and Molecular Biology Reviews, 69*(4), 585-607.

Dmitri D. Iarikov, Mehdi Kargar, Ali Sahari, Lauren Russel, Katelyn T. Gause, Bahareh Behkam, & William A. Ducker. (2014). Antimicrobial Surfaces Using Covalently Bound Polyallylamine. *Biomacromolecules, 15*, 169-176.

Dobbins, S. C., McGrath, D. E., & Bernards, M. T. (2012). Nonfouling hydrogels formed from charged monomer subunits. *The Journal of Physical Chemistry B, 116*(49), 14346-14352.

Dong-Kuk Lee, J. R. B., Michele F. M. Sciacca, Janarthanan Krishnamoorthy, Changsu Yu, Ayyalusamy Ramamoorthy. (2013). Lipid Composition-Dependent Membrane Fragmentation and Pore-Forming Mechanisms of Membrane Disruption by Pexiganan (MSI-78). *Biochemistry, 52*, 3254-3263.

Edgar HH Wong, Mya Mya Khin, Vikashini Ravikumar, Zhangyong Si, Scott A Rice, & Chan-Park, M. B. (2016). Modulating antimicrobial activity and mammalian cell biocompatibility with glucosamine-functionalized star polymers. *Biomacromolecules, 17*(3), 1170-1178.

Elizabeth J. Brisbois, Terry C. Major, Marcus J. Goudie, Mark E. Meyerhoff, Robert H. Bartlett, & Handa, H. (2016). Attenuation of thrombosis and bacterial infection using dual function nitric oxide releasing central venous catheters in a 9 day rabbit model. *Acta Biomaterialia, 44*, 304-312.

Emilie A. Porter, Bernard Weisblum, & Gellman, S. H. (2002). Mimicry of Host-Defense Peptides by Unnatural Oligomers: Antimicrobial â-Peptides. *Journal of American Chemisty Society, 124*, 7324-7330.

Emilisa Frirdich, Jacob Biboy, Calvin Adams, Jooeun Lee, Jeremy Ellermeier, Lindsay Davis Gielda, . . . Gaynor, E. C. (2012). Peptidoglycan modifying enzyme Pgp1 is required for helical cell shape and pathogenicity traits in Campylobacter jejuni. *PLoS Pathogens*.

Entsar I. Rabea, Mohamed E.-T. Badawy, Christian V. Stevens, Guy Smagghe, & Walter Steurbaut. (2003). Chitosan as Antimicrobial Agent: Applications and Mode of Action. *Biomacromolecules, 4*(6), 1457-1465.

Errington, R. A. D. a. J. (2003). Control of Cell Morphogenesis in Bacteria: Two Distinct Ways to Make a Rod-Shaped Cell. *Cell, 113*.

Fabíola Costa, Isabel F. Carvalho, Ronald C. Montelaro, P. Gomes, & Martins, M. C. L. (2011). Covalent immobilization of antimicrobial peptides (AMPs) onto biomaterial surfaces. *Acta Biomaterialia, 7*, 1431-1440.

Fan Fan, Chunyu Zhou, Xu Wang, & Szpunar, J. (2015). Layer-by-Layer Assembly of a Self-Healing Anticorrosion Coating on Magnesium Alloys. *ACS Applied Materials & Interfaces, 7*, 27271-27278.

Fan Zhang, F. J. Xu, E. T. Kang, & Neoh, K. G. (2006). Modification of Titanium via Surface-Initiated Atom Transfer Radical Polymerization (ATRP). *Industrial & Engineering*

Chemistry Research, 45, 3067-3073.
Flores-Mireles, A. L., Walker, J. N., Caparon, M., & Hultgren, S. J. (2015). Urinary tract infections: epidemiology, mechanisms of infection and treatment options. *Nature Reviews Microbiology, 13*(5), 269.
FME Wagenlehner, & KG Naber. Urinary Tract Infections - General http://www.antimicrobe.org/e4e.asp. Retrieved from http://www.antimicrobe.org/e4e.asp
Fox, J. L. (2013). Antimicrobial peptides stage a comeback. *Nature Biotechnology, 31*(5), 379-382. doi:10.1038/nbt.2572
Frans Ricardo Tamara, Chi Lin, Fwu-Long Mi, & Yi-Cheng Ho. (2018). Antibacterial Effects of Chitosan/Cationic Peptide Nanoparticles. *Nanomaterials, 8*(88).
Frédéric Kerff, Petrella, S., Frédéric Mercier, Eric Sauvage, Raphaël Herman, Anne Pennartz, . . . Paulette Charlier. (2010). Specific structural features of the N-acetylmuramoyl-L-alanine amidase AmiD from Escherichia coli and mechanistic implications for enzymes of this family. *Journal of Molecular Biology, 397*, 249–259.
G.W Richter, Y. K. (1967). Electron microscopy of a strain of Bordetella bronchiseptica. *Journal of bacteriology, 94*(4), 1216.
Gang Cheng, Hong Xue, Zheng Zhang, Shengfu Chen, & Jiang, S. (2008). A Switchable Biocompatible Polymer Surface with Self-Sterilizing and Nonfouling Capabilities. *Angewandte Chemie International Edition, 47*, 8831-8834.
Gaurav Misra, E. R. R., Ajay Gopinathan, Kerwyn Casey Huang. (2013). Mechanical Consequences of Cell-Wall Turnover in the Elongation of a Gram-Positive Bacterium. *Biophys Journal, 104*, 2342-2352.
Geoffrey W. Stone, Qin Zhang, Rosario Castillo, V. Ramana Doppalapudi, Analia R. Bueno, Jean Y. Lee, . . . Georgopapadakou, N. H. (2004). Mechanism of Action of NB2001 and NB2030, Novel Antibacterial Agents Activated by beta-Lactamases. *Antimicrobial agents and chemotherapy, 48*(2), 477-483.
George Fleming, Jenny Aveyard, Joanne L. Fothergill, Fiona McBride, Rasmita Raval, & Raechelle A. D'Sa. (2017). Nitric Oxide Releasing Polymeric Coatings for the Prevention of Biofilm Formation. *Polymer, 9*(601).
Guozhu Li, Gang Cheng, Hong Xue, Shenfu Chen, Fengbao Zhang, & Jiang, S. (2008). Ultra low fouling zwitterionic polymers with a biomimetic adhesive group. *Biomaterials, 29*, 4592-4597.
Haibo Mu, Fan Guo, Hong Niu, Qianjin Liu, Shunchun Wang, & Jinyou Duan. (2014). Chitosan Improves Anti-Biofilm Efficacy of Gentamicin through Facilitating Antibiotic Penetration. *International journal of molecular sciences, 15*, 22296-22308.
Haifeng Gao, & Matyjaszewski, K. (2007). Synthesis of Molecular Brushes by “Grafting onto” Method: Combination of ATRP and Click Reactions. *Journal of American Chemisty Society, 129*, 6633-6639.
Haiyong Ao, Shengbing Yang, a., Binen Nie, Qiming Fan, Quanchao Zhang, Jiajia Zong, . . . Tngting Tang. (2019). Improved antibacterial properties of collagen I/hyaluronic acid/quaternized chitosan multilayer modified titanium coatings with both contact-killing and release-killing functions. *Journal of Materials Chemistry B, 7*, 1951-1961.
Hans-Curt Flemming, Jost Wingender, Ulrich Szewzyk, Peter Steinberg, Scott A. Rice, & and Staffan Kjelleberg. (2016). Biofilms: an emergent form of bacterial life. *Nature Reviews Microbiology, 14*, 563-575.
Hao Meng, Pegah Kord Forooshani, Pratik U. Joshi, Julie Osborne, Xue Mi, Christa Meingast, . . . Lee, B. P. (2019). Biomimetic recyclable microgels for on-demand generation of hydrogen peroxide and antipathogenic application. *Acta Biomaterialia, 83*, 109-118.
Hayssam Khalil, Tao Chen, Rene´e Riffon, Rutao Wang, & Zhao Wang. (2008). Synergy between Polyethylenimine and Different Families of Antibiotics against a Resistant Clinical Isolate of Pseudomonas aeruginosa. *Antimicrobial agents and chemotherapy, 52*(5), 1635-1641.
Heidrich, C., M.F. Templin, A. Ursinus, et al. (2001). Involvement of N-acetylmuramyl-L-alanine

amidases in cell separation and antibiotic-induced autolysis of Escherichia coli. *Mol. Microbiol, 41*, 167-178.

Heijenoort, J. v. (2011). Peptidoglycan Hydrolases of Escherichia coli. *Microbiological and Molecular Biology Reviews, 75*(4).

Helio S. Sader, K. A. F., Robert P. Rennie, Shelley Stevens, Ronald N. Jones. (2004). Omiganan Pentahydrochloride (MBI 226), a Topical 12-Amino-Acid Cationic Peptide: Spectrum of Antimicrobial Activity and Measurements of Bactericidal Activity. *Antimicrobial agents and chemotherapy, 48*(8), 3112–3118.

Herzberg, M., Sweity, A., Brami, M., Kaufman, Y., Freger, V., Oron, G., . . . Kasher, R. (2011). Surface properties and reduced biofouling of graft-copolymers that possess oppositely charged groups. *Biomacromolecules, 12*(4), 1169-1177.

Ho-Wook Jun, Lakeshia J. Taite, & West, J. L. (2005). Nitric Oxide-Producing Polyurethanes. *Biomacromolecules, 6*, 838-844.

Holmlin, R. E., Chen, X., Chapman, R. G., Takayama, S., & Whitesides, G. M. (2001). Zwitterionic SAMs that resist nonspecific adsorption of protein from aqueous buffer. *Langmuir, 17*(9), 2841-2850.

Hong Chen, Chao Zhao, Mingzhen Zhang, Qiang Chen, Jie Ma, & Zheng, J. (2016). Molecular Understanding and Structural-Based Design of Polyacrylamides and Polyacrylates as Antifouling Materials. *Langmuir, 32*, 3315-3330.

Hongbin Zhang, & Mu Chiao. (2015). Anti-fouling Coatings of Poly(dimethylsiloxane) Devices for Biological and Biomedical Applications. *Journal of Medical and Biological Engineering, 35*, 143-155.

https://www.csun.edu/~hcbio027/biotechnology/lec4a/gram.html. Cell Wall and Gram-Negative Cell Envelope.

Hyung-Sik Won, S.-J. K., Wahn-Soo Choi, Bong-Jin Lee. (2011). Activity Optimization of an Undecapeptide Analogue Derived from a Frog-Skin Antimicrobial Peptide. *Molecules and Cells, 31*, 49-54.

Hyyryla, H.-L., ¨inen‡, M. V., Joanne Thwaite§, Hongyan Wu‡, Matti Sarvas‡,, & Colin R. Harwood§, V. P. K., and Keith Stephenson. (2000). D-Alanine Substitution of Teichoic Acids as a Modulator of Protein

Folding and Stability at the Cytoplasmic Membrane/Cell Wall

Interface of Bacillus subtilis. *The Journal of biological chemistry, 275*(35), 26696–26703.

Infection: Prevention and Control of Healthcare-Associated Infections in Primary and Community Care: Partial Update of NICE Clinical Guideline 2-Long term urinary catheters. (2012). Retrieved from https://www.ncbi.nlm.nih.gov/books/NBK115272/

Inna S Radzishevsky1, S. R., Dmitry Bourdetsky, Shiri Navon-Venezia, Yehuda Carmeli, Amram Mor. (2007). Improved antimicrobial peptides based on acyl-lysine oligomers. *Nature Biotechnology, 25*(6), 657-659.

Isabelle Richard, Marc Thibault, Gregory De Crescenzo, Michael D. Buschmann, & Lavertu, M. (2013). Ionization Behavior of Chitosan and Chitosan–DNA Polyplexes Indicate That Chitosan Has a Similar Capability to Induce a Proton-Sponge Effect as PEI. *Biomacromolecules, 14*(6), 1732-1740.

Jacob N. Lockhart, Thomas J. Spoonmore, Michael W. McCurdy, Bridget R. Rogers, Scott A. Guelcher, & Harth, E. (2018). Poly(glycidol) Coating on Ultrahigh Molecular Weight Polyethylene for Reduced Biofilm Growth. *ACS Applied Materials & Interfaces, 10*, 4050-4056.

Jae Kyu Ryu, Mark A. Petersen, Sara G. Murray, Kim M. Baeten, Anke Meyer-Franke, Justin P. Chan, . . . Akassoglou, K. (2015). Blood coagulation protein fibrinogen promotes autoimmunity and demyelination via chemokine release and antigen presentation. *Nature Communication, 6*.

Jagath L. Kadurugamuwa, Lin Sin, Eddie Albert, Jun Yu, Kevin Francis, Monica DeBoer, . . . Contag, P. R. (2003). Direct Continuous Method for Monitoring Biofilm Infection in a Mouse Model. *71*(2), 882-890.

Jarmila Vinová, E. V. (2011). Chitosan Derivatives with Antimicrobial, Antitumour and

Antioxidant Activities - a Review. *Current Pharmaceutical Design, 17*, 3596-3607.

Jean-Luc Dewez, Aurora Doren, Yves-Jacques Schneider, & Rouxhet, P. G. (1999). Competitive adsorption of proteins: Key of the relationship between substratum surface properties and adhesion of epithelial cells. *Biomaterials, 20*, 547-559.

Ji-Hoon Kim, Daeung Yu, Sung-Hwan Eom, Song-Hee Kim, Junghwan Oh, Won-Kyo Jung, & Kim, Y.-M. (2017). Synergistic Antibacterial Effects of Chitosan-Caffeic Acid Conjugate against Antibiotic-Resistant Acne-Related Bacteria. *Marine Drugs, 15*(167).

Jianghua Li, Kaixi Zhang, Lin Ruan, Seow Fong Chin, Nirmani Wickramasinghe, Hanbin Liu, . . . Chan-Park, M. B. (2018). Block Copolymer Nanoparticles Remove Biofilms of Drug-Resistant Gram-Positive Bacteria by Nanoscale Bacterial Debridement. *Nano letters, 18*, 4180-4187.

Jiangna Guo, Jing Qin, Yongyuan Ren, Bin Wang, Hengqing Cui, Yingying Ding, . . . Yan, F. (2018). Antibacterial activity of cationic polymers: side-chain or main-chain type? *Polymer Chemistry, 9*.

Jianhui Tian, A. S., Basil I. Swanson, Byron Goldstein, S. Gnanakaran. (2013). Taste of Sugar at the Membrane: Thermodynamics and Kinetics of the Interaction of a Disaccharide with Lipid Bilayers. *Biophysical Journal, 104*, 622-632.

Jie Gao, Wenting Zheng, Jimin Zhang, Di Guan, Zhimou Yang, Deling Kong, & Zhao, Q. (2013). Enzyme-controllable delivery of nitric oxide from a molecular hydrogel. *Chemical Communications*(80).

Jiezhao Zhan, Lin Wang, Sa Liu, Junjian Chen, Li Ren, & Wang, Y. (2015). Antimicrobial Hyaluronic Acid/Poly(amidoamine) Dendrimer Multilayer on Poly(3-hydroxybutyrate-co-4-hydroxybutyrate) Prepared by a Layer-by-Layer Self-Assembly Method. *ACS Applied Materials & Interfaces, 7*, 13876-13881.

Jingxiao Tian, Jiangyan Zhang, Jiangtao Yang, Lingyun Du, Hao Geng, & Cheng, Y. (2017). Conjugated Polymers Act Synergistically with Antibiotics to Combat Bacterial Drug Resistance. *ACS Applied Materials & Interfaces, 9*, 18512-18520.

Jon Ladd, Zheng Zhang, Shengfu Chen, Jason C. Hower, & Shaoyi Jiang. (2008). Zwitterionic Polymers Exhibiting High Resistance to Nonspecific Protein Adsorption from Human Serum and Plasma. *Biomacromolecules, 9*(5).

Jonas Marschall, Leonard A. Mermel, Mohamad Fakih, Lynn Hadaway, Alexander Kallen, Naomi P. O'Grady, . . . Deborah S. Yokoe. (2014). Strategies to Prevent Central Line–Associated Bloodstream Infections in Acute Care Hospitals: 2014 Update. *Infection Control & Hospital Epidemiology, 35*(7), 753-771.

Jong-Bum Kim, Wenxi Huang, Merlin L. Bruening, & Gregory L. Baker. (2002). Synthesis of Triblock Copolymer Brushes by Surface-Initiated Atom Transfer Radical Polymerization. *Macromolecules, 35*, 5410-5416.

Joon-Il, J., Ki-Hyun, K., & Lester, L. (2015). The Matricellular Protein CCN1 Mediates Neutrophil Efferocytosis in Cutaneous Wound Healing. *Nature Communication, 6*.

Jun Cao, Yi, F., Qiufeng Tian, Dang, G., Si, W., Liu, S., & Yu, S. (2017). Targeting the gram-negative bacteria peptidoglycan synthase MraY as a new approach for monoclonal antibody anti-bacterial activity. *Human Vaccines & Immunotherapeutics, 13*(9), 2086-2091.

Justin O. Zoppe, Nariye Cavusoglu Ataman, Piotr Mocny, Jian Wang, John Moraes, & Klok, H.-A. (2017). Surface-Initiated Controlled Radical Polymerization: State-of-the-Art, Opportunities, and Challenges in Surface and Interface Engineering with Polymer Brushes. *Chemical Reviews, 117*, 1105-1318.

K.Y. Lee, I.C. Kwon, Y.-H. Kim, W.H. Jo, & Jeong, S. Y. (1998). Preparation of chitosan self-aggregates as a gene delivery system. *Journal of Controlled Release, 51*, 213-220.

Kagya A. Amoako, Harihara S. Sundaram, Ahmed Suhaib, Shaoyi Jiang, & Cook, K. E. (2016). Multimodal, Biomaterial-Focused Anticoagulation via Superlow Fouling Zwitterionic

Functional Groups Coupled with Anti-Platelet Nitric Oxide Release. *Advanced Material Interfaces, 3*.

Kaiyang Lim, Ray Rong Yuan Chua, Ho Bow, Paul Anantharajah Tambyah, Kunn Hadinoto, & Susanna Su Jan Leong. (2015). Development of a catheter functionalized by a polydopamine peptide coating with antimicrobial and antibiofilm properties. *Acta Biomaterialia, 15*, 127-138.

Karin, S., Wyn, B., & Robert, J. (1994). Micellar Sphere-to-Rod Transition in an Aqueous Triblock Copolymer System. A Dynamic Light Scattering Study of Translational and Rotational Diffusion. *Macromolecules, 27*(17), 4825-4832

Kay E. B. Doncom, Nicholas J. Warren, & Armes, S. P. (2015). Polysulfobetaine-based diblock copolymer nanoobjects via polymerization-induced self-assembly. *Polymer Chemistry, 6*, 7264.

Keefer, L. K. (2011). Fifty Years of Diazeniumdiolate Research. From Laboratory Curiosity to Broad-Spectrum Biomedical Advances. *ACS chemical biology, 6*, 1147-1155.

Keiji Fujimoto, Yoshihiro Takebayashi, Hiroyuki Inoue, & Ikada, Y. (1993). Ozone-induced graft polymerization onto polymer surface. *Polymer Chemistry, 31*(4), 1035-1043.

Keisuke Kurita, Hiroyuki Ikeda, Manabu Shimojoh, & Jin Yang. (2007). N-Phthaloylated Chitosan as an Essential Precursor for Controlled Chemical Modifications of Chitosan: Synthesis and Evaluation. *Polymer Journal, 39*(9), 945-952.

Kevin J. Hallock, D.-K. L., A. Ramamoorthy. (2003). MSI-78, an Analogue of the Magainin Antimicrobial Peptides, Disrupts Lipid Bilayer Structure via Positive Curvature Strain. *Biophysical Journal, 84*(5), 3052–3060.

KH, S. (1972). Peptidoglycan types of bacterial cell walls and their taxonomic implications. *Bacteriological reviews, 36*(4).

King, A., Chakrabarty, S., Zhang, W., Zeng, X. M., Ohman, D. E., Wood, L. F., . . . Wynne, K. J. (2014). High Antimicrobial Effectiveness with Low Hemolytic and Cytotoxic Activity for PEG/Quaternary Copolyoxetanes. *Biomacromolecules, 15*(2), 456-467. doi:10.1021/bm401794p

Koch, A. L. (2003). Bacterial Wall as Target for Attack. *Clinical Microbiology and Reviews, 16*(4), 673-687.

Kohji Ohno, Ying Ma, Yun Huang, Chizuru Mori, Yoshikazu Yahata, Yoshinobu Tsujii, . . . Perrier, S. (2011). Surface-Initiated Reversible Addition Fragmentation Chain Transfer (RAFT) Polymerization from Fine Particles Functionalized with Trithiocarbonates. *Macromolecules, 44*, 8944-8945.

Laschewsky, A. (2014). Structures and Synthesis of Zwitterionic Polymers. *polymers, 6*, 1544-1601.

Lei Yang, Evan S. Feura, Mona Jasmine R. Ahonen, & Schoenfisch, M. H. (2018). Nitric Oxide–Releasing Macromolecular Scaffolds for Antibacterial Applications. *Advanced Healthcare Materials, 7*.

Lincoln W Pasquina, John P Santa Maria, & Walker, S. (2013). Teichoic acid biosynthesis as an antibiotic target. *Current Pharmaceutical Design, 16*(5), 1.

Lindsey M. Gottler, A. R. (2009). Structure, membrane orientation, mechanism, and function of pexiganan — A highly potent antimicrobial peptide designed from magainin. *Biochimica et Biophysica Acta, 1788*(8), 1680-1686.

Lorke, D. (1983). A new approach to practical acute toxicity testing. *Archives of Toxicology, 54*(4).

M.S. Benhabiles, R. Salah, H. Lounici, N. Drouiche, M.F.A. Goosen, & N. Mameri. (2012). Antibacterial activity of chitin, chitosan and its oligomers prepared from shrimp shell waste. *Food Hydrocolloids, 29*, 48-56.

Maan Hayyan, Mohd Ali Hashim, & AlNashef, I. M. (2016). Superoxide Ion: Generation and Chemical Implications. *Chemical Reviews, 116*, 3029-3085.

Martti Vaara, & Porro, M. (1996). Group of Peptides That Act Synergistically with Hydrophobic Antibiotics against Gram-Negative Enteric Bacteria. *Antimicrobial agents and chemotherapy, 40*(8), 1801-1805.

Maryam Mazloumpour, Priya Malshe, Ahmed El-Shafei, & Hauser, P. (2013). Conferring durable

antimicrobial properties on nonwoven polypropylene via plasma-assisted graft polymerization of DADMAC. *Surface and Coatings Technology*, 1-7.

Matthew A. Jorgenson, K. D. Y. (2016). Interrupting Biosynthesis of O Antigen or the Lipopolysaccharide

Core Produces Morphological Defects in Escherichia coli by

Sequestering Undecaprenyl Phosphate. *Journal of bacteriology, 198*(22).

Merve Gultekinoglu, Yeliz Tunc Sarisozen, Ceren Erdogdu, Meral Sagiroglu, Eda Ayse Aksoy, Yoo Jin Oh, . . . Ulubayram, K. Designing of dynamic polyethyleneimine (PEI) brushes on polyurethane (PU) ureteral stents to prevent infections. *Acta Biomaterialia, 21*, 44-54.

Mi, L., & Jiang, S. (2014). Integrated antimicrobial and nonfouling zwitterionic polymers. *Angewandte Chemie International Edition, 53*(7), 1746-1754.

Michael F. Mesleh, Premraj Rajaratnam, Mary Conrad, Vasu Chandrasekaran, Christopher M. Liu, Bhaumik A. Pandya, . . . Moy, T. I. (2015). Targeting Bacterial Cell Wall Peptidoglycan Synthesis by Inhibition of Glycosyltransferase Activity. *Chemical Biology & Drug Design, 87*(2), 190-199.

Michael Stenger, Kasper Klein, Rasmus B. Grønnemose, Janne K. Klitgaard, Hans J. Kolmos, Jes S. Lindholt, . . . Andersen, T. E. (2016). Co-release of dicloxacillin and thioridazine from catheter material containing an interpenetrating polymer network for inhibiting device-associated Staphylococcus aureus infection. *Journal of Controlled Release, 241*, 125-134.

Michal, B., & Ger, K. (1997). Proton Binding Characteristics of Branched Polyelectrolytes. *Macromolecules, 30*(7), 2151.

Miller, S. I. (2016). Antibiotic Resistance and Regulation of the Gram-Negative Bacterial Outer Membrane Barrier by Host Innate Immune Molecules. *mBio, 7*(5).

Ming Kong, Xi Guang Chen, Ke Xing, & Park, H. J. (2010). Antimicrobial properties of chitosan and mode of action: A state of the art review. *International Journal of Food Microbiology, 144*, 51-63.

Mingrui He, Kang Gao, Linjie Zhou, Zhiwei Jiao, Mengyuan Wu, Jialin Cao, . . . Jiang，, Z. (2016). Zwitterionic materials for antifouling membrane surface construction. *Acta Biomaterialia, 40*, 142-152.

Mir-Morteza Sadat Ebrahimi, Yvonne Voss, & Schönherr, H. (2015). Rapid Detection of Escherichia coli via Enzymatically Triggered Reactions in Self-Reporting Chitosan Hydrogels. *ACS Applied Materials & Interfaces, 7*(36), 20190-20199.

Mygind, P. H., Fischer, R. L., Schnorr, K. M., Hansen, M. T., Sonksen, C. P., Ludvigsen, S., . . . Kristensen, H. H. (2005). Plectasin is a peptide antibiotic with therapeutic potential from a saprophytic fungus. *Nature, 437*(7061), 975-980. doi:10.1038/nature04051

Nana Cai, Qingsi Li, Jiamin Zhang, Tong Xu, Weiqiang Zhao, Jing Yang, & Zhang, L. (2017). Antifouling zwitterionic hydrogel coating improves hemocompatibility of activated carbon hemoadsorbent. *Journal of Colloid and Interface Science, 503*, 168-177.

Nathan A. Stasko, & Schoenfisch, M. H. (2006). Dendrimers as a Scaffold for Nitric Oxide Release. *Journal of American Chemisty Society, 128*, 8265-8271.

Nermina Malanovic, K. L. (2015). Gram-positive bacterial cell envelopes: The impact on the activity of antimicrobial peptides. *Biochimica et Biophysica Acta*, 936-946.

Neu, H. C. (1973). Antimicrobial agents. Mechanisms of action and clinical usage. *Current Problems in Surgery, 10*(6), 1-64.

Ng，, V. W. L., Xiyu Ke, Ashlynn L. Z. Lee, James L. Hedrick, & Yang, Y. Y. (2013). Synergistic Co-Delivery of Membrane-Disrupting Polymers with Commercial Antibiotics against Highly Opportunistic Bacteria. *Advanced Materials, 25*(46).

Nicolas Barraud, Bharat G. Kardak, Nageshwar R. Yepuri, Robert P. Howlin, Jeremy S. Webb, Saul N. Faust, . . . Kelso, M. J. (2012). Cephalosporin-3'-diazeniumdiolates: Targeted NO-Donor Prodrugs for Dispersing Bacterial Biofilms. *Angewandte Chemie International Edition, 51*, 9057-9060.

Nicole J. Afacan, A. T. Y. Y., Olga M. Pena, Robert E.W. Hancock. (2012). Therapeutic Potential

of Host Defense Peptides in Antibiotic-resistant Infections. *Current Pharmaceutical Design, 18*, 807-819.
Nicolle, L. E. (2014a). Catheter associated urinary tract infections. *Antimicrob Resist Infect Control, 3*. Retrieved from https://www.ncbi.nlm.nih.gov/pmc/articles/PMC4114799/#
Nicolle, L. E. (2014b). Catheter associated urinary tract infections. *Antimicrobial Resistance and Infection Control, 3*. Retrieved from https://www.ncbi.nlm.nih.gov/pmc/articles/PMC4114799/#
Nikaido, H. (2009). Multidrug Resistance in Bacteria. *Annual Reviews in Biochemistry, 78*, 119-146.
Norma, G. (2007). Analysis of The Kinetics of Folding of Proteins and Peptides Using Circular Dichroism. *Nature Protocols, 1*(6), 2891-2899.
O'Neill, T. (1972). Grafting of Acrylic Acid onto Radiation-Peroxidized Polypropylene Film in the Presence of Ferrous Ion. *Journal of Polymer Science: Part A, 10*, 569-580.
Ögmundur Vidar Rúnarsson, Clemens Malainer, Jukka Holappa, Snorri Th. Sigurdsson, & Már Másson. (2008). tert-Butyldimethylsilyl O-protected chitosan and chitooligosaccharides: useful precursors for N-modifications in common organic solvents. *Carbohydrate Research, 343*, 2576-2582.
Omar. S. Sakr, & Borchard, G. (2013). Encapsulation of Enzymes in Layer-by-Layer (LbL) Structures: Latest Advances and Applications. *Biomacromolecules, 14*, 2117-2135.
P. Stoodley, K. Sauer, D. G. Davies, & J.W. Costerton. (2002). Biofilms as complex differentiated communities. *Annual Reviews in Microbiology, 56*, 187-209.
Peng Li, C. Z., Shahrzad Rayatpisheh, Kai Ye, Yin Fun Poon, Paula T. Hammond , Hongwei Duan , Mary B. Chan-Park (2012). Cationic Peptidopolysaccharides Show Excellent Broad-Spectrum Antimicrobial Activities and High Selectivity. *Advanced Materials, 24*, 4130-4137.
Per H. Mygind, R. L. F., Kirk M. Schnorr, Mogens T. Hansen, Carsten P. So¨nksen, Svend Ludvigsen, Dorotea Ravento, Steen Buskov, Bjarke Christensen, Leonardo De Maria. (2005). Plectasin is a peptide antibiotic with therapeutic potential from a saprophytic fungus. *Nature, 437*(13), 975-980.
Philip S Stewart, & Costerton, J. W. (2001). Antibiotic resistance of bacteria in biofilms. *The Lancet, 358*(9276), 135-138.
Phillips, R. (2014). Blocking bacterial biofilms on urinary bladder catheters. *Nature Reviews Urology, 11*(12), 660-661.
Piddock, L. J. V. (2006). Multidrug-resistance efflux pumps—not just for resistance. *Nature Reviews Microbiology, 4*.
Pornpen Sae-ung, Kristopher W. Kolewe, Ying Bai, Eric W. Rice, Jessica D. Schiffman, Todd Emrick, & Hoven, V. P. (2017). Antifouling Stripes Prepared from Clickable Zwitterionic Copolymers. *Langmuir, 33*(28), 7028-7035.
Priyanka Sahariah, Kasper K. Sørensen, Martha A. Hjalmarsdottir, Olafur E. Sigurjonsson, Knud J. Jensen, Mar Massonn, & Thygesen, M. B. (2015). Antimicrobial peptide shows enhanced activity and reduced toxicity upon grafting to chitosan polymers. *Chemical Communications, 51*.
Punia, A., Mancuso, A., Banerjee, P., & Yang, N. L. (2015). Nonhemolytic and Antibacterial Acrylic Copolymers with Hexamethyleneamine and Poly(ethylene glycol) Side Chains. *ACS Macro Letters, 4*(4), 426-430. doi:10.1021/acsmacrolett.5b00102
Qiaohong Liu, Priyadarshini Singha, Hitesh Handa, & Locklin, J. (2017). Covalent Grafting of Antifouling Phosphorylcholine-Based Copolymers with Antimicrobial Nitric Oxide Releasing Polymers to Enhance Infection-Resistant Properties of Medical Device Coatings. *Langmuir, 33*, 13105-13113.
Regev-Shoshani Gilly, Ko Mary, Miller Chris, & Av-Gay Yossef. (2010). Slow release of nitric oxide from charged catheters and its effect on biofilm formation by Escherichia coli. *Antimicrobial agents and chemotherapy, 54*(1), 273-279.
Richard Wheeler, R. D. T., Richard G. Bailey, Bartłomiej Salamaga, Stéphane Mesnage, Sharifah A. S. Mohamad, Emma J. Hayhurst, Malcolm Horsburgh, Jamie K. Hobbs, Simon J.

Foster. (2015). Bacterial Cell Enlargement Requires Control of Cell Wall Stiffness Mediated by Peptidoglycan Hydrolases. *mBio, 6*(4).

Robert E W Hancock, & Chapple, D. S. (1999). Peptide Antibiotics. *Antimicrobial agents and chemotherapy, 43*(6), 1317-1323.

Robert E W Hancock, H.-G. S. (2006). Antimicrobial and host-defense peptides as new anti-infective therapeutic strategies. *Nature Biotechnology, 24*, 1551-1557.

Robert J. Soto, Lei Yang, & Schoenfisch, M. H. (2016). Functionalized Mesoporous Silica via an Aminosilane Surfactant Ion Exchange Reaction: Controlled Scaffold Design and Nitric Oxide Release. *ACS Applied Materials & Interfaces, 8*, 2220-2231.

Romeis T. (1994). Penicillin-binding protein 7/8 of Escherichia coli is a DD-endopeptidase. *European Journal Of Biochemistry, 224*.

Romeis, T., W. Vollmer & J.-V. H¨oltje. (1993). Characterization of three different lytic transglycosylases in Escherichia coli. *FEMS Microbiol. Lett, 111*(141-146).

S, S. R., Zheng, Z., Michael, B., Jun, L., S, L. H., R, B. G., . . . Arthur, C. (2012). Vascular catheters with a nonleaching poly-sulfobetaine surface modification reduce thrombus formation and microbial attachment. *Science translational medicine, 4*(153), 153ra132-153ra132.

Saira Javed, Farrukh Azeem, Sabir Hussain, Ijaz Rasul, Muhammad Hussnain Siddique, Muhammad Riaz, . . . Habibullah Nadeem. (2018). Bacterial lipases: A review on purification and characterization. *Progress in Biophysics and Molecular Biology, 132*, 23-34.

Salah M. Tawfik, & Hassan H. Hefni. (2016). Synthesis and antimicrobial activity of polysaccharide alginate derived cationic surfactant–metal(II) complexes. *International Journal of Biological Macromolecules, 82*, 562-572.

Salzer, W. L. (2018). Peritoneal dialysis-related peritonitis: challenges and solutions. *International Journal of Nephrology and Renovascular Disease, 11*(173-186).

San Tin, Chu Sing Lim, Meena Kishore Sakharkar, & Sakharkar, K. R. (2010). Synergistic Combinations of Chitosans and Antibiotics in Staphylococcus aureus. *Letters in Drug Design & Discovery, 7*, 31-35.

Shakeela Sayed, Tatiana Millard, & Jardine, A. (2018). Expedient synthesis and properties of 6-deoxy-6-amino chitosan. *Carbohydrate Polymers, 196*, 187-198.

Shelley S. Magill, Jonathan R. Edwards, Wendy Bamberg, Zintars G. Beldavs, Ghinwa Dumyati, Marion A. Kainer, . . . Scott K. Fridkin. (2014). Multistate Point-Prevalence Survey of Health Care–Associated Infections. *The New England Journal of Medicine, 370*(13).

Shenfu Chen, Lingyan Li, Chao Zhao, & Zheng, J. (2010). Surface hydration: Principles and applications toward low-fouling/nonfouling biomaterials. *Polymer, 51*, 5283-5293.

Shih, Y.-J., Chang, Y., Quemener, D., Yang, H.-S., Jhong, J.-F., Ho, F.-M., . . . Chang, Y. (2014). Hemocompatibility of polyampholyte copolymers with well-defined charge bias in human blood. *Langmuir, 30*(22), 6489-6496.

Shinpei Yamamoto, Muhammad Ejaz, Yoshinobu Tsujii, & Fukuda, T. (2000). Surface Interaction Forces of Well-Defined, High-Density Polymer Brushes Studied by Atomic Force Microscopy. 2. Effect of Graft Density. *Macromolecules, 33*, 5608-5612.

Shrinivas Venkataraman, Ashlynn L. Z. Lee, Jeremy P. K. Tan, Yi Chien Ng, Amelia Lee Yi Lin, Jaron Y. K. Yong, . . . Yang, Y. Y. (2019). Functional cationic derivatives of starch as antimicrobial agents. *Polymer Chemistry, 10*.

Shu J. Lam, Neil M. O'Brien-Simpson, Namfon Pantarat, Adrian Sulistio, Edgar H. H. Wong, Yu-Yen Chen, . . . Qiao, G. G. (2016). Combating multidrug-resistant Gram-negative bacteria with structurally nanoengineered antimicrobial peptide polymers. *Nature Microbiology, 1*, 1.

Silvia Schwank, Zarko Rajacic, Werner Zimmerli, & Blaser, J. (1998). Impact of Bacterial Biofilm Formation on In Vitro and In Vivo Activities of Antibiotics. *Antimicrobial agents and chemotherapy, 42*(4), 895-898.

Sirijan Santajit, & Indrawattana, N. (2016). Mechanisms of Antimicrobial Resistance in ESKAPE

Pathogens. *BioMed Research International, 2016*.
Smith, R. S., Zhang, Z., Bouchard, M., Li, J., Lapp, H. S., Brotske, G. R., . . . Coury, A. (2012). Vascular catheters with a nonleaching poly-sulfobetaine surface modification reduce thrombus formation and microbial attachment. *Science translational medicine, 4*(153), 153ra132-153ra132.
Srinivas, N., Jetter, P., Ueberbacher, B. J., Werneburg, M., Zerbe, K., Steinmann, J., . . . Robinson, J. A. (2010). Peptidomimetic Antibiotics Target Outer-Membrane Biogenesis in Pseudomonas aeruginosa. *Science, 327*(5968), 1010-1013. doi:10.1126/science.1182749
Steele, M. F. (2016). https://www.nlm.nih.gov/medlineplus/news/fullstory_159074.html.
Stefano, F., Luigi, M., Giorgio, C., & Luciano, P. (2012). Charge Density Quantification of Polyelectrolyte Polysaccharides by Conductometric Titration: An Analytical Chemistry Experiment. *Journal of Chemical Education, 89*(1), 121-124
Steve Edmondson, Vicky L. Osborne, & Huck, W. T. S. (2004). Polymer brushes via surface-initiated polymerizations. *Chemical Society Reviews*(1).
Surendra H. Mahadevegowda, Shuai Hou, Jielin Ma, Damien Keogh, Jianhua Zhang, Asadulla Mallick, . . . Chan-Park, M. B. (2018). Raman-encoded, multivalent glycannanoconjugates for traceable specific binding and killing of bacteria. *Biomaterials Science, 6*.
Sycuro, L. K., T.J. Wyckoff, J. Biboy, et al. (2012). Multiple peptidoglycan modification networks modulate Helicobacter pylori's cell shape, motility, and colonization potential. *PLoS Pathogens*.
T. Goto, Y. Nakame, M. Nishida, & Ohi, Y. (1999). Bacterial biofilms and catheters in experimental urinary tract infection. *International Journal of Antimicrobial Agents, 11*, 227-231.
Tejero，, R., Gutiérrez，, B., DanielLópez，, FátimaLópez-Fabal，, L.Gómez-Garcés，, J., & MartaFernández-García. (2015). Copolymers of acrylonitrile with quaternizable thiazole and triazole side-chain methacrylates as potent antimicrobial and hemocompatible systems. *Acta Biomaterialia, 25*, 86-96.
Thien-Fah C Mah, & O'Toole, G. A. (2001). Mechanisms of biofilm resistance to antimicrobial agents. *Trends in Microbiology, 9*(1), 34-39.
Tsung-Shing Andrew Wang, T. J. L., Yuto Sumida, Hirokazu Tsukamoto, Yihui Wu, Yuriy Rebets, Daniel E. Kahne, and Suzanne Walker. (2011). Primer Preactivation of Peptidoglycan Polymerases. *Journal of the American Chemical Society, 133*(22).
Tuanwei Liu, Wei Zhang, Xinlin Yang, & Li, C. (2015). Hollow polymer nanoparticles with S-nitrosothiols as scaffolds for nitric oxide release. *Journal of Colloid and Interface Science, 459*, 115-122.
Vaara, M. (1992). Agents That Increase the Permeability of the Outer Membrane. *Microbiological Reviews, 56*(3), 395-411.
Vale´rio R. F. Matias, T. J. B. (2006). Native Cell Wall Organization Shown by Cryo-Electron Microscopy Confirms the Existence of a Periplasmic Space in Staphylococcus aureus. *Journal of bacteriology, 188*(3), 1011-1021.
Vasil ML, Graham LM, Ostroff RM, Shortridge VD, & Vasil AI. (1991). Phospholipase C: molecular biology and contribution to the pathogenesis of Pseudomonas aeruginosa. *Antibiotics and Chemotherapy, 44*, 34-47.
Vitaly V. Komnatnyy, Wen-Chi Chiang, Tim Tolker-Nielsen, Michael Givskov, & Thomas E. Nielsen. (2014). Bacteria-Triggered Release of Antimicrobial Agents. *Angewandte Chemie International Edition, 53*, 439-441.
W. H. Yu, E. T. Kang, & Neoh, K. G. (2005). Controlled Grafting of Comb Copolymer Brushes on Poly(tetrafluoroethylene) Films by Surface-Initiated Living Radical Polymerizations. *Langmuir, 21*, 450-456.
Wael Elhenawy, R. M. D., Jutta Fero, Nina R. Salama, Mario F. Felman, Natividad Ruiz. (2016). The O-Antigen Flippase Wzk Can Substitute for MurJ in Peptidoglycan Synthesis in Helicobacter pylori and Escherichia coli. *PLOS one, 11*(8), 1-16.

Waldemar Vollmer, B. J., Paulette Charlier, Simon Foster. (2008). Bacterial peptidoglycan(murein) hydrolases. *Federation of European Microbiological Societies*.

Warayuth Sajomsang, S. T., Varawut Tangpasuthadol, William H. Daly. (2008). Synthesis of methylated chitosan containing aromatic moieties: Chemoselectivity and effect on molecular weight. *Carbohydrate Polymers, 72*, 740–750.

Warayuth Sajomsang, S. T., Varawut Tangpasuthadol, William H. Daly. (2009). Quaternization of N-aryl chitosan derivatives: synthesis, characterization, and antibacterial activity. *Carbohydrate Research, 344*, 2502–2511.

Wei Wang, Yang Lu, Hui Zhu, & Cao, Z. (2017). Superdurable Coating Fabricated from a Double-Sided Tape with Long Term "Zero" Bacterial Adhesion. *Advanced Materials, 29*.

Wei Wang, Yang Lu, Jinbing Xie, Hui Zhu, & Cao, Z. (2016). A zwitterionic macro-crosslinker for durable non-fouling coatings. *Chemistry Communications, 52*.

Wei Wang, Yang Lu, Jinbing Xie, Hui Zhu, & Zhiqiang Cao. (2016). A zwitterionic macro-crosslinker for durable non-fouling coatings. *Chemistry Commnunications, 52*.

Wei Yang, Chanjuan Liu, & Chen, Y. (2018). Stability of Polydopamine Coatings on Gold Substrates Inspected by Surface Plasmon Resonance Imaging. *Langmuir, 34*(12), 3565-3571.

Wenjie Yuan, Yakai Feng, Heyun Wang, Dazhi Yang, Bo An, Wencheng Zhang, . . . Guo, J. (2013). Hemocompatible surface of electrospun nanofibrous scaffolds by ATRP modification. *Materials Science and Engineering, 33*, 3644-3651.

Wufang Yang, & Zhou, F. (2017). Polymer brushes for antibiofouling and lubrication. *Biosurface and Biotribology*, 97-114.

Xia-Chao Chen, Ke-Feng Ren, Jia-Hui Zhang, Dan-Dan Li, Emily Zhao , Zhong Jonathon Zhao, . . . Jian Ji. (2015). Humidity-Triggered Self-Healing of Microporous Polyelectrolyte Multilayer Coatings for Hydrophobic Drug Delivery. *Advanced Functional Materials, 25*, 7470-7477.

Xiaona Yang, Dawei Chen, & Zhao, H. (2016). Silica particles with immobilized protein molecules and polymer brushes. *Acta Biomaterialia, 29*, 446-454.

Xiaowu Fan, Lijun Lin, Jeffrey L. Dalsin, & Phillip B. Messersmith. (2005). Biomimetic Anchor for Surface-Initiated Polymerization from Metal Substrates. *Journal of American Chemisty Society, 127*, 15843-15847.

Xiaoying Zhu, & Loh, X. J. (2015). Layer-by-layer assemblies for antibacterial applications. *Biomaterials Science, 3*.

Xingxing Jin, Jiang Yuan, & Shen, J. (2016). Zwitterionic polymer brushes via dopamine-initiated ATRP from PET sheets for improving hemocompatible and antifouling properties. *Colloids and Surfaces B: Biointerfaces, 145*, 275-284.

Xinhua, L., Weihua, D., Haiyan, J., Nianhua, D., & Juxia, G. (2015). Preparation and Evaluation of a Novel pADM-derived Micro- and Nano-electrospun Collagen Membrane. *RSC Advances, 5*(64), 52079-52087

Xintao Cao, Y. Z., Ruoyu Mao, Da Teng, Xiumin Wang, Jianhua Wang. (2015). Design and recombination expression of a novel plectasin-derived peptide MP1106 and its properties against Staphylococcus aureus. *Applied Microbiology and Biotechnology, 99*, 2649–2662.

Xinyuan Wan, Y. Z., Ya Deng, Qin Zhang,a Jiehua Li, Kunjie Wang, Jianshu Li, Hong Tan, Qiang Fua. (2015). Effects of interaction between a polycation and a nonionic polymer on their cross-assembly into mixed micelles. *Soft Matter, 11*, 4197.

Yajuan Su, Liang Tian, Meng Yu, Qiang Gao, Dehui Wang, Yuewei Xi, . . . Peng Li. (2017). Cationic peptidopolysaccharides synthesized by'click' chemistry with enhanced broad-spectrum antimicrobial activities. *Polymer Chemistry, 8*.

Yamamura, H., Sugiyama, Y., Murata, K., Yokoi, T., Kurata, R., Miyagawa, A., . . . Katsu, T. (2014). Synthesis of antimicrobial cyclodextrins bearing polyarylamino and polyalkylamino groups via click chemistry for bacterial membrane disruption. *Chemical Communications, 50*(41), 5444-5446. doi:10.1039/c3cc49543d

Yan Li, & Lee, P. I. (2009). Controlled Nitric Oxide Delivery Platform Based on S-Nitrosothiol

Conjugated Interpolymer Complexes for Diabetic Wound Healing. *Molecular Pharmaceutics, 7*(1), 254-266.

Yaqi Wo, Elizabeth J. Brisbois, Robert H. Bartlett, & Mark E. Meyerhoff. (2016). Recent advances in thromboresistant and antimicrobial polymers for biomedical applications: just say yes to nitric oxide (NO). *Biomaterials Science, 4*.

Yaqi Wo, Zi Li, Elizabeth J. Brisbois, Alessandro Colletta, Jianfeng Wu, Terry C. Major, . . . Meyerhoff, M. E. (2015). Origin of Long-Term Storage Stability and Nitric Oxide Release Behavior of CarboSil Polymer Doped with S-Nitroso-N-acetyl-D-penicillamine. *Acs Applied Materials & Interfaces, 7*, 22218-22227.

Yazan Haddadin, & Regunath, H. (2019a). Central Line Associated Blood Stream Infections (CLABSI). *StatPearls*. Retrieved from https://www.ncbi.nlm.nih.gov/books/NBK430891/

Yazan Haddadin, & Regunath, H. (2019b). Central Line Associated Blood Stream Infections (CLABSI). Retrieved from https://www.ncbi.nlm.nih.gov/books/NBK430891/

Yi He, T. L. (2013). Activity Determinants of Helical Antimicrobial Peptides: A Large-Scale Computational Study. *PLOS one, 8*(6).

Yingzi Zhao, Paul M. Vanhoutte, & Leung, S. W. S. (2015). Vascular nitric oxide: Beyond eNOS. *Journal of Pharmacological Sciences, 129*, 83-94.

Yongqiang Gao, Lei Liang, Song Zhao, Yunlong Qi, Wen Zhang, Xuefei Sun, . . . Baodong Song. (2018). Hydrophilic and antimicrobial core–shell nanoparticles containing guanidine groups for ultrafiltration membrane modification. *RSC Advances, 8*.

Youling Yuan, Fei Ai, Xiaopeng Zang, Wei Zhuang, Jian Shen, & Lin, S. (2004). Polyurethane vascular catheter surface grafted with zwitterionic sulfobetaine monomer activated by ozone. *Colloids and Surfaces B: Biointerfaces, 35*.

Yuanzi Wu, Yanyi Huang, & Hongwei Ma. (2007). A Facile Method for Permanent and Functional Surface Modification of Poly(dimethylsiloxane). *Journal of American Chemisty Society, 129*, 7226-7227.

Yuchong Yang, Zhengguo Cai, Zehuan Huang, Xiaoyan Tang, & Zhang, X. (2018). Antimicrobial cationic polymers: from structural design to functional control. *Polymer Journal, 50*, 33-44.

Yuji Pu, Zheng Hou, Mya Mya Khin, Rubi Zamudio-Vázquez, Kar Lai Poo, Hongwei Duan, & Chan-Park, M. B. (2017). Synthesis and Antibacterial Study of Sulfobetaine/Quaternary Ammonium-Modified Star-Shaped Poly[2-(dimethylamino)ethyl methacrylate]-Based Copolymers with an Inorganic Core. *Biomacromolecules, 18*(1), 44-55.

Yury, S., Valentina, P., Olga, O., Irina, S., & Ekaterina, G. (2016). Characterization of Clusters and Unimers in Associating Solutions of Chitosan by Dynamic and Static Light Scattering. *Macromolecular chemistry and physics, 217*(14), 1636-1644

Yuxin Chen, Michael T. Guarnieri, Adriana I. Vasil, Michael L. Vasil, Colin T. Mant, & Robert S. Hodges. (2007). Role of Peptide Hydrophobicity in the Mechanism of Action of alpha-Helical Antimicrobial Peptides. *Antimicrobial agents and chemotherapy, 51*(4), 1398-1406.

Zachary K. Zander, & Becker, M. L. (2018). Antimicrobial and Antifouling Strategies for Polymeric Medical Devices. *ACS Macro Letters, 7*, 16-25.

Zahra Assadia, Giti Emtiazib, & Zarrabia, A. (2018). Novel synergistic activities of tetracycline copper oxide nanoparticles integrated into chitosan micro particles for delivery against multiple drug resistant strains: Generation of reactive oxygen species (ROS) and cell death. *Journal of Drug Delivery Science and Technology, 44*, 65-70.

Zahra Sadrearhami, Farah Nabilah Shafiee, Kitty K. K. Ho, Naresh Kumar, Marta Krasowska, Anton Blencowe, . . . Cyrille Boyer. (2019). Antibiofilm Nitric Oxide-Releasing Polydopamine Coatings. *ACS Applied Materials & Interfaces, 11*, 7320-7329.

Zelun Zhi, Yajuan Su, Yuewei Xi, Liang Tian, Miao Xu, Qianqian Wang, . . . Huang, W. (2017). Dual-Functional Polyethylene Glycol-b-polyhexanide Surface Coating with in Vitro and in Vivo Antimicrobial and Antifouling Activities. *ACS Applied Materials & Interfaces, 9*, 10383-10397.

Zheng Hou, Yogesh Vikhe Shankar, Yang Liu, Feiqing Ding, Jothy Lachumy Subramanion, Vikashini Ravikumar, . . . Chan-Park, M. B. (2017). Nanoparticles of Short Cationic Peptidopolysaccharide Self-Assembled by Hydrogen Bonding with Antibacterial Effect against Multidrug-Resistant Bacteria. *ACS Applied Materials & Interfaces, 9*(44), 38288-38303.

Zheng Zhang, Gang Cheng, Louisa R. Carr, Hana Vaisocherova, Shengfu Chen, & Jiang, S. (2008). The hydrolysis of cationic polycarboxybetaine esters to zwitterionic polycarboxybetaines with controlled properties. *Biomaterials, 29*, 4719-4725.

Zhi Xiang Voo, Majad Khan, Qingxing Xu, Karthikeyan Narayanan, Brandon W. J. Ng, Raidah Bte Ahmad, . . . Yan, Y. Y. (2016). Antimicrobial coatings against biofilm formation: the unexpected balance between antifouling and bactericidal behavior. *Polymer Chemistry, 7*.

Zhimei Zhong, P. L., Ronge Xing, Song Liu. (2009). Antimicrobial activity of hydroxylbenzenesulfonailides derivatives of chitosan, chitosan sulfates and carboxymethyl chitosan. *International Journal of Biological Macromolecules, 45*, 163–168.

Zhimei Zhong, R. X., Song Liu, Lin Wang, Shengbao Cai, Pengcheng Lia. (2008). Synthesis of acyl thiourea derivatives of chitosan and their antimicrobial activities in vitro. *Carbohydrate Research, 343*, 566–570.

Zhiyi Bao, Merlin L. Bruening, & Baker, G. L. (2006). Control of the Density of Polymer Brushes Prepared by Surface-Initiated Atom Transfer Radical Polymerization. *Macromolecules, 39*, 5251-5258.

Zhou, Z., & Meyerhoff, M. E. (2005). Preparation and characterization of polymeric coatings with combined nitric oxide release and immobilized active heparin. *Biomaterials, 26*(33), 6506-6517.